PERFORMANCE OF CONFINED CONCRETE COLUMNS UNDER SIMULATED LIFE CYCLES

by

STEVEN D. HART

B.S., United States Military Academy, 1988
M. Eng., Virginia Tech, 1998

AN ABSTRACT OF A DISSERTATION

submitted in partial fulfillment of the requirements for the degree

DOCTOR OF PHILOSOPHY

Department of Civil Engineering
College of Engineering

KANSAS STATE UNIVERSITY
Manhattan, Kansas

2008

Abstract

Over the past 30 years, FRP composites (carbon, glass, or aramid fibers) have arisen as a method of retrofitting existing reinforced concrete structures to bring them up to current code standards of confinement and ductility. The development of stress-strain models for FRP confined concrete began with the adaptation of steel confinement models then progressed to models specifically developed based on test results from FRP confined specimens. State of the art stress-strain models for FRP confined concrete models may now be validated against a wide variety of published experimental results. Recent publications show researchers branching out and looking at other aspects of FRP confined concrete behavior, including the impact of sustained service loads on long term and ultimate behavior. An experimental program which examines the effects of sustained service loading on the ultimate axial performance of FRP confined concrete is presented. The program's purpose is to determine whether or not a material model developed without the presence of a sustained load accurately predicts the ultimate stress-strain response of FRP confined concrete previously subjected to a sustained service load. Equipment and procedures were developed to model the critical events in a building life cycle: construction, sustained service loading, minor critical events, rehabilitation, and ultimate performance. Varying the order of these events produces a simulated life cycle allowing analysis of the impact of strain history on ultimate performance. The results of the experimental program indicate that the presence of a sustained service load changes the expected failure mode from FRP rupture to FRP de-lamination and the stress-strain response of a specimen is approximately 10% below published models when sustained service loads are included in the life cycle. A comprehensive modeling process is proposed for modeling significant events in a structure's life cycle. Impacts on earthquake engineering and reliability studies are addressed and future research suggested. This research shows that life cycle modeling can improve the design and rehabilitation of structures so that they meet safety requirements in future seismic events.

PERFORMANCE OF CONFINED CONCRETE COLUMNS UNDER SIMULATED LIFE CYCLES

by

STEVEN D. HART

B.S., United States Military Academy, 1988
M. Eng., Virginia Tech, 1998

A DISSERTATION

submitted in partial fulfillment of the requirements for the degree

DOCTOR OF PHILOSOPHY

Department of Civil Engineering
College of Engineering

KANSAS STATE UNIVERSITY
Manhattan, Kansas

2008

Approved by:

Major Professor
Asad Esmaeily

Abstract

Over the past 30 years, FRP composites (carbon, glass, or aramid fibers) have arisen as a method of retrofitting existing reinforced concrete structures to bring them up to current code standards of confinement and ductility. The development of stress-strain models for FRP confined concrete began with the adaptation of steel confinement models then progressed to models specifically developed based on test results from FRP confined specimens. State of the art stress-strain models for FRP confined concrete models may now be validated against a wide variety of published experimental results. Recent publications show researchers branching out and looking at other aspects of FRP confined concrete behavior, including the impact of sustained service loads on long term and ultimate behavior. An experimental program which examines the effects of sustained service loading on the ultimate axial performance of FRP confined concrete is presented. The program's purpose is to determine whether or not a material model developed without the presence of a sustained load accurately predicts the ultimate stress-strain response of FRP confined concrete previously subjected to a sustained service load. Equipment and procedures were developed to model the critical events in a building life cycle: construction, sustained service loading, minor critical events, rehabilitation, and ultimate performance. Varying the order of these events produces a simulated life cycle allowing analysis of the impact of strain history on ultimate performance. The results of the experimental program indicate that the presence of a sustained service load changes the expected failure mode from FRP rupture to FRP de-lamination and the stress-strain response of a specimen is approximately 10% below published models when sustained service loads are included in the life cycle. A comprehensive modeling process is proposed for modeling significant events in a structure's life cycle. Impacts on earthquake engineering and reliability studies are addressed and future research suggested. This research shows that life cycle modeling can improve the design and rehabilitation of structures so that they meet safety requirements in future seismic events.

Table of Contents

List of Figures

List of Tables

Acknowledgements

The assistance of my committee members, Dr. Esmaeily, Dr. Rasheed, Dr. Melhem, Dr. Das, and Dr. Rebello is gratefully acknowledged. Special thanks are due to Dr. Esmaeily for providing the funding for this research and to Dr. Rasheed for securing the FRP materials. Special thanks go to VSL Strengthening Products for providing the carbon fiber and the epoxy materials.

Dedication

This work is dedicated to the glory of God, in loving memory of my grandparents, in honor of my parents, in love to my wife and children, and in memory of "the ones who couldn't make it."

1. Introduction

1.1 Overview

In an introductory course in mechanics of materials, aspiring engineers first learn to develop the relationships between the loads applied to a specimen and the resulting deformations. In the Mechanics Lab, the young engineers conduct a tensile test on a steel coupon and plot their first stress-strain curves. From this, they begin to understand Hooke's Law, Young's Modulus, strain hardening, and ultimate strength. Armed with this knowledge, they proceed to learn the basics of linear elastic structural analysis. At this point, reality begins to intrude when one young engineer, in an "AH-HAH" moment, points out that the computer told him that the axial stress in a column was 52 ksi, but that the steel should have yielded at 36 ksi. Now the concept of a yield point becomes very real and the effects of residual stresses and buckling further complicate analysis problems. Then come courses in reinforced and pre-stressed concrete where material non-linearity, creep, and shrinkage make our aspiring engineers long for the days of "homogeneous, isotropic, linear, elastic behavior." However, those days are long gone as reality, once exposed, never fades away. Next come real world design experience and graduate school with exposure to cyclic loading, vibration analysis, earthquake design, advanced matrix structural analysis, and finite element analysis where non-linear behavior is a daily occurrence. So our engineers come full circle—they start with a basic linear elastic material model and end with a complex non-linear material model that is the basis for everything.

The importance of accurate material stress-strain models can be seen in a variety of applications, particularly those related to earthquake engineering. In a study for the Pacific Earthquake Engineering Research Center (PEER), Esmaeily and Xiao (2002) examine the response of bridge columns subjected to gravity and seismic load combinations. They also develop a computer program for predicting the performance of bridge piers subjected to these seismic loads. The program employs a non-linear stress strain model to predict the hysteretic response of a reinforced concrete section. Without the material model, the program cannot function and the accuracy of the program cannot exceed the accuracy of the model. Additionally, both matrix structural analysis and finite element analysis are only valid up to the

yield point of the structural material unless some method is present to account for behavior which is beyond the material's elastic limit. These methods involve the use of materials models which may be simple, bi-linear models like the elasto-plastic assumption of mild steel behavior or complex, multi-parameter models like that proposed by Moran and Pantelides (2002) for the behavior of Fiber Reinforced Polymer (FRP) confined concrete. In addition to their use in computer analysis, these material models also play a crucial role in earthquake design codes.

The Federal Emergency Management Administration (FEMA) has sponsored the development of two model earthquake engineering codes. The first, *NEHRP Recommended Provisions for Seismic Regulations for New Buildings and Other Structures (FEMA 450)*, was most recently published in 2003 by the Building Seismic Safety Council (BSSC). The *Provisions* address minimum life safety requirements by proportioning structures to resist the forces and moments generated by the design earthquake with the expectation that this procedure will provide acceptable levels of performance in less severe seismic events (BSSC, 2003). This document represents over 75 years of development of the lateral force methodologies first published in 1927 and is the basis for the earthquake provisions in other model codes like the International Building Code (IBC). The second, the *Prestandard and Commentary for the Seismic Rehabilitation of Buildings* (*Prestandard*) developed by the American Society of Civil Engineers (ASCE) and released by FEMA in 2000, provides guidance for the survey, evaluation, and rehabilitation of older structures that do not comply with current seismic standards. It codifies a performance based earthquake engineering methodology by establishing four levels of target building performance and matching them against four levels of earthquake hazards to enable design to a desired level of performance against a specific earthquake hazard (ASCE, 2000).

While the two documents promulgate very different design approaches, (Hart and Esmaeily, 2007), they are both based on the fact that earthquake loading produces a highly non-linear response in individual members and the structure as a whole. From the understanding that the "inelastic response of a structure is very sensitive to the inelastic behavior of critical regions," the *Provisions* employ a response modification factor, R, based on the inelastic response of the building's structural system to enable a linear elastic analysis to predict a non-linear response (BSSC, 2003). Before any rehabilitation analysis is performed, the *Prestandard* requires that each individual element be classified as either force-controlled or deformation-

controlled based on the element's actual force-deformation curve. Using Figure 1-1, a component with a Type 3 force-deformation (i.e. non-ductile) curve is classified as a force controlled member while a member with a Type 1 or 2 force-deformation response would be considered a deformation controlled member, provided 'a' and 'b' were sufficiently large. In this it can be seen that a true understanding of the stress-strain behavior of an individual structural member is essential to properly classifying the member and predicting its response to a seismic event.

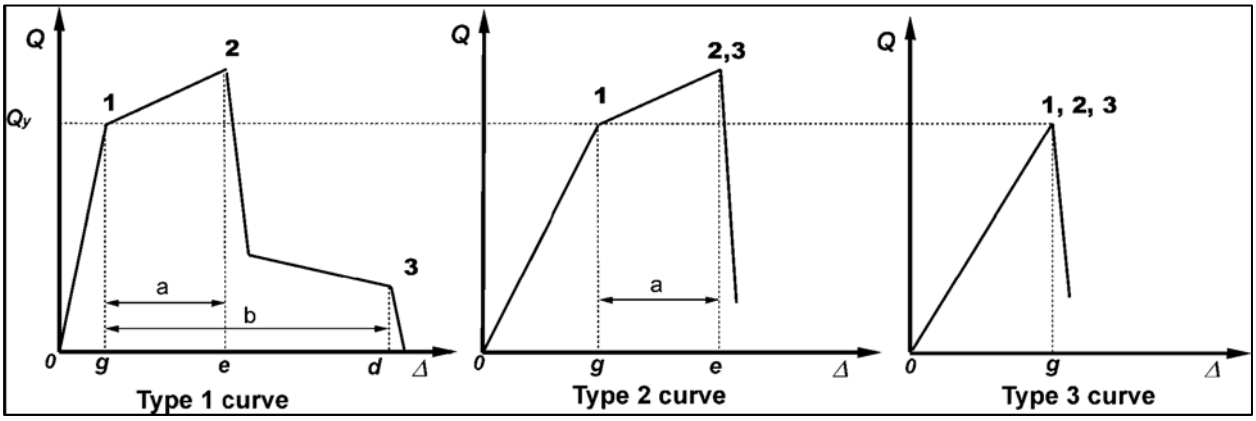

Figure 1-1 FEMA 356 Component Force vs. Deformation Curve

The record of performance of reinforced concrete structures subjected to seismic events has shown that sufficient ductility of the columns is essential to adequate performance of the structure. When considering a steel reinforced column, this ductility is achieved by confining the core concrete using a tightly wound steel spiral. Structures designed in accordance with the current state of the art are expected to have satisfactory performance even in extreme circumstances. Difficulties arise, however, when one considers that older structures do not meet current codes. How, then, can such structures be retrofitted to provide the necessary ductile behavior to prevent a catastrophic structural collapse?

Over the past 30 years, FRP composites (carbon, glass, or aramid fibers) have arisen as a method to retrofit existing reinforced concrete structures to bring them up to current code standards in terms of confinement and ductility. FRP is an attractive solution as it is externally applied to an existing structure and has proven cost effective in achieving the desired results. The development of material models for FRP confined concrete began 25 years ago when early pioneers adapted steel confinement models to work with this new confining material (Fardis and Khalili, 1982 and Saadatmanesh, et al., 1994). Following these developments, new models were proposed that were specifically developed based on test results from FRP confined specimens. A

variety of parameters were considered and both design oriented and analysis oriented models were published (Teng and Lam, 2004). With the large variety of experimental results available, the state of the art for stress-strain models of FRP confined concrete is now highly developed. More recent scholarship and publications have researchers branching out and looking at other aspects of FRP confined concrete behavior. One of the most significant of these may prove to be the impact of sustained service loads on long term and ultimate behavior. Whereas previous research has tended to focus on monotonic, cyclic, or sustained loading, this research will investigate the integration of all three loading types in conjuction with a variety of life cycle events.

1.2 Research Objectives

This study investigates the performance of confined concrete subjected to construction, rehabilitation, service loading, and ultimate loading in patterns that replicate these same events for actual buildings. The research will determine whether or not the duration and magnitude of sustained load, the conditions of application of the FRP, and the prior strain history of an element are necessary parameters in the development of a stress-strain model. If so, appropriate modifications to an existing model, or a new model, will be offered. The scope of this research is focused soley on a member's axial response. Time and equipment constraints prevent other investigations.

This goal requires four supporting objectives. First, the events of a structural life cycle must be defined and apparatuses constructed to simulate these events. Specimen groups will be established to investigate the influence of particular life cycle events on the FRP confined concrete stress-strain curve. Second, changes in the specimen group's behavior due to life cycle events will be identified. Third, these results will be compared to an existing stress-strain model so points of convergence and divergence can be identified. Finally, a model or combination of models will be proposed to accurately model the stress-strain life cycle of confined concrete columns.

1.3 Organization of Report

This dissertation is divided into five chapters. Chapter 1 introduces the problem and summarizes the research. Chapter 2 reports on a survey of the applicable literature. The development of confined concrete models is traced over its 80 year history with a focus on research that significantly advanced the state of the art. The review ends with conclusions based on the strengths and weaknesses of the current research. Chapter 3 explains the experimental procedures used to achieve the research objectives. The purpose and design of the devices employed are explained as well as the procedures for conducting the various required tests. Experimental data are reported for each specimen and specimen group. In Chapter 4 the results of each experimental test are examined. Twelve investigations are conducted to examine the impact of each life cycle event. Findings from these investigations lead to a better understanding of FRP confined concrete behavior and the proposal of life cycle modeling procedures. Impacts of the results are addressed along with suggestions for future research. Finally, Chapter 5 summarizes the research and proposed models and provides general conclusions.

2. Literature Review

Research on the behavior of confined concrete has an eighty year history which has led to the publication of a large body of work. To provide organization and focus, the literature review is grouped into eight categories based on the development of the state of the art. Reviews of selected papers are presented to describe substantial advances in the state of the art in each category. Equations are rendered using a common notation rather than the notation of the original paper. This is done to allow for cross-comparison of concepts and formats between authors. Appendix A contains the definitions of all applicable terms.

2.1 Foundational Research

The papers reviewed in this section are best described as foundational—that is almost all subsequent papers refer to one or more of these authors as initially proposing critical concepts that were the basis for subsequent research efforts.

2.1.1 Richart, et al. (1928)

The initial discovery that radial confinement increased the ultimate compressive strength of concrete was published by Richart, et al. (1928). He placed a concrete specimen in a triaxial state of stress using pressurized water as the confining mechanism and developed an expression to predict the increased ultimate strength and ultimate strain of the confined concrete. Richart did not present an expression for the resulting stress-strain curve of confined concrete. Equations (2.1) and (2.2) have been used ever since as the fundamental expressions for confined concrete behavior and are cited directly or indirectly, in most papers on the subject. Other authors have also offered alternate values of k_1 and k_2 based on further experiments.

$$f'_{cc} = f'_{co}\left(1 + k_1\left(\frac{f'_l}{f'_{co}}\right)\right) \quad with\ k_1 = 4.1 \tag{2.1}$$

$$\varepsilon_{cu} = \varepsilon_{co}\left(1 + k_2\left(\frac{f'_{cc}}{f'_{co}}\right)\right) \quad with\ k_2 = 5 \tag{2.2}$$

2.1.2 Popovics (1973) and Richard & Abbott (1975)

In the mid Twentieth Century, several models were proposed for the stress-strain curve of plain concrete. Two of these have been frequently modified by subsequent researchers to model the stress-strain behavior of confined concrete. Popovics (1973) proposed a single equation, (2.3), to model stress-strain behavior which is valid for uniaxial compression at a constant rate of strain.

$$f_c = f'_{co}\frac{\varepsilon_c}{\varepsilon_{co}}\frac{n}{n-1+\left(\frac{\varepsilon_c}{\varepsilon_{co}}\right)^n} \quad with \;\; n = 0.004 f'_{co} + 1.0 \tag{2.3}$$

Equation (2.3) has the advantage of being a closed form equation which can generate a stress-strain curve simply by varying ε_c. Alternatively, Richard and Abbott (1975) proposed Equation (2.4), a three parameter stress-strain model requiring iteration.

$$\sigma = \frac{E_{co}\varepsilon_c}{\left(1+\left|\frac{E_{co}\varepsilon_c}{\sigma_o}\right|^n\right)^{1/n}} + E_p\varepsilon_c \tag{2.4}$$

where E_p is the plastic modulus and n is the shape parameter of the stress-strain curve obtained from the numerical iteration of Equation (2.5) or using a chart provided by Richard and Abbott.

$$A^n - 1\frac{1}{2^n}\left(B^n - 1\right) = 0 \tag{2.5}$$

Evaluation of Equation (2.5) requires the use of two points on the stress strain curve (ε_a, σ_a) and (ε_b, σ_b) taken so that $\varepsilon_b = 2\varepsilon_a$ and the expressions

$$A = \frac{E_1}{\left(E_a - E_p\right)} \quad with \quad E_a = \frac{\sigma_a}{\varepsilon_a}$$

$$B = \frac{E_1}{\left(E_b - E_p\right)} \quad with \quad E_b = \frac{\sigma_b}{\varepsilon_b}$$

$$E_1 = E_{co} - E_p$$

2.2 Steel Spiral Confinement

In the 1960s and 1970s advances in earthquake engineering demonstrated that the need for increased ductility in concrete columns could be satisfied by confining the concrete using a tightly spaced steel spiral. Several models were developed, including Sheikh and Uzumeri (1982), Fafitis and Shah (1985), Mander, Priestly, and Park (1988) and Cusson and Paultre (1995). These models, while different, share some common characteristics. First, the initial behavior of confined concrete is similar to, and is governed by, the material properties of the plain concrete. Second, the steel spiral confinement substantially increases the ultimate strength of the specimens. Finally, once the ultimate strength is achieved, the steel spiral confinement provides a significant increase in ductility over plain concrete. After reaching $f'_{cc,}$ some models like Mander, et al. (1988) predict an ever decreasing load capacity as strain increases while others like Sheikh and Uzumeri (1992) showing a constant stress plateau prior to a loss of capacity. The decrease in post-peak strength is due to the fact that when the steel yields, it provides a constant confining pressure that decreases in effectiveness as the applied load increases.

2.2.1 Mander, et al. (1988) Stress Strain Relationship for Cyclic Loading

Mander, Priestly, and Park's model which is based on Povpovics' (1973) expression has proven popular. It is reasonably accurate and easy to use as it employs a single closed form expression to model the entire stress-strain curve. This model is well explained in the referenced paper. The monotonic stress-strain relationship is not reproduced here as it is not used in this research. The cyclic relationship, however, will be adapted for use in FRP confined concrete and is therefore included here for reference.

Figure 2-1 illustrates Mander, et al.'s cyclic stress-strain model for steel spiral confined concrete. It is based on the approach used by Takiguchi et al. (1976), but is modified to account for the changes in behavior caused by the confining steel spirals. It employs three equations to model the three parts of a cyclic response: unloading, reloading, and transition to the envelope curve. The unloading and transition branches are represented by curves while the reloading relationship is linear.

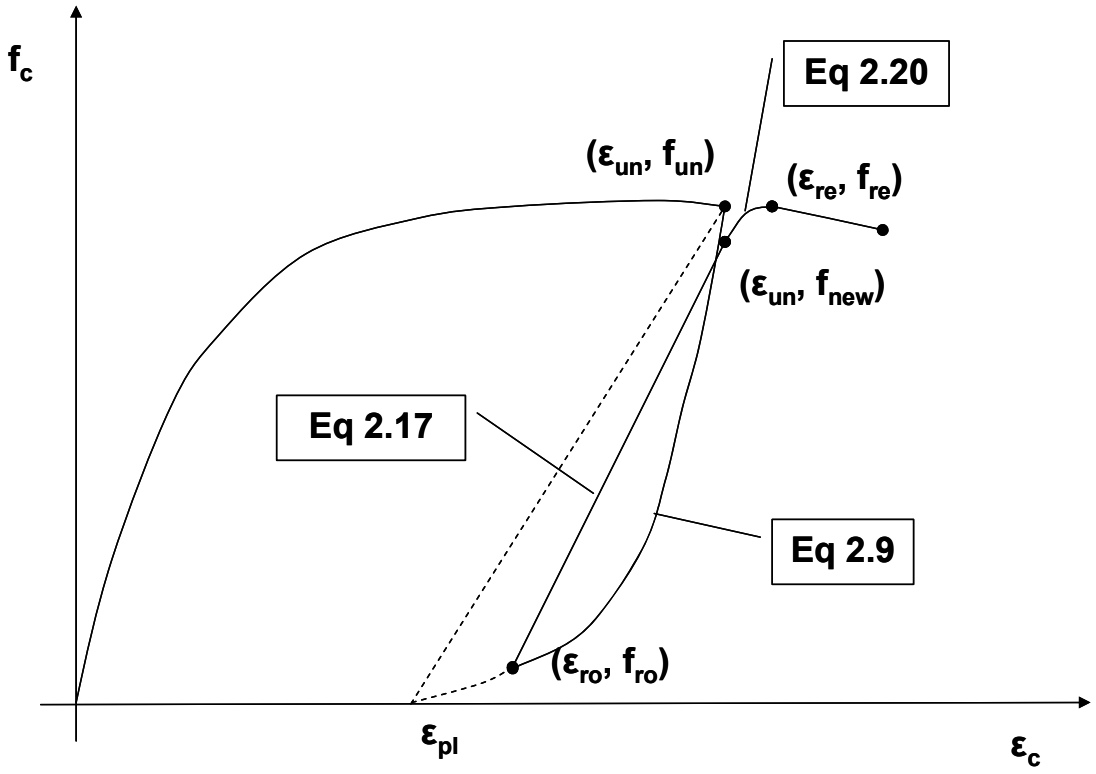

Figure 2-1 Cyclic Stress-Strain Relationship from Mander et al. (1988)

Unloading Branch

The unloading branch requires the calculation of the plastic strain, ε_{pl}. It is found using Equation (2.8) and lies on the plastic unloading secant slope defined between the unloading strain, ε_{un}, and the reference strain, ε_a. Equation (2.6) supported by Equation (2.7) gives the value for ε_a.

$$\varepsilon_a = a\sqrt{\varepsilon_{un}\varepsilon_{cc}} \tag{2.6}$$

$$a = \left| \frac{\varepsilon_{cc}}{\varepsilon_{cc} + \varepsilon_{un}} \quad or \quad \frac{0.09\varepsilon_{un}}{\varepsilon_{cc}} \right|_{max} \tag{2.7}$$

$$\varepsilon_{pl} = \varepsilon_{un} - \frac{(\varepsilon_{un} + \varepsilon_a) f_{un}}{(f_{un} + E_c \varepsilon_a)} \tag{2.8}$$

The unloading curve is defined by Equation (2.9) where the supporting values are given by Equations (2.10) to (2.15). E_u is the initial modulus of elasticity at the point of unloading and

is given by Equation (2.13). The coefficients a, b, and c given by Equations (2.7), (2.14), and (2.15) were selected by the researcher to provide a best fit to the experimental data.

$$f_c = f_{un} - \frac{f_{un}\, x\, r}{r - 1 + x^r} \tag{2.9}$$

$$r = \frac{E_u}{E_u - E_{\sec}} \tag{2.10}$$

$$E_{\sec} = \frac{f_{un}}{\varepsilon_{un} - \varepsilon_{pl}} \tag{2.11}$$

$$x = \frac{\varepsilon_c - \varepsilon_{un}}{\varepsilon_{pl} - \varepsilon_{un}} \tag{2.12}$$

$$E_u = b\, c\, E_c \tag{2.13}$$

$$b = \frac{f_{un}}{f'_{co}} \geq 1 \tag{2.14}$$

$$c = \left(\frac{\varepsilon_{cc}}{\varepsilon_{un}} \right)^{0.5} \leq 1 \tag{2.15}$$

Reloading Branch

The reloading branch is a linear relationship between the reloading point and a new reference stress, f_{new}, which accounts for the strength degradation from the cyclic loading. Equation (2.16) provides for the calculation of f_{new} and Equation (2.18) for the modulus of the reloading branch. Using these terms, Equation (2.17) yields the stress along the reloading branch.

$$f_{new} = 0.92 f_{un} + 0.08 f_{ro} \tag{2.16}$$

$$f_c = f_{ro} + E_r \left(\varepsilon_c - \varepsilon_{ro} \right) \tag{2.17}$$

$$E_r = \frac{f_{ro} - f_{new}}{\varepsilon_{ro} - \varepsilon_{un}} \tag{2.18}$$

Transition Curve

The return from the cyclic stress-strain relationship to the Mander et al. monotonic envelope is accomplished with a parabolic function. First, the return strain, ε_{re}, is calculated with Equation (2.19), then the return stress, f_{re}, and modulus, E_{re}, are read on the envelope curve at ε_{re}. Then the terms in Equations (2.21) and (2.22) are calculated and used to formulate the transition relationship given by Equation (2.20).

$$\varepsilon_{re} = \varepsilon_{un} + \frac{f_{un} - f_{new}}{E_r\left(2 + \frac{f'_{cc}}{f'_{co}}\right)} \tag{2.19}$$

$$f_c = f_{re} + E_{re}x + Ax^2 \tag{2.20}$$

$$x = \left(\varepsilon_c - \varepsilon_{re}\right) \tag{2.21}$$

$$A = \frac{E_r - E_{re}}{-4\left[\left(f_{new} - f_{re}\right) - E_r\left(\varepsilon_{un} - \varepsilon_{re}\right)\right]} \tag{2.22}$$

2.3 Steel Confinement Based Models for FRP Confined Concrete

The early models for the stress-strain behavior of FRP confined concrete were extensions of models developed for steel confined concrete. These early models were of limited utility because they did not yet recognize the differences in behavior between steel and FRP confining materials that later research would show.

2.3.1 Fardis and Khalili (1982)

Fardis and Khalili (1982) applied experiences in structural steel tube confined concrete and prestressed concrete cylinders to experiments on rigid FRP tubes. They developed expressions that model the ultimate stress, Equation (2.24), and ultimate strain, Equation (2.25), of FRP confined concrete as well as predict the entire stress-strain curve, Equation (2.23).

$$f_c = \frac{E_{co}\varepsilon_c}{1 + \varepsilon_c\left(\frac{E_{co}}{f'_{cc}} - \frac{1}{\varepsilon_{cc}}\right)} \tag{2.23}$$

$$f'_{cc} = f'_{co}\left[1 + 4.1\left(2\frac{f_{frp}t}{df'_{co}}\right)\right] \tag{2.24}$$

$$\varepsilon_{cc} = 0.002 + 0.001\frac{E_{frp}t}{df'_{co}} \tag{2.25}$$

Their research was limited to rigid FRP tubes which acted both as forms and confining material. They quantified the increased strength and ductility due to the FRP confinement as well as identifying future research needs.

2.3.2 Saadatmanesh et al. (1994)

Saadatmanesh et al. (1994) conducted research on steel reinforced concrete columns that had been wrapped with either individual FRP rings or continuous FRP spirals as shown in Figure 2-2, but did not test a completely wrapped specimen.

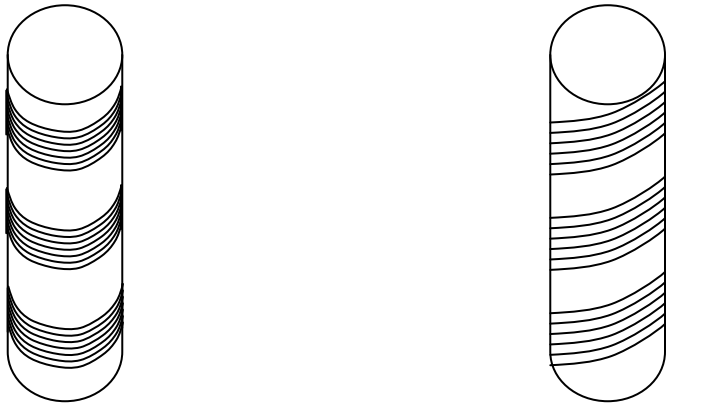

Individual FRP Rings Continuous FRP spiral

Figure 2-2 FRP Confinement Configurations

Mander, Priestly, and Park's expressions for the stress-strain curve were employed, but Equation (2.26) was used in place of the expression for steel confining pressure, to calculate the confining pressure provided by the FRP.

$$f_l = \frac{2f_{frp}A_{st}}{ds} \tag{2.26}$$

Saadatmanesh et al. identified that FRP confinement provided a greater increase in both the axial strength and ductility of concrete members than it did in moment capacity. Additionally, they reported that, for a constant level of confinement, the rate of increase in ultimate capacity diminishes with increasing concrete strength. Both of these observations presage details quantified by later researchers.

2.4 Early FRP Specific Models

In the 1990's researchers began to develop stress-strain models which identified and explained the differences in behavior between steel and FRP confined concrete. Other issues were identified, but were not solved until after significantly more research was completed and enough data were available.

2.4.1 Nanni and Bradford (1995)

In a pioneering study, Nanni and Bradford (1995) evaluated Fardis and Khalili's (1982) and Saadatmanesh, et al.'s (1994) models. They describe how the transverse dilation of concrete causes the FRP to produce the confining force. In lieu of Poisson's Ratio, Nanni and Bradford use 'strain ratio' to describe the ratio of transverse to axial strain "since in the cracked states, the ratio is no longer a material property." The strain ratio of FRP confined concrete can be described by Equation (2.27).

$$\nu_c = \nu_{co}\left[1.0 + 1.3763\,\varepsilon_c/\varepsilon_{co} - 5.36\left(\varepsilon_c/\varepsilon_{co}\right)^2 + 8.586\left(\varepsilon_c/\varepsilon_{co}\right)^3\right] \tag{2.27}$$

The strain ratio of FRP confined concrete has a value of about 0.20 through 85% of f'_c, then 0.50 up to f'_c, and 1.2 or more above f'_c.

Nanni and Bradford opined that because of the low strain ratio of uncracked concrete, the presence of an FRP jacket does not significantly impact the behavior at stresses below f'_c and reported that, "The ultimate strain in the FRP jacket appears to be much larger than that measured in uniaxial tension." Both of these findings would later be disputed by other researchers who came to the opposite conclusions. Supporting the conclusions of Mansur, et al. (1995), the additional confining effect caused by friction between the load platens and the specimen is described. Finally, Nanni and Bradford did not propose a specific stress-strain model of their own.

2.4.2 Sammaan, Mirmiran, and Shahawy (1998)

Sammaan, Mirmiran, and Shahawy (1998) conducted research on 6"x12" cylinders confined by FRP tubes of 6, 10, and 14 plies. The model they developed was one of the first to recognize the principal difference between steel spiral and FRP confined concrete: while the confining stress provided by a steel spiral is constant once the spiral yields, the confining stress provided by FRP increases linearly, based on the stiffness of the FRP, until it ruptures. This lead to the development of a bi-linear model where the transition point is near the unconfined compressive strength of plain concrete and the second slope is a function of the stiffness of the jacket. This would prove to be the fundamental form of future models.

The proposed model, given by Equation (2.28), modifies Richard and Abbot's (1975) equation to account for the observed bilinear nature of FRP confined concrete behavior. The subsequent equations provide the values necessary to evaluate Equation (2.28).

$$f_c = \frac{(E_1 - E_2)\varepsilon_c}{\left[1 + \left(\frac{(E_1 - E_2)\varepsilon_c}{f_o}\right)^n\right]^{\frac{1}{n}}} + E_2\varepsilon_c \tag{2.28}$$

$$f_l = \frac{2 f_{frp} t}{d} \tag{2.29}$$

$$f_o = 0.872 f'_{co} + 0.371 f_l + 0.908 [ksi] \tag{2.30}$$

$$E_1 = 47.586\sqrt{1.000 f'_{co}}\,[ksi] \tag{2.31}$$

$$E_2 = 52.411 f'^{0.2}_{co} + 1.3456 \frac{E_{frp} t}{d} [ksi] \tag{2.32}$$

$$f'_{cc} = f'_{co} + 3.38 f_l^{0.7} [ksi] \tag{2.33}$$

The curve defined by these equations terminates at the ultimate strain given in Equation (2.34).

$$\varepsilon_{cc} = \frac{f'_{cc} - f_o}{E_2} \tag{2.34}$$

The shape parameter 'n' controls the curve shape in the transition region. A value of 1.5 is proposed, but the model is not very sensitive to this value.

This model can be extended to the radial direction where radial strain is related to axial concrete stress by Equation (2.35)

$$f_c = \frac{(E_{1r} - E_{2r})\varepsilon_r}{\left[1 + \left(\frac{(E_{1r} - E_{2r})\varepsilon_r}{f_{or}}\right)^{n_r}\right]^{\frac{1}{n_r}}} + E_{2r}\varepsilon_r \tag{2.35}$$

Equation (2.36), originally proposed by Ahmad (1981), provides the value for the 1st branch elastic modulus where υ is Poisson's ratio of concrete which has a commonly accepted value between 0.15 and 0.22.

$$E_{1r} = \frac{E_1}{\upsilon} \tag{2.36}$$

The next two parameters, E_{2r} and n_r, are a function of the ultimate dilation rate, μ_u, as originally proposed by Mirmiran and Shahawy (1997), and given in Equation (2.37).

$$\mu_u = -0.187 \ln\left(\frac{E_{frp}t}{f_c'r}\right) + 0.881 \tag{2.37}$$

$$E_{2r} = \frac{E_2}{\mu_u} \tag{2.38}$$

$$n_r = \frac{n_1}{\mu_u} \tag{2.39}$$

The radial reference plastic stress, f_{or}, is based on the compressive strength of plain concrete and the confining pressure and is found by Equation (2.40) while the ultimate radial strain is given by Equation (2.41).

$$f_{or} = 0.636 f'_{co} + 0.233 f_l + 0.661[ksi] \tag{2.40}$$

$$\varepsilon_{ru} = \frac{f'_{cc} - f_{or}}{E_{2r}} \tag{2.41}$$

2.4.3 Toutanji (1999) and Saffi, Toutanji, and Li (1999)

In 1999, Toutanji proposed a model based on FRP wrapped cylinders while Saffi, Toutanji, and Li suggested a similar model for concrete placed in and confined by FRP tubes. Both models represent stress-strain behavior with two curves and a defined transition point.

Using an expression first proposed by Sargin (1971) and subsequently adapted by Ahmad and Shah (1982) for use in steel spiral confined concrete, Toutanji developed an analytic model to predict the entire stress-strain curve of FRP confined concrete. In this model the first branch is similar in performance to plain concrete while the second is primarily controlled by the properties of the confining FRP.

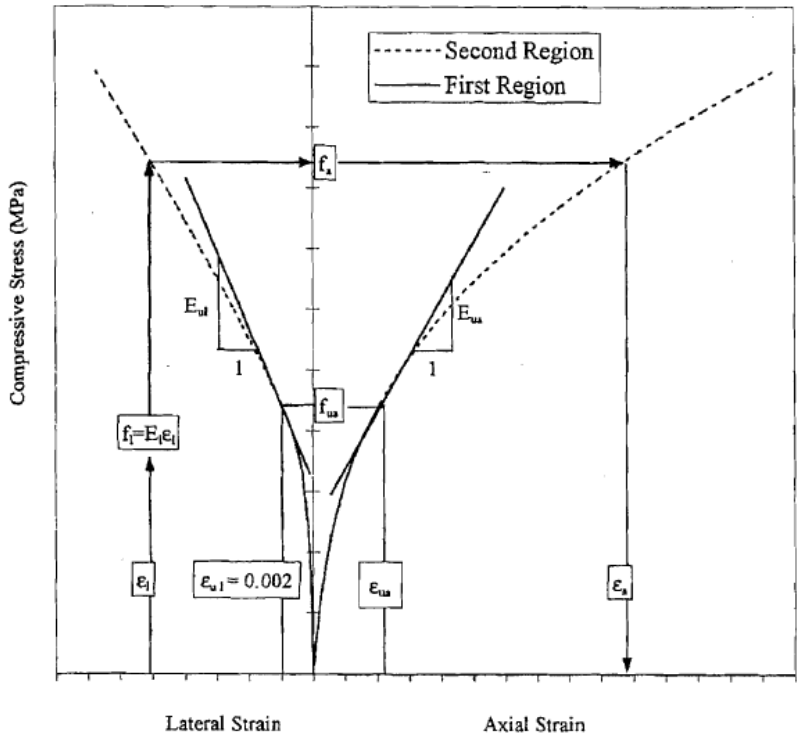

Figure 2-3 Analytical Stress-Strain Curves by Toutanji (1999)

Figure 2-3 shows the process for formulating the stress-strain curve using Toutanji's model. Calculations begin by developing the 2nd branch first. The transition between the first and the second branches is marked by a radial strain of 0.002. Above this strain, the confining stress is calculated by varying ε_r then finding f_l by Equation (2.42).

$$f_l = E_l \varepsilon_r \quad with \quad E_l = \frac{2E_{frp}t}{d} \tag{2.42}$$

Next, the corresponding axial concrete stress is found by Equation (2.43) and then, finally, a corresponding axial concrete strain by Equation (2.44) .

$$f_c = f'_{co}\left[1 + 3.5\left(\frac{f_l}{f'_{co}}\right)^{0.85}\right] \tag{2.43}$$

$$\varepsilon_c = \varepsilon_{co}\left[1 + (310.57\varepsilon_r + 1.90)\left(\frac{f_c}{f'_{co}} - 1\right)\right] \tag{2.44}$$

In the axial direction, the transition point, (ε_{ua}, f_{ua}) corresponding to the radial strain of 0.002 is given by Equations (2.45) and (2.46). Below this point, Equation (2.47) is employed to generate the stress strain curve.

$$\varepsilon_{ua} = \varepsilon_{co}\left[1 + 0.0448\left(\frac{E_l}{f'_c}\right)^{0.85}\right] \tag{2.45}$$

$$f_{ua} = f'_{co}\left[1 + 0.0178\left(\frac{E_l}{f'_{co}}\right)^{0.85}\right] \tag{2.46}$$

$$f_a = \frac{E_{ia}\varepsilon_a}{1 + \left(\frac{E_{ia}}{f_{ua}} - \frac{2}{\varepsilon_{ua}} + \frac{E_{ua}E_{ia}\varepsilon_{ua}}{f_{ua}^2}\right)\varepsilon_a + \left(\frac{1}{\varepsilon_{ua}^2} - \frac{E_{ua}E_{ia}}{f_{ua}^2}\right)\varepsilon_a^2} \tag{2.47}$$

with $E_{ia} = 10200\sqrt[3]{f'_c}$ and $E_{ua} = 0.3075\frac{f'_c}{\varepsilon_o}$ in MPa

Toutanji also reports reliable agreement between his model and the experimental results of Pitcher et al. (1996), Harmon et al. (1995), Miyauchi et al. (1997), and Nanni and Bradford

(1995). The model, however, overestimates axial stress in FRP encased (as opposed to wrapped) columns.

Saafi, Toutanji, and Li's model employs the same fundamental equation as Toutanji's, but has different calibration constants due to the difference in behavior between FRP wraps and FRP tubes. At the early stages of loading, the FRP tubes do not contribute to the stiffness of the FRP-concrete composite member since the Poisson's ratio of the concrete is lower than that of the tube. The first branch of the stress-strain curve, in both the axial and radial directions, is described by Equation (2.48) with the appropriate values of elastic modulus substituted in the expressions for A, B, and C. (note: The constants in this model are calibrated for SI units)

$$f_c = \frac{A\varepsilon}{1 + B\varepsilon + C\varepsilon^2} \tag{2.48}$$

with:

$$A = E_1$$

$$B = \frac{E_1}{f_c} - \frac{2}{\varepsilon_1} + \frac{E_2 E_1 \varepsilon_1}{f_c}$$

$$C = \frac{1}{\varepsilon_1^2} - \frac{E_2 E_1}{f_c{}^2}$$

$$E_{1a} = 10{,}200\left(f_c'\right)^{\frac{1}{3}}$$

$$E_{2a} = 0.272\frac{f_c'}{\varepsilon_{co}}$$

and

$$E_{1r} = \frac{E_{1a}}{\upsilon_o}$$

$$E_{2r} = 5\left(\frac{2t_{com}E_{com}}{df_c'}\right)^{0.16}$$

The concrete axial stress, f'$_c$, is calculated by assuming a strain, finding A, B, and C, and then calculating the stress. Equation (2.48) is valid until the transition point, defined by Equations (2.49) and (2.50), is reached.

$$f_{1c} = f_{co}'\left(1 + 0.0213\left(\frac{tE_{frp}}{df_{co}'}\right)^{0.84}\right) \tag{2.49}$$

$$\varepsilon_{1c} = \varepsilon_{co}\left(1 + 0.0783\left(\frac{tE_{frp}}{df'_{co}}\right)^{0.84}\right) \tag{2.50}$$

Calculation of the second branch begins with the assumption of a radial (lateral) strain and then the calculation of the confining pressure with Equation (2.51) which enables the calculation of axial stress by Equation (2.52) and then axial strain by Equation (2.53).

$$f_l = \frac{2t_{frp}E_{frp}\varepsilon_r}{d} \tag{2.51}$$

$$f(\varepsilon_r) = f'_{co}\left(1 + 2.2\left(\frac{f_l}{f'_{co}}\right)^{0.84}\right) \tag{2.52}$$

$$\varepsilon_c = \varepsilon_{co}\left(1 + (537\varepsilon_r + 2.6)\left(\frac{f(\varepsilon_l)}{f'_{co}} - 1\right)\right) \tag{2.53}$$

The model terminates with at the ultimate stress and strain defined by Equations (2.54) and (2.55), respectively.

$$f'_{cc} = f'_{co}\left(1 + 2.2\left(\frac{2tf_{frp}}{df'_{co}}\right)^{0.84}\right) \tag{2.54}$$

$$\varepsilon_{cc} = \varepsilon_{co}\left(1 + (537\varepsilon_{fpr} + 2.6)\left(\frac{f'_{cc}}{f'_{co}} - 1\right)\right) \tag{2.55}$$

When the results of these two studies are considered together, it must be noted that a model calibrated to predict the behavior of concrete confined with an FRP tube will not accurately predict the response of concrete confined by FRP wraps and vice versa. Though both are FRP, the behaviors are different enough as to require different calibration constants in the modeling equations.

2.4.4 Spolestra and Monti (1999)

Building on the work of Popovics' (1973) stress-strain model, Mander, Priestly, and Park's (1988) curves modeling the effect of confinement, and Pantazopoulou and Mills' (1995) damage model, Spolestra and Monti (1999) developed an analytic, iterative model suitable for either steel or FRP confined concrete and intended for use in a fiber type finite element model. The model is suitable for either type of confinement because it recognized that FRP, properly applied, provides an ever increasing confining pressure while a steel spiral provides a constant confining pressure upon yield.

The process constructs a stress-strain curve that crosses a series of Mander, Priestly, and Park curves that are each calculated for a constant confining stress which is based on a corresponding lateral strain. The iterative process requires seven equations and the following sequence.

1. Impose ε_c.
2. Set confining stress $f_l = f_{lp}$ from previous iteration.
3. Calculate $f'_{cc}(f_l)$ using Equation (2.56)
4. Calculate current stress $f_c(f'_{cc})$ from Equation (2.57) with Equation (2.58)
5. Update radial strain $\varepsilon_r(f'_c)$ from Equation (2.59)
6. Update confining stress f_l from Equation (2.60)
7. Is $f_l = f_{lp}$? If yes, go to 1 and impose next step. If no, go to 2.

$$\frac{f'_{cc}}{f'_{co}} = 2.254\sqrt{1+7.94\frac{f_l}{f'_{co}}} - 2\frac{f_l}{f'_{co}} - 1.254 \tag{2.56}$$

$$f'_c = \frac{f'_{cc}\cdot x \cdot r}{r-1+x^r} \tag{2.57}$$

$$x = \frac{\varepsilon_c}{\varepsilon_{cc}}$$

$$\varepsilon_{cc} = \varepsilon_{co}\left[1+5\left(\frac{f'_{cc}}{f'_{co}}-1\right)\right] \tag{2.58}$$

$$r = \frac{E_c}{E_c - E_{sec}}$$

$$\varepsilon_r(\varepsilon_c, f_l) = \frac{E_c\varepsilon_c - f'_c(\varepsilon_c, f_l)}{2\beta f'_c(\varepsilon_c, f_l)} \tag{2.59}$$

$$f_l = 2\frac{t}{d}E_{frp}\varepsilon_r \tag{2.60}$$

Evaluations performed by Spolestra and Monti indicate that the procedure converges rapidly on an acceptably accurate solution. The model compares favorably with the experimental result of Picher et al.(1996) and Kawashima et al. (1997) but shows some discrepancy with the results of Mirmiran and Shahawy (1997).

Based on this model, Spolestra and Monti also developed exact and approximate expressions for the ultimate stress and strain of FRP confined specimens. Determination of the exact expression for the ultimate compressive stress and strain begins by calculating the ultimate confining pressure by Equation (2.61)

$$f_{lu} = 2\frac{t_j}{d_j}f_{ju} \tag{2.61}$$

Next, the Mander stress strain curve parameters corresponding to the ultimate confining pressure are calculated by Equations (2.62) and (2.63).

$$f'_{cc} = f'_{co}\left(2.254\sqrt{1+7.94\frac{f_{lu}}{f'_{co}}} - 2\frac{f_{lu}}{f'_{co}} - 1.254\right) \tag{2.62}$$

$$\varepsilon_{cc} = \varepsilon_{co}\left[1+5\left(\frac{f'_{cc}}{f'_{co}}-1\right)\right] \tag{2.63}$$

Then the secant modulus of elasticity is determined by Equation (2.64) which allows the finding of the ultimate compressive stress and strain by Equations (2.65) and (2.66).

$$E_{\sec u} = \frac{E_{co}}{1 + 2\beta f_{frp} / E_{frp}} \qquad with \qquad \beta = \frac{E_c}{|f'_{co}|} - \frac{1}{|\varepsilon_{co}|} \tag{2.64}$$

$$\varepsilon_{cu} = \varepsilon_{cc}\left(\frac{E_{\sec}\left(E_c - E_{\sec u}\right)}{E_{\sec u}\left(E_c - E_{\sec u}\right)}\right)^{\frac{1-E_{\sec}}{E_c}} \tag{2.65}$$

$$f'_{cu} = E_{\sec u}\varepsilon_{cu} \qquad where \qquad E_{\sec} = f'_{cc} / \varepsilon_{ee} \tag{2.66}$$

Alternatively, an approximate expression for the ultimate stress and strain may be found by using basic material properties to determine the three independent parameters of Equation (2.67) which are then substituted into Equations (2.68) and(2.69) to determine f'$_{cu}$ and ε_{cu}.

$$\bar{f}_{lu} = \frac{f_{lu}}{f'_{co}}; \quad \varepsilon_{frp}; \quad \bar{E} = \frac{E_{co}}{f'_{co}} \tag{2.67}$$

$$\varepsilon_{cu} = \varepsilon_{co}\left(0.2 + 1.25\bar{E}_c\varepsilon_{frp}\sqrt{f_{lu}}\right) \tag{2.68}$$

$$f'_{cu} = f'_{co}\left(0.2 + 3\sqrt{f_{lu}}\right) \tag{2.69}$$

One of Spolestra and Monti's most significant contributions was the quantification of effective confinement. An FRP confined specimen is said to be effectively or sufficiently confined if the second branch of the stress-strain curve has a positive slope, in other words, the stress always increases with increasing strain. If the second branch has a descending slope, the specimen is said to be insufficiently confined. For a specimen to be sufficiently confined, the ratio of confining stress to unconfined compressive strength of the plain concrete must exceed 0.07 as shown in Equation (2.70).

$$\frac{f_{lu}}{f'_{co}} \geq 0.07 \tag{2.70}$$

This relationship quantified the observation by Saadatmanesh et al. (1994) that for a given level of confinement, incremental increases in compressive strength produced smaller and smaller improvements in ultimate confined performance. Prior to this time, levels of confinement were often simply reported as 1, 2, or 3 wraps. Subsequent to this, a confinement effectiveness ratio could be reported in a standardized manner.

2.5 Advanced FRP Confinement Models

At the start of the 21st Century, the state of the art of FRP confined concrete models was advancing rapidly. The results of a large number of experiments by a variety of authors under many different conditions had been published. This allowed researchers to validate models for many different conditions. Additionally, the general aspects of FRP confined concrete behavior had been well established and researchers were able to focus on nuances and specific parameters to fine tune models. Teng and Lam (2004) describe how models adopt either an analysis oriented or design oriented approach. Analysis oriented models required an iterative procedure and are mainly suitable for incorporation into finite element or other computer models while design oriented models provide a closed form equation to generate a stress strain curve. Selected models are introduced below. The models of Moran and Pantelides (2002) and Karabinis and Rousakis (2002) were selected to show the level of complexity and detail in current analytical models. Lam and Teng (2003) was selected as a simple, accurate, and broadly based design oriented model while Berthet, et al.'s (2004 to 2006) model demonstrates research on a comprehensive model of FRP confined concrete behavior.

2.5.1 Moran and Pantelides, (2002)

Moran and Pantelides (2002) developed an analytical model that combines aspects of both the Richard and Abbott (1975) and Popovics (1973) models. The model is applicable to both wrapped FRP jackets and bonded FRP tubes. The model combines two aspects of FRP confined concrete behavior: strain-softening parameters to account for the cracking of the concrete core with subsequent loss of strength, and strain-hardening parameters which account for the increase in strength due to the confinement provided by the FRP. The authors validated their model by comparing it to a variety of tests by other researchers. Good agreement between the model and the experimental results of Mirmiran (1997), Wu and Xiao (2000), Picher et al. (1996), and Rochette and Labossiere (2000) was demonstrated. The model is complex requiring

a substantial number of equations and a flow chart to explain the calculation of the strain hardening parameters and strain softening coefficients. The model is suitable for use in either spreadsheet or other computer language programs for moment-curvature analysis or for finite element analysis of FRP confined concrete members.

2.5.2 Karabinis and Rousakis, (2002)

Karabinis and Rousakis (2002) conducted experimental studies on 22 cylindrical specimens with low confinement ratios (1, 2, or 3 wraps of FRP). Specimens with only 1 wrap proved to be insufficiently confined using Spolestra and Monti's (1999) criteria and showed a descending second branch in the stress-strain curve. Specimens with 2 wraps were sufficiently confined, but barely. Based on their experiments, Karabinis and Rousakis employed a Drucker-Prager type constitutive model requiring 14 material parameters (2 elastic, 3 failure-yield, 6 hardening, and 3 dilation) to develop an analytic model which showed good agreement with their results and those of other researchers. Their research further demonstrated the need to achieve a sufficient level of confinement to realize the increase in strength and ductility that FRP confinement provides.

Of the 22 specimens tested, premature failure at the overlap was reported for two of the specimens. These specimens achieved a comparable ultimate strength to those that did not fail prematurely, but failed at approximately $0.6\varepsilon_{cc}$ when compared to fully mature failure. Additionally, one of these specimens exhibited second region behavior that was substantially different from the typical bi-linear stress strain curve. This behavior is similar to some of the experimental results presented in this paper.

2.5.3 Lam and Teng, (2003)

Lam and Teng (2003), using a database of 76 specimens from a variety of researchers, developed a design type model which addresses behavioral aspects that were not included in most previous models. First, they confirm Spoletra and Monti's (1999) requirement for sufficient confinement. Second, they advanced the understanding of the first branch of the bi-linear stress-strain curve. Many previous models based the equation for this curve on one of the expressions for plain concrete and stated that the presence of FRP did not affect behavior in this region. Lam and Teng demonstrate that the FRP confinement becomes effective once the concrete behavior becomes non-linear and that the first branch model must include the

contribution of the FRP. Third, many previous researchers reported that models failed to predict the ultimate strain accurately and that the FRP jackets ruptured at a lower strain than expected. Lam and Teng indicate that the rupture strain of the FRP jacket, when employed on a circular column, should be taken as 58.6% of the tensile coupon rupture strain.

Lam and Teng's model uses two closed form equations to generate the stress-strain curve. First, the actual maximum confining stress is calculated by Equation (2.71) which includes a correction for the aforementioned FRP rupture strain.

$$f_{l,act} = \frac{2E_{frp}t\varepsilon_{h,rup}}{d} \qquad with \qquad \varepsilon_{h,rup} = 0.586\varepsilon_{frp} \tag{2.71}$$

Next, the ultimate strain and stress can be found by Equations (2.72) and (2.73).

$$\frac{\varepsilon_{cu}}{\varepsilon_{co}} = 1.75 + 5.53\left(\frac{f_{l,act}}{f'_{co}}\right)\left(\frac{\varepsilon_{frp}}{\varepsilon_{co}}\right)^{0.45} \tag{2.72}$$

$$\frac{f'_{cc}}{f'_{co}} = 1 + 3.3\frac{f_{l,a}}{f'_{co}} \tag{2.73}$$

This allows the calculation of the entire stress-strain curve using Equation (2.74) for strains between zero and the branch transition strain of ε_t and Equation (2.75) for strains above ε_t.

$$f_c = E_c\varepsilon_c - \frac{(E_c - E_2)^2}{4f_o}\varepsilon_c^2 \tag{2.74}$$

$$f_c = f_0 + E_2\varepsilon_c \tag{2.75}$$

The transition strain is calculated based on the transition reference stress which is taken as the unconfined compressive strength of concrete as shown in Equation (2.76) and the elastic modulus, E_2, of the second branch of the stress strain curve as found in Equation (2.77). When these parameters are known, the transition strain, ε_t, can be found by Equation (2.78)

$$f_o = f'_{co} \tag{2.76}$$

$$E_2 = \frac{f'_{cc} - f_o}{\varepsilon_{cu}} \tag{2.77}$$

$$\varepsilon_t = \frac{2 f_o}{\left(E_c - E_2\right)} \tag{2.78}$$

Lam and Teng's model represents the current state of the art in design oriented models. Based on a wide variety of tests from various researchers, it accurately models FRP confined concrete behavior. Its closed form equations and use of readily available material parameters make it very user friendly an applicable to programming in a spreadsheet. Its principal drawback is that the reference database only includes specimens that failed in FRP rupture. Other failure modes are excluded from the database and the results comparison.

2.5.4 Berthet, et al., (2004 to 2006)

Berthet, et al. published three papers between 2004 and 2006 detailing a comprehensive study of FRP confined concrete behavior. The first (2004) described the experimental setup and testing parameters, the second (2006a) presented a stress-strain model, and the third (2006b) described the results of short and long term creep tests. The proposed stress-strain model addressed the need for sufficient confinement and included the reduction of FRP strain capacity when used as a column wrap, but, contrary to Lam and Teng's (2003) model, based the first branch behavior on plain concrete properties only.

First, the ultimate strain and stress are predicted by Equations (2.79) and (2.80)

$$\varepsilon_{cu} = \varepsilon_{co} + \sqrt{2} \cdot \left(\frac{E_l}{f'^2_{co}} \right)^{2/3} \cdot \left(\varepsilon_{frp} - \nu_c \cdot \varepsilon_{co} \right) \tag{2.79}$$

$$f'_{cc} = f'_{co} + k_1 \cdot \frac{t}{r} \cdot E_{frp} \cdot \varepsilon_{frp} = f'_{co} + k_1 \cdot E_l \cdot \varepsilon_{frp} \tag{2.80}$$

where

$$k_1 = 3.45 \quad for\ 20 \le f'_{co} \le 50\ MPa$$

$$k_1 = \frac{9.5}{\left(f'_{co}\right)^{1/4}} \quad for\ 50 \le f'_{co} \le 200\ MPa$$

and the confinement modulus, E_l, is defined by Equation (2.81). (NOTE: analysis of this model by Sutherland (2007) found an error in this procedure to predict the ultimate stress. Attempts to contact the authors to resolve the discrepancy were not successful.)

$$E_l = \frac{t}{r} \cdot E_{frp} \tag{2.81}$$

The second branch begins at a reference stress and strain f'_{cp} and ε_{ap} calculated using Equations (2.83) and (2.84). Then the second branch is modeled by Equation (2.82).

$$f'_c = f'_{cp} + \theta_r \left[(\nu_c - \gamma)\varepsilon_{co} - \varepsilon_{rp} \right] + \theta_r \cdot \gamma \cdot \varepsilon_c \quad for\ \varepsilon_c \geq \varepsilon_{ap} \tag{2.82}$$

where $\theta_r = 2.73 \cdot E_l - 163$

$$f'_{cp} = f'_{cc} - \theta_r \cdot (\varepsilon_{fu} - \varepsilon_{rp}) \tag{2.83}$$

$$\varepsilon_{ap} = \varepsilon_{co} + \frac{\varepsilon_{rp} - \varepsilon_{ro}}{\gamma} \tag{2.84}$$

The reference strain, ε_{rp}, is taken as 0.002, ε_{ro} is radial strain corresponding to ε_{co} calculated using Poisson's Ratio, and ε_{co} is taken as 0.002 for the ultimate axial strain of plain concrete. The parameter, γ, is calculated by Equation (2.85)

$$\gamma = \frac{1}{\sqrt{2}} \left(\frac{E_l}{f'^2_{co}} \right)^{-2/3} \tag{2.85}$$

Finally, based on a model originally proposed by Ahmad and Shah (1982), the first zone is modeled by Equation (2.90)

$$f'_c = \frac{A\varepsilon}{1 + B\varepsilon + C\varepsilon^2} \tag{2.86}$$

where A, B, and C are determined by boundary conditions and are given by Equations (2.87), (2.88), and (2.89) and E^*_a is given by Equation (2.90).

$$A = E_a^* \tag{2.87}$$

$$B = \frac{E_a^*}{f'_{cp}} - \frac{2}{\varepsilon_{ap}} + \theta_r \frac{E_a^* \varepsilon_{ap}}{f'^2_{cp}} \tag{2.88}$$

$$C = \frac{1}{\varepsilon_{ap}^2} - \theta_r \frac{E_a^*}{f'^2_{cp}} \tag{2.89}$$

$$E_a^* = E_c \frac{E_c + (1 - \nu_c) E_l}{E_c + (1 - \nu_c - 2\nu_c^2) E_l} \tag{2.90}$$

The third paper (2006b) sought to extend the results of the above model to account for the effects of concrete creep. The main parameters investigated were level of confinement (1, 2 or 3 layers) and level of sustained load. In the short term creep tests, the sustained load always exceeded f'_c and either 85 or 90% of f'_{cc}. In the long term tests, the sustained load exceeded 80% of f'_c and 40% of f'_{cc}, all depending on confinement configurations. The goal of the short term tests was to fail the specimens in three days to determine an appropriate load level for the long term tests so that the specimens would not fail in creep under the sustained load.

Within the first region, Berthet, et al. state that, "The creep of composite is neglected because of the low stress in the carbon fibers and because the anchorage length of the FRP wrap is enough to neglect any sliding in the resin." Berthet's modified behavioral model is based on the Eurocode 2 (EC2) (CEB-FIP 1990) double power model which is valid for linear creep at a load that does not exceed 60% of the maximum strength. Equations (2.91) and (2.92) show that the creep strains are a function of age of load application, t_0, duration of load, t, and level of sustained load, σ_0, along with the EC2 creep function $\varphi(t, t_0)$.

$$\varepsilon_a(t, t_0, \sigma_0) = \sigma_0 \left(\frac{\left(\frac{r}{t}\right) \bullet \left(\frac{\upsilon_{frp}}{E_{frp}} \bullet \frac{\upsilon_c}{E_c(t, t_0)} \right)}{\left(\frac{r}{E_{frp} t} \right) + \frac{1}{E_c(t, t_0)} - \frac{\upsilon_c}{E_c(t, t_0)}} \right) \tag{2.91}$$

$$E_c(t, t_0) = \frac{1}{E_{c0}(1 + \varphi(t, t_0))} \tag{2.92}$$

Within the second region, creep strains can be calculated by Equation (2.93) using the parameters determined by the subsequent equations with χ=0.2 and δ=0.353.

$$\varepsilon_a(t,t_0,\sigma_0)=\frac{\sigma_0(t)-f'_{cc}}{\theta_r\cdot\gamma}+\frac{\left[\varepsilon_{frp}-(\upsilon_c-\gamma\cdot\varepsilon_{a0})\right]}{\gamma}+\psi(t,t_0) \tag{2.93}$$

$$\psi(t,t_0)=\alpha\left(\frac{1+\beta\cdot t^{\delta}}{1+\chi\cdot t^{\delta}}\right) \tag{2.94}$$

$$\beta=\left(0.379\frac{E_l}{\sigma_0}-10.6\right) \tag{2.95}$$

$$\begin{aligned}\alpha&=0.0019-0.0009\left(\frac{E_l}{\sigma_0^2}\right) \quad if \quad \frac{f'_c}{\sigma_0}\le 1\\ \alpha&=0.0129-0.008\left(\frac{E_l}{\sigma_0^2}\right) \quad if \quad \frac{f'_c}{\sigma_0}\ge 1\end{aligned} \tag{2.96}$$

Both the short and long term experiments conducted by Berthet et al. showed good agreement with the equations presented. They caution that the data set was small and that the creep functions should be compared to other tests for further validation. The specimens were not, however, loaded to failure at the conclusion of the creep testing so the effects of creep on the post sustained load behavior were not determined.

2.6 Codes and Standards

Two codes and one standard are included in this section. ACI Codes 209-R and 440.2R give the current industry standards for the prediction of creep and the performance of FRP retrofitted specimens. ASTMC469-02 provides the standard for the strength testing of plain concrete cylinders.

2.6.1 ACI209-R, Prediction of Creep Shrinkages and Temperature Effects in Concrete Structures (1997)

ACI209 was released in 1992 and then re-approved in 1997. It provides procedures for predicting creep, shrinkage, and temperature effects in structures. Creep is defined as the "time-dependent increase of strain in hardened concrete subjected to sustained stress" while shrinkage

is the decrease of concrete volume over time due to changes in the moisture content. The value of creep strain can be found by measuring the total strain then subtracting the initial instantaneous strain (usually considered elastic), shrinkage strain, and thermal strain, if any. One method of calculating creep strain is to multiply the initial instantaneous strain, ε_i, by the creep coefficient, ν_t, as calculated by Equation (2.97) where t is time in days after loading . This equation is valid for moist cured concrete loaded at 7 days of age or steam cured concrete loaded at 1-3 days of age. The factor γ_c corrects for different curing, loading, and construction conditions.

$$\upsilon_t = \frac{t^{0.60}}{10 + t^{0.60}} \upsilon_u \quad \textit{where} \quad \upsilon_u = 2.35\gamma_c \tag{2.97}$$

For loading ages later than 7 days for moist cured concrete and if other correction factors are not required (as is the case for this report), γ_c can be calculated using Equation (2.98) where t_{la} is the age of the concrete at first application of load.

$$\gamma_c = \gamma_{la} = 1.25(t_{la})^{-0.118} \tag{2.98}$$

Other methods for predicting creep and shrinkage are mentioned and references given that include the double power law used by Berthet et al, (2006b) as discussed above.

2.6.2 ACI440.2R-02, Design and Construction of Externally Bonded Systems for Strengthening Concrete Structures (2002)

ACI440.2R (2002) describes FRP materials, provides recommended construction requirements, and gives design recommendations for both flexural and axial strengthening. The recommendations for axial strengthening are based primarily on the work of Nanni and Bradford (1995), Spolestra and Monti (1999), and Toutanji (1999). This code provides for the calculation of ultimate compressive strength using Equation (2.99) where the maximum confining stress is provide by Equation (2.100). Once the ultimate compressive strength is known, the design strength of a retrofitted member can be found using Equation (2.101a) for non-prestressed members with spiral reinforcement or (2.101b) for non-prestressed members with tied reinforcement. ψ_f is and additional FRP strength reduction factor and is recommended as 0.95

for this application. The maximum usable compressive strain for circular members can be calculated using Equation(2.102).

$$f'_{cc} = f'_c\left[2.25\sqrt{1+7.9\frac{f_l}{f'_c}}-2\frac{f_l}{f'_c}-1.25\right] \tag{2.99}$$

$$f_l = \frac{2t_{frp}\varepsilon_{frp}E_{frp}}{D} \tag{2.100}$$

$$\phi P_n = 0.85\phi\left[0.85\psi_f f'_{cc}\left(A_g - A_{st}\right)+ f_y A_{st}\right] \tag{2.101a}$$

$$\phi P_n = 0.80\phi\left[0.85\psi_f f'_{cc}\left(A_g - A_{st}\right)+ f_y A_{st}\right] \tag{2.101b}$$

$$\varepsilon_{cc} = \frac{1.71\left(5f'_{cc} - 4f'_c\right)}{E_c} \tag{2.102}$$

2.6.3 ASTM C469-02 Standard Test Method for Static Modulus of Elasticity and Poisson's Ratio of Concrete in Compression

This ASTM publication contains the standards for determining Young's Modulus and Poisson's Ratio for plain concrete using standard test cylinders. For hydraulic test machines a constant load rate of 35 ± 5 psi per second in the elastic region is specified while a travel rate of 0.05 inches per minute is given for screw-type testing machines. The modulus of elasticity is to be calculated using points corresponding to 50με and the stress at 40% of the ultimate load.

2.7 Related Papers

This section contains papers that address various aspects of the long term behavior of concrete under varying conditions. Song, et al. (1995) examined changes in plain concrete properties over a one year time frame. Naguib and Mirmiran (2003) studied creep of FRP wrapped specimens. Han, Tao, and Liu (2004) examined the sustained load and post-sustained load behavior of concrete filled hollow structural steel sections. While they deal with a variety of topics, each paper provides a different perspective on the time dependent behavior of concrete. Lessons learned from these papers were used to set the time and sustained load parameters in the current research. See Table 3-1.

2.7.1 Song, et al. (1995)

As part of the quality control procedures for the Wolsung-2 nuclear power plant in South Korea, Song et al. (1995) carried out tests of creep, modulus of elasticity, and Poisson's ratio to determine the long term response of plain concrete. All tests were conducted according to the appropriate ASTM or DIN standard. Tests were conducted to enable the verification of the projected pre-stress losses at this critical facility.

Compressive strength tests were conducted at 7, 28, 90, 180, and 365 days after casting. Concrete ultimate strength was found to increase with time for the first 90 days and thereafter plateau. The concrete strength at 90 days and beyond was 38% greater than the strength at 28 days.

Modulus of elasticity and Poisson's Ratio tests were conducted at the same time intervals as compressive strength tests. The value of the elastic modulus tends to increase over time with the rate of increase being reasonably constant. On the other hand, the long term value of Poisson's Ratio remains relatively constant and slightly lower than the 28 day value.

The specimen sets tested for creep were loaded after 7, 28, 90, 180, and 365 days of moist curing and then held under a sustained load for one year. The sustained load was 35% of the ultimate compressive strength as determined at the time of loading. Drying shrinkage was shown to stabilize after about 90 days. After 1 year, the total deformation of specimens loaded at 7, 28, and 90 days was approximately the same, although the path was slightly different. The specimens loaded at 180 and 365 days showed similar total deformation but less that that of the 7, 28, and 90 day groups. No test specimens were reloaded to failure after being subjected to creep loading.

2.7.2 Naguib and Mirmiran (2003) based on Naguib (2001)

Based on the Ph.D. research of Naguib (2001), Naguib and Mirmiran (2003) reported the results of creep tests conducted on Concrete Filled FRP Tubes (CFFT) and Fiber Wrapped Concrete Columns (FWCC) to determine their time dependent behavior under sustained axial loads. Analytical issues of concern included:

1. The triaxial state of stress resulting from lateral confinement is expected to reduce creep.

2. The FRP in a FWCC creeps in the hoop direction while the FRP in a CFFT creeps in both directions.
3. Most retrofitted columns have already experienced creep strains prior to wrapping so a discrepancy may exist between real world and laboratory conditions.

To address these issues, Naguib and Mirmiran developed a creep model for both CFFT and FWCC that, "utilized the double power law creep function in the framework of rate of flow method for concrete, and the power law creep function for FRP." The model is applied in the following steps. Only FWCC are discussed as CFFTs are not pertinent to this paper.

1. In a FWCC, the concrete carries the entire axial load. Based on this load, the short-term (static) axial concrete stress is found at time t_0 according to Equation (2.103)

$$f_{ca} = \frac{P_c}{A_c} \tag{2.103}$$

Then, the corresponding axial and radial strain, ε_{ca} and ε_{cr}, are calculated according to the model of Samaan et al. (1998) as outlined in Chapter 2.4.2. Let the hoop strain in the jacket, ε_{frp}, equal the concrete radial strain, ε_{cr}, and find the hoop stress in the FRP by Equation (2.104).

$$f_{fh} = E_{frp}\varepsilon_{cr} \tag{2.104}$$

Calculate the effective creep Poisson's ratio, ε_{epr}, by dividing ε_{cr} by ε_{ca} and record for later use.

2. Increment the time step by Δt.

3. Calculate the uniaxial creep strain in the axial direction, $\varepsilon_{ca\text{-}uniaxial}$, using the rate of flow method (RFM) and double power law function based on current level of applied load and duration of time step

4. Apply Equation (2.105) to calculate the axial creep strain in the FWCC.

$$\varepsilon_{ca} = \varepsilon_{ca-uniaxial} - 2\upsilon_c J(t,t_0) f_l \tag{2.105}$$

5. Calculate radial creep in the FWCC by Equation (2.106) where υ_{ERP} is the effective creep Poisson's Ratio from step 1.

$$\varepsilon_{cr} = \upsilon_{ERP}\varepsilon_{ca} \tag{2.106}$$

6. Using the hoop stress in the jacket found in Equation (2.104) and Findley's (1960) power law of FRP creep as in Equation (2.107), find the lateral creep strain in the FRP, ε_{jh}.

$$\varepsilon = \varepsilon'_o + \varepsilon'_t t^n \tag{2.107}$$

where

ε=total elastic plus time dependent strain

ε'_o = stress-dependent and time-independent elastic strain

ε'_t = stress-dependent and time-independent coefficient

n = dimensionless material constant independent of stress magnitude

t = time after loading in hours

7. Compare ε_{cr} and ε_{jh}. If the difference is out of a pre-set tolerance, adjust ε_{jh} and calculate a new confining pressure, f_l, and repeat 4 through 7.

8. Iterate until the desired time is achieved or the FRP shell ruptures as predicted by Samaan, et al. (1998)

This model was verified using glass fiber wrapped specimens subjected to sustained loads of 15% and 30% of f'_c for 90 and 150 days. As can be seen in Figure 2-4, the FWCC specimens reached about70% of their 90 day behavior in 30 days. Additionally, the model described above accurately predicts the time based creep behavior of the FWCC specimens.

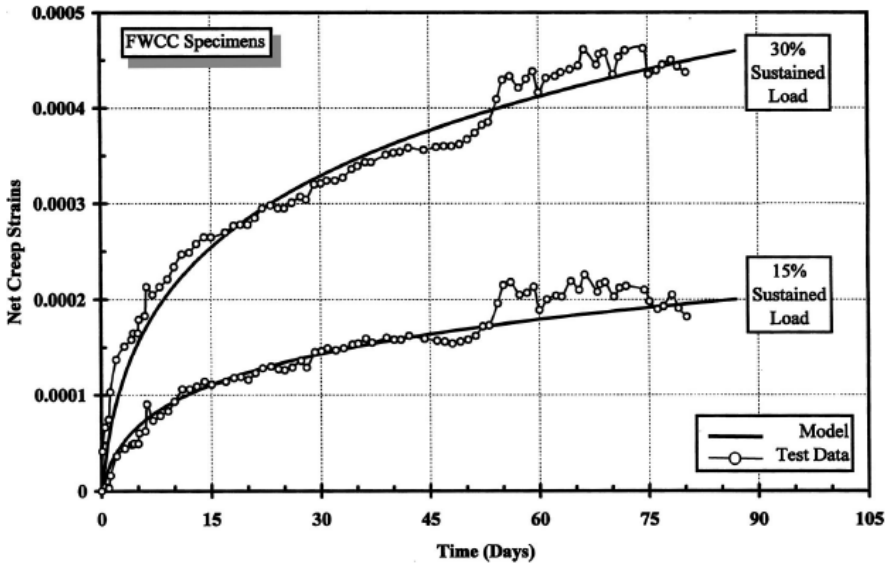

Figure 2-4 Creep Strains of FWCC Specimens by Naguib and Mirmiran (2003)
(With permission from ASCE)

When Naguib unloaded the specimens in Figure 2-4, he collected data on the creep recovery strains for three weeks. Then both specimens were tested to determine reserve capacity strength. The results are shown in Figure 2-5. The failure patterns and ultimate strengths observed in the post-sustained load tests were the same as those in the virgin test, but the transition region between the first and second branches of the stress-strain curve showed variations in curvature and transition points. The change in transition points also applied to the calculation of Poisson's Ratio as load increased. Naguib (2001) suggested that the change in transition points "may be attributed to the internal compaction of the concrete particles" due to the long term sustained loads. Additionally, the ultimate strain for specimen FWCC40 was about 70% of the ultimate strain value of the virgin curve. This is similar to the behavior observed by Karabinis and Rousakis (2002) and discussed in Chapter 2.5.2 and selected results presented in this paper. Naguib and Mirmiran did not give a definitive explanation for this behavioral difference. This analysis cannot be said to be life cycle modeling as not structure is unloaded for three weeks prior to ultimate loading. While this technique may provide insight into material behavior, it is not consistent with real world conditions.

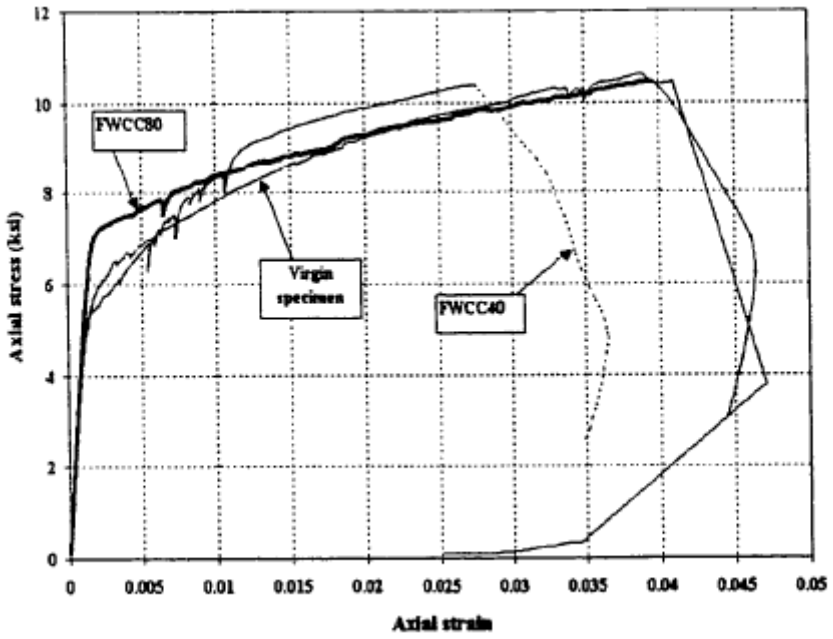

Figure 2-5 Virgin and Reserve Capacity Comparisons by Naguib (2001)

2.7.3 Han, Tao, and Liu, (2004)

Han, Tao, and Liu (2004) report that over a 50 year history of studies on the behavior of concrete filled hollow structural sections (HSS) little attention has been given to the effects of sustained load on member behavior. To remedy this shortcoming, they evaluated the effects of 120 day sustained loads on concrete filled HSS and endeavored to predict behavior using the ACE 209R-92 model. The sustained load was 62% of the predicted ultimate load and was applied using tension rods. Under the effects of a sustained load within this system, axial strain in the test specimens achieved 80-90% of its maximum value in 30 days and tended to stabilize in about 100 days as seen in Figure 2-6.

Han, et al. included the effects of a sustained stress, $\sigma_{\tau 0}$, applied at τ_0, by multiplying the short term strain in a standard stress-strain curve by the creep parameter $\{1+\varphi(t, \tau_0)\}$. For any time $(t - \tau_0)$, Figure 2-7 shows the modified stress strain curve resulting from this process. It is reported that this procedure is expected to be valid for sustained loads between 20% and 60% of the ultimate load. This procedure is then used to predict the ultimate behavior of four experimental specimens. Table 2-1 shows these results. It can be seen that the ultimate strength of a specimen subjected to a sustained load typically equals or exceeds that of a specimen without a sustained load. These results are for test specimens with a very low slenderness ratio.

Additional data show that as slenderness increases, the presence of a sustained load can cause a loss of up to 20% of the ultimate section capacity.

Additionally, Han, et al. suggest a Strength Index (SI) formula that includes the effects of slenderness, reinforcement ratio, and eccentricity for the prediction of the ultimate load of a composite column that has been subjected to a sustained load. It is interesting to note that the level of sustained load is not a parameter. The formula, however, is only valid for sustained loads between 20 and 60% of the ultimate load.

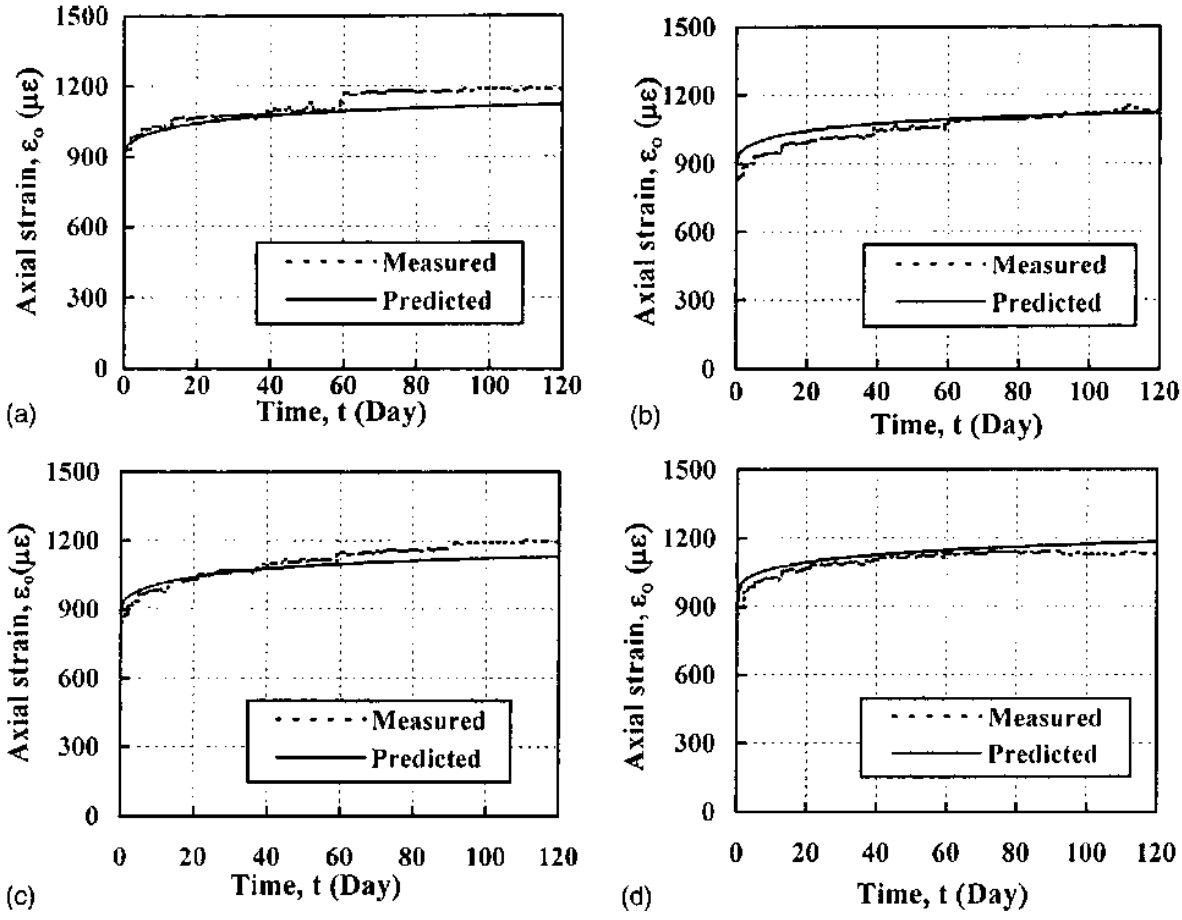

Figure 2-6 Time History of Axial Strain by Han, et al. (2004) (With permission from ASCE)

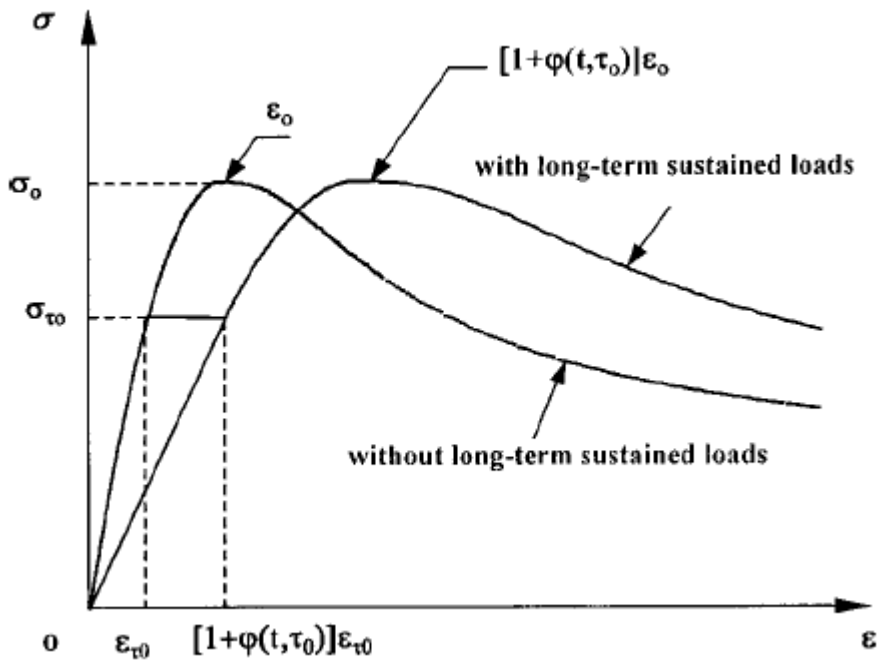

Figure 2-7 Stress-Strain Diagram Modified due to Sustained Load from Han, et al. (2004) (With permission from ASCE)

Specimen	Sustained Load (kN)	Duration (day)	Ultimate Load (kN)	Predicted Load (kN)
S-1	none	---	802	734
S-1-L-1	360	120	800	716
S-1-L-2	360	120	853	716
S-2	none	---	1054	1044
S-2-L-1	470	120	1088	993
S-2-L-2	470	120	1144	993

Table 2-1 Han, et al. (2004) Test Results

Han, et al.'s research investigates similar behavior to that contained in this report. The methodology is similar and useful parallels exist. First, a sustained load applied for 40 days will produce 80 to 90% of the long term deformation. Second, a creep function may be used to modify a stress-strain curve to account for the effects of sustained load on ultimate, post-sustained load behavior. Finally, a Strength Index (SI) may be used to further quantify the relationship of laboratory loading conditions to actual service loading conditions. The principal difference between the study of Han, et al. and this study is that while steel as a confining mechanism does not creep, FRP does.

2.8 Recent Publications

Until recently, the development of models for FRP confined concrete has focused on basic material parameters with only limited attention given to aspects of behavior under typical in-service conditions. Recently, in addition to Berthet et al. (2006b) reported in Section 2.5.4, Maalej, Tangongsval, and Paramasivam, (2003) and Shan, Xiao, and Gou, (2006), have raised questions about how FRP confined concrete behaves under sustained service loading. All indicate that sustained loading does have an effect on the behavior of FRP confined concrete, but that this behavior has not been isolated, tested, modeled, or understood.

2.8.1 Maalej, Tangongsval, and Paramasivam, (2003)

Recognizing that the effects of sustained loading on concrete column retrofit had not been explored, Maalej, et al. (2003) undertook an investigation to predict the ultimate load and the complete load-displacement response of wall-like reinforced concrete columns strengthened with FRP. A wall-like column is a rectangular column with a high width to depth aspect ratio.

The behavior of wall-like columns is substantially different from circular ones. Most significantly, the FRP confinement is much less effective in a rectangular column which results in a different bi-linear response. Maalej, et al. modeled the first branch as a parabola using confined concrete model proposed by Saatcioglu and Razvi, (1992) because it allows for the superposition of the effects of reinforcing steel and externally applied FRP. The second branch descends in a wall-like column and is modeled as a straight line between the peak of the Saatcioglu and Razvi curve and the failure point defined by the buckling of the longitudinal reinforcing rods. These equations are not reproduced here because of the substantial difference between the behavior of rectangular and circular columns. However, Maalej, et al.'s method of accounting for sustained loads merits inclusion.

When accounting for the effects of sustained loads, the axial strains, ε_c, in the proposed equations are reduced by the strains caused by sustained loads so that all ε_c terms are replaced by $(\varepsilon_c - \varepsilon_{sustained})$. Additionally, the loss in confining pressure due to the absence of FRP during the sustained load phase results in modifications to the expressions for the contribution of both core and cover concrete to the ultimate strength of the section. Although the proposed models show good agreement with a limited number of tests, Maalej, et al. clearly recognize the importance of the sustained load effect in their first conclusion:

The effect of sustained loading on the strengthening efficiency should be accounted for in the designing of column strengthening schemes. More experimental studies are however required to fully correlate the strengthening ratio to various levels of sustained loading.

2.8.2 Shan, Xiao, and Gou, (2006)

Many structures in California, particularly bridges, have been retrofitted with various forms of FRP to improve seismic performance. The principal philosophy employed is that an FRP retrofit should allow the structure to survive one extreme seismic event. This philosophy, however, raises additional questions in regards to non-critical seismic events and routine service loading including:

1. What levels of sustained stress can be safely induced in the FRP jacket?
2. What are the criteria and duration of sustained load that structure can handle without a creep failure of FRP jacket?
3. How would retrofitted columns damaged in one earthquake perform in the next earthquake?
4. What is the economic and safety justification for retrofit?

To address these issues, Shan, et al. conducted experiments on eight specimens designed to simulate 1970s era bridge columns (Figure 2-8) subjected to simulated seismic flexural loading followed by sustained service loading. The columns were retrofitted with two layers of glass or carbon FRP. Additional layers were applied at the column-base interface.

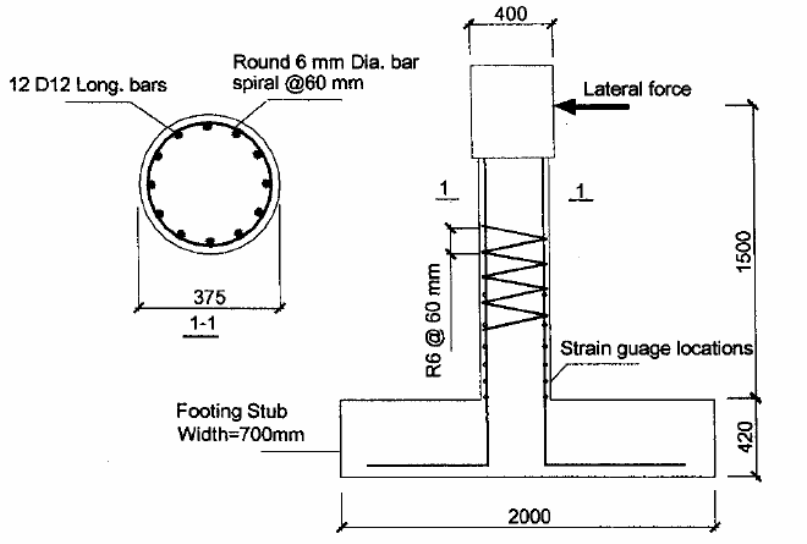

Figure 2-8 Shan, et al. (2006) Column Model Details (With permission from ASCE)

Using the apparatus shown in Figure 2-9 , each specimen was subjected to a constant axial load of $0.2f'_cA_g$ and then cyclic lateral load that ended at a drift ratio of 10% to simulate earthquake damage. Following this, each specimen was moved to a long term sustained load frame shown in Figure 2-10 and a sustained axial load of $0.2f'_cA_g$ was applied. Strains were recorded for a period of 30 days until they became stable.

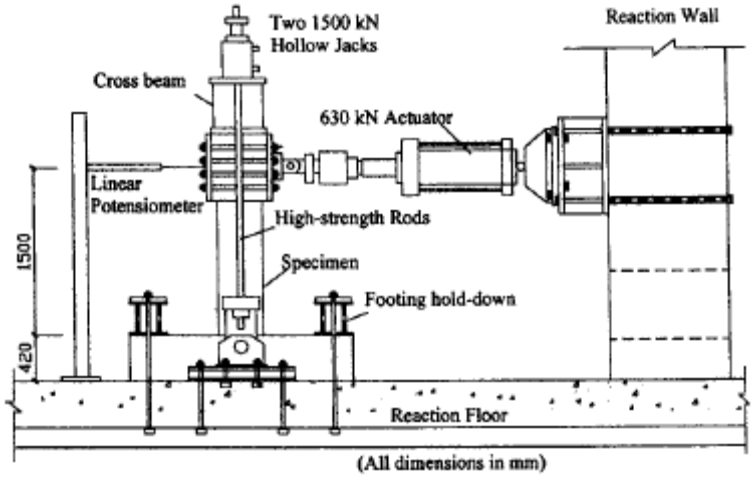

Figure 2-9 Shan, et al. (2006) Combined Lateral and Axial Load Device (With permission from ASCE)

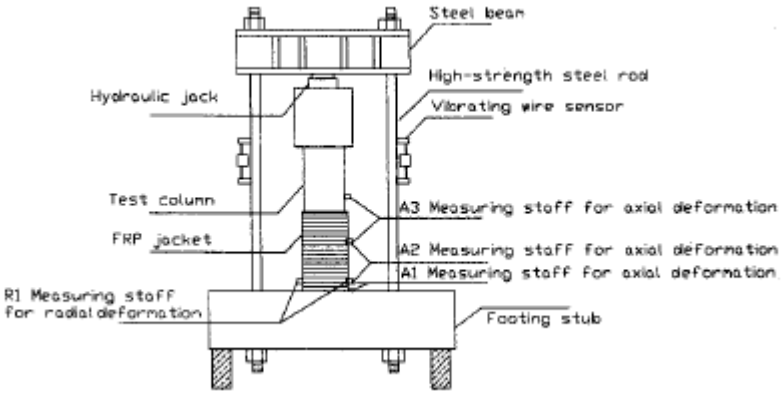

Figure 2-10 Shan, et al. (2006) Long Term Axial Load Device (With permission from ASCE)

Based on the data collected Shan, et al. used a modification factor, α, to allow the confined concrete model suggest by Xiao and Wu (2000) and Xiao (2004) to predict the immediate axial strain, ε_{ia}, of a damaged specimen. See Equation (2.108) where ε'_{ia} is the immediate axial strain of an undamaged specimen and α has an average value of 1.98 for the tested conditions. The value of ε_{ia} can then be multiplied by the ACI209-92 creep coefficient presented in Chapter 2.6.1 to predict the creep strain behavior at any time t of a specimen

subjected to both simulated seismic damage and long term sustained loads. A sample of Shan, et al.'s results shown in Figure 2-11 demonstrates that this procedure provides a good approximation of the creep behavior of damaged specimens.

$$\varepsilon_{ia} = \alpha \varepsilon'_{ia} \tag{2.108}$$

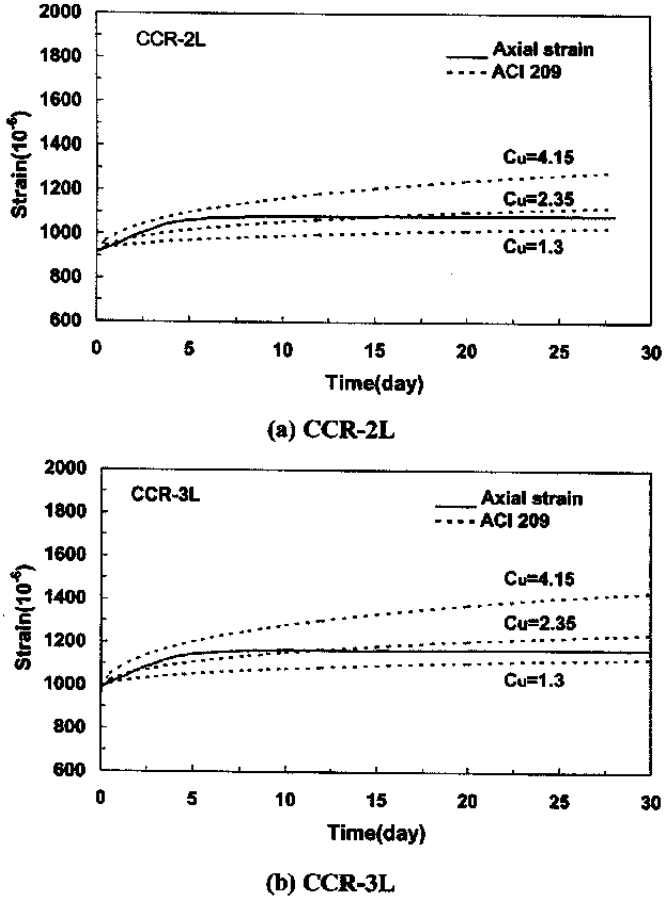

Figure 2-11 Shan, et al. (2006) Creep Strains of Damaged, FRP Retrofitted Specimen Compared to ACI 209 (With permission from ASCE)

Shan, et al. conclude that the ACI 209 model can provide a good prediction of the post damage creep provided that the initial strains are modified to account for the damage. Additionally, the average effective creep Poisson's Ratio for these specimens was found to be 0.15, and the development of long term deformations was found to be related to both the level of damage and the elastic modulus of the FRP. It is interesting to note that in spite of the question

posed about residual capacity, Shan, et al. did not report on whether or not the specimens were reloaded to failure at the conclusion of the creep testing.

2.8.3 Cyclic Modeling based on Shao (2003)

The only discussions of cyclic modeling of FRP confined concrete found for this research are based on the PhD dissertation of Shao (2003). This work was later published by Shao, Zhu, and Mirmiran in 2006.

Shao's model uses the stress-strain model of Samaan, Mirmiran, and Shahawy (1998) (see Section 2.4.2) to predict the envelope curve. The unloading path is given by Equation (2.109) supported by (2.110), (2.111), and (2.112).

$$f_c = \frac{(1-x)^2}{(1+2x)^2} f_{un,env} \tag{2.109}$$

$$x = \frac{\varepsilon_c - \varepsilon_{un,env}}{\varepsilon_{pl} - \varepsilon_{un,env}} \tag{2.110}$$

$$\varepsilon_{pl} = \varepsilon_{un,env} - \frac{f_{un,env}}{E_{\sec,u}} \tag{2.111}$$

$$E_{\sec,u} = E_c \begin{cases} 1 & 0 \le f_{un.env}/f'_{co} < 1 \\ -0.44 f_{un,env}/f'_{co} + 1.44 & 1 \le f_{un.env}/f'_{co} < 2.5 \\ 0.34 & f_{un.env}/f'_{co} \ge 2.5 \end{cases} \tag{2.112}$$

The reloading path is a straight line defined by the point of plastic strain (ε_{pl}, 0) and the new reference stress given by Equation (2.113) at the original unloading strain (ε_{un}, f_{new}). For simplicity, this linear relationship is used until the cyclic response returns to the envelope curve.

$$f_{new} = 0.9 f_{un,env} \tag{2.113}$$

Shao states that for each unloading point on the envelope curve (ε_{un}, f_{un}) there exists a unique plastic strain, ε_{pl}, and new reference stress, f_{new}. For a given unloading point, the hysteretic response cycles between (ε_{pl}, 0) and (ε_{un}, f_{new}) without further degradation.

Lam, et al. (2006) conducted cyclic loading tests on 18 standard 6"x12" specimens wrapped with either one or two layers of CFRP. One set of specimens was subjected to a series of single cycles that began at a prescribed displacement level followed by unloading to near zero stress followed by a reloading to the next prescribed displacement level. The other set of specimens underwent the same procedure except that three cycles were conducted at each prescribed displacement level. Lam, et al. used the model of Lam and Teng (2003) (see Section 2.5.3) to evaluate the envelope performance of the specimens and the model of Shao (2003) to evaluate the cyclic performance.

Lam, et al. found that Shao's model did not correlate well with their test results as it was "unable to predict the cumulative effect of loading history on the permanent strain and stress deterioration of FRP confined concrete." Shao's concept of a unique plastic strain and hysteretic response was not substantiated by Lam, et al.'s tests and was repudiated in their conclusions. It was also reported that the FRP jacket hoop rupture strain, ultimate stress, and ultimate strain of the cyclically loaded specimens were about 15% higher that those in monotonically loaded specimens. Additionally, the results showed that cyclic loading has very little effect on the stress-strain response envelope. Following a cyclic load, the response tended to return to the envelope curve predicted by the model of Lam and Teng (2003). Lam, et al. did not propose a new or modified cyclic model.

2.8.4 LRFD for FRP

Three papers discuss the necessity for and concepts behind developing appropriate resistance factors and design guidance for the use of FRP products in construction and rehabilitation. Ellingwood (2003) and Oline (2003) both explain the principals behind the limit states/LFRD design philosophy. Both state because of the code based nature of structural design, FRP based construction and rehabilitation will not be widely accepted until suitable LRFD codes are published and accepted. Both authors describe the difficulty of the process because of the substantial variability of FPR base construction. In particular, FRP has time and environmental effects that are not fully studied or quantified. Atadero and Karbhari (2005) describe how the high coefficient of variation for FPR composite members affects the determination of appropriate design strengths. Atadero and Karbhari suggest that the resistance factor, φ, consider only variations in modeling, geometry, and materials other than FRP for a specific limit state while an

FRP resistance factor, ψ, is included to account for the variation in FRP based properties. While the use of two resistance factors increases the difficulty of design strength calculations, it allows for a better prediction of behavior when the wide variation of FRP materials, behavior, and environmental are considered. Atadero and Karbhari do not propose value for ψ for various limit states or FRP conditions.

2.9 Conclusions

With the exception of one cyclic model, all of the models currently available for FRP confined concrete focus on monotonic loading without any effects from sustained loading. Recently published models have been validated against the large variety of published experimental results available. Both design oriented and analysis oriented models are available for a variety of applications. With this in mind, researchers are branching out and looking at other aspects of FRP confined concrete behavior. One of the most significant of these may prove to be the impact of sustained service loads.

When comparing the development of experimental based models and field service conditions of structures, it is apparent that the life cycles of a test specimen and an actual building are different. A test specimen is created, instrumented, and tested, and then a model is developed based on these results. An actual structure sees the gradual application of dead load during construction, then a variable application of service loads over extended periods of time, and any number of combinations of renovations, rehabilitations, and extreme events. This raises the proposed question of verisimilitude: Does an experimental based model which experiences construction, loading, and destruction in a matter of weeks accurately reflect the behavior of a real structure which experiences long term sustained service loading prior to critical events? This research will determine whether or not the duration and magnitude of sustained load, the conditions of application of the FRP, and the prior strain history of an element are necessary parameters in the development of a stress-strain model

3. Experimental Program

3.1 Conceptual Development

The focus of this research was to understand the constitutive relationship of confined concrete over its life cycle and determine the effects of strain history on the ultimate behavior. This understanding is necessary to the proper prediction of structural behavior under extreme events because earthquakes, hurricanes, and tornadoes typically arrive years after a structure has been constructed. To achieve this objective, specific life cycle events must be identified, defined, and modeled in a way that approximates the actual life cycle of a structure yet fits within a reasonable research timeframe.

3.1.1 Material Properties

Commercial ready-mix concrete was used for all specimens. Concrete was placed on February 12, 2007. This was Day 1 of the experimental program. Day numbers for all life cycle events were counted from this day. The plain concrete compressive strength was 3,568 psi at 7 days, 5,455 psi at 28 days, and 5,457 psi at 219 days. Accordingly a value of 5,455 psi is used for f'_c in all calculations and 4,210 ksi is used for E_c according to ACI 8.5.1. Enough cylinders were cast to allow poorly formed ones to be rejected, to validate procedures prior to testing record specimens, and to have replacement cylinders if needed. Figure 3-1 shows the placement of the 4 inch specimens for strength determination.

The FRP used was V-Wrap C100 from VSL Strengthening Products. The manufacturer's published properties are as follows:

f_{frp}	550 ksi
E_{frp}	33,000 ksi
ε_{frp}	0.0167 strain
thickness of 1 layer	0.0065 in

Local tests confirm the manufacturer's values.

Figure 3-1 Cylinder Placement

3.1.2 Life Cycle Definitions

The specimens in this program were subjected to a combination of five events: construction, sustained service loading, minor critical event, rehabilitation, and extreme critical event (ultimate loading). The variations in groupings explained in Section 3.2 allow the impact of each variable to be observed.

Construction: This event is the building of the specimen. For a real structure it incorporates the entire process from groundbreaking to ribbon cutting. It is characterized by the gradual application of dead load as the structure is constructed and, for concrete structures, the gradual growth in capacity as the concrete cures. For this research, the construction phase simply consisted of casting the concrete test cylinders which were demolded after 24 hours and then moist cured for seven days. No further events occurred until after the concrete had dry cured for an additional 21 days. The timeframes were selected to mimic typical construction procedures. Forms are usually stripped in one or two days. Moist curing is typically provided for few days, at most, so additional formwork can then be placed and construction may continue.

Sustained Service Loading: Most structures, most of the time, see a sustained service loading that is much lower than the code-required design loads. A typical office design live load is 50 psf yet the average daily load in an office is only 11 psf (Murray, 1997). Naguib (2001) reports that sustained loads in bridge piers are typically 20% of the pier's capacity while sustained loads at the lower levels of a high rise structure may rise to 35% of its capacity.

Accordingly, the target sustained loading for specimens in this research is 25% to 30% of the 28 day plain concrete compressive strength. For f'_c of 5.455 ksi, the target sustained stress is between 1.36 and 1.64 ksi.

Within a real structure, the duration of the sustained load is measured in years or decades. This timeframe is not practical for routine research so a shorter time period must be selected. Typical magnitudes and durations of sustained loadings used in prior research are shown in Table 3-1 along with the percentage of the final creep strains attained at the end of the first 30 days of loading. Clearly any duration of sustained loading that exceeds 30 days will allow most of the effect of the loading to be observed. A target of 40 days was selected as it met the minimum duration of 30 days while being the maximum value possible to ensure completion of the research on schedule.

	Song, et al. (1995)	Naguib and Mirmiran (2003) based on Naguib (2001)	Han, Tao, and Liu, (2004)	Shan, Xiao, and Gou, (2006)
Sustained Load as a % of Ultimate Load	35%	15% and 30%	62%	20%
Duration of Sustained Load	365 days	80 days	120 days	30 days
% of final creep attained in 30 days	75%	75% and 72%	75%	---

Table 3-1 Magnitude and Duration of Sustained Loadings

Minor Critical Event: Minor critical events occur during the life cycle of a structure when a given load exceeds its service level value but does not reach its maximum design value. These events could include an earthquake at the 50% probability of exceedence in 50 years level, winds from a category II hurricane, or an impact loading from either a blast or collision. In the laboratory, this was approximated by loading the test specimens to a sufficient level to induce some damage, but not to a level to cause failure. For specimens confined with FRP, the 'minor critical event' was defined as monotonic loading to about 7.5 ksi followed by three loading cycles between zero and the specimen strain resulting from the 7.5 ksi load. 7.5 ksi was chosen because it represents a point approximately halfway between f'_c and f'_{cc}. For specimens confined with steel spirals, it was defined as two cycles between 0.0 ksi and 4.0 ksi. 4.0 ksi is 55% of the f'_{cc} value using the Mander model. This value was selected to be large enough to cause some damage to the concrete, but small enough to prevent spalling of the cover concrete.

It was necessary to keep the cover concrete intact to allow for effective application of the FRP during rehabilitation.

Rehabilitation: For this research, rehabilitation (or retrofit) of the concrete specimens was accomplished by the application of two layers of carbon FRP according to the manufacturer's instructions. A 5 inch (1/4 wrap) overlap was provided to ensure proper bonding of the free edge of the FRP. At the top and bottom of each specimen, two additional 1.5 inch wide layers of FRP were provided. Preliminary experiments showed a tendency to fail prematurely at the ends. The additional end reinforcement ensured that the failure occurred at mid-height on the specimen. Figure 3-2 shows the rehabilitation of one specimen while under load in the sustained load device.

Figure 3-2 Rehabilitation of Test Specimens Under Load

Extreme Critical Event: An actual structure experiences an extreme critical event when a seismic or wind load reaches its lifetime maximum value and the structure experiences its ultimate loading condition. In the laboratory, this was achieved by loading the specimen monotonically to failure. All specimens were loaded in displacement-control mode to ensure that data could be collected on the second branch of the stress-strain curve as well as for the safety of the operators and the equipment. The loading rate for each specimen was 1392 με/min or 0.0167 inches per minute for a standard 12 inch specimen. This rate is consistent with the rate used by many researchers as shown in Table 3-2. Both strain rates and displacement rates

applied to 12 inch specimens are shown. This rate was fast enough to ensure that specimens fail in compressive loading rather than creep, yet slow enough to allow for good data collection.

Researcher	Strain Rate	Displacement Rate (6"x12" specimen)
Matthys (2006)	250 με/min	0.00300 in/min
Saafi (1999)	694 με/min	0.00833 in/min
This Research	**1392 με/min**	**0.01670 in/min**
Karabinis (2002)	1892 με/min	0.02270 in/min
Berthet (2004)	6250 με/min	0.07500 in/min
Shahaway (2000)	18333 με/min	0.22000 in/min

Table 3-2 Published Displacement Control Rates

3.1.3 Sustained Load Device

Applying a long term sustained load to a concrete specimen has always proven challenging. Passive methods of applying load such as tension rods required constant adjustment since concrete creep leads to a reduction in the confining force. Active methods including various hydraulic or pneumatic pumps require the dedication of critical resources and are subject to mechanical or electrical failure as occurred with Berthet, et al. (2006b). For this research, a sustained load device was designed and constructed to enable a constant axial load to be applied to twelve standard 6"x12" concrete test cylinders. Details of the design are shown in Appendix B and Figure 3-3 shows the device in operation. The device employs the basic principles of statics and hydraulics to apply a 42 kip load to up to 12 test specimens. Figure 3-4 shows the stability of the sustained load over time. For this group of specimens, the load was always within 2% of the target load. Additionally, the configuration of the tension rods provided sufficient space to allow FRP to be applied to the specimens under load as was necessary in some cases.

The only drawback to this device is that the specimens must be removed from the device, and thus the sustained load, prior to transferring the specimen to the load frame for ultimate loading. This modeling technique is not consistent with real world behavior, but it is common to most research as different systems are required for sustained and ultimate loading.

Figure 3-3 Sustained Load Device

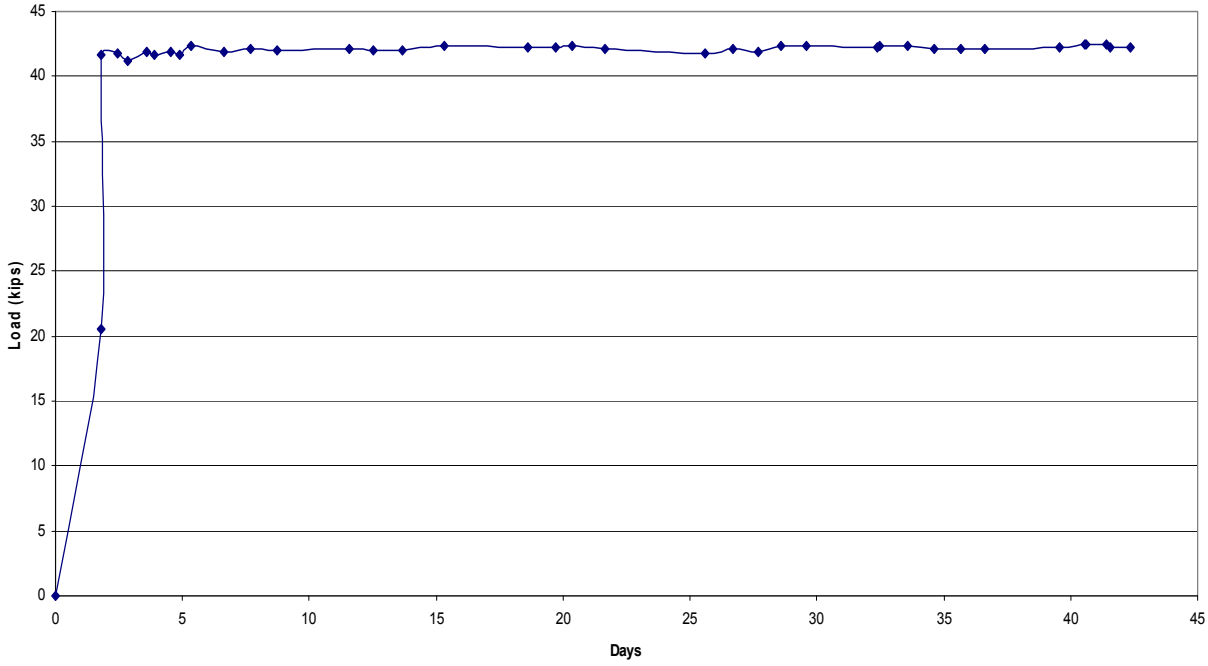

Figure 3-4 Magnitude of Sustained Loads

3.1.4 Ultimate Loading Systems

The KSU structural testing laboratory possesses two relevant machines. 'Big Purple' is a 400 kip capacity, hydraulically activated compression testing system suitable for determining the ultimate strength of concrete specimens. It is difficult to maintain a constant loading rate on the

machine and the lack of a feedback control system makes determination of the post peak stress-strain behavior impossible. The only data collected by the system is load, stress, and time. 'Big Purple' does not have a programmable control system so cyclic load cannot be accurately applied. The load cell data cannot be directly exported to the MEGADAC data collection system.

The 'MTS' system is a 150 kip capacity, servo-controlled, hydraulic actuator. The computer control system allows it to function in either displacement or force control methods. Load and displacement data are easily transferred to the MEGADAC data collection system. The computer control-system allows a program to be used to control the application of load in either a monotonic or a cyclic manner or a combination of both. The principal drawback of this system is its capacity. It can only produce an axial stress of about 5 ksi on a 6 inch concrete test cylinder which is too low for the purposes of this research.

To remedy this situation, a load amplification device was designed and constructed which enables the MTS system to exert up to 450 kips of load or 15 kis on a standard 6 inch by 12 inch specimen. The completed load amplification device is shown in Figure 3-5. Details of its design, calibration, and construction are in Appendix C.

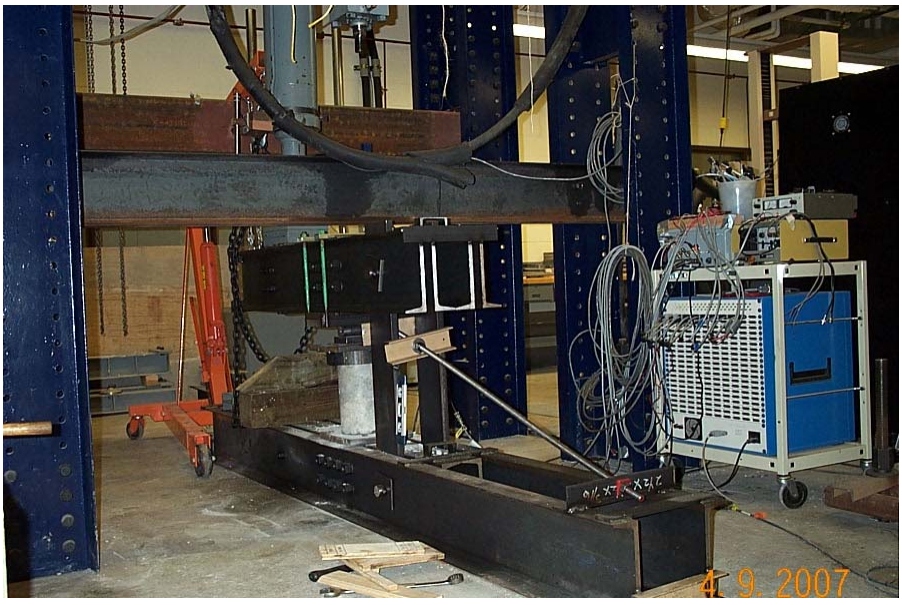

Figure 3-5 Load Amplification Device

3.1.5 Instrumentation

Each cylinder was instrumented in the axial (longitudinal) direction with three 2 inch long strain gages placed at mid-height at the third points on the circumference. These gages were consistently designated L1, L2, and L3. Circumferential strain was collected by two 2 inch long strain gages, designated R1 and R2, diametrically opposed at mid-height. R1 was positioned adjacent to L1 and R2 to L2. Data was collected using P3500 strain gage indicators together with SB-10 switch and balance units during the sustained loading phase and the MEGADAC data collection system during ultimate testing in the load frame. Figure 3-6 shows the instrumentation of the test specimens with a schematic of the gage locations.

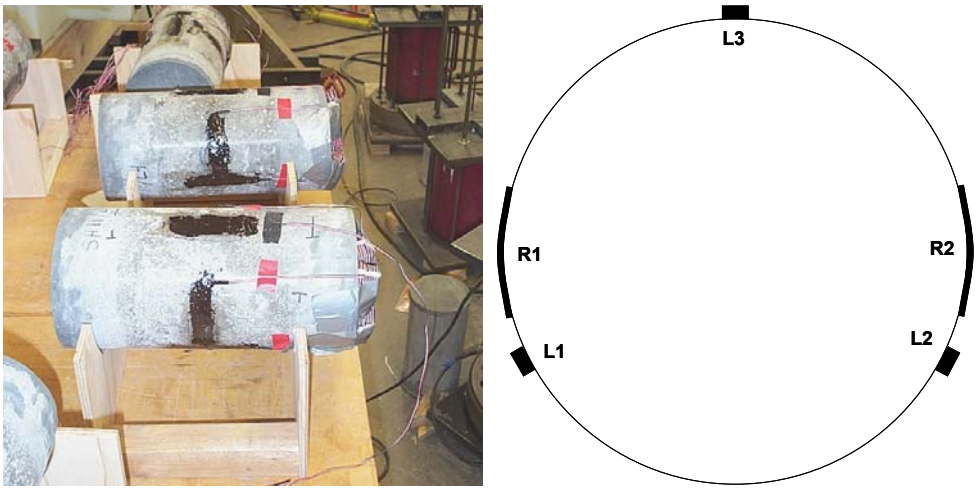

Figure 3-6 Test Specimen Instrumentation

3.2 Experimental Groupings

The test specimens were placed in four groups. The parameters were varied for each group so that the group addresses one specific aspect of life cycle behavior.

3.2.1 Control Group

This group established the base line behavior. Specimens were constructed, retrofitted, and tested in the manner which normally precedes stress-strain model development. That is, the specimens were cast, wrapped with FRP, and then tested. Four specimens, C1, C2, C3, and C4 were tested monotonically to failure. Specimens C5 and C6 were multi-function specimens. For control purposes, C5 and C6 were subjected to a minor critical event to establish the cyclic behavior of a specimen without a prior sustained load. Following the minor critical event, these

specimens were placed in the sustained load device for 44 days, and then were tested monotonically to failure to provide further data for post minor critical event analysis.

3.2.2 Lab Group

This group was so named because the specimens underwent a life cycle typically seen only by lab specimens. Cylinders were cast, instrumented, and wrapped with FRP. Then, they were placed in the sustained load device for 41 days and tested. Specimens L1 and L2 were loaded monotonically to failure. Specimens L3 and L4 were loaded through a minor critical event then pushed monotonically from this point to failure. Specimens L5 and L6 were subjected to a minor critical event then returned to the sustained load device for an additional 40 days. Following this, they were tested monotonically to failure.

Lab group results were compared to control group results to determine if the presence of a sustained service load changes the stress-strain behavior of FRP confined concrete.

3.2.3 Retrofit Group

This group is designated 'Retrofit' because it models the life cycle of a member in an actual structure. Six cylinders were cast and instrumented, then placed in the sustained load device. After a period of sustained loading, the specimens were retrofitted with FRP which simulates an FRP retrofit in an actual structure. Specimens R1, R3, R4, and R6 were wrapped under load after 30 days of sustained loading. Specimens R2 and R5 were wrapped after 39 days of sustained loading. After 41 days of total loading, the specimens were tested. R1, R2, R3, R5, and R6 were tested monotonically to failure while R4 was subjected to a minor critical event, returned to the sustained load device for 40 days, and then tested monotonically to failure.

The Retrofit group is differentiated from the Lab group by the time of application of the FRP. FRP was applied to the Lab group prior to the application of any load. FRP was applied to the Retrofit group after the application of sustained load.

Retrofit group results were compared to control group and lab group results to determine the impact of sustained load history and time of application of FRP on the stress-strain behavior of FRP confined concrete.

3.2.4 Steel Group

This group contains eight specimens that were cast with a confining steel spiral consisting of a ¼ inch, A36 steel rod with a 3 inch pitch and a 5 inch diameter of spiral. Spirals were manufactured in the Civil Engineering shop using a mandrel and lathe as shown in Figure 3-7. Figure 3-8 shows a completed steel spiral just prior to specimen construction.

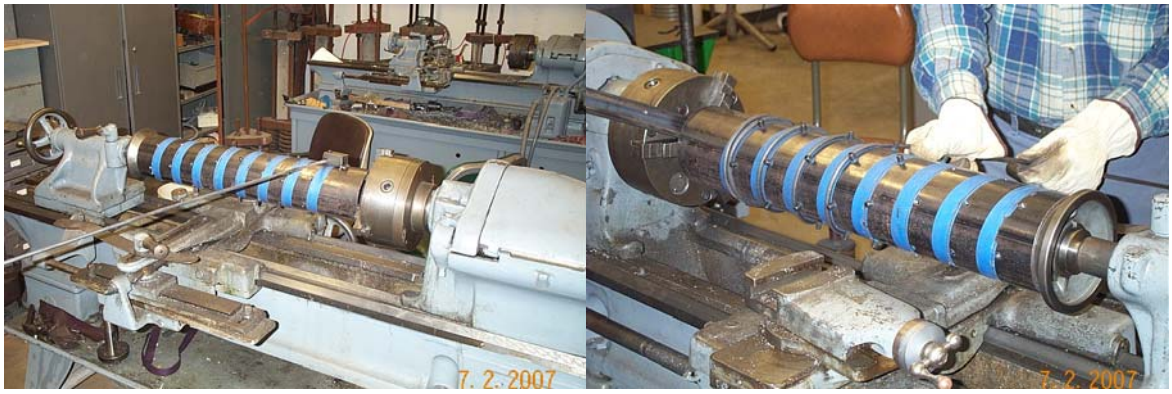

Figure 3-7 Steel Spiral Fabrication

Figure 3-8 Steel Spiral Prepared for Placement in a Specimen

The Steel Group was designed to examine the interaction of steel spirals, FRP retrofits, sustained loading, and minor critical events on the behavior of concrete confined by both FRP and steel spirals. Specimen S7 failed prematurely and was excluded from all analysis. Specimen S8 was tested monotonically to failure without sustained load or retrofit to establish the baseline behavior. Specimens S1 to S6 were subjected to 42 days of sustained loading. After 26 days of sustained loading, specimens S1, S2, S3, and S4 were subjected to a minor critical event and

returned to the sustained load device. At this point, specimens S3 and S4 underwent a retrofit and were wrapped with two layers of FRP. Specimens S5 and S6, which were undamaged at this time, also were retrofitted. After an additional 16 days of sustained loading, specimens S1 to S6 were tested monotonically to failure. Specimens S1 and S2 allow an investigation of the residual capacity remaining in a steel spiral confined specimen following a minor critical event. Specimens S3 and S4 demonstrate the effectiveness of FRP as a retrofit strategy for a damaged steel spiral confined specimen. Specimen S5 and S6 provide an assessment of the difference in capacity between a damaged and undamaged retrofitted specimen as well as a comparison between specimens with and without steel spiral confinement.

3.3 Experimental Results

This section reports the experimental results of each specimen. The life cycle history of each specimen is provided along with the strain data from each strain gage in each event. For minor and extreme critical events, axial strains are shown as positive and circumferential strains as negative in each figure. For a sustained load, both axial and circumferential strains are shown as positive. For some specimens, individual data points were missing due to gages going out of range. These values were estimated and explained as indicated for each specimen. The data plots of some tests, particularly for specimens C1, C2, C6, and R6, display results that are not consistent with expectations. The causes of these discrepancies and the comparison and analysis of all the results is covered in Chapter 4.

Loading of specimens for both minor critical events (sub-ultimate, cyclic) and extreme critical events (ultimate, monotonic) were applied with the load amplification device. Specimens were pre-loaded to 30.75 kips, unloaded to 9.25 kips, and then reloaded for either a minor or extreme critical event. This pre-loading was to ensure that the specimen was properly seated and that the test equipment was functioning within acceptable limits.

Multiple failure modes were observed and are defined as follows:

- FRP rupture: a breaking of the carbon fiber strands
- De-lamination: a failure of the epoxy matrix resulting in intact sheets of carbon fiber pealing off the specimen
- Yielding: an increase in strain with no increase in load (Note: it would be incorrect to say that the specimen has ‘yielded’ in the same way a steel tensile coupon yields,

but the common understanding of the term best describes what is observed in some specimens.)

- Crushing: spalling of the cover concrete followed by a compressive failure of the core concrete. This failure mode only applied in steel spiral specimens without FRP retrofit.

Tests were stopped at the first indication of a failure mode for safety of both operators and equipment. Accordingly, some specimens show complete, spectacular failures while others show only small ruptures. Yielding failures were observed using the peak load detectors of the MTS system. When the data collectors indicated a drop in load for an increase in displacement, the test was terminated.

3.3.1 Control Group Results

Specimen C1

This specimen was wrapped on day 109 and tested on day 117. No sustained load was applied. When the specimen was tested, longitudinal strain gage 1 failed almost immediately and produced no usable data. Gages L2 and L3 when averaged, did not provide an accurate measure of the response. Therefore, since readings were available for radial gage R1, a value for L1 was estimated by dividing the L2 reading by R2 to estimate a strain ratio then multiplying the result by the R1 reading. This value was then averaged with L2 and L3 to produce an average longitudinal strain. The specimen failed at 8.07 ksi and 7,914 (average) με by FRP rupture. Failure occurred at the base of the specimen rather than at mid-height (Figure 3-9). To ensure failure at mid-height in future tests, all subsequent specimens were reinforced at the top and bottom of the cylinder by two additional layers of 1.5 inch wide FRP. This technique was successful in directing the failure to mid-height where the instrumentation was located. Figure 3-10 shows the response of the individual gages and Figure 3-11 shows the average stress-strain response of the specimen. The strange shape of the stress-strain curve between 1.5 and 3.0 ksi will be addressed under Specimen C2 which exhibited similar behavior.

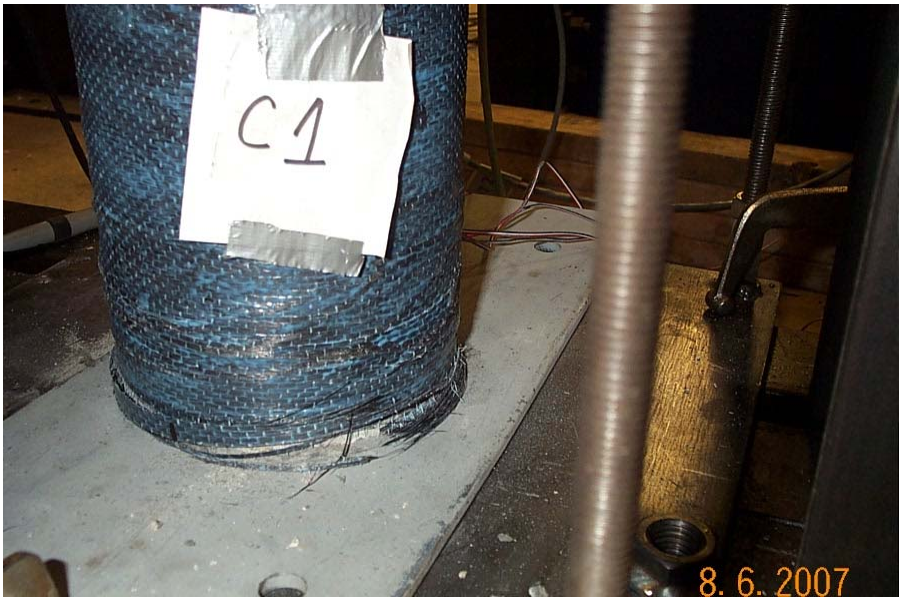

Figure 3-9 Specimen C1 Failure Mode

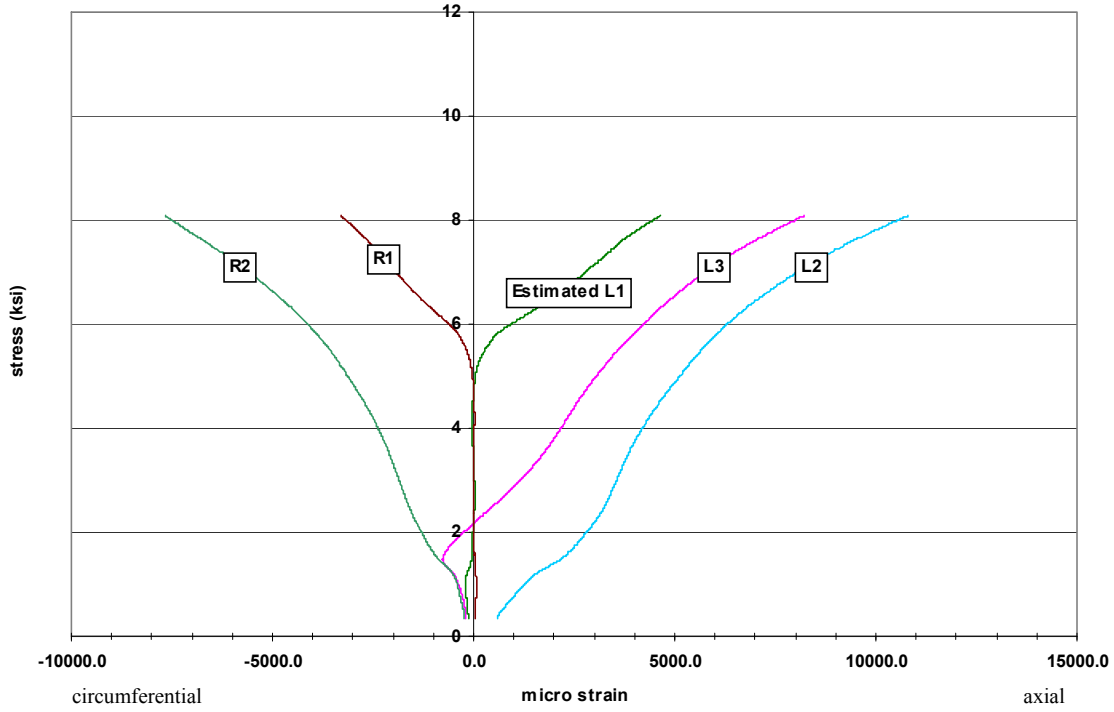

Figure 3-10 Specimen C1, Individual Gage Data

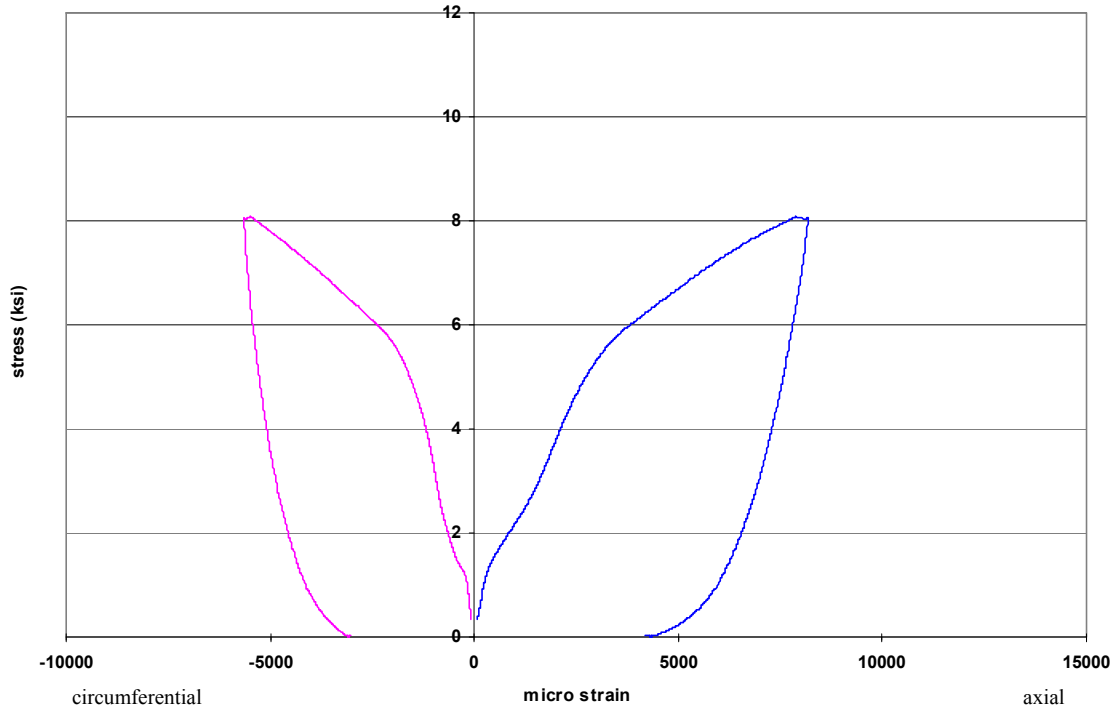

Figure 3-11 Specimen C1, Stress Strain Response

Specimen C2

Specimen C2 was wrapped on day 109 and broken on day 120. No sustained load was applied, and the specimen was loaded monotonically. Strain gage L2 did not function properly so the value was estimated using gage R2 in the same manner as described for specimen C1. Failure occurred at 9.49 ksi and 9,918 (average) με by FRP rupture as shown in Figure 3-12. Figure 3-13 shows the response of the individual gages and Figure 3-14 shows the stress-strain response of the specimen. The shape of the curve within the stress range of 1.5 ksi to 3 ksi is similar to specimen C1.

Up to 1.5 ksi, the stress-strain curves of both C1 and C2 align closely with expected results. Between 1.5 and 3.0 ksi, both exhibit a shift to the right which seems to indicate either excessive deformation for the recorded load or an under-recording of the applied load. In other words, the stress-strain curve in this region should be shifted left, up, or a combination of both to get the proper response. It is suspected that this discrepancy in behavior was caused by the base plate being too flexible. Observations of the plate after the test showed a substantial amount of bending. Accordingly, the base plate was replaced with a 1 inch thick plate for all subsequent

tests. As this softening phenomenon was not observed again, it can be reasonably concluded to have been caused by the more flexible base plate. Further discussion of the problems with specimens C1 and C2 is in Section 4.2.1.

Figure 3-12 Specimen C2, Failure Mode

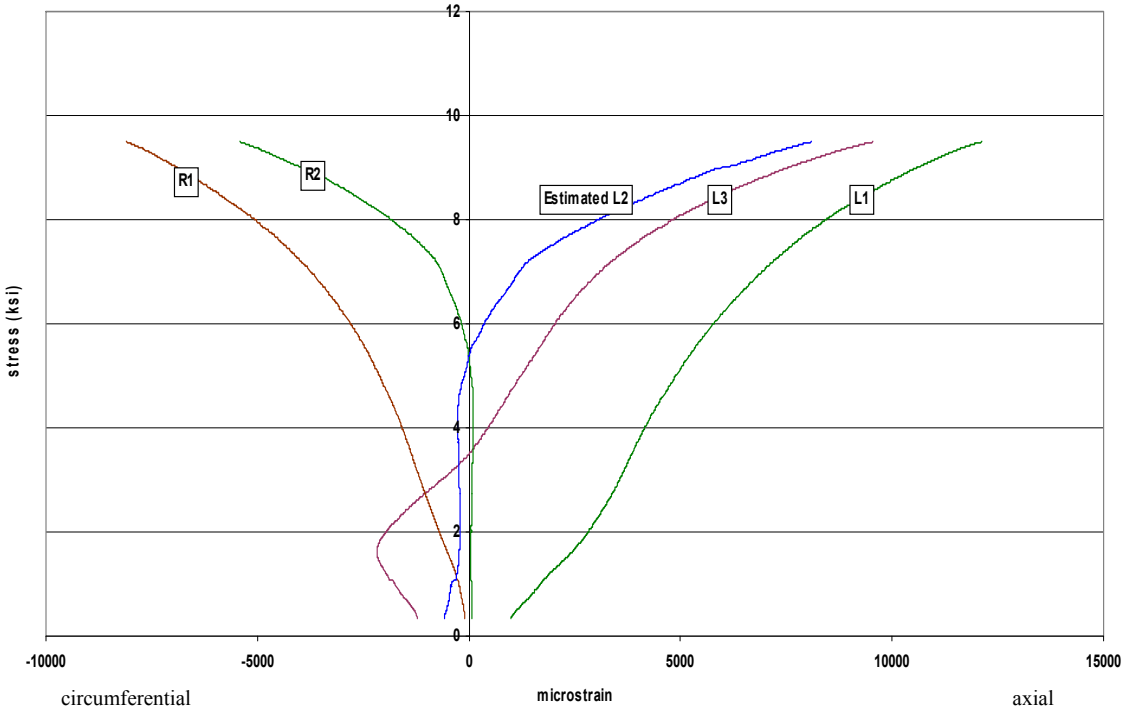

Figure 3-13 Specimen C2, Individual Gage Data

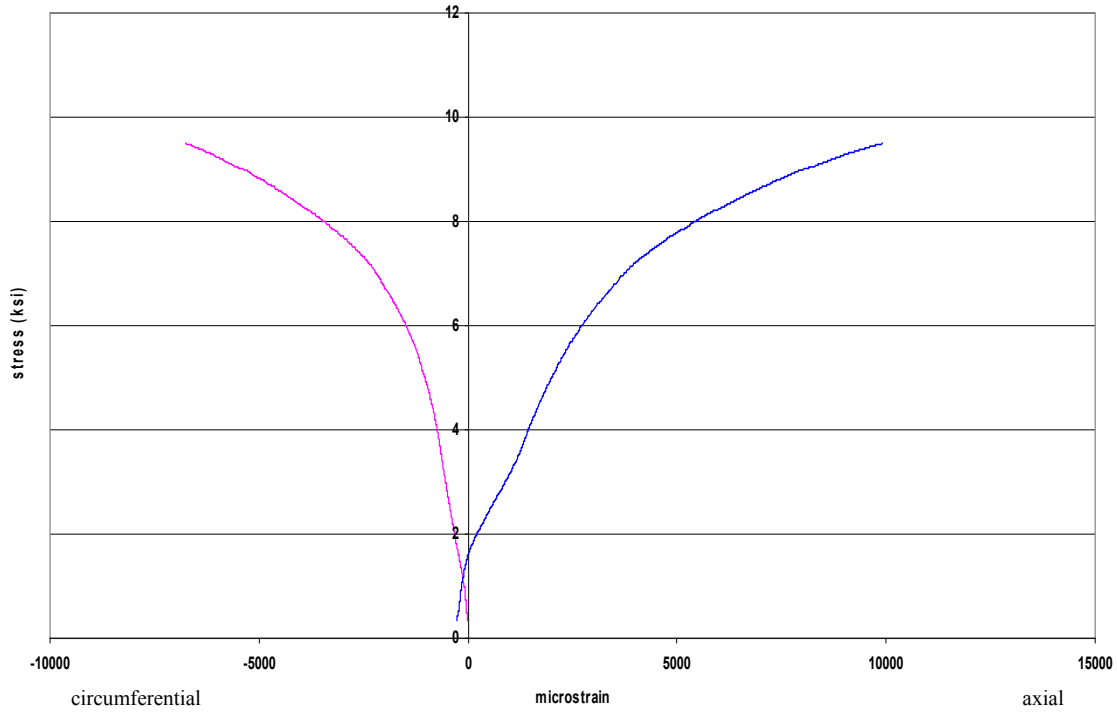

Figure 3-14 Specimen C2 Stress-Strain Response

Specimen C3

Specimen C3 was wrapped on day 109 and broken on day 124. No sustained load was applied, and the specimen was loaded monotonically. All strain gages functioned until longitudinal gage 2 failed at 9.22 ksi and 8,473 (average) με. Gage behavior at this point was linear so forward extrapolation of data was reasonable to the point of specimen failure which occurred at 9.89 ksi and 10,412 (average) με. FRP rupture or delamination was not observed so the failure point was determined by increasing strain without an increase in stress. Figure 3-15 shows the response of individual gages and Figure 3-16 shows the final stress-strain response of the specimen.

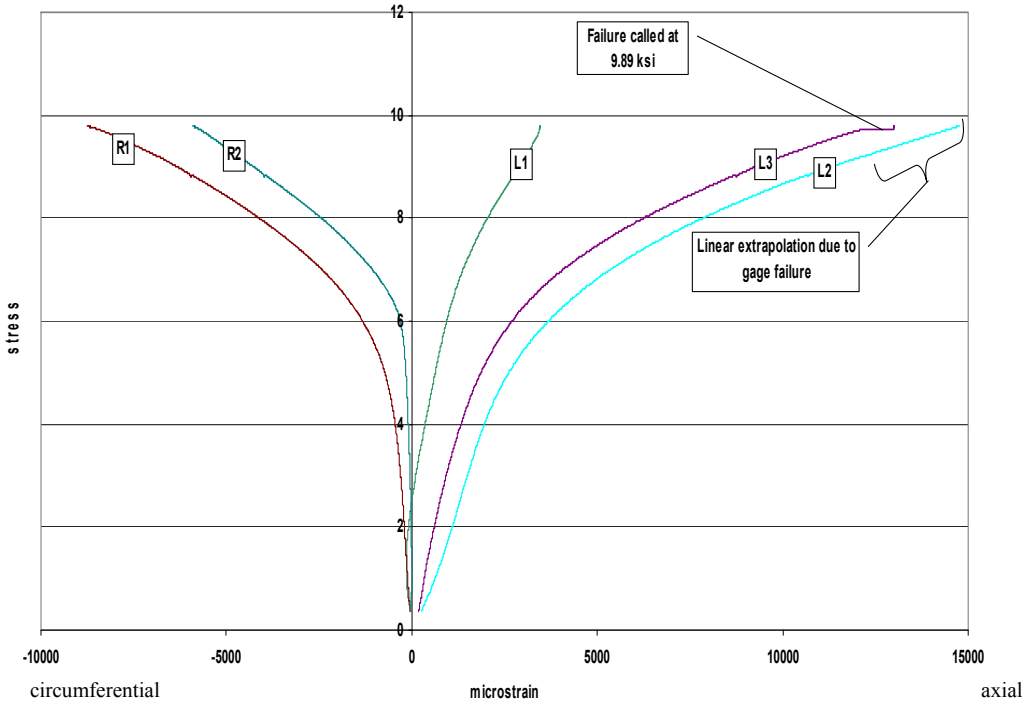

Figure 3-15 Specimen C3, Individual Gage Data

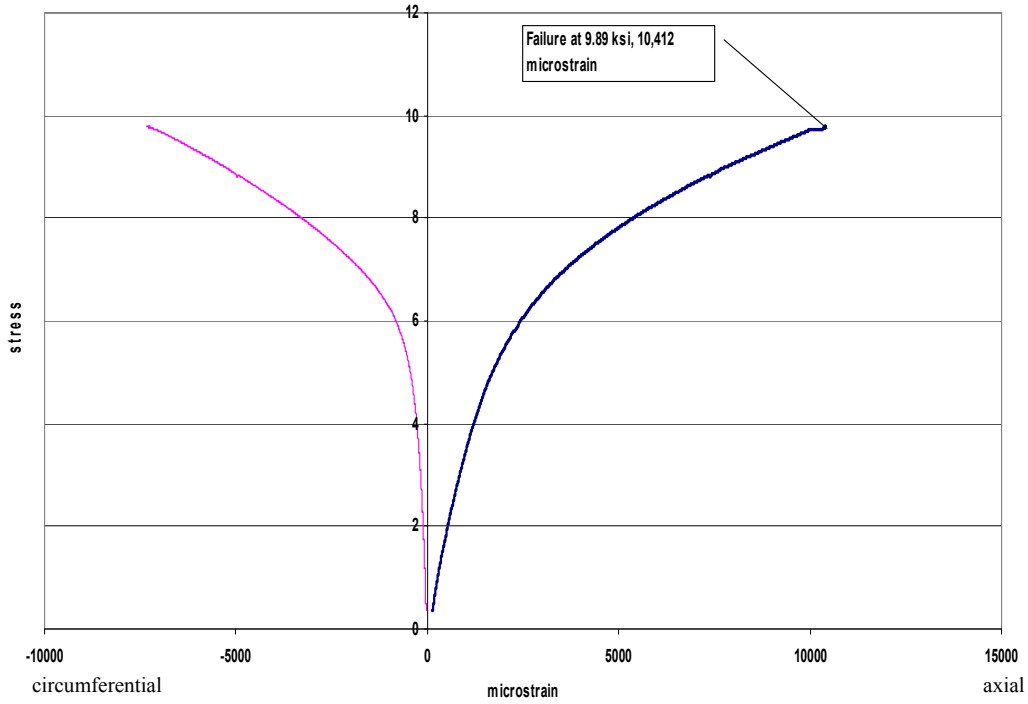

Figure 3-16 Specimen C3, Stress-Strain Response

Specimen C4

Specimen C4 was wrapped on day 109 and broken on day 128. No sustained load was applied, and the specimen was loaded monotonically. All longitudinal gages functioned properly throughout the test. Radial gage R1 failed at 9.47 ksi. Radial strain is not shown past this point as failure was imminent. Specimen failure occurred at 9.52 ksi and 7,490 (average) με. The failure mode was FRP delamination as shown in Figure 3-17. This specimen was the last of a group of four wrapped with the same pot of epoxy adhesive. At the time of mixing, the epoxy was at the end of its pot life, but not beyond it. Figure 3-18 shows the data collected from each strain gage while Figure 3-19 shows the average stress-strain response of the specimen.

Figure 3-17 Specimen C4 Failure Mode

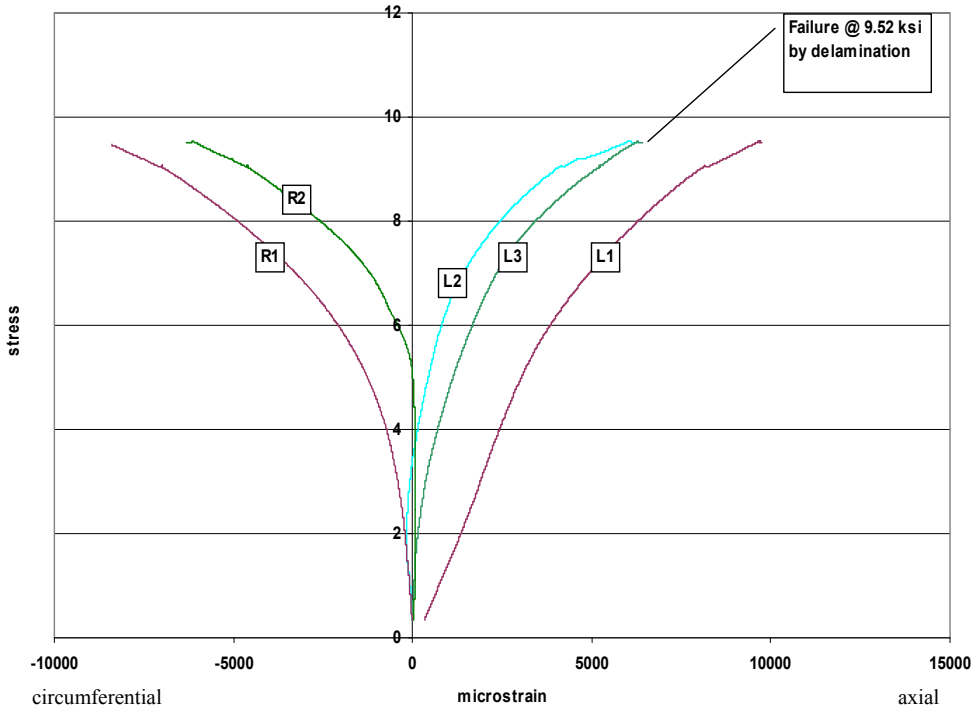

Figure 3-18 Specimen C4, Individual Gage Data

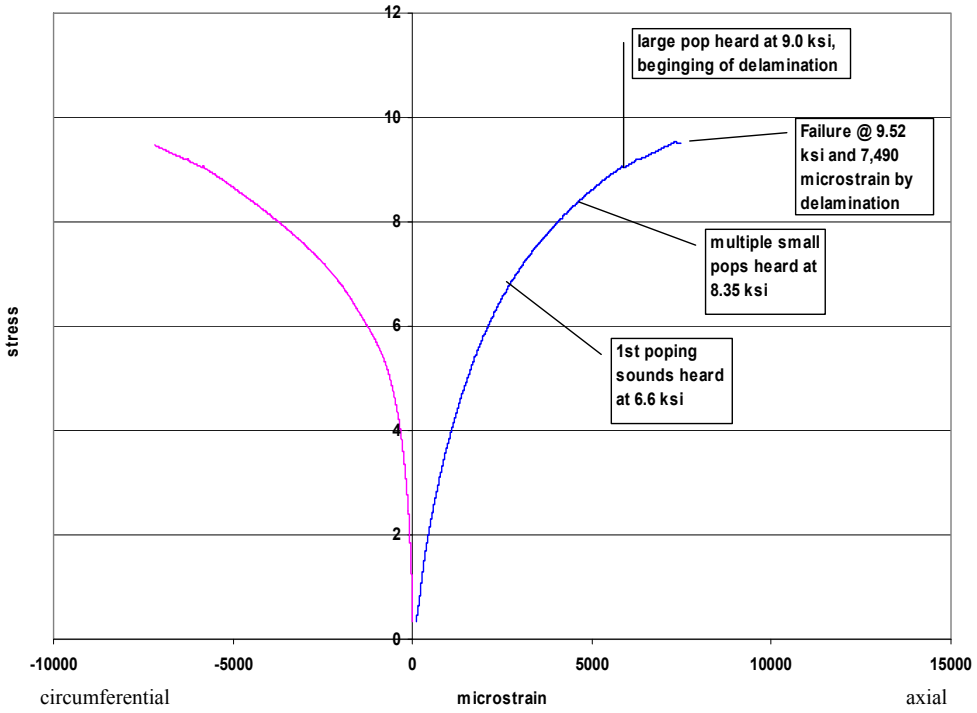

Figure 3-19 Specimen C4, Stress-Strain Response

Specimen C5

Specimen C5 was wrapped on day 109, subjected to a minor critical event on day 135, and placed under sustained service load on day 135. After 44 days, the specimen was removed from the sustained load device and loaded monotonically to failure on day 179. Failure occurred at 9.415 ksi and 10,992 (average total) με. All strain gages functioned correctly throughout all tests so no corrections or extrapolations were required. No external failure was observed and the final test was terminated when the strain began to increase without a corresponding increase in load. Figure 3-20 shows the individual gage data from the minor critical event loading and Figure 3-21 shows the individual gage data from the 44-day sustained service loading. The large change in the readings of gages L1 and L2 on day 24-25 was caused by the removal of the sustained service loading for the installation of two additional test cylinders in the same load frame. Although a change in the accidental eccentricity resulted in large variations of the individual gage readings, the average behavior remained unchanged. Figure 3-22 shows the individual gage data from the second loading without accounting for the residual strain resulting from the initial minor critical event and the sustained service loads. Figure 3-23 shows the average stress-strain response of the final ultimate loading both with and without the inclusion of the residual strains from prior events. Figure 3-24 shows the combined stress-strain response over the 44 day loading history.

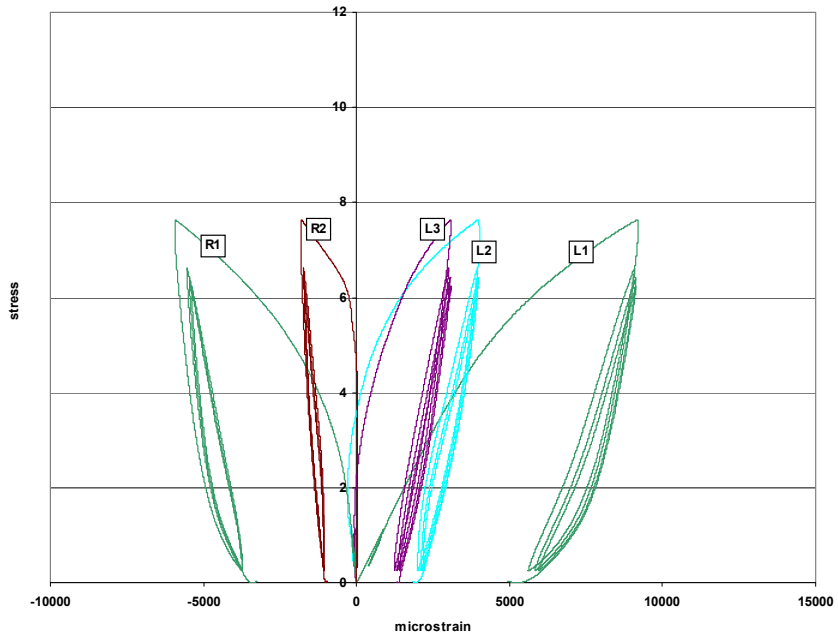

Figure 3-20 Specimen C5, Individual Gage Data for Minor Critical Event

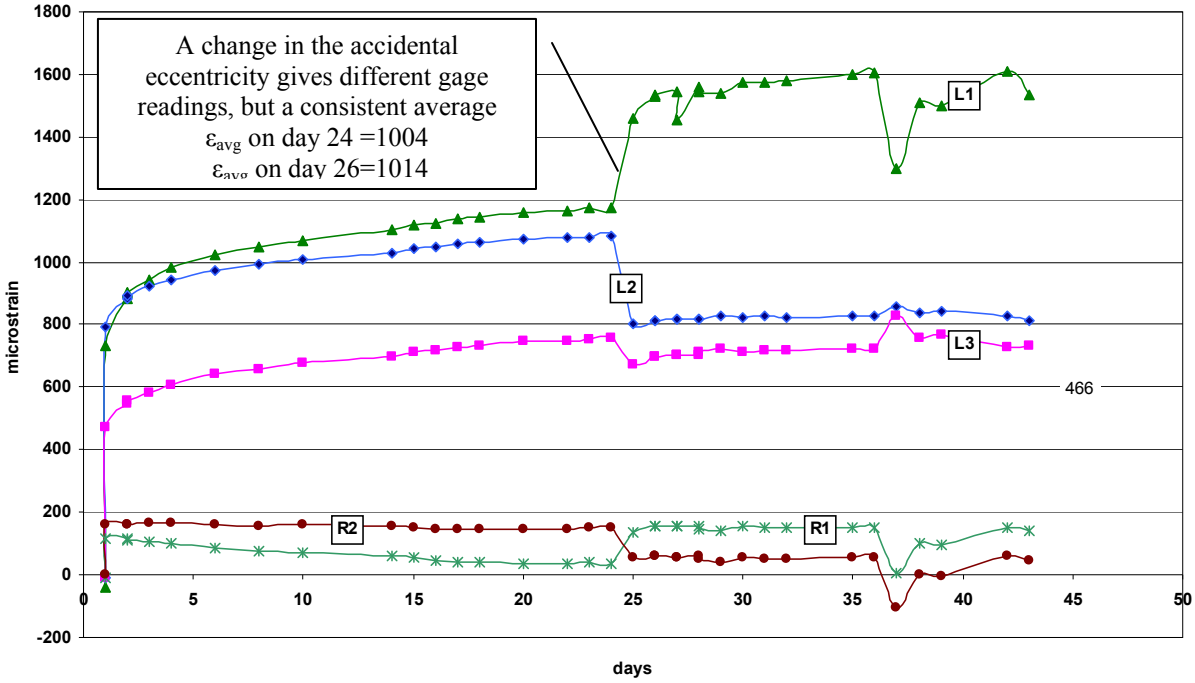

Figure 3-21 Specimen C5, Strains Under Sustained Load

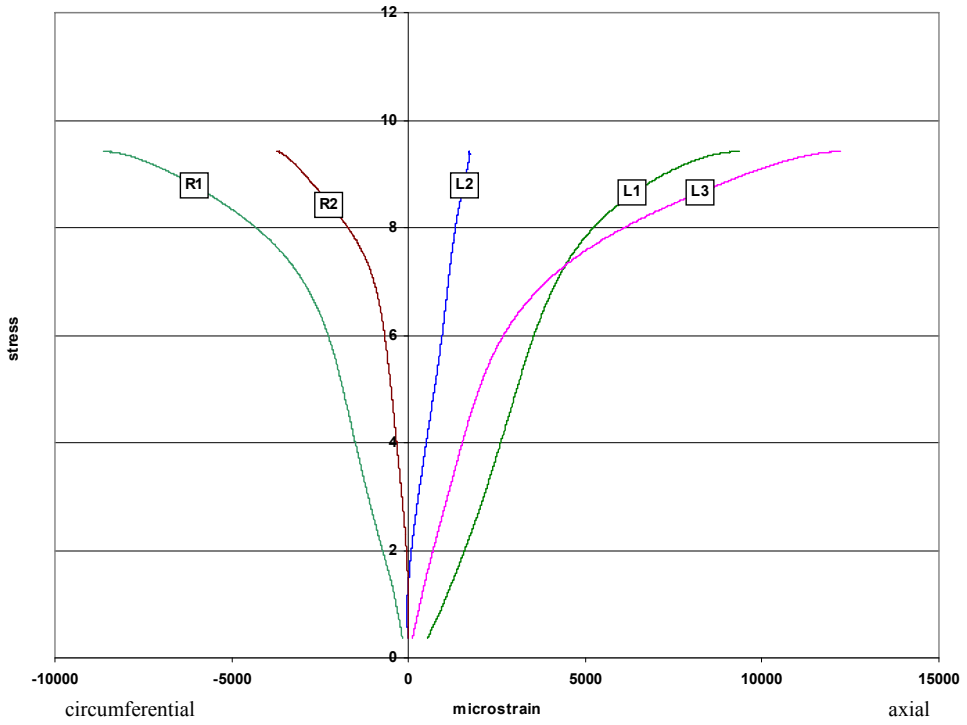

Figure 3-22 Specimen C5, Ultimate (Second) Loading, Individual Gage Data

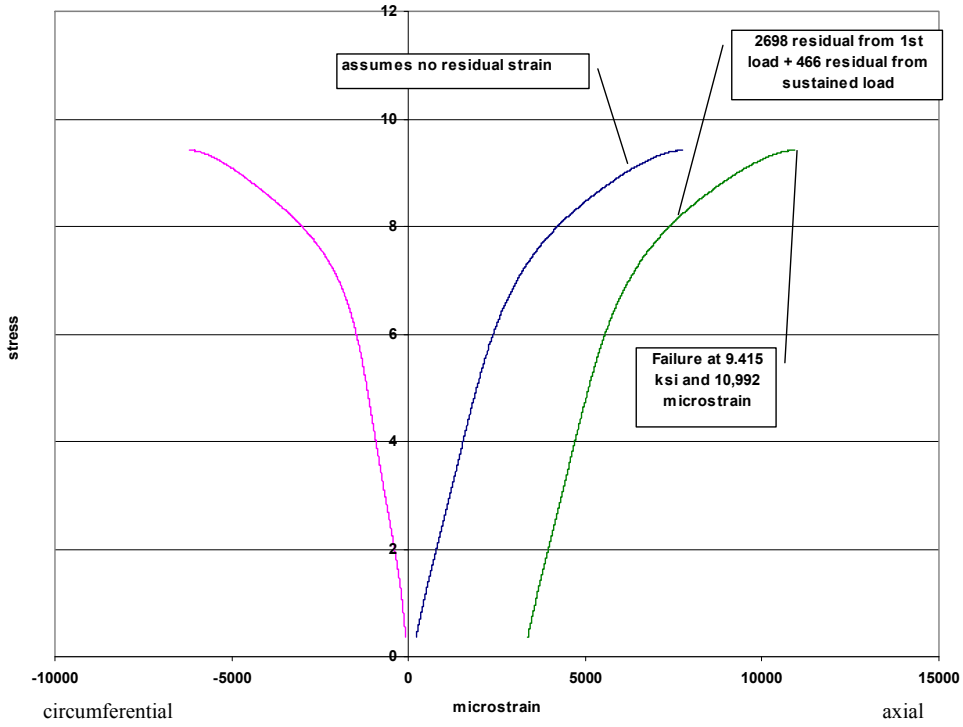

Figure 3-23 Specimen C5, Stress-Strain Response with Effects of Residual Strains

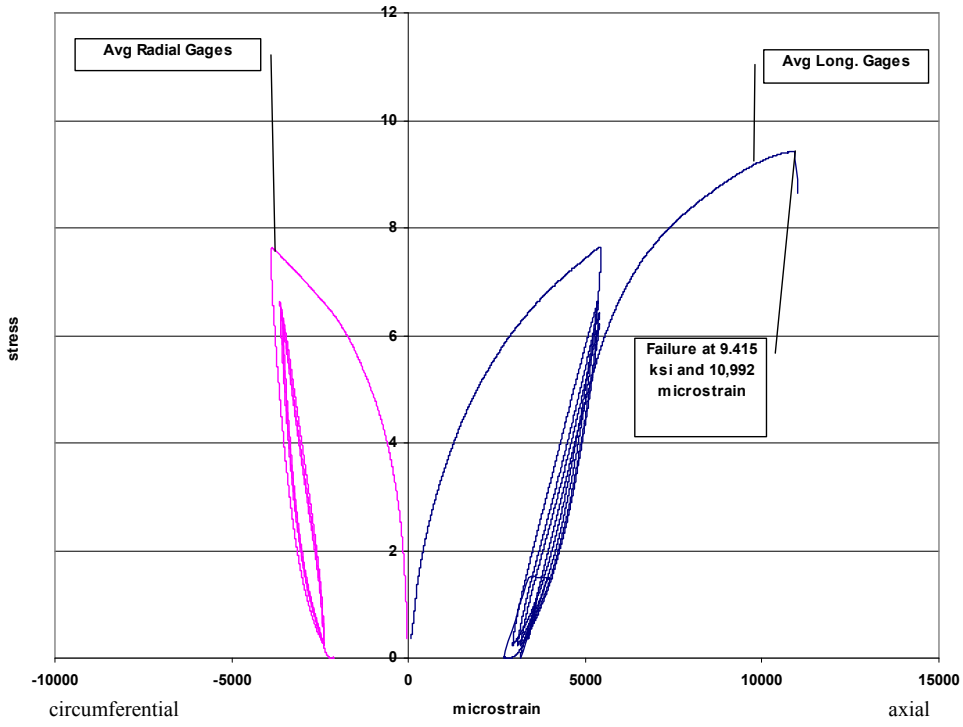

Figure 3-24 Specimen C5, Combined Average Stress Strain Response

Specimen C6

Specimen C6 was wrapped on day 109, subjected to a minor critical event on day 135, and placed under sustained service load on day 135. After 44 days, the specimen was removed from the sustained load device and loaded monotonically to failure on day 179. Failure occurred at 9.479 ksi and 9,365 (average total) με. All longitudinal strain gages functioned properly, but gage R2 failed upon the initial loading and gage R1 failed during the sustained loading phase and was not available for the final load test. No external failure was observed and the final test was terminated when strain began to increase without a corresponding increase in load. Figure 3-25 shows the individual gage data from the minor critical event loading and Figure 3-26 shows the individual gage data from the 44 day sustained service loading. The large change in the readings of gages L1 and L2 on day 24-25 was previously explained under Specimen C5. Figure 3-27 shows the individual gage data from the second loading without accounting for the residual strain resulting from the initial minor critical event and the sustained service load. Figure 3-28 shows the average stress-strain response of the final ultimate loading both with and without the residual strains from prior events. Figure 3-29 shows the combined stress-strain response over the 44 day loading history. The apparent tensile response in this figure is addressed in Section 4.2.1.

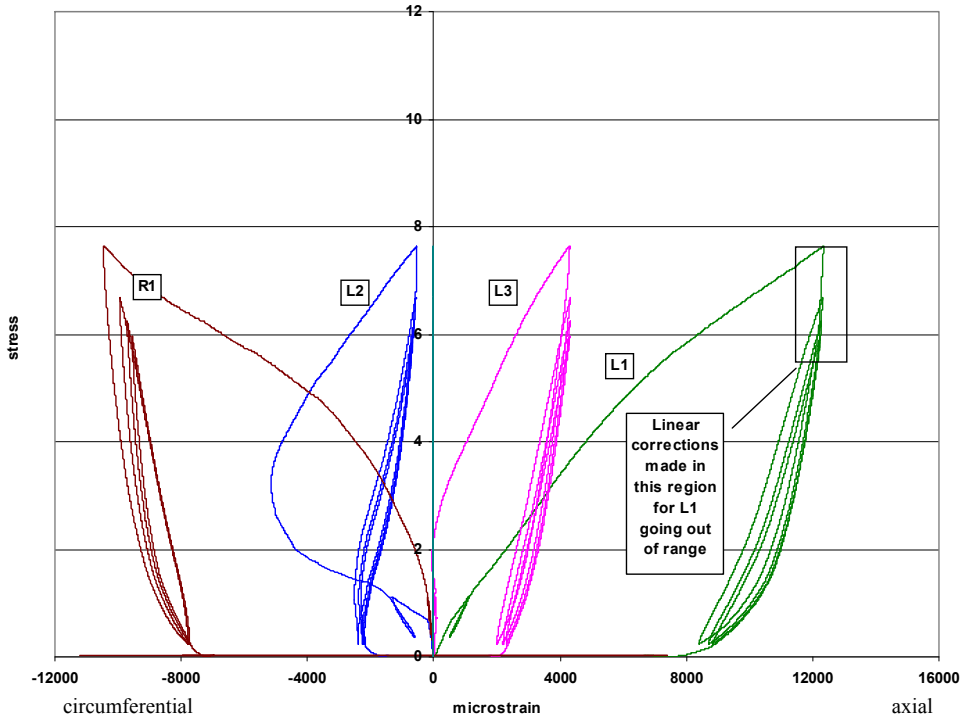

Figure 3-25 Specimen C6, Individual Gage Data for Minor Critical Event

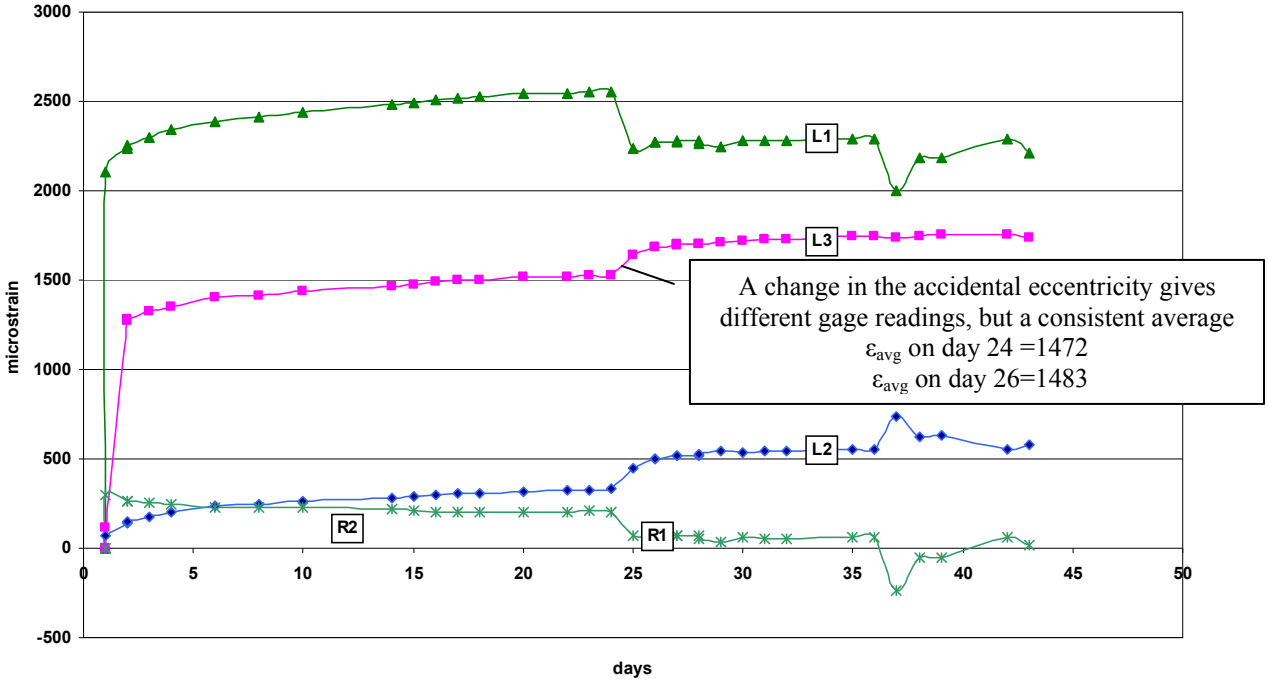

Figure 3-26 Specimen C6, Strains Under Sustained Load

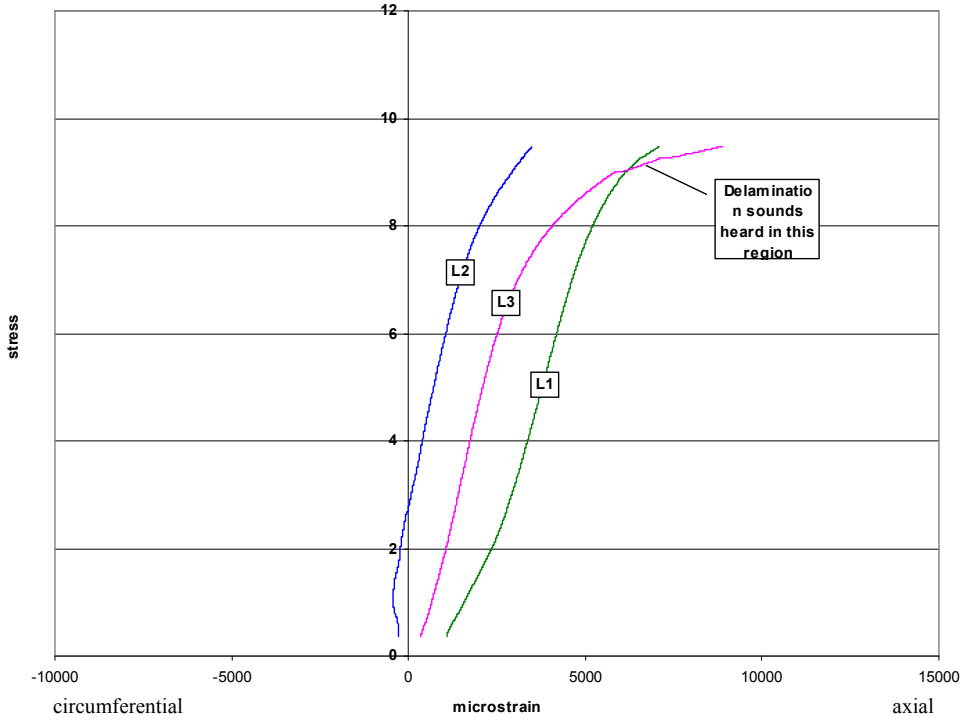

Figure 3-27 Specimen C6, Ultimate (Second) Loading, Individual Gage Data

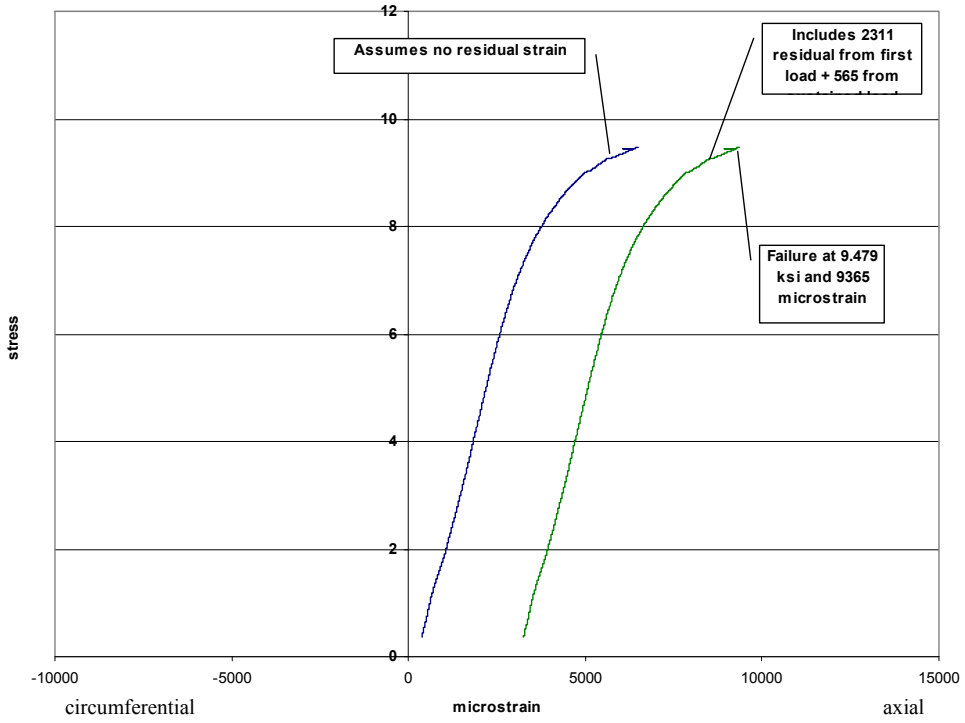

Figure 3-28 Specimen C6, Stress-Strain Response with Effects of Residual Strains

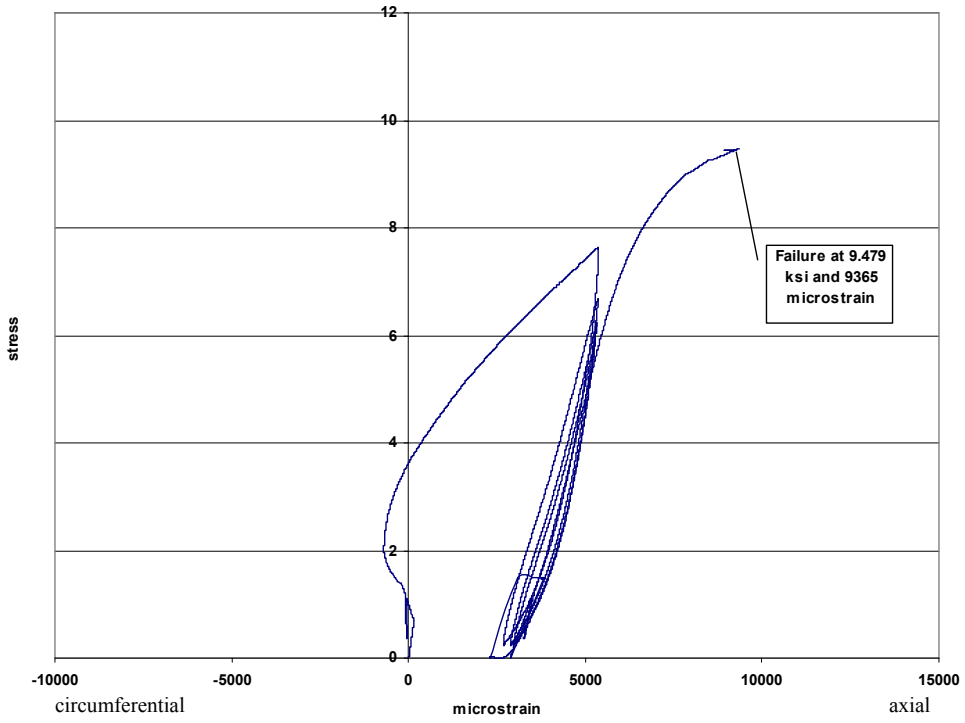

Figure 3-29 Specimen C6, Combined Average Stress Strain Response

Control Group Data Summary

Table 3-3 shows a summary of the ultimate data from control group.

Specimen	f'_{cc} (ksi)	ε_{cc} (microstrain)	Failure Mode	Sustained Load
C1	8.07	7,914	FRP Rupture	No
C2	9.49	9,918	FRP Rupture	No
C3	9.89	10,9412	Yielding	No
C4	9.52	7.490	De-lamination,	No
C5	9.42	10.992	Yielding	Yes
C6	9.48	9,366	Yielding	Yes

Table 3-3 Control Group Data Summary

3.3.2 Lab Group Results

Specimen L1

Specimen L1 was wrapped on day 109, placed under a sustained service load for 41 days starting on day 117, and broken monotonically on day 158. Specimen L1 failed at 9.141 ksi and 10,169 (average total) με by de-lamination as seen in Figure 3-30. All gages functioned throughout the test. Figure 3-31 shows the strain under the sustained loads and Figure 3-32 shows the individual gage responses under the ultimate loading. Figure 3-33 shows the combined stress-strain response resulting from the sustained service loading followed by the ultimate loading. The final stress-strain curve is the average of the individual gage responses plus a residual strain of 256 microstrain resulting from the sustained loading.

Figure 3-30 Specimen L1, Failure Mode

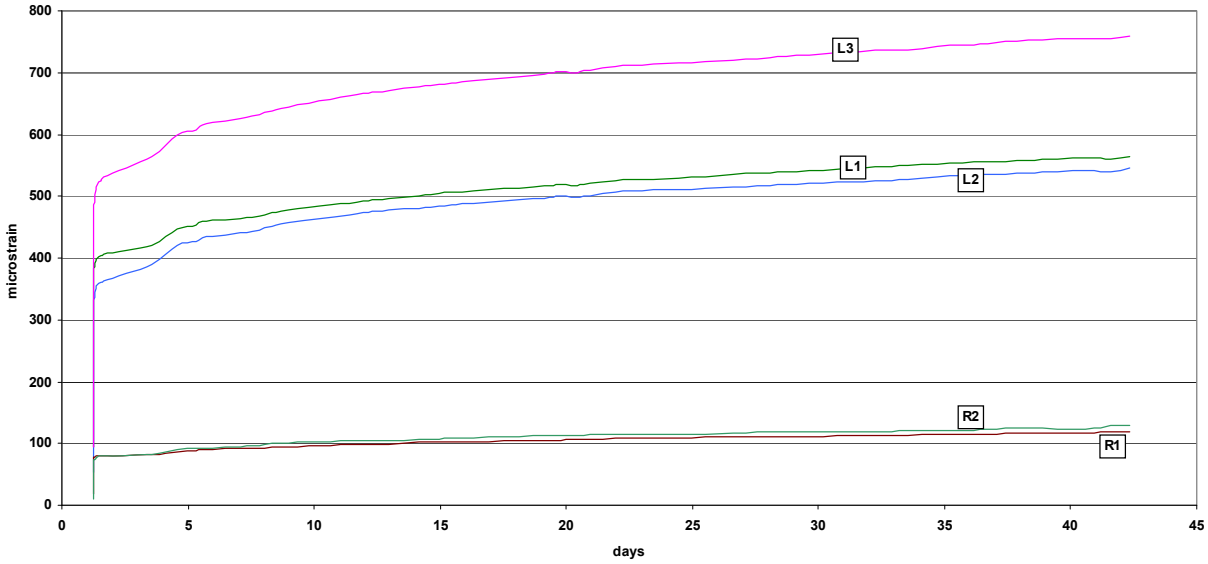

Figure 3-31 Specimen L1, Strains under Sustained Load

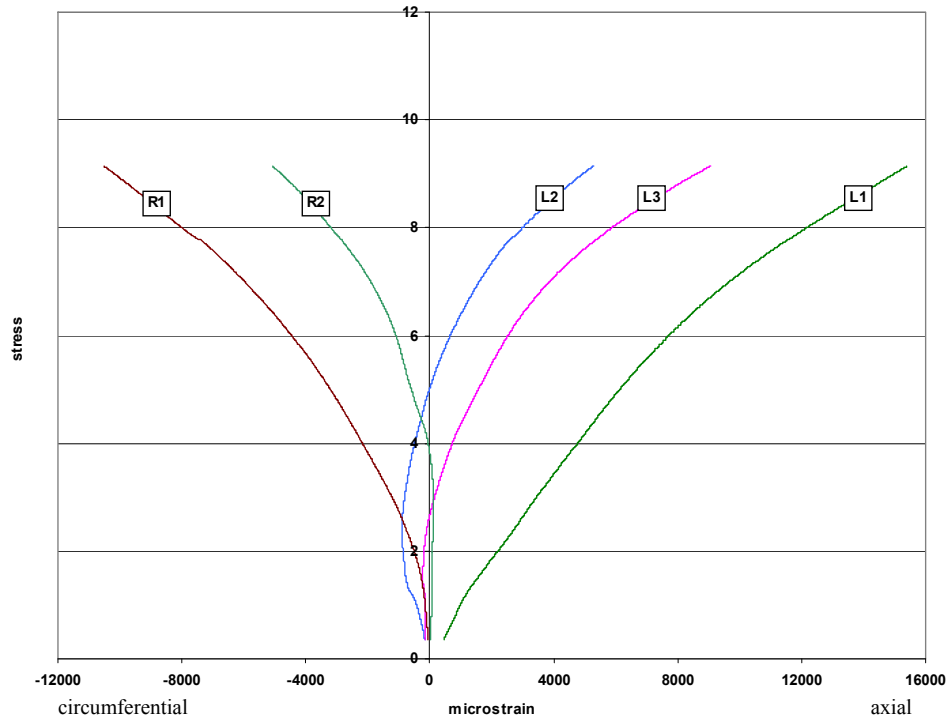

Figure 3-32 Specimen L1, Individual Gage Data

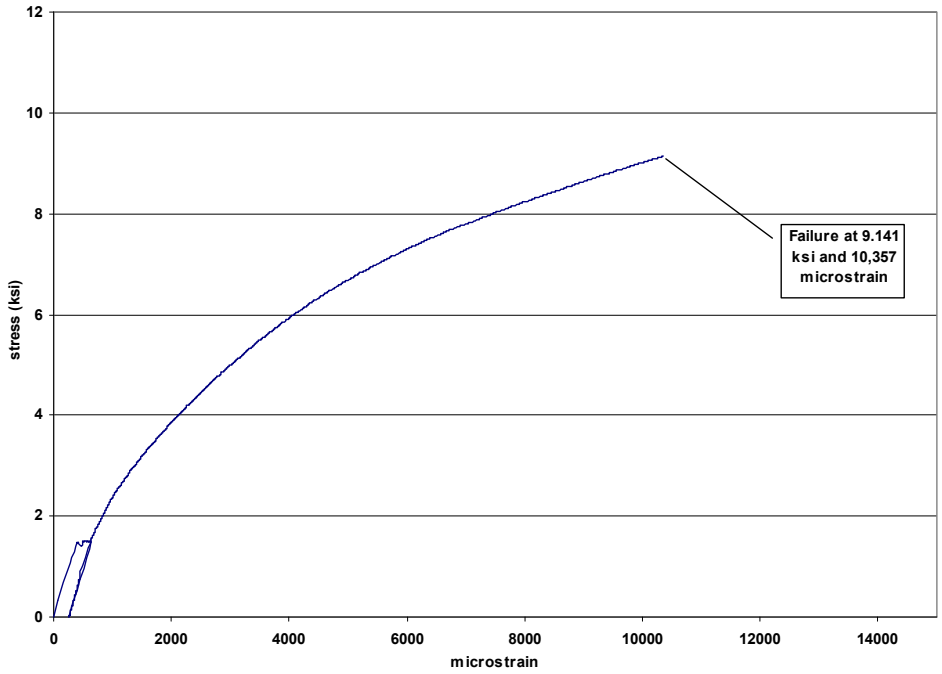

Figure 3-33 Specimen L1, Combined Stress-Strain Response

Specimen L2

Specimen L2 was wrapped on day 109, placed under a sustained service load for 41 days starting on day 117, and broken monotonically on day 158. It L2 failed at 9.893 ksi and 9,893 (average total) με by de-lamination as seen in Figure 3-34. All gages functioned throughout the test. Figure 3-35 shows the strain under the sustained loads and Figure 3-36 shows the individual gage responses under the ultimate loading. Figure 3-37 shows the combined stress-strain response resulting from the sustained service loading followed by the ultimate loading. The final stress-strain curve is the average of the individual gage responses plus a residual strain of 200 microstrain resulting from the sustained loading

Figure 3-34 Specimen L2, Failure Mode

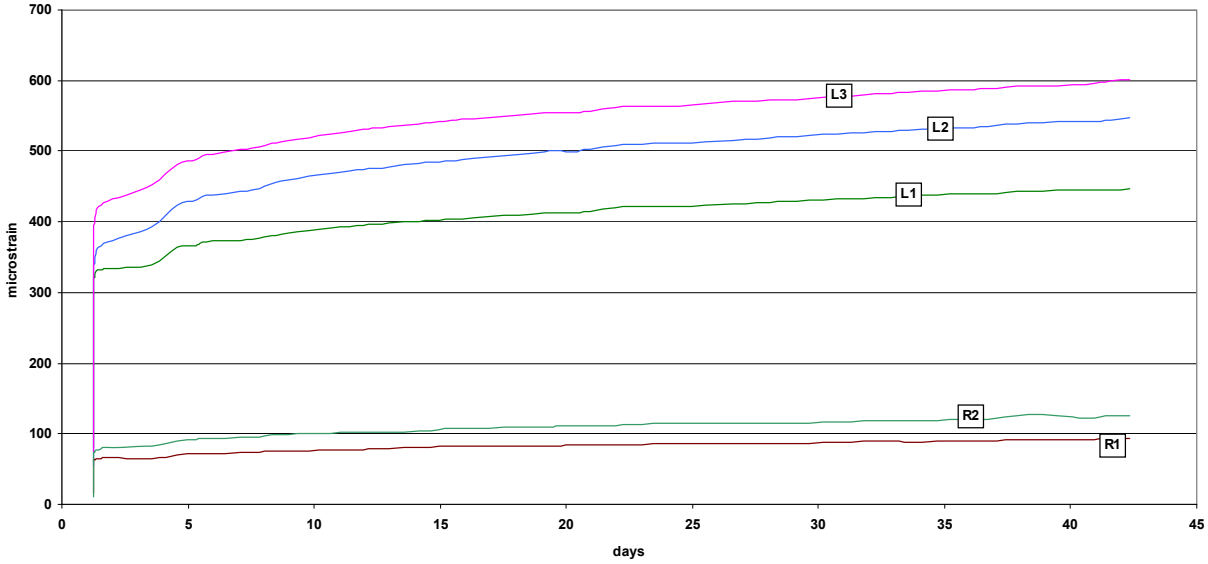

Figure 3-35 Specimen L2, Strains under Sustained Load

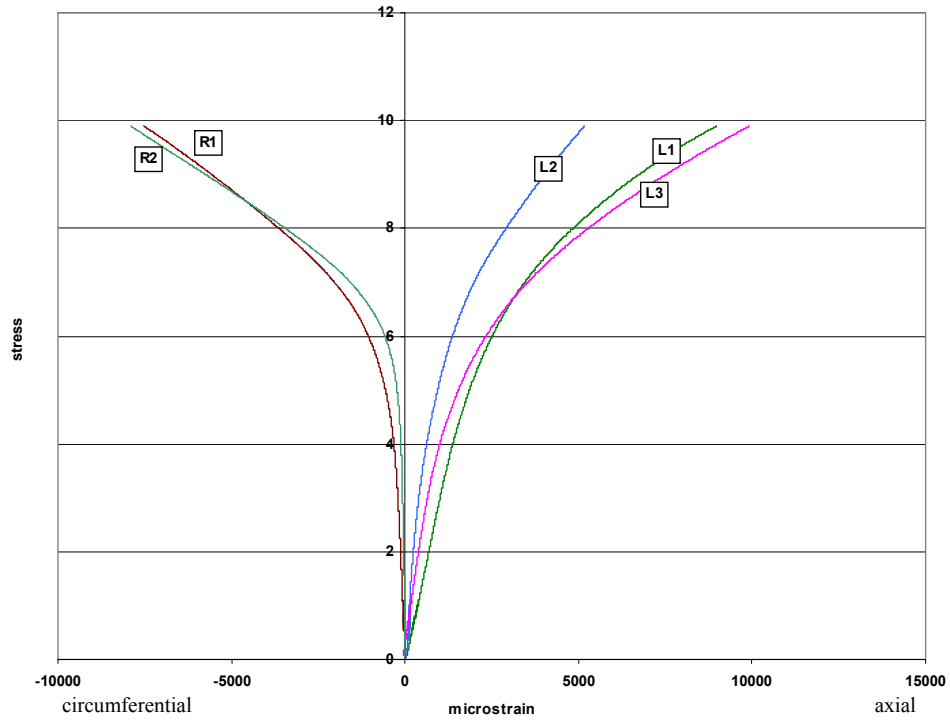

Figure 3-36 Specimen L2, Individual Gage Data

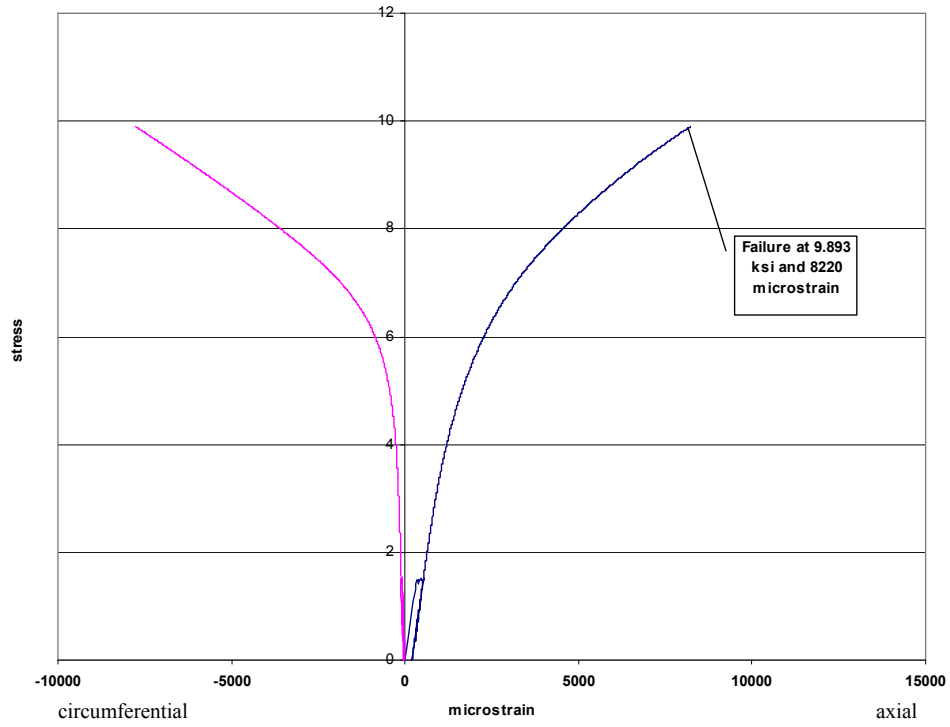

Figure 3-37 Specimen L2, Combined Stress-Strain Response

Specimen L3

Specimen L3 was wrapped on day 109, placed under a sustained service load for 41 days starting on day 117, and broken cyclically on day 158. Specimen L3 was initially loaded in the load amplification device. All strain gages functioned normally until after the start of the first unloading cycle at 216 kips. On the downward path, strain gage L3 failed at 154.45 kips. Based on the data available to this point, the future values of L3 were estimated at 0.91 of the values of L1. After completing three cycles, the plan called for a monotonic load increase to failure. However, when strain gage L1 also stopped reporting, the test was terminated as strain data could no longer be accurately collected. The specimen was placed in 'Big Purple' and loaded monotonically to failure which occurred at 9.658 ksi. Based on this failure stress and the prior load history, the failure strain was estimated at 12,562 (average total) με. The failure mode was FRP de-lamination as seen in Figure 3-38. Figure 3-39shows the strain under the sustained loads and Figure 3-40 shows the individual gage responses under the cyclic loading until the test was stopped due to gage failure. Figure 3-41 shows the combined stress-strain response resulting from the sustained service loading followed by the cyclic loading. The estimated failure point is indicated by the cross. The final stress-strain curve is the average of the individual gage responses plus a residual strain of 308 microstrain resulting from the sustained loading

Figure 3-38 Specimen L3, Failure Mode

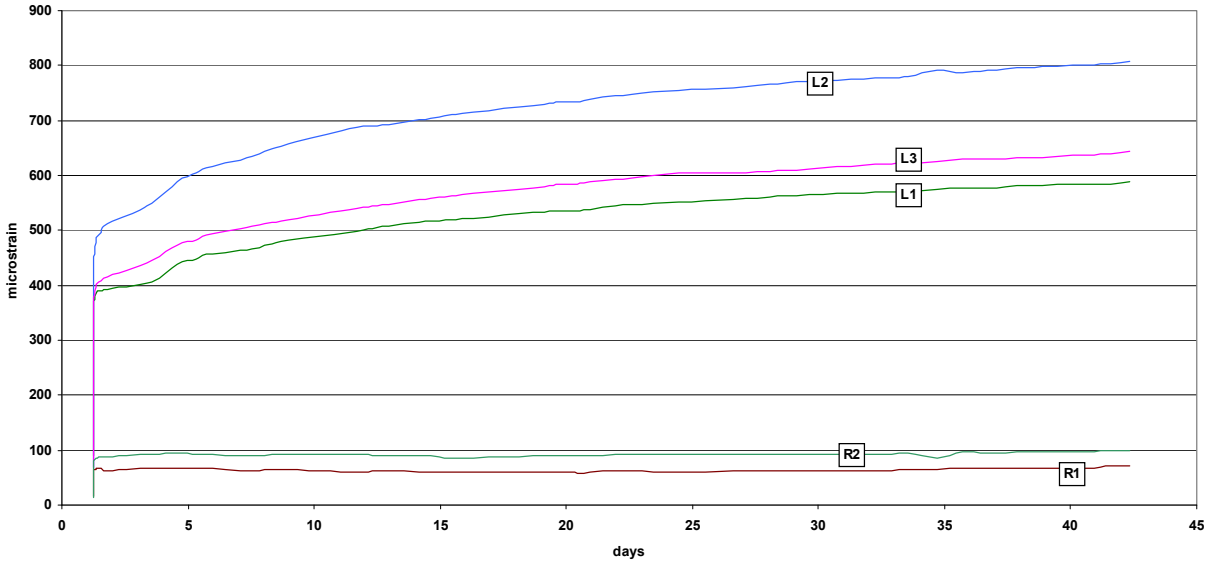

Figure 3-39 Specimen L3, Strains under Sustained Load

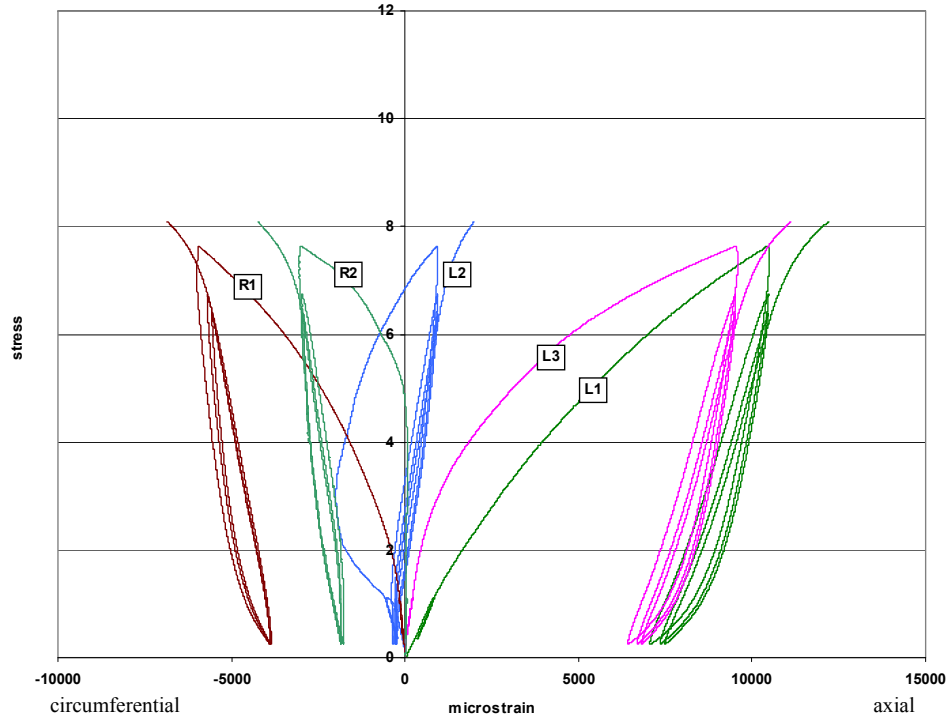

Figure 3-40 Specimen L3, Individual Gage Data

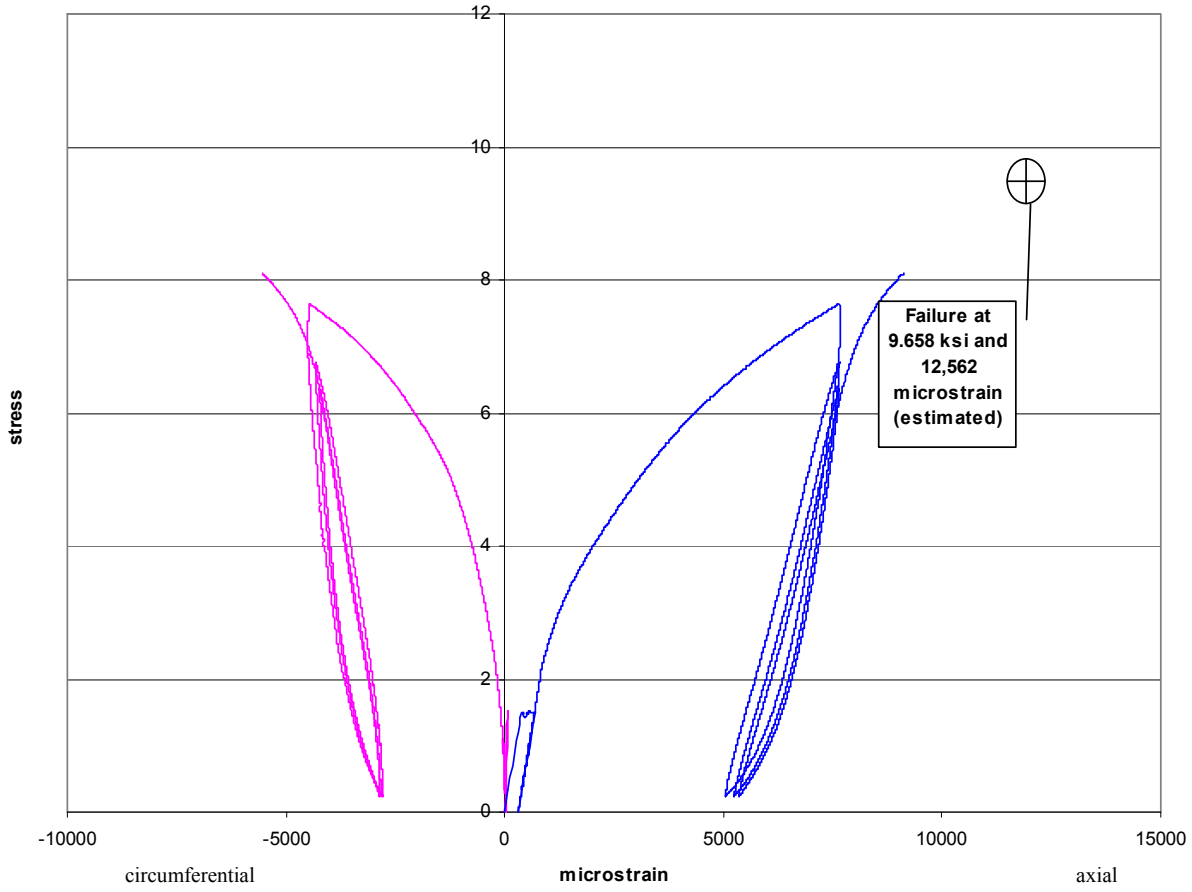

Figure 3-41 Specimen L3 Combined Stress Strain Response

Specimen L4

Specimen L4 was wrapped on day 109, placed under a sustained service load for 42 days starting on day 117, and broken cyclically on day 159. The residual strain resulting from the sustained loading was 309(average total) με. All strain gages functioned normally until strain gage L1 failed after the three load cycles at 240.76 kips. The subsequent values for L1 were estimated by a linear extrapolation of the slope prior to failure. Specimen L4 failed at 9.438 ksi and 11,704 (average total) με by de-lamination as seen in Figure 3-42. Figure 3-43 shows the strain under the sustained loads and Figure 3-44 shows the individual gage responses under the cyclic loading. Figure 3-45 shows the combined stress-strain response resulting from the sustained service loading followed by the cyclic loading. The final stress-strain curve is the average of the individual gage responses plus a residual strain of 309 microstrain resulting from the sustained loading

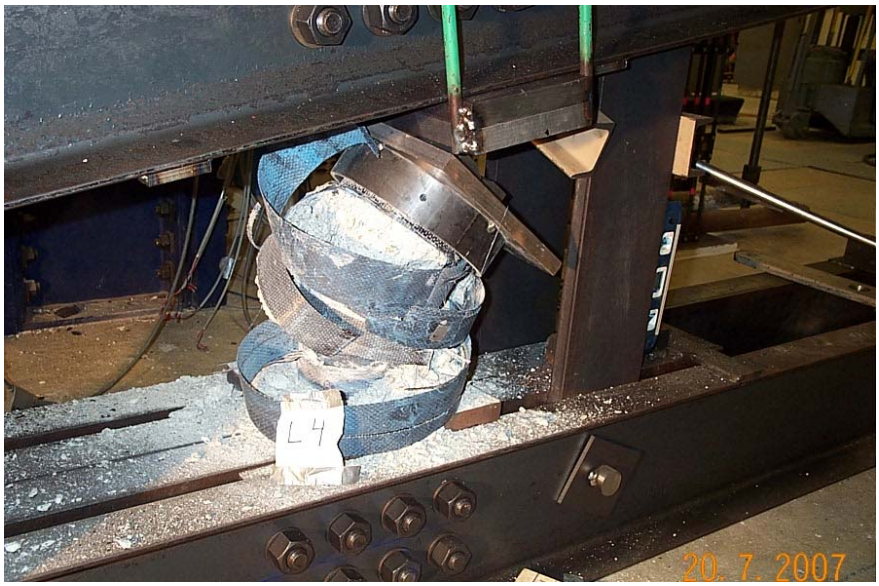

Figure 3-42 Specimen L4, Failure Mode

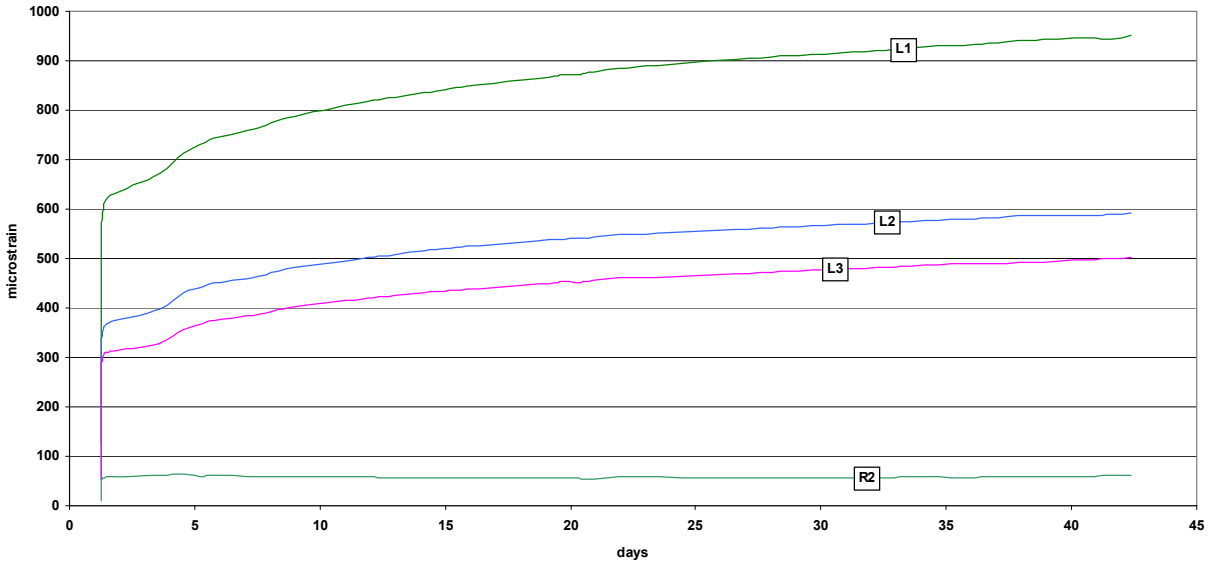

Figure 3-43 Specimen L4, Strain under Sustained Loads

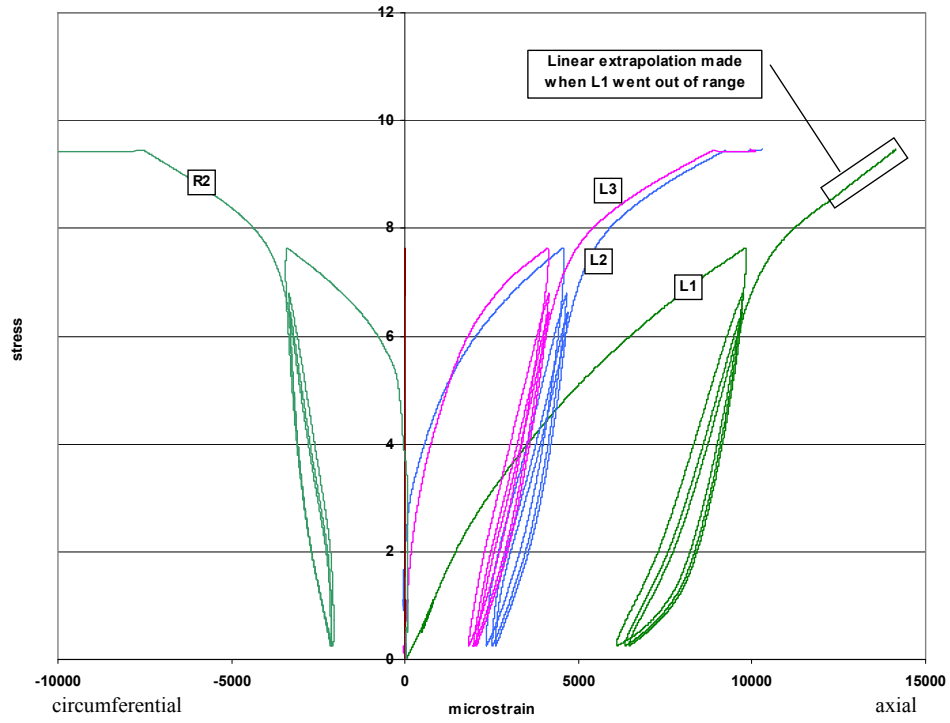

Figure 3-44 Specimen L4, Individual Gage Data

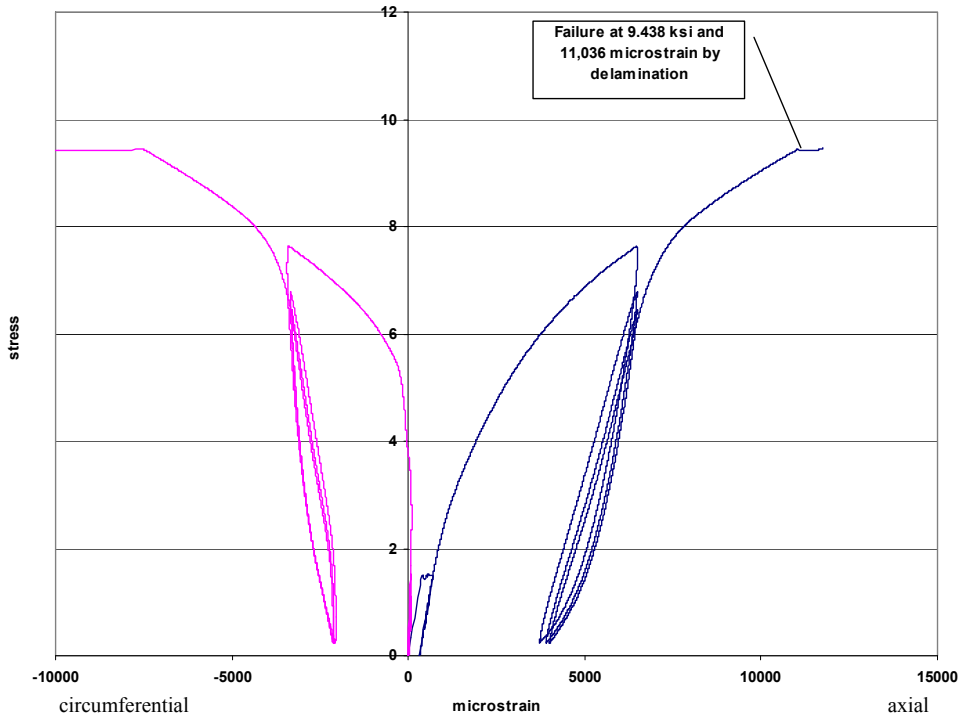

Figure 3-45 Specimen L4 Combined Stress Strain Response

Specimen L5

Specimen L5 was wrapped on day 109, placed under a sustained service load for 42 days starting on day 117, subjected to a minor critical event on day 159, and again placed under a sustained service load for an additional 40 days. This specimen was broken monotonically on day 199. It failed at 9.658 ksi and 14,981(average total) με. Strain gage L1 went out of range on the minor critical event test. Data was linearly approximated based on the readings when the gage functioned properly. This gage functioned properly on the remaining tests. Failure occurred by a combination of a small FRP rupture (Figure 3-46) concurrent with a yield type failure. Figure 3-47 shows the individual gage strains under the first sustained load and Figure 3-48 shows the individual gage data, as measured from a point of zero strain, from the minor critical event. Figure 3-49 shows the individual gage strains, measured from zero strain, for the second sustained which followed the minor critical event. The large change in the readings of the strain gages on day 20 was caused by the removal of the sustained service loading to allow for the removal of two test cylinders from the same load frame. The average behavior remained constant. Figure 3-50 shows the individual gage data from the final ultimate loading as measured from a point of zero strain, and Figure 3-51 shows the combined average stress-strain history of specimen L5 where the permanent strain offsets from each load step are accounted for in subsequent behavior.

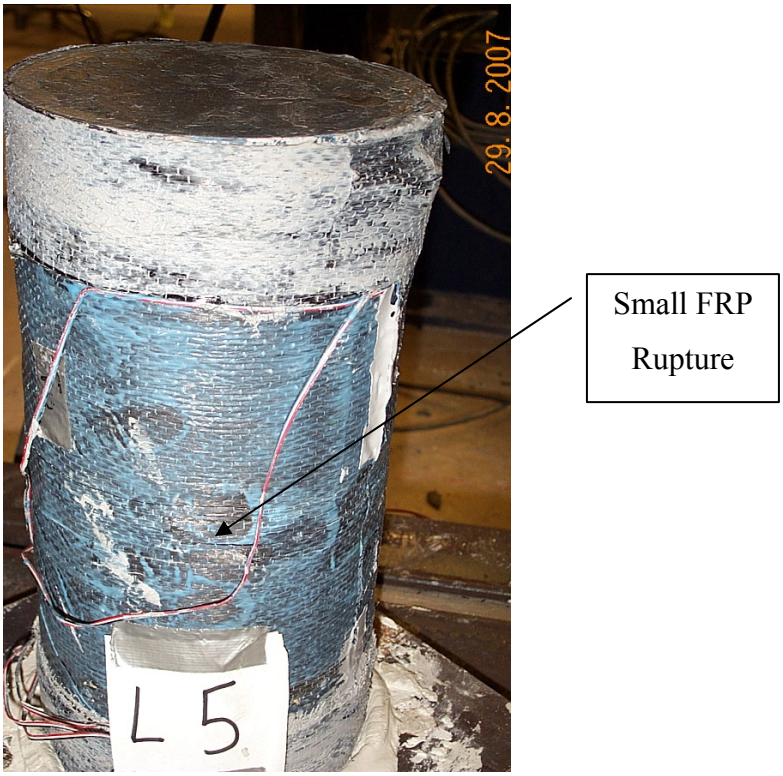

Figure 3-46 Specimen L5, Failure Mode

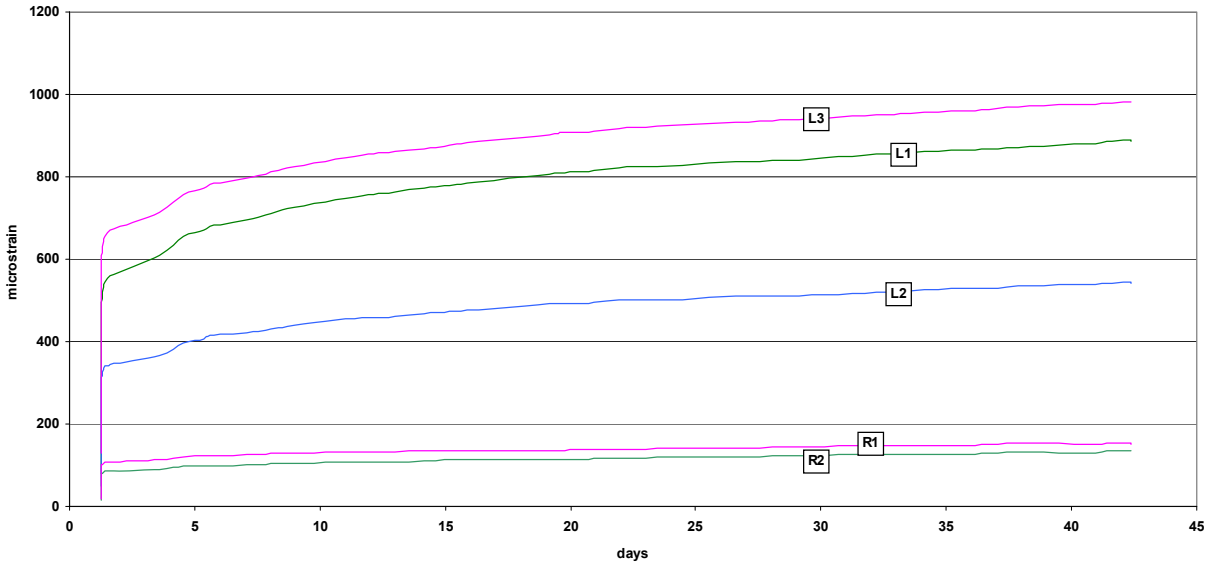

Figure 3-47 Specimen L5, First Sustained Load

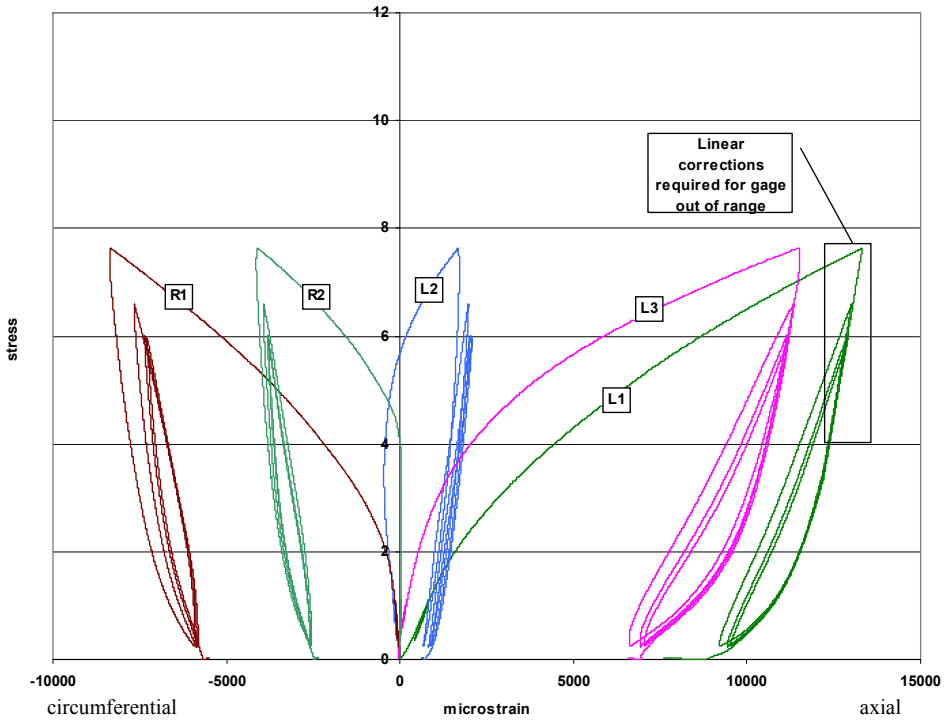

Figure 3-48 Specimen L5, Minor Critical Event, Individual Gage Data

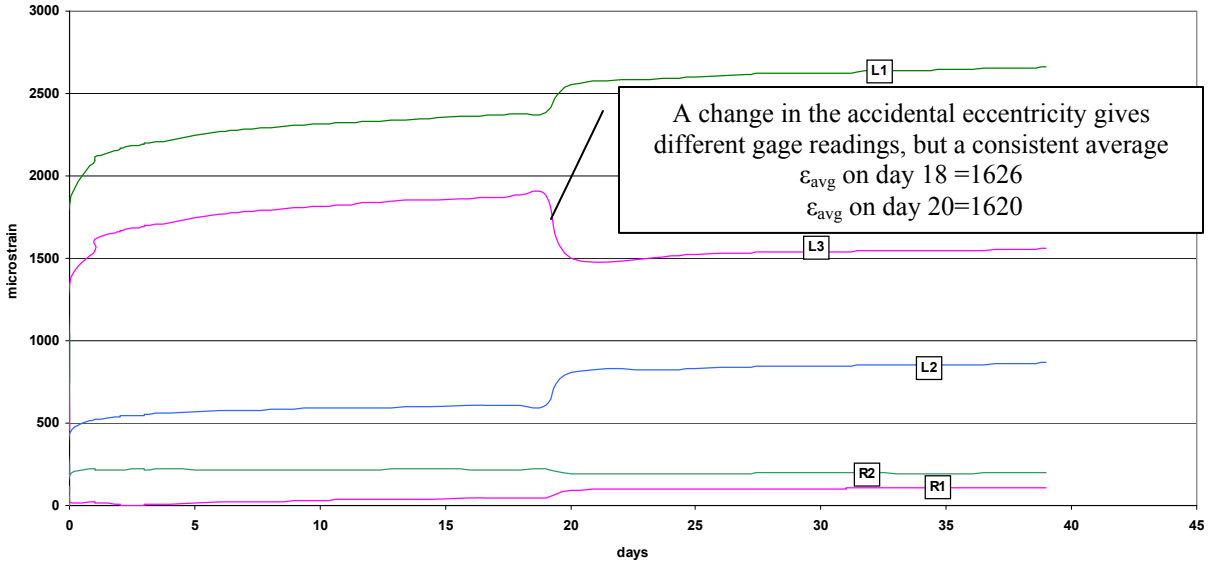

Figure 3-49 Specimen L5, Second Sustained Loading

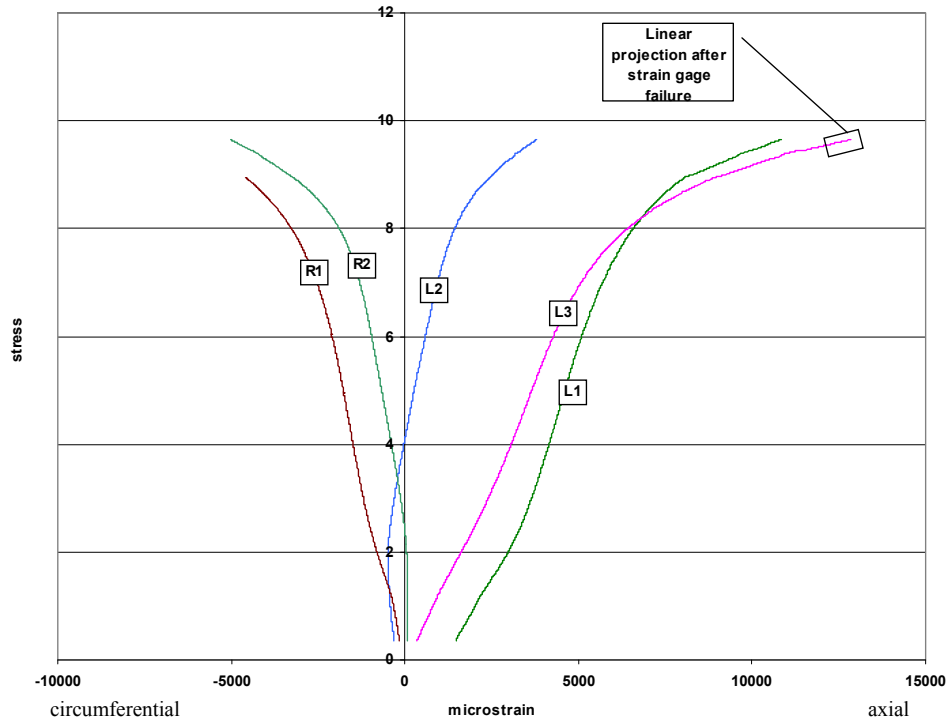

Figure 3-50 Specimen L5, Ultimate Loading, Individual Gage Data

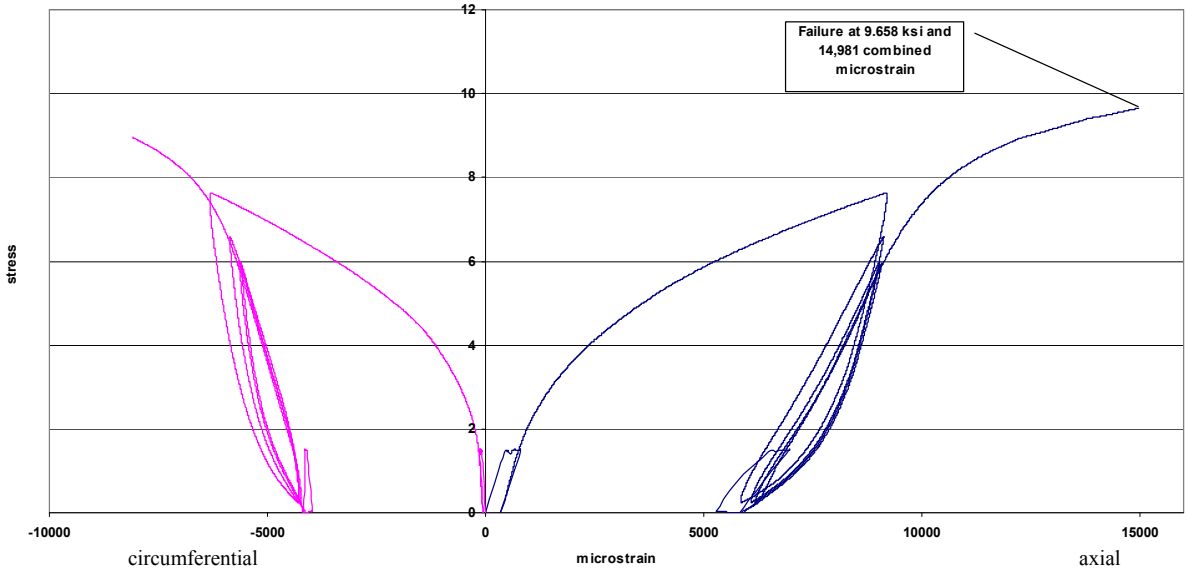

Figure 3-51 Specimen L5, Combined Stress-Strain Response

Specimen L6

Specimen L6 was wrapped on day 109, placed under a sustained service load for 42 days starting on day 117, subjected to a minor critical event on day 159, and again placed under a

sustained service load for an additional 40 days. This specimen was broken monotonically on day 199. It failed at 8.811 ksi and 10,147 (average total) με. All strain gages functioned for all tests, but strain gage R1 displayed erratic behavior on both sustained load tests. No reason could be determined. Failure occurred by de-lamination as seen in Figure 3-52 concurrent with a yield type failure. Figure 3-53 shows the individual gage strains under the first sustained load and Figure 3-54 shows the individual gage data, as measured from a point of zero strain, from the minor critical event. Figure 3-55 shows the individual gage strains, measured from zero strain, for the second sustained load which followed the minor critical event. The large change in the readings of the strain gages on day 20 was caused by the removal of the sustained service loading to allow for the removal of two test cylinders from the same load frame. The average behavior remained constant. Figure 3-56 shows the individual gage data from the final ultimate loading as measured from a point of zero strain, and Figure 3-57 shows the combined average stress-strain history of specimen L6 where the permanent strain offsets from each load step are accounted for in subsequent behavior.

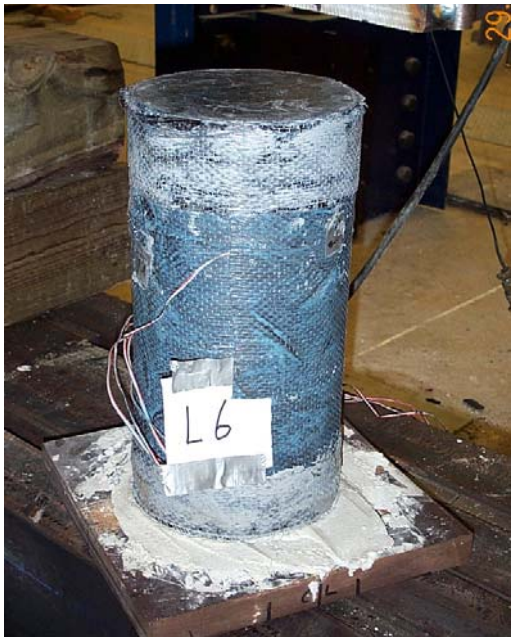

Figure 3-52 Specimen L6, Failure Mode

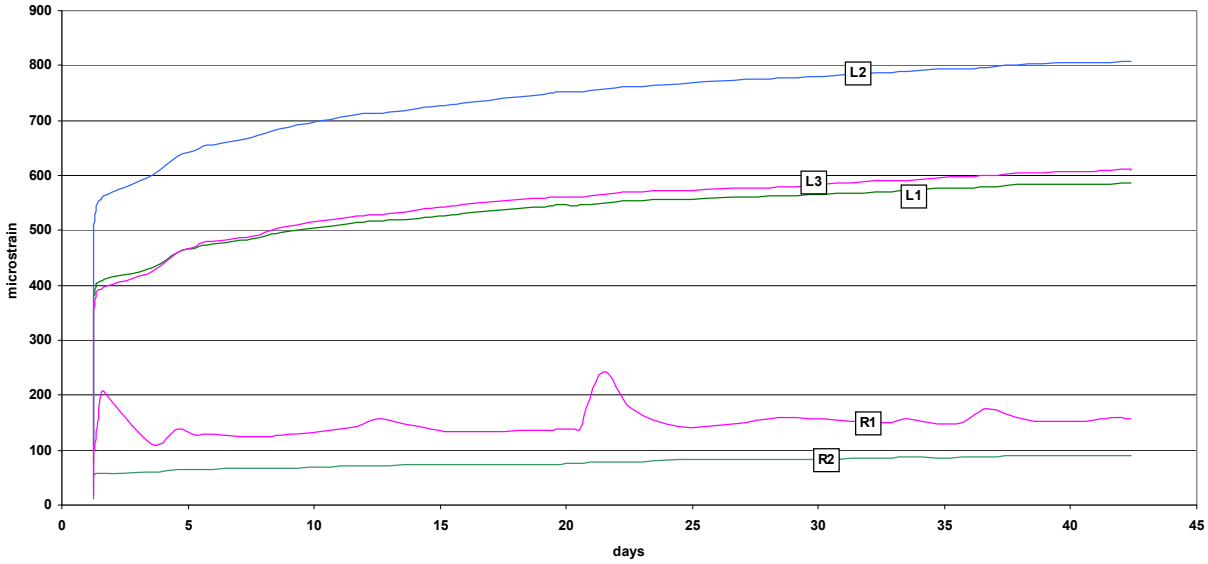

Figure 3-53 Specimen L6, First Sustained Load

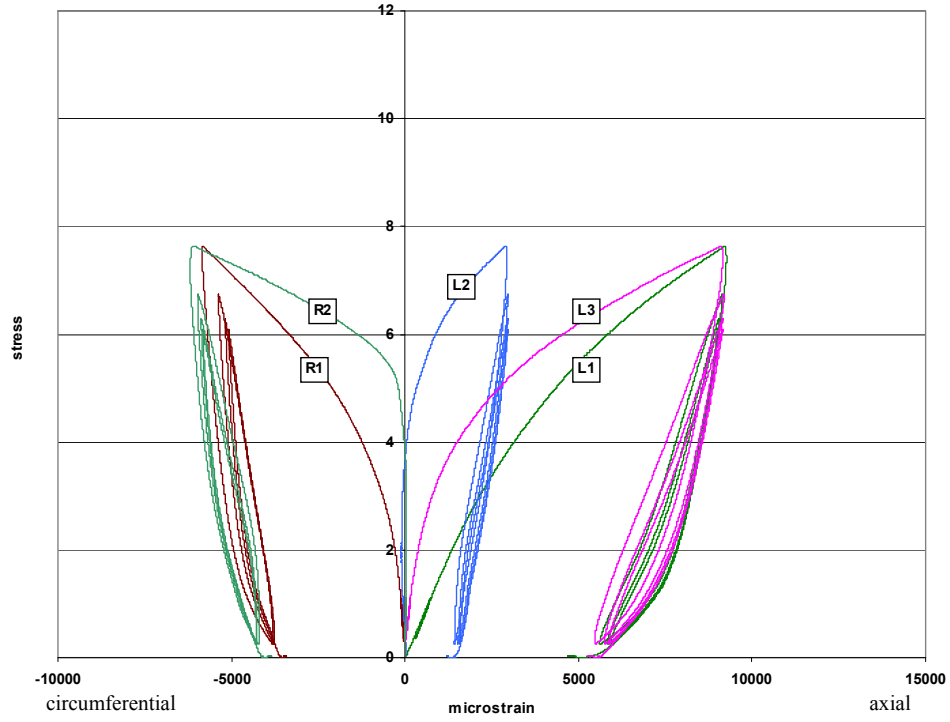

Figure 3-54 Specimen L6, Minor Critical Event, Individual Gage Data

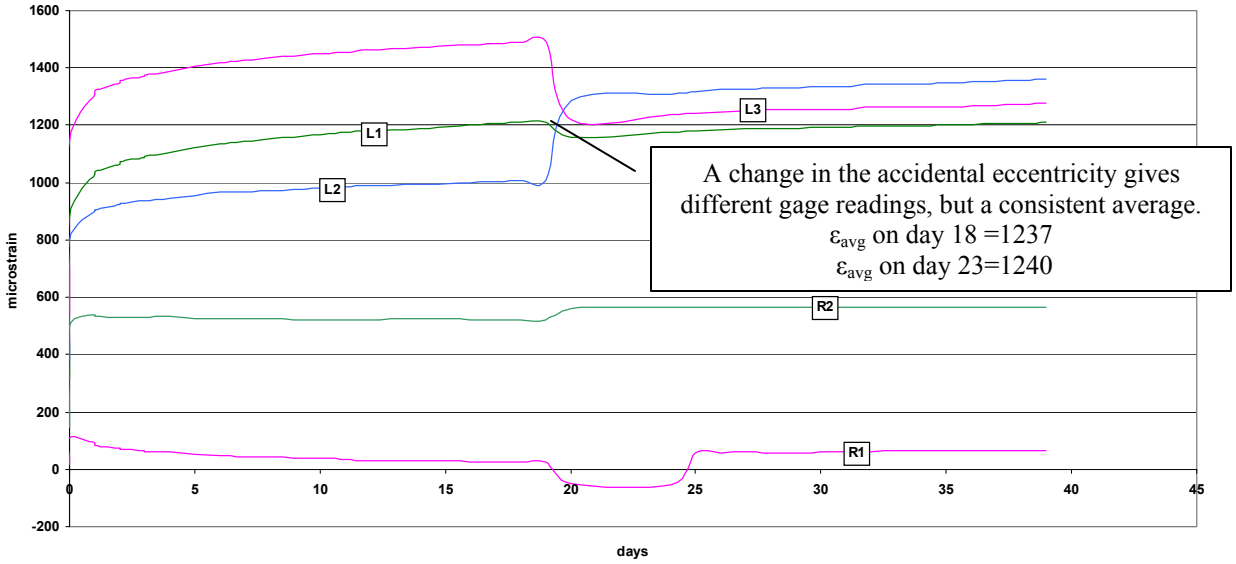

Figure 3-55 Specimen L6, Second Sustained Load

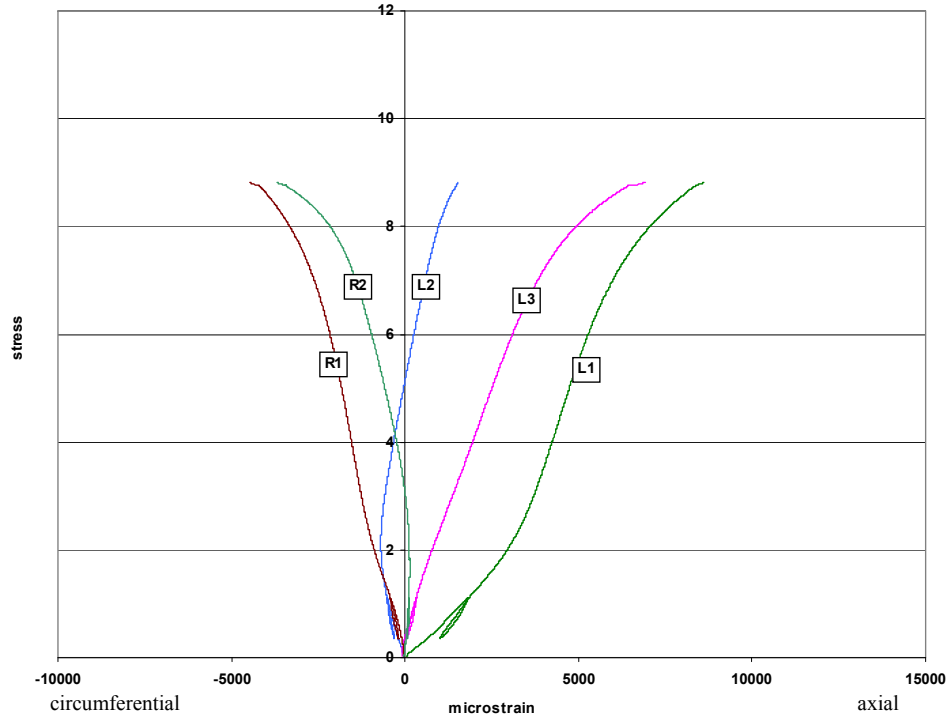

Figure 3-56 Specimen L6, Ultimate Loading, Individual Gage Data

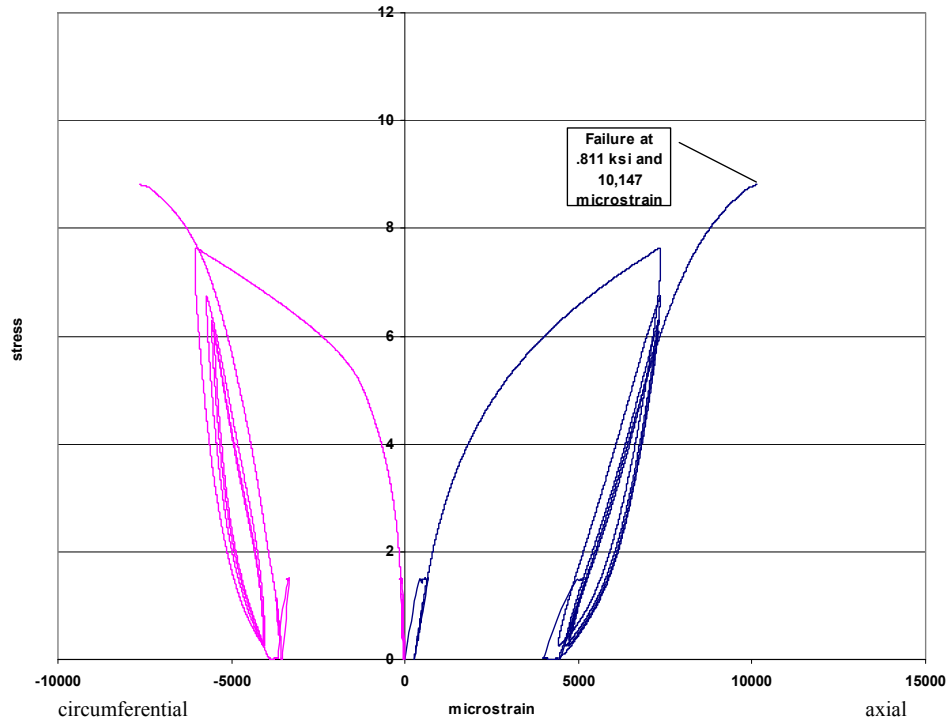

Figure 3-57 Specimen L6, Combined Stress-Strain Response

Lab Group Data Summary

Table 3-4 shows a summary of the ultimate data from the lab group. Specimens L5 and L6 were subjected to a minor critical event after 42 days of sustained loading then returned for an additional 40 days of sustained loading.

Specimen	f'_{cc} (ksi)	ε_{cc} (microstrain)	Failure Mode	Sustained Load
L1	9.141	10,357	de-lamination	41 days
L2	9.893	8,220	de-lamination	41 days
L3	9.658	12,562 (estimate)	de-lamination	41 days
L4	9.438	11,036	de-lamination	42 days
L5	9.658	14,981	rupture + yield	42+40 days
L6	8.811	10,147	de-lam. + yield	42+40 days

Table 3-4 Lab Group Data Summary

3.3.3 Retrofit Group

Specimen R1

Specimen R1 was placed under a sustained service load for 42 days starting on day 159. The specimen was wrapped under load on day 190 and broken monotonically on day 201. It failed at 8.771 ksi and 11,953 (average total) με. Strain gage L1 went out of range at 6.859 ksi and 12,260 με. Further values were estimated by a linear projection of the response from this point. Failure occurred by FRP rupture as seen in Figure 3-58. Figure 3-59 shows the individual gage strains under the first sustained load and Figure 3-60 shows the individual gage data, as measured from a point of zero strain. Figure 3-61 shows the combined average stress-strain history of specimen R1 where the permanent strain offsets from each load step are accounted for in subsequent behavior.

Figure 3-58 Specimen R1, Failure Mode

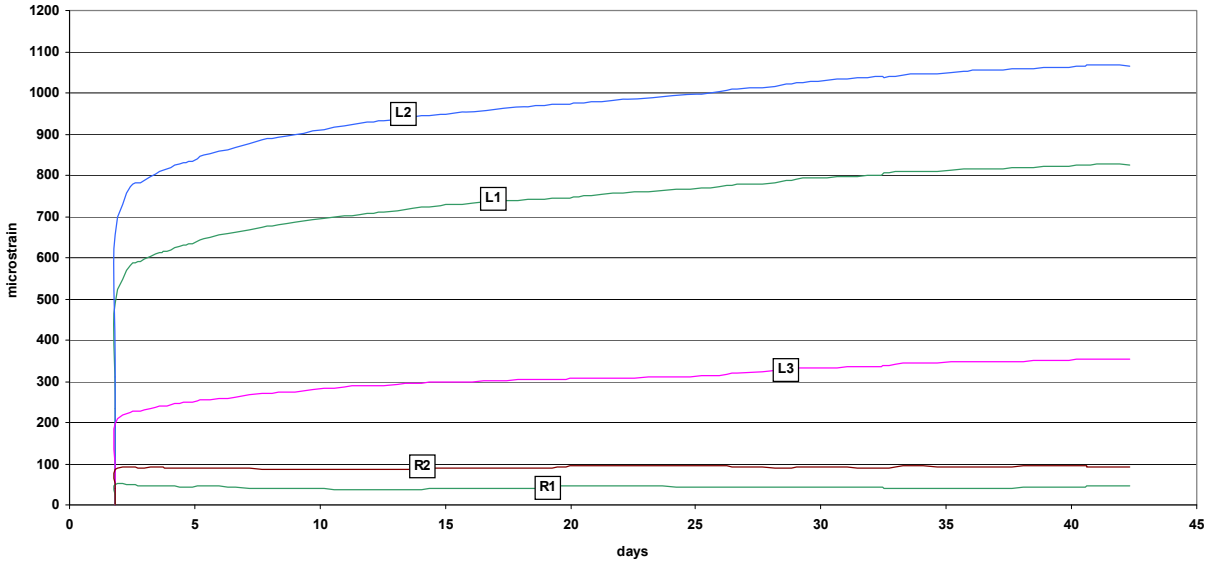

Figure 3-59 Specimen R1, Strain under Sustained Load

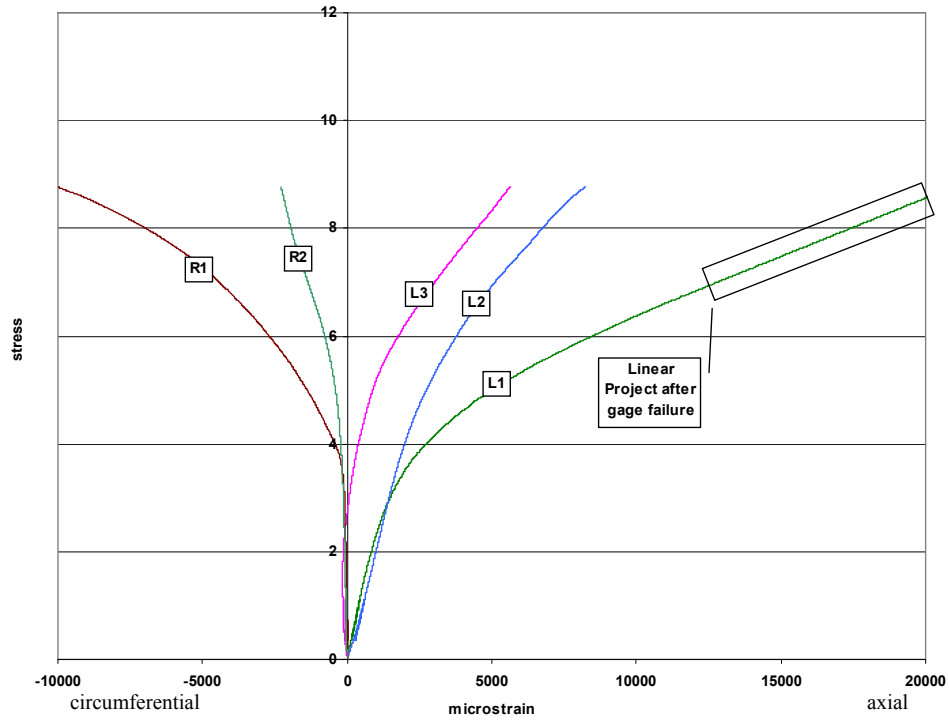

Figure 3-60 Specimen R1, Individual Gage Data

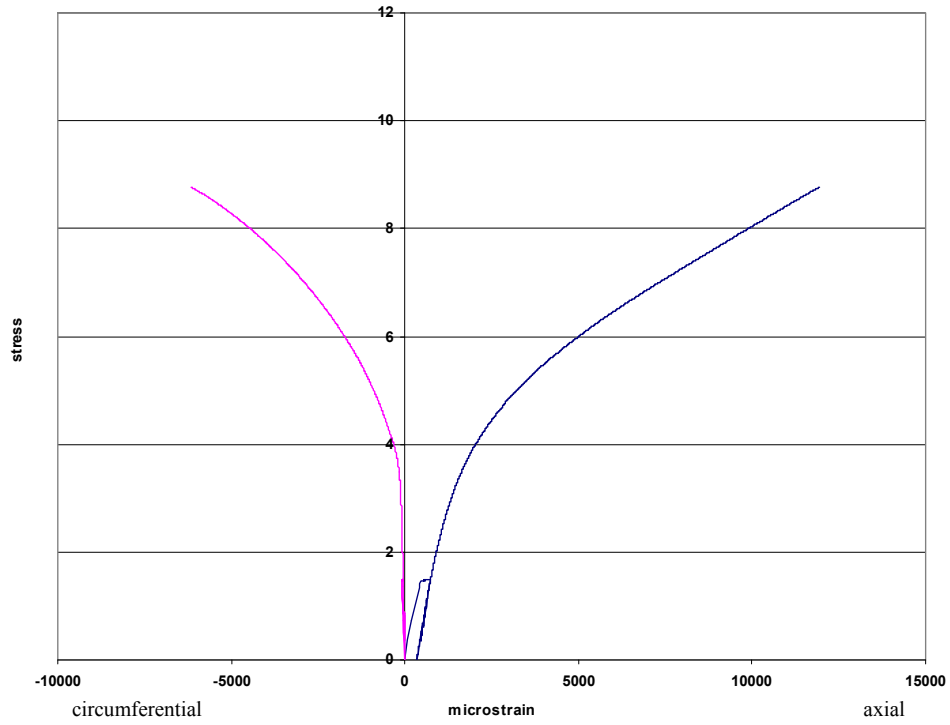

Figure 3-61 Specimen R1, Combined Stress-Strain Response

Specimen R2

Specimen R2 was placed under a sustained service load for 42 days starting on day 159. The specimen was wrapped under load on day 198 and broken monotonically on day 201. It failed at 7.337 ksi and 9,593 (average total) με. Strain gageL1 went out of range at 7.200 ksi and 12,283 με. Further values were estimated by a linear projection of the response from this point. Failure occurred by FRP de-lamination as seen in Figure 3-62. Figure 3-63 shows the individual gage strains under the first sustained load and Figure 3-64 shows the individual gage data for the ultimate loading, as measured from a point of zero strain. Figure 3-65 shows the combined average stress-strain history of specimen R2 where the permanent strain offsets from each load step are accounted for in subsequent behavior. Figure 3-64 and Figure 3-65 also demonstrates the progressive nature of the de-lamination in this specimen. The de-lamination began at about 7.1 ksi which resulted in a load re-distribution in the FRP jacket followed by an additional increase in load until failure. This is the only specimen to exhibit this behavior to this degree.

Figure 3-62 Specimen R2, Failure Mode

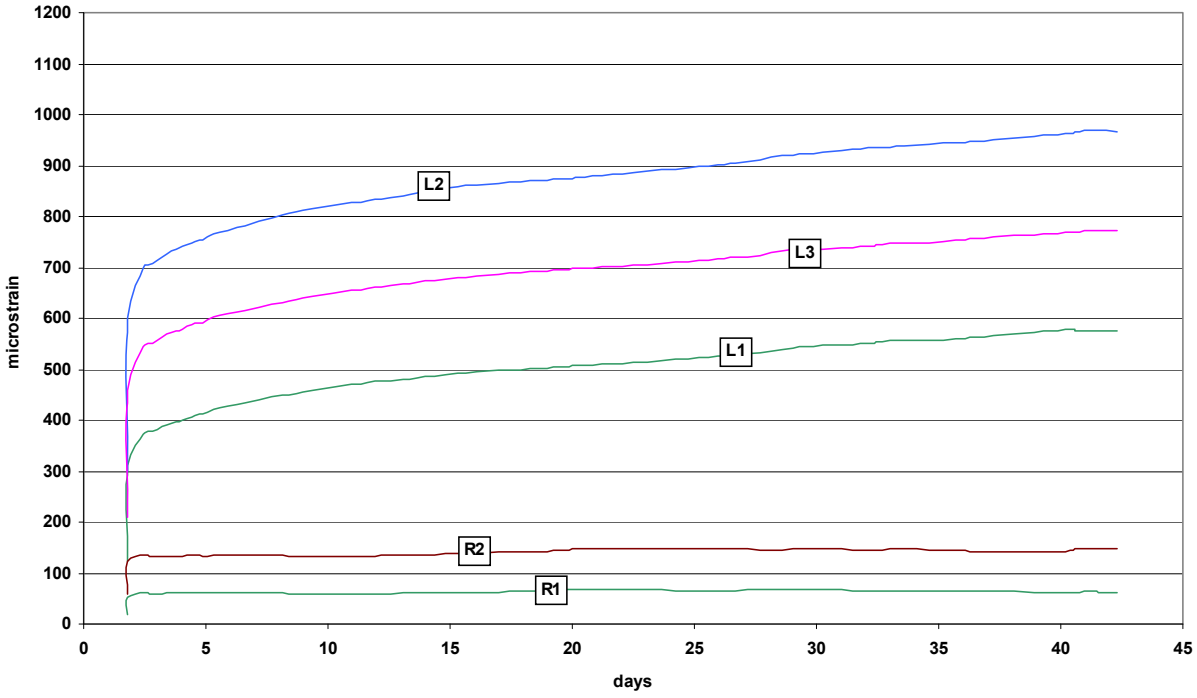

Figure 3-63 Specimen R2, Strain under Sustained Load

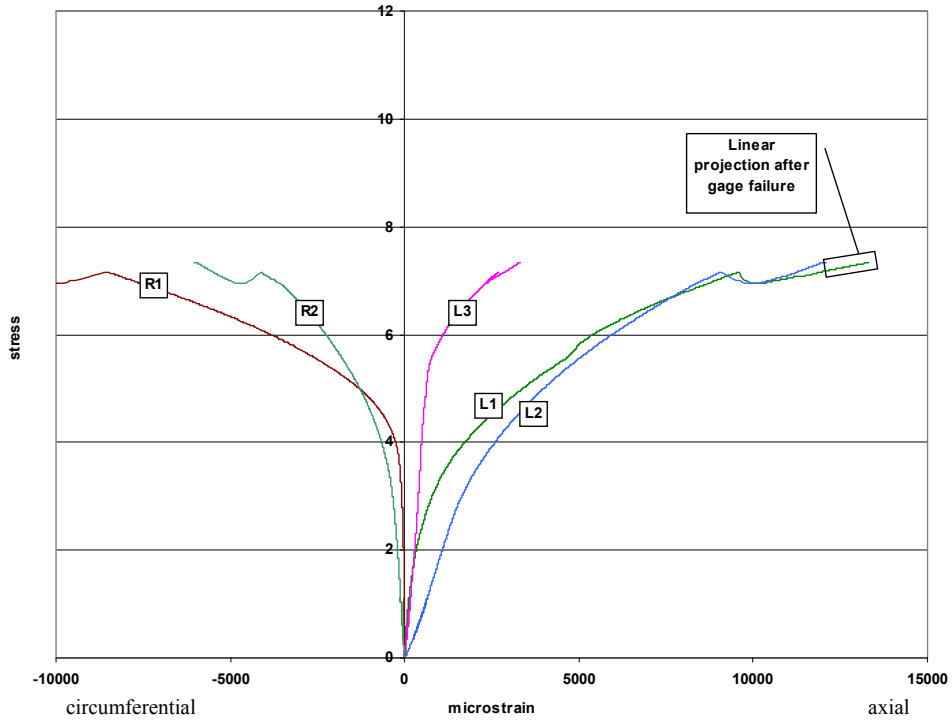

Figure 3-64 Specimen R2, Individual Gage Data

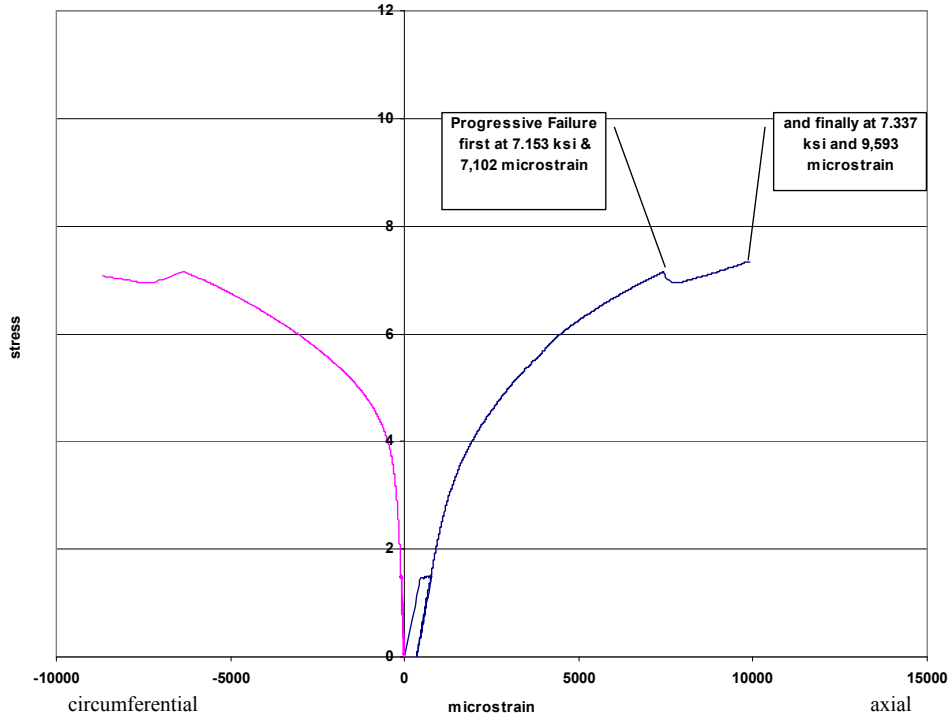

Figure 3-65 Specimen R2, Combined Stress-Strain Response

Specimen R3

Specimen R3 was placed under a sustained service load for 42 days starting on day 159. The specimen was wrapped under load on day 190 and broken monotonically on day 201. It failed at 10.147 ksi and 10,764 (average total) με. Strain gage L3 went out of range at 8.468 ksi and 12,260 με. Further values were estimated by a linear projection of the response from this point. Failure occurred by FRP de-lamination as seen in Figure 3-66. Figure 3-67 shows the individual gage strains under the first sustained load and Figure 3-68 shows the individual gage data for the ultimate loading, as measured from a point of zero strain. Figure 3-69 shows the combined average stress-strain history of specimen R3 where the permanent strain offsets from each load step are accounted for in subsequent behavior.

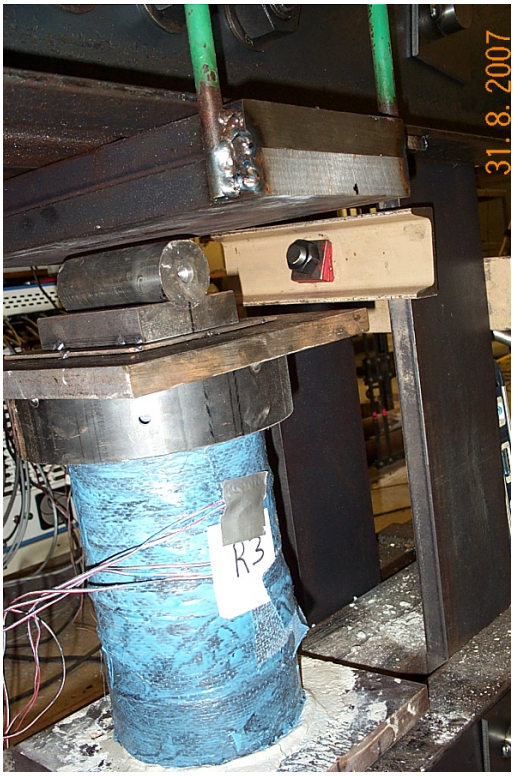

Figure 3-66 Specimen R3, Failure Mode

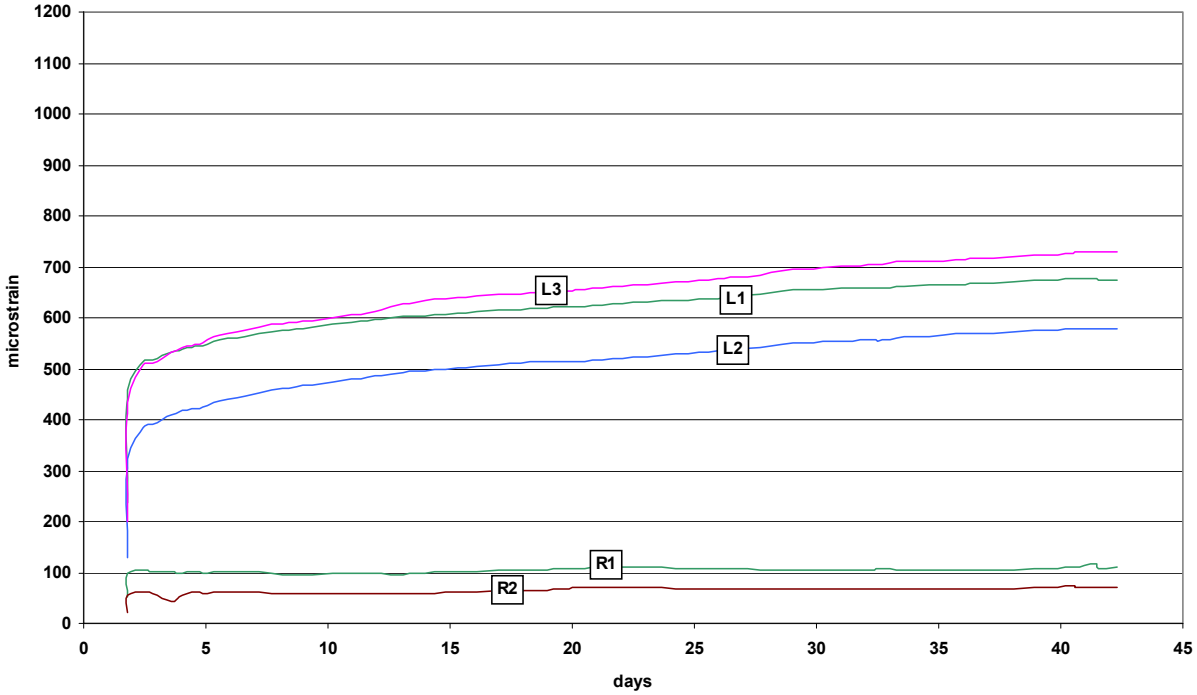

Figure 3-67 Specimen R3, Strain under Sustained Load

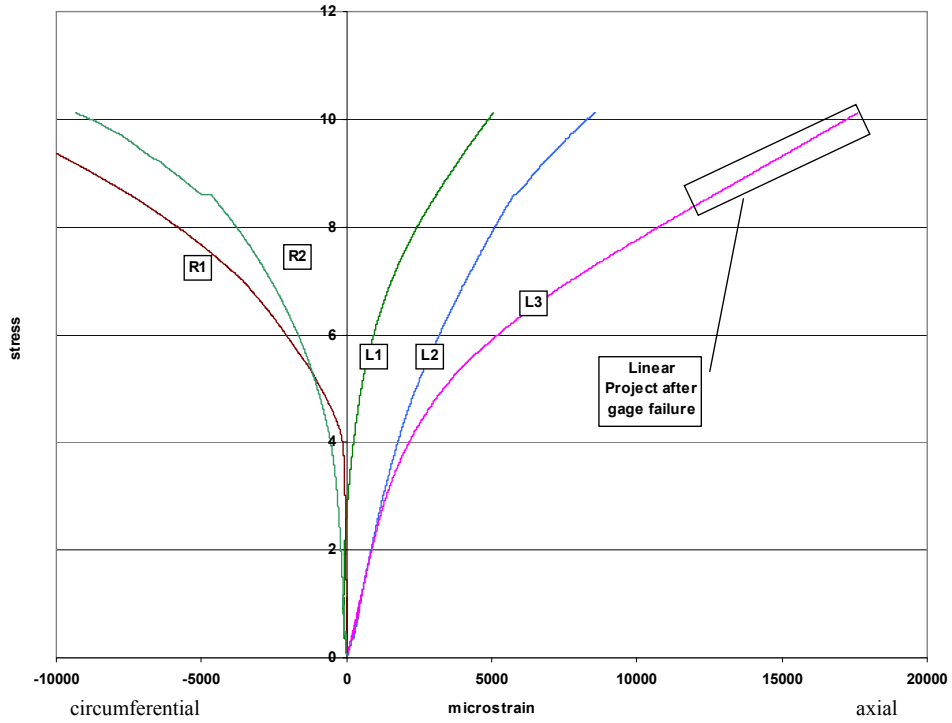

Figure 3-68 Specimen R3, Individual Gage Data

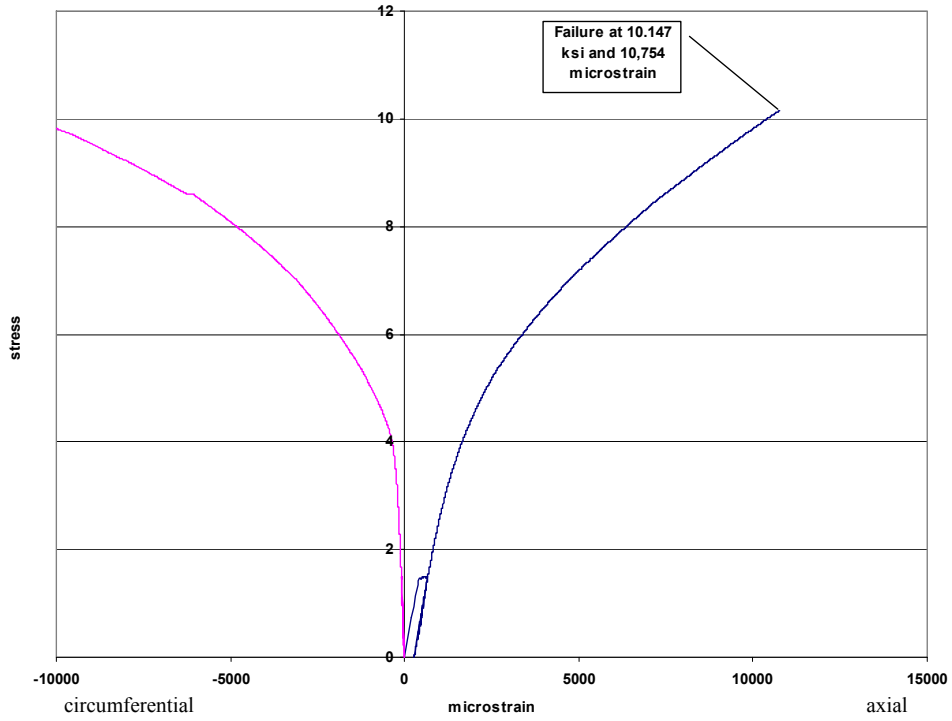

Figure 3-69 Specimen R3, Combined Stress-Strain Response

Specimen R4

Specimen R4 was placed under a sustained service load for 41 days starting on day 159. The specimen was wrapped under load on day 190. R4 was subjected to a minor critical event on day 200 then returned to the sustained load device until day 240 when it was broken monotonically. The specimen failed at 9.494 ksi and 15,932 (average total) με. The second loading took place initially in the load amplification device. When this device reached its displacement limit, the specimen was removed and broken in 'Big Purple'. Failure occurred by FRP de-lamination as seen in Figure 3-70. Figure 3-71 shows the individual gage strains under the first sustained load and Figure 3-72 shows the individual gage data for the minor critical event loading, as measured from a point of zero strain. Strain Gage R1 did not function during this test. Figure 3-73 show the results of the second sustained service loading and Figure 3-74 shows the individual gage data, again measured from zero strain, of the second, ultimate loading. Strain Gage L2 went out of range at 9.088 ksi and 4,300 με. As strain gage R2 was functioning at the time and had a good load history, the missing values for L2 were estimated using the strain

ratio of R2 to L2. Figure 3-75 shows the combined average stress-strain history of specimen R4 where the permanent strain offsets from each load step are accounted for in subsequent behavior.

Figure 3-70 Specimen R4, Failure Mode

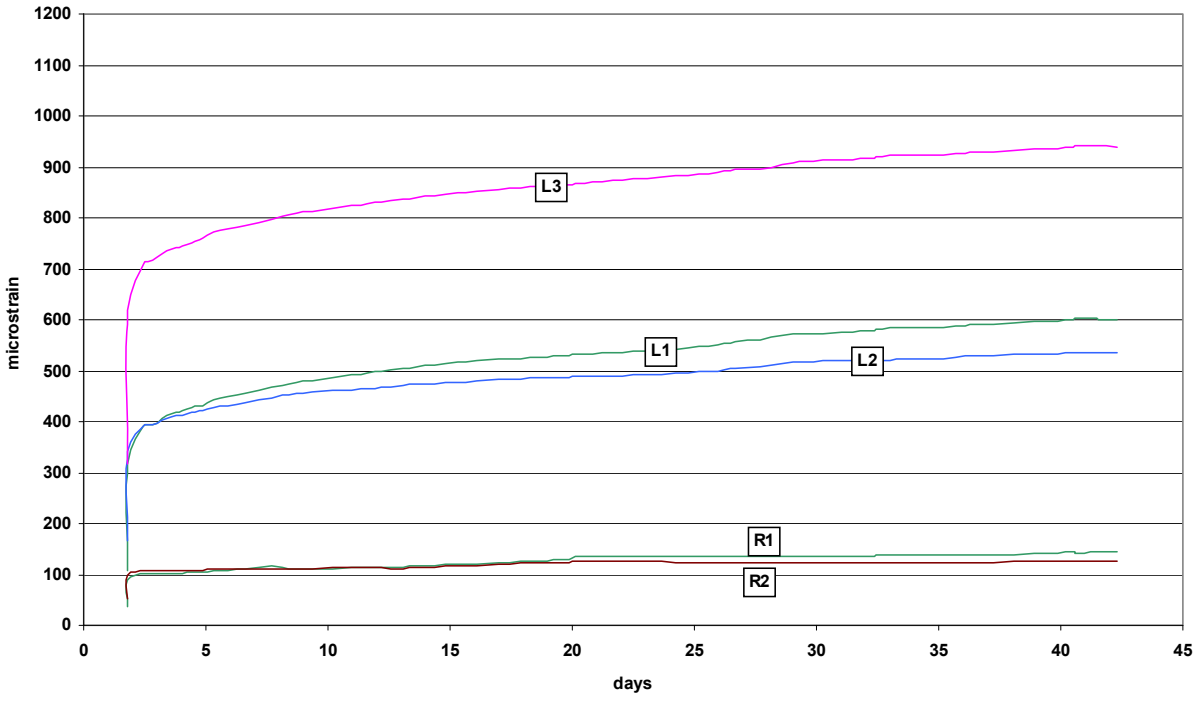

Figure 3-71 Specimen R4, Strain Under First Sustained Load

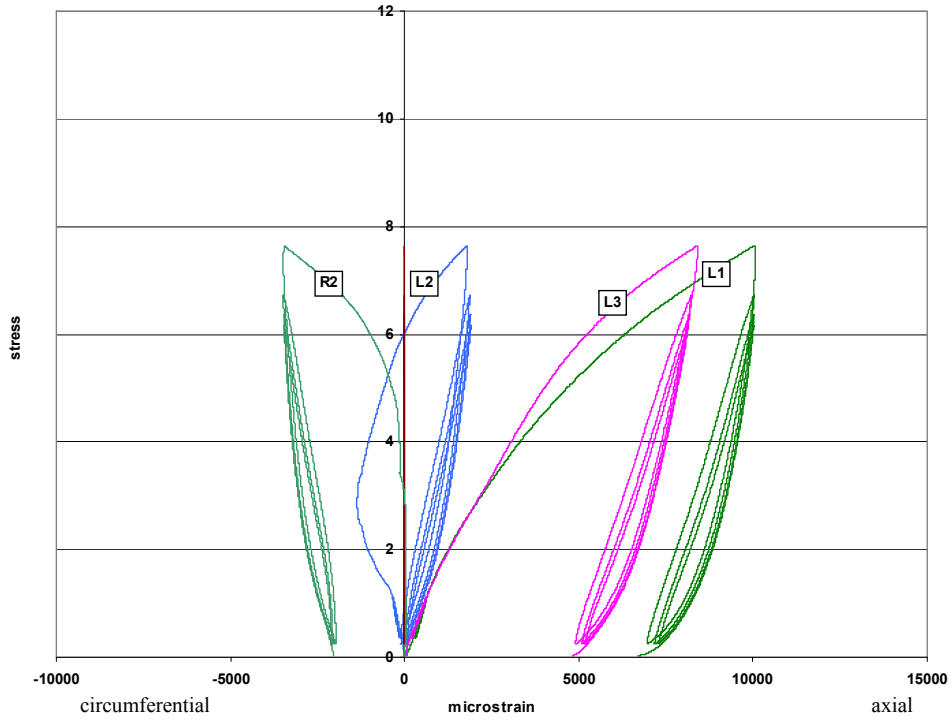

Figure 3-72 Specimen R4, Minor Critical Event, Individual Gage Data

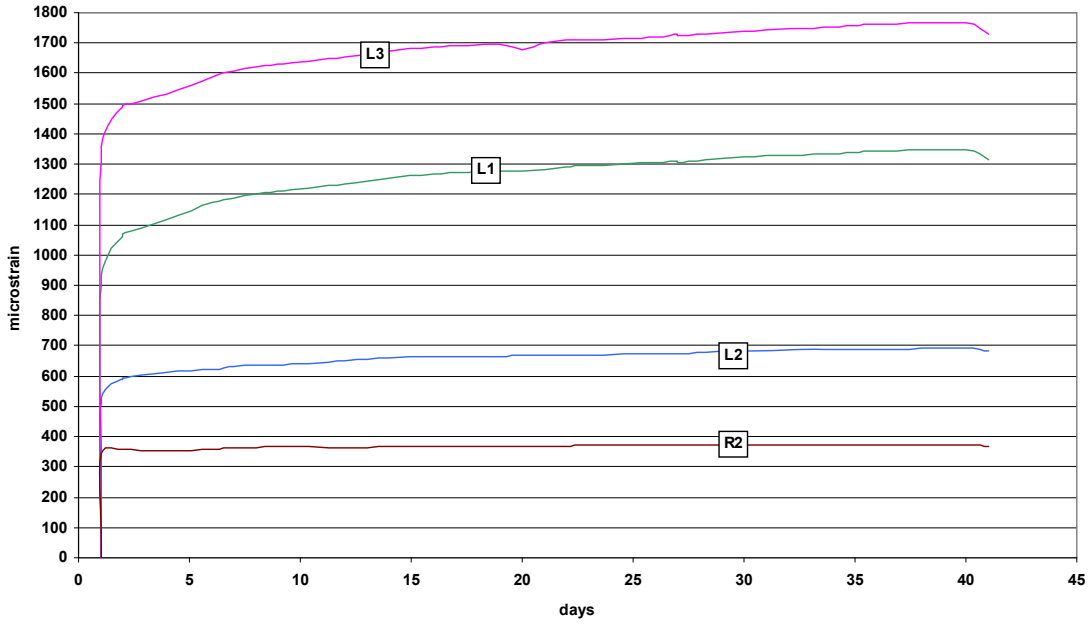

Figure 3-73 Specimen R4, Strain Under Second Sustained Load

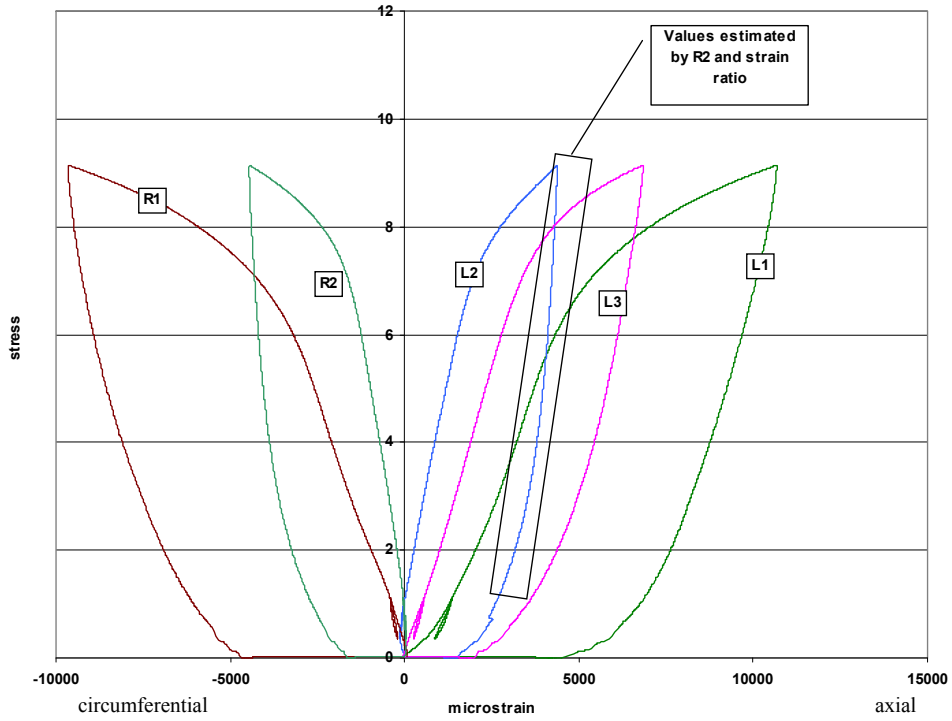

Figure 3-74 Specimen R4, Ultimate Loading, Individual Gage Data

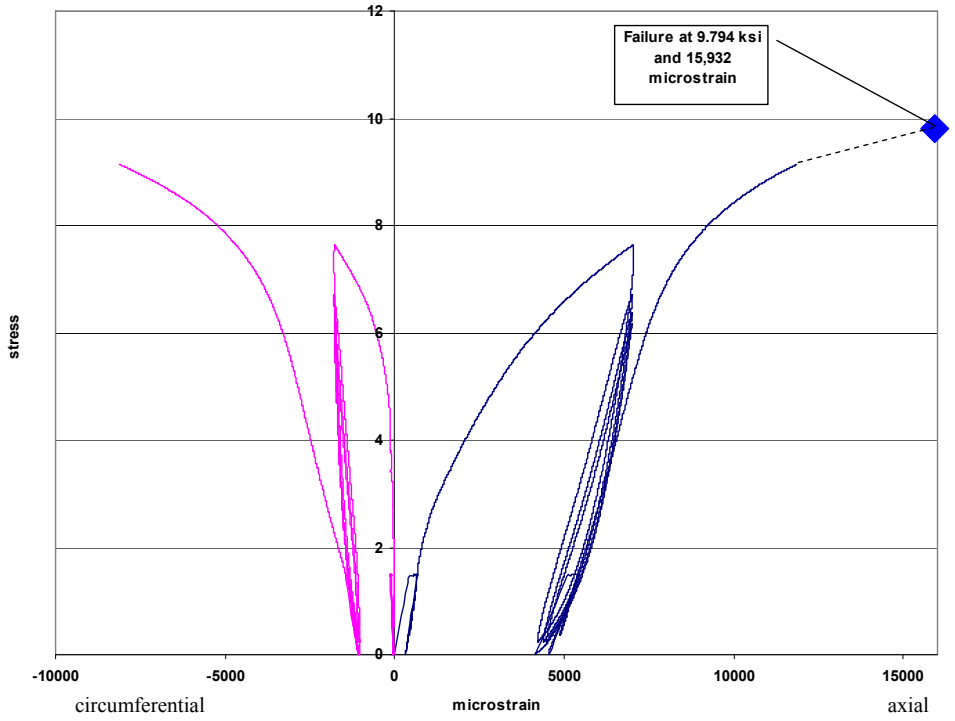

Figure 3-75 Specimen R4, Combined Stress-Strain Response

Specimen R5

Specimen R5 was placed under a sustained service load for 41 days starting on day 159. The specimen was wrapped under load on day 198 and broken monotonically on day 200. It failed at 8.088 ksi and 8,161 (average total) με. All strain gages functioned normally throughout the tests. Failure occurred by FRP de-lamination as seen in Figure 3-76. Figure 3-77 shows the individual gage strains under the sustained load and Figure 3-78 shows the individual gage data for the ultimate loading, as measured from a point of zero strain. Figure 3-79 shows the combined average stress-strain history of the specimen.

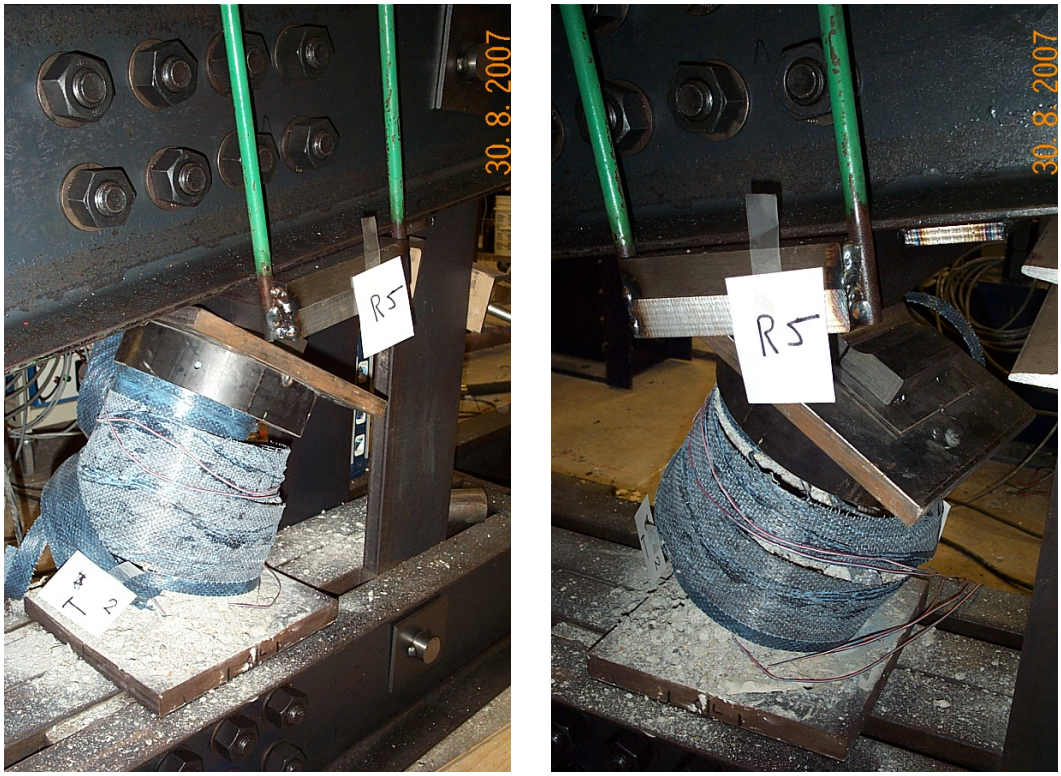

Figure 3-76 Specimen R5, Failure Mode

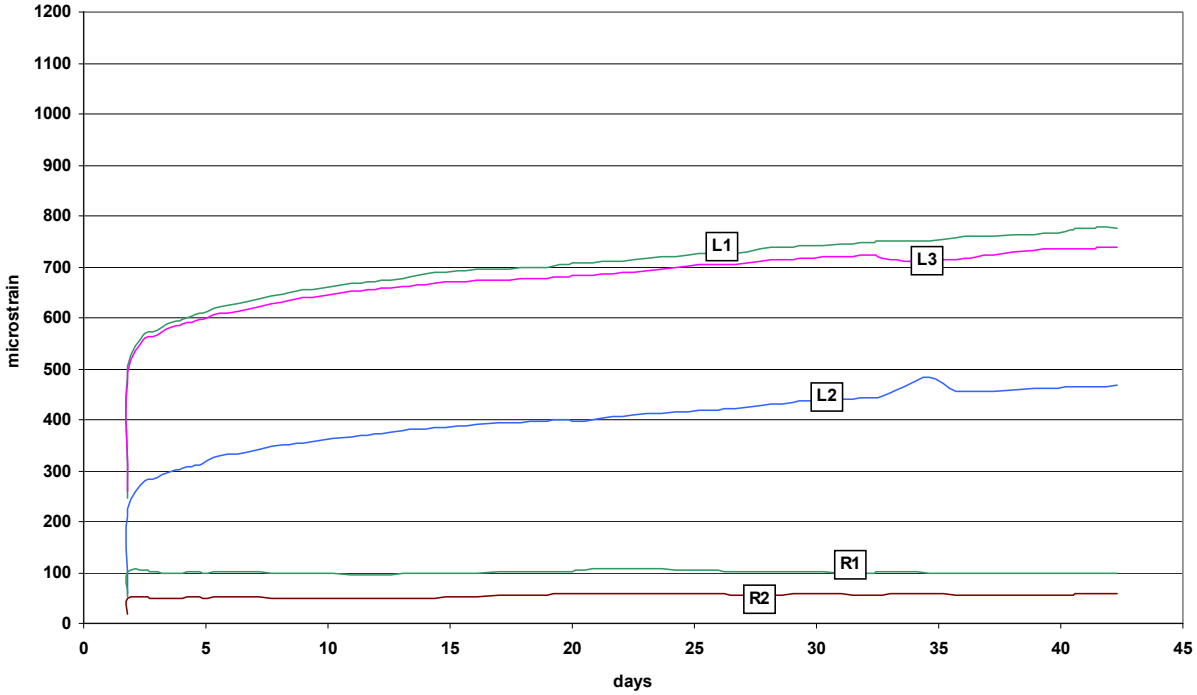

Figure 3-77 Specimen R5, Strain under Sustained Load

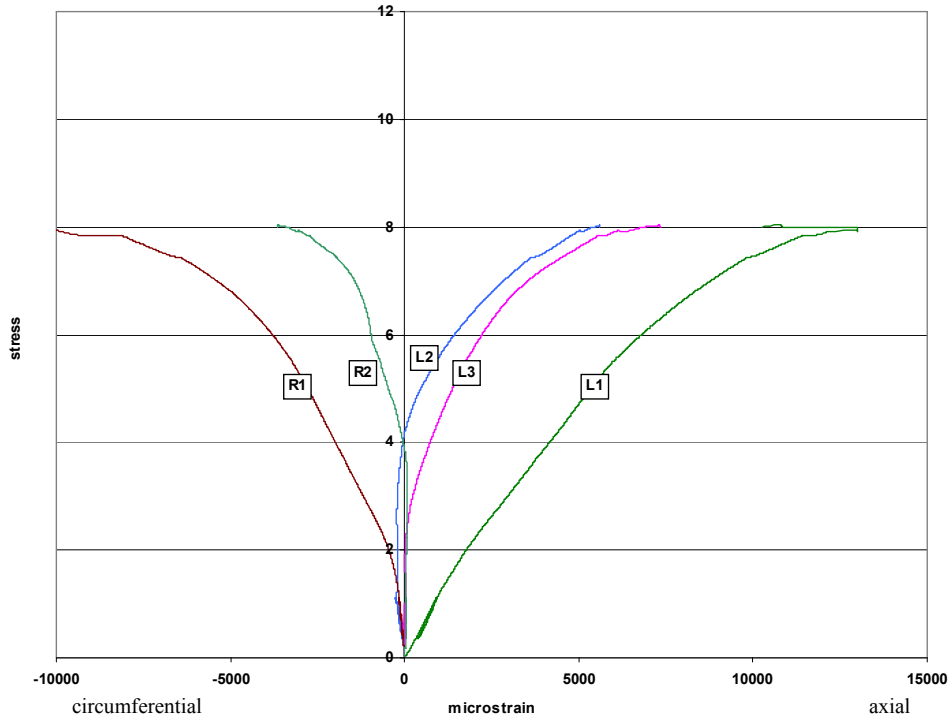

Figure 3-78 Specimen R5, Ultimate Load, Individual Gage Data

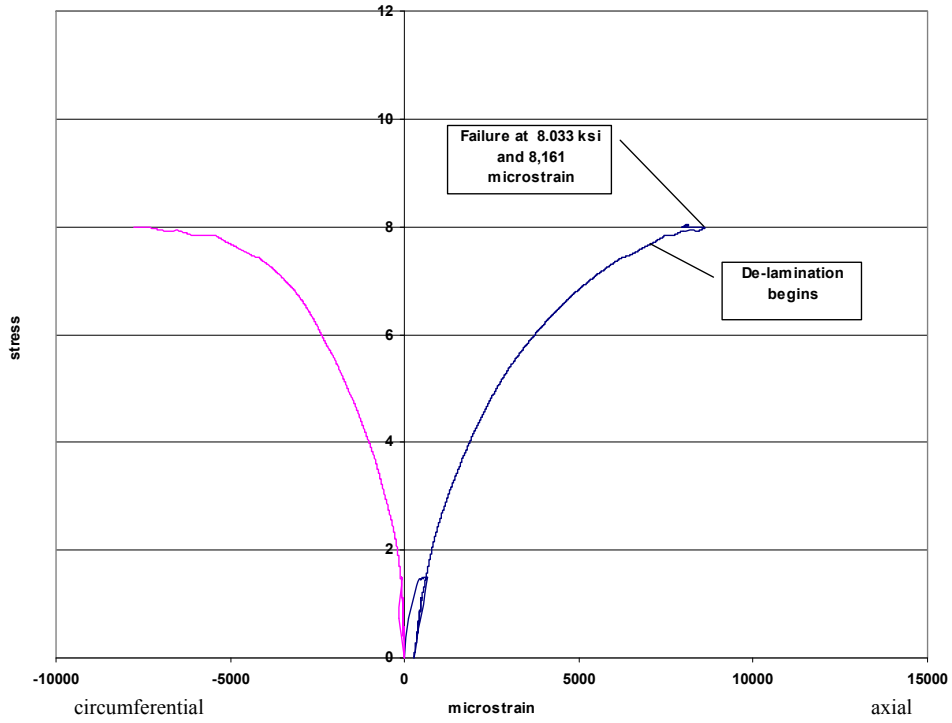

Figure 3-79 Specimen R5, Combined Stress-Strain Response

Specimen R6

Specimen R6 was placed under a sustained service load for 41 days starting on day 159. The specimen was wrapped under load on day 190 and broken monotonically on day 200. It failed at 7.460 ksi and 13,796 (average total) με. All strain gages functioned normally until they reach a strain of about 12,200 με. Beyond this strain, a linear projection was used to estimate the values of strain gages L1, L2, and L3. Failure occurred by FRP de-lamination as seen in Figure 3-80. Figure 3-81 shows the individual gage strains under the sustained load and Figure 3-82 shows the individual gage data for the ultimate loading, as measured from a point of zero strain. Figure 3-83 shows the combined average stress-strain history of specimen R6. The first attempt at an ultimate loading produced a highly eccentric result as seen in Figure 3-82. Strain gage L1 experienced an extreme compressive strain while L2 showed a large tensile strain. As this was observed, the test was terminated, the specimen reset in the load amplification device, and then reloaded. This second loading functioned as expected, but previous eccentric load may have damaged the specimen such that it could not reliably be compared to other results. It was intended for Specimen R6 to experience the same loading pattern as R4, but this did not occur as

it failed below the cycling stress of 7.64 ksi. Because of the abnormal performance of this specimen, it was excluded from all analysis in Chapter 4.

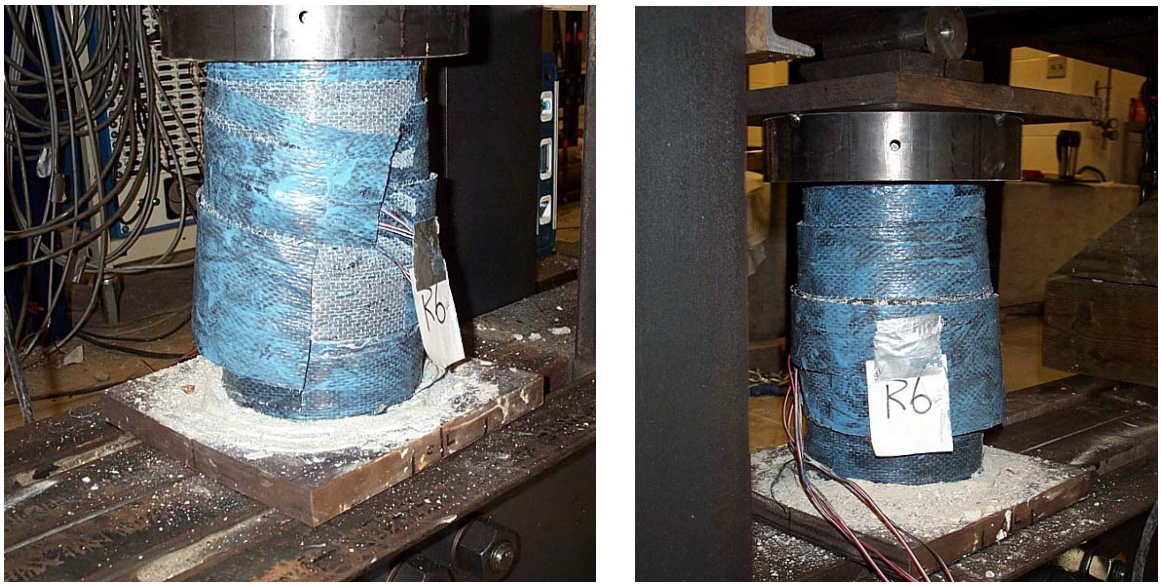

Figure 3-80 Specimen R6, Failure Mode

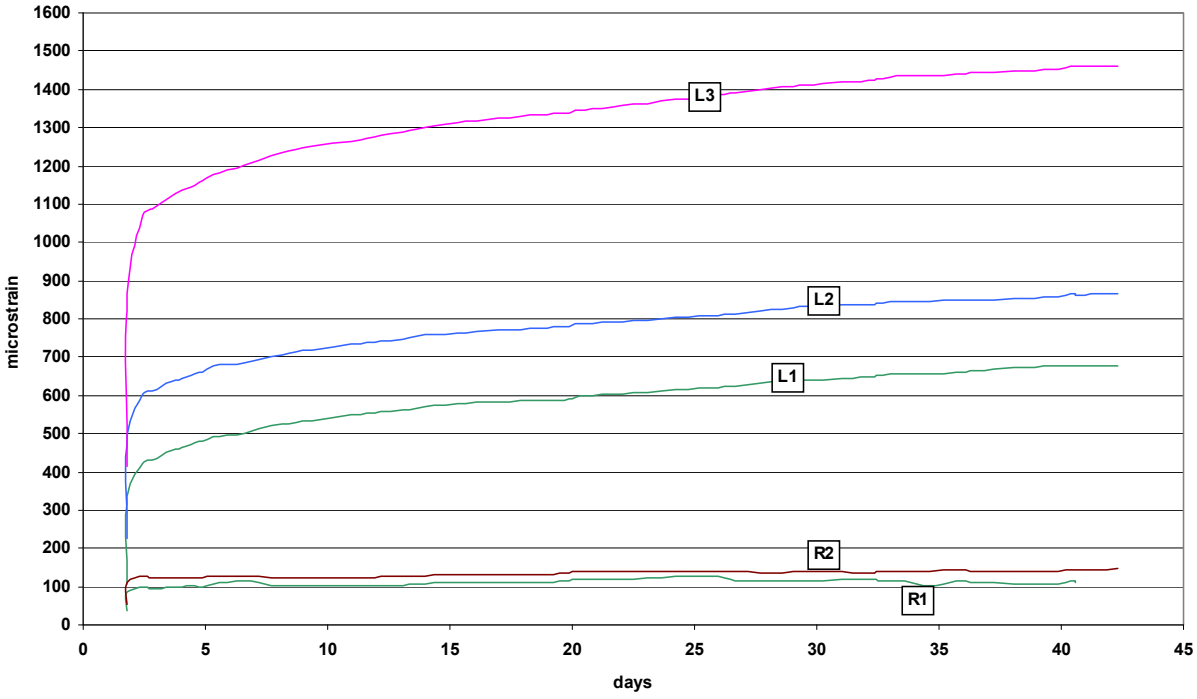

Figure 3-81 Specimen R6, Strain under Sustained Load

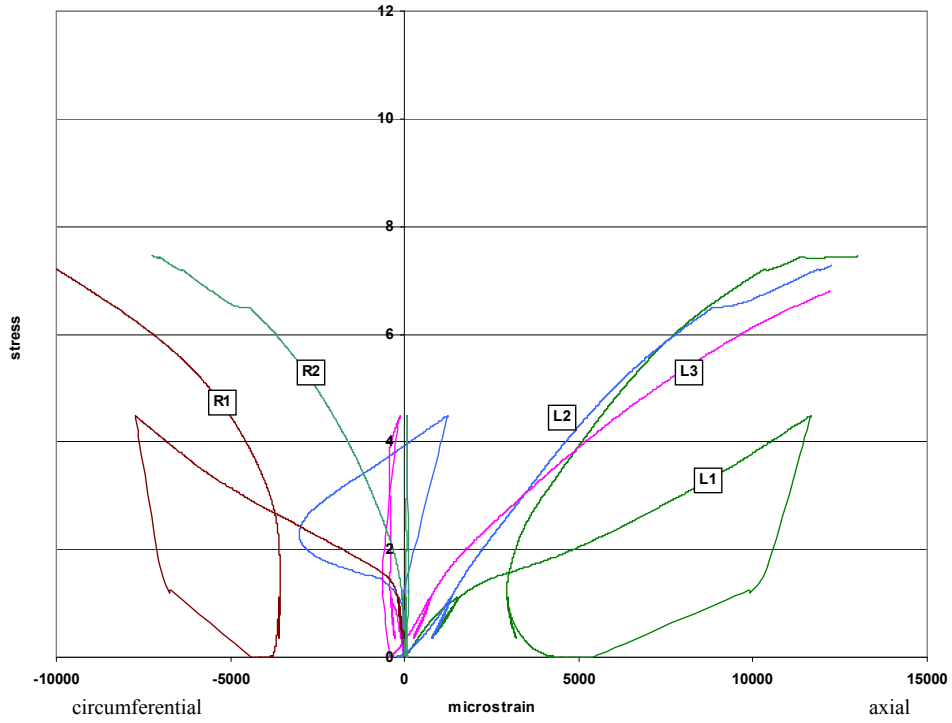

Figure 3-82 Specimen R6, Ultimate Loading, Individual Gage Data

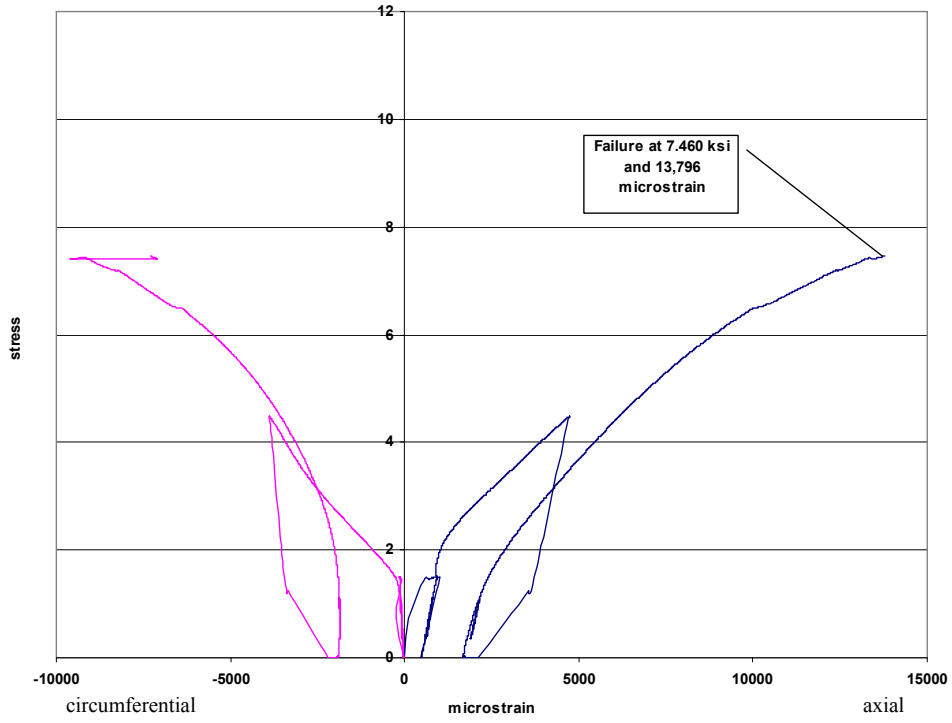

Figure 3-83 Specimen R6, Combined Stress-Strain Response

Retrofit Group Data Summary

Table 3-5 shows a summary of the ultimate data from the Retrofit group. Specimens R4 was subjected to a minor critical event after 41 days of sustained loading then returned for an additional 40 days of sustained loading. It is interesting to note that specimens R2 and R5 that were wrapped only for 3 and 2 days respectively prior to the ultimate loading failed at a much lower stress than expected. The decreased strength may be attributed to incomplete cure, an error in epoxy preparation, or similar but undetermined factors.

Specimen	f'_{cc} (ksi)	ε_{cc} (microstrain)	Failure Mode	Sustained Load	
				total	w/FRP
R1	8.771	11,953	rupture	42 days	11 days
R2	7.337	9,593	de-lamination	42 days	3 days
R3	10.147	10,764	de-lamination	42 days	11 days
R4	9.494	15,932	de-lamination	41 + 40 days	10 + 40 days
R5	8.088	8,161	de-lamination	41 days	2 days
R6	7.460	13,799	de-lamination	41 days	10 days

Table 3-5 Retrofit Group Data Summary

3.3.4 Steel Group

Specimen S1

Specimen S1 was placed under a sustained service load for 27 days starting on day 199. The specimen was subjected to a minor critical event on day 226 and then returned to the sustained load device for an additional 14 days. It was broken monotonically on day 240. The failure stress was 5.826 ksi. The failure strain could not be determined since the strain gages ceased functioning when the cover concrete spalled off. Figure 3-84 shows the failure of specimen S1.

Figure 3-84 Specimen S1, Failure Mode

Specimen S2

Specimen S2 was placed under a sustained service load for 27 days starting on day 199. The specimen was subjected to a minor critical event on day 226 and then returned to the sustained load device for an additional 14 days. It was broken monotonically on day 240. The failure stress was 5.947 ksi. The failure strain could not be determined since the strain gages ceased functioning when the cover concrete spalled off. Figure 3-85 shows the failure of specimen S2.

Figure 3-85 Specimen S2, Failure Mode

Specimen S3

Specimen S3 was placed under a sustained service load for 27 days starting on day 199. The specimen was subjected to a minor critical event on day 226, after which it was wrapped with FRP and then returned to the sustained load device for an additional 14 days. The FRP was applied without the presence of the sustained load, but the cure took place under the sustained load. Specimen S3 was broken monotonically on day 240. The test took place in the load amplification device and was stopped prior to identifying the failure mode and load. A photo is not shown as there is nothing to observe. The maximum load achieved was 8.950 ksi at a 6,312 (average total) με.

Figure 3-86 shows the strains resulting from the first application of sustained load which was followed by the minor critical event shown in Figure 3-87. Following the damage of the minor critical event, the specimen was wrapped with FRP and return to the sustained load device which resulted in the strains shown in Figure 3-88. Figure 3-89 shows the data from each longitudinal strain gage during the ultimate loading and Figure 3-90 shows the combined stress strain response of specimen S3 to all loading events.

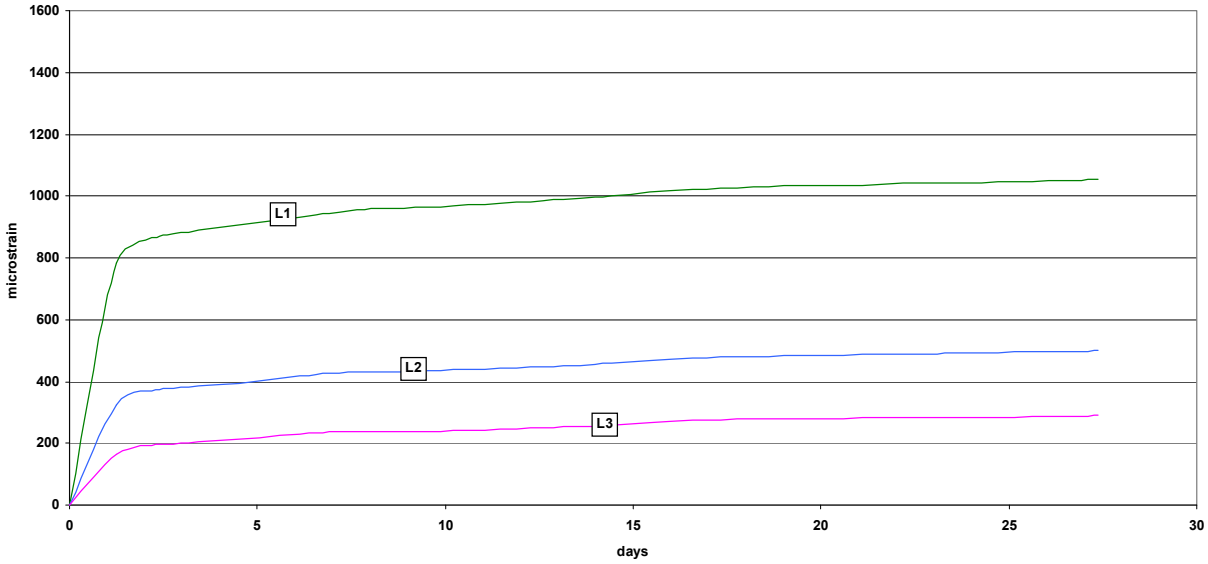

Figure 3-86 Specimen S3, First Sustained Load

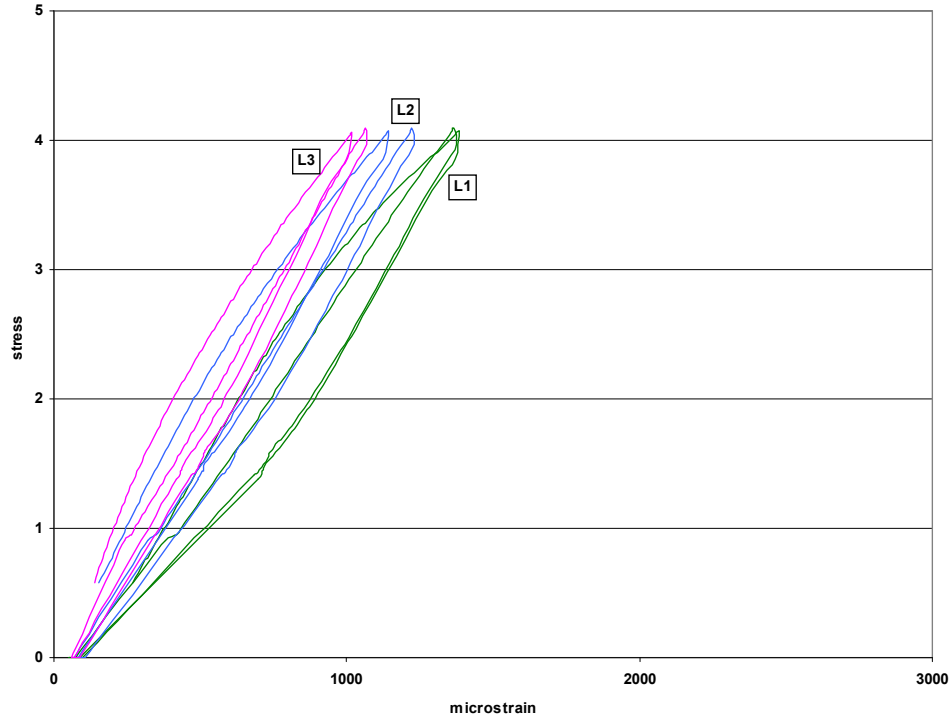

Figure 3-87 Specimen S3, Minor Critical Event

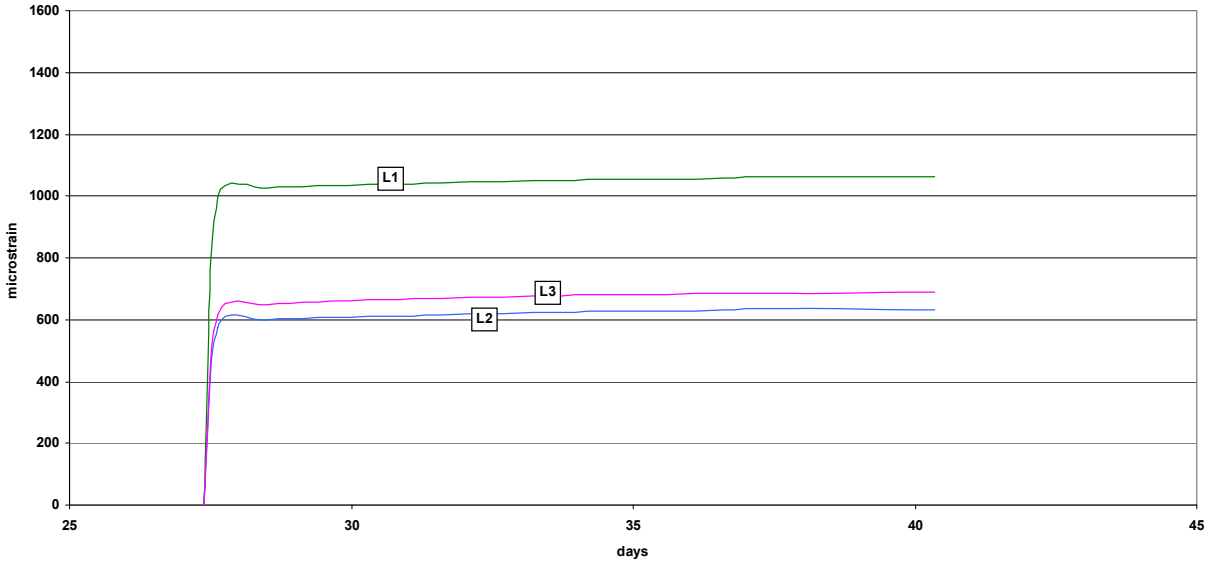

Figure 3-88 Specimen S3, Second Sustained Load

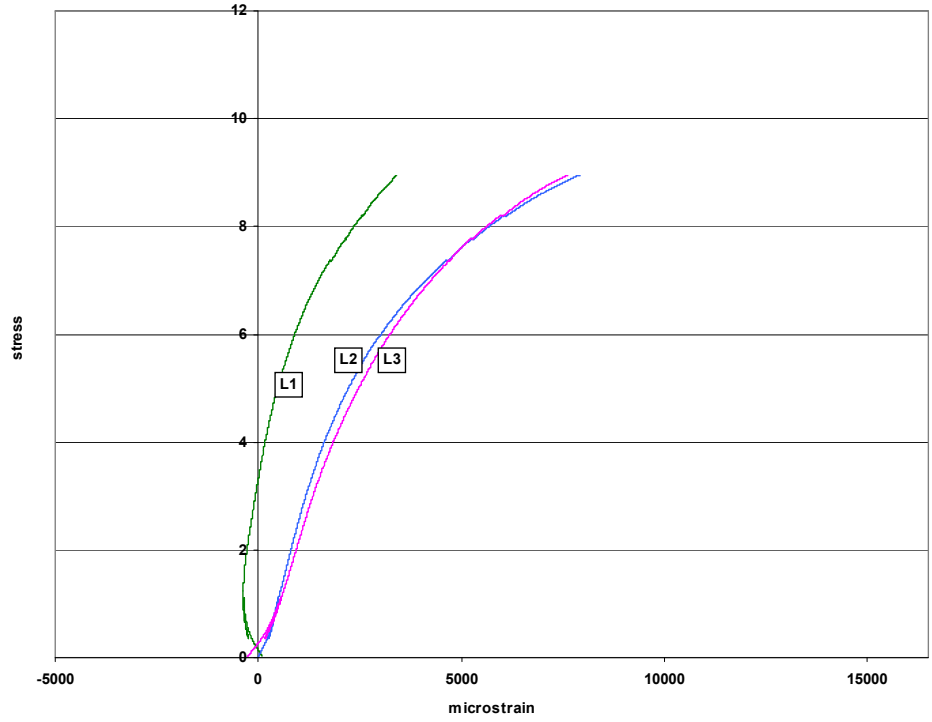

Figure 3-89 Specimen S3, Ultimate Loading, Individual Gage Data

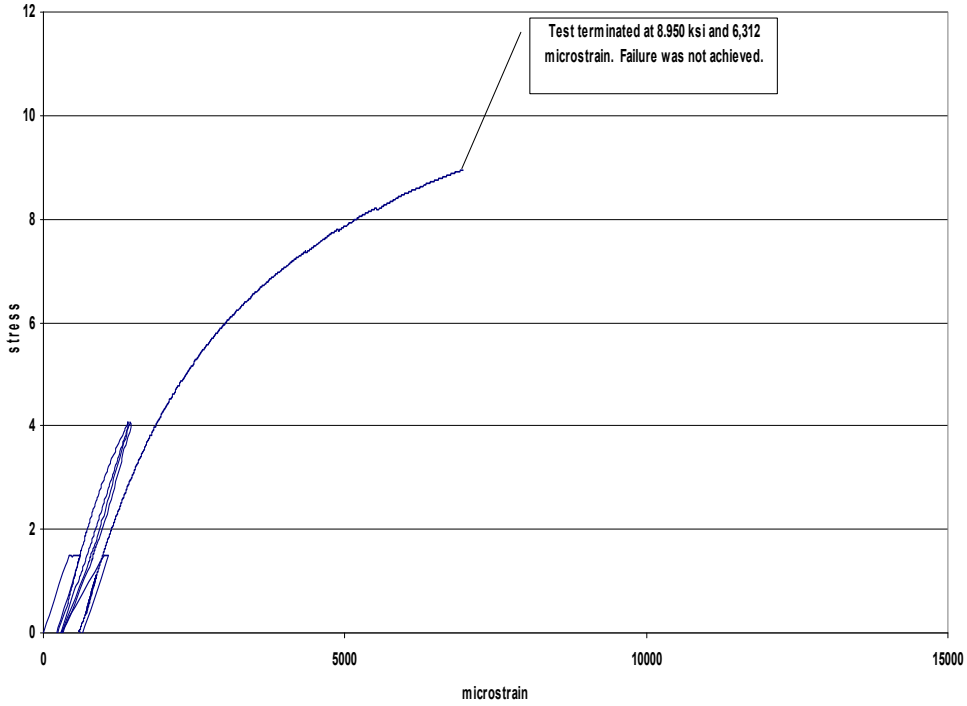

Figure 3-90 Specimen S3, Combined Stress Strain Response

Specimen S4

Specimen S4 was placed under a sustained service load for 27 days starting on day 199. The specimen was subjected to a minor critical event on day 226, after which it was wrapped with FRP and then returned to the sustained load device for an additional 14 days. The FRP was applied without the presence of the sustained load, but the cure took place under the sustained load. Specimen S4 was broken monotonically on day 240. The test took place in the load amplification device the specimen failed in de-lamination as shown in Figure 3-91 at 8.835 ksi and 9,213 (average total) με.

Figure 3-92 shows the strains resulting from the first application of sustained load which was followed by the minor critical event shown in Figure 3-93. Following the damage of the minor critical event, the specimen was wrapped with FRP and return to the sustained load device which resulted in the strains shown in Figure 3-94. Figure 3-95 shows the data from each longitudinal strain gage during the ultimate loading and Figure 3-96 shows the combined stress strain response of specimen S4 to all loading events.

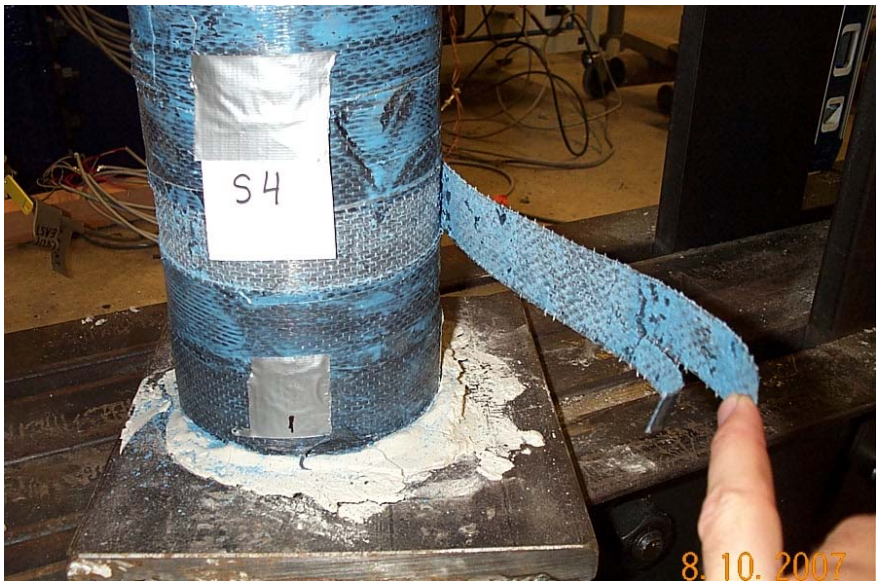

Figure 3-91 Specimen S4, Failure Mode

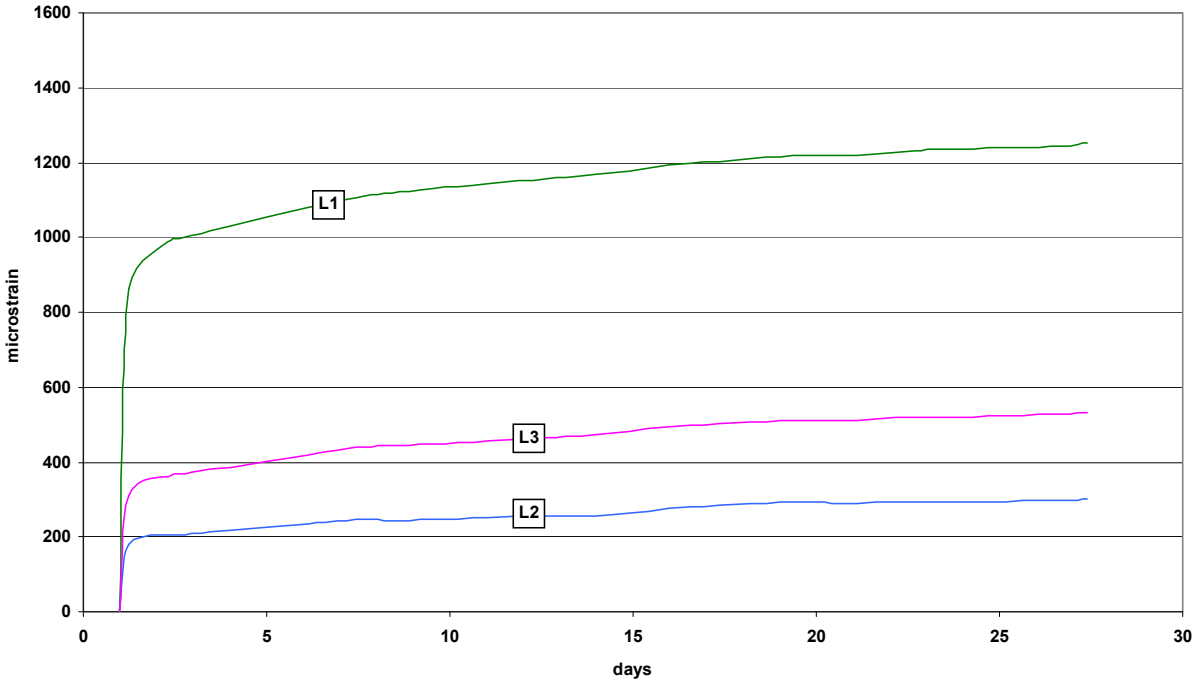

Figure 3-92 Specimen S4, First Sustained Load

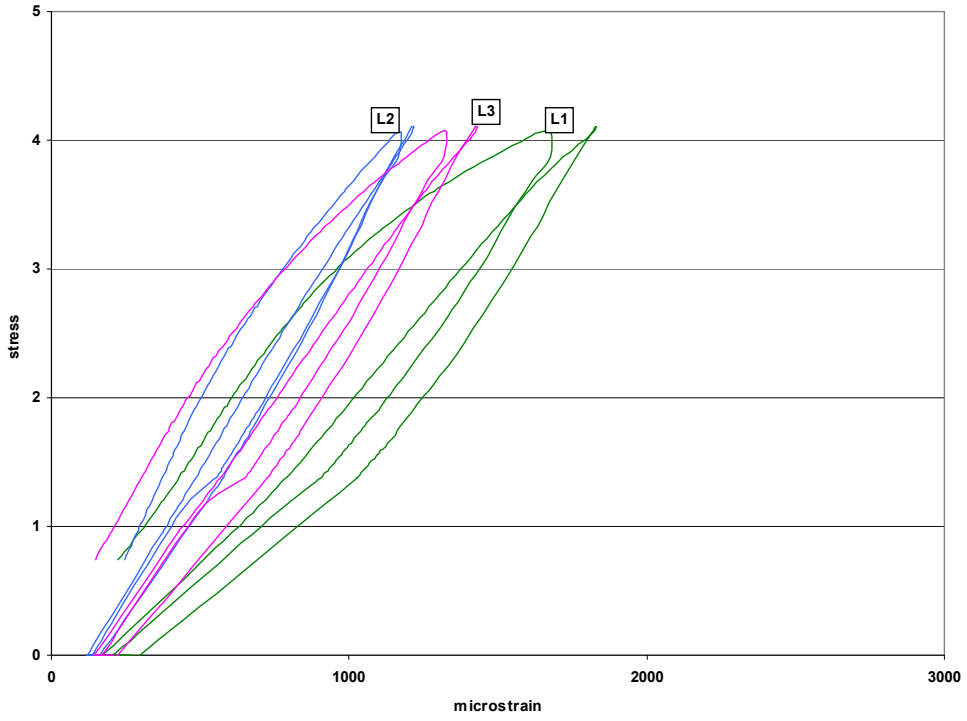

Figure 3-93 Specimen S4, Minor Critical Event

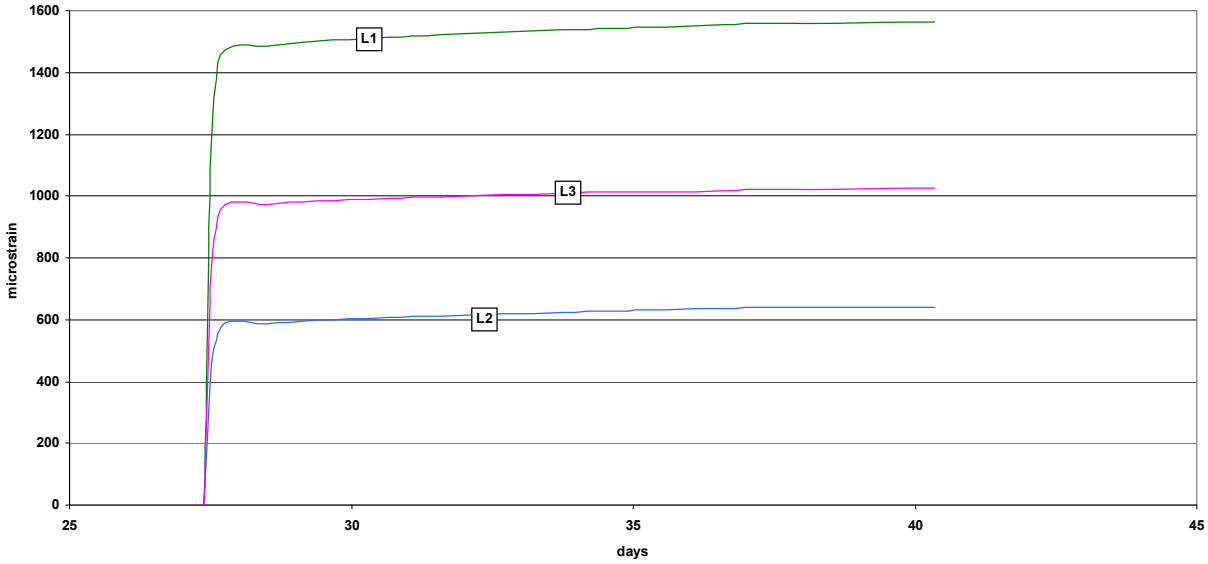

Figure 3-94 Specimen S4, Second Sustained Load

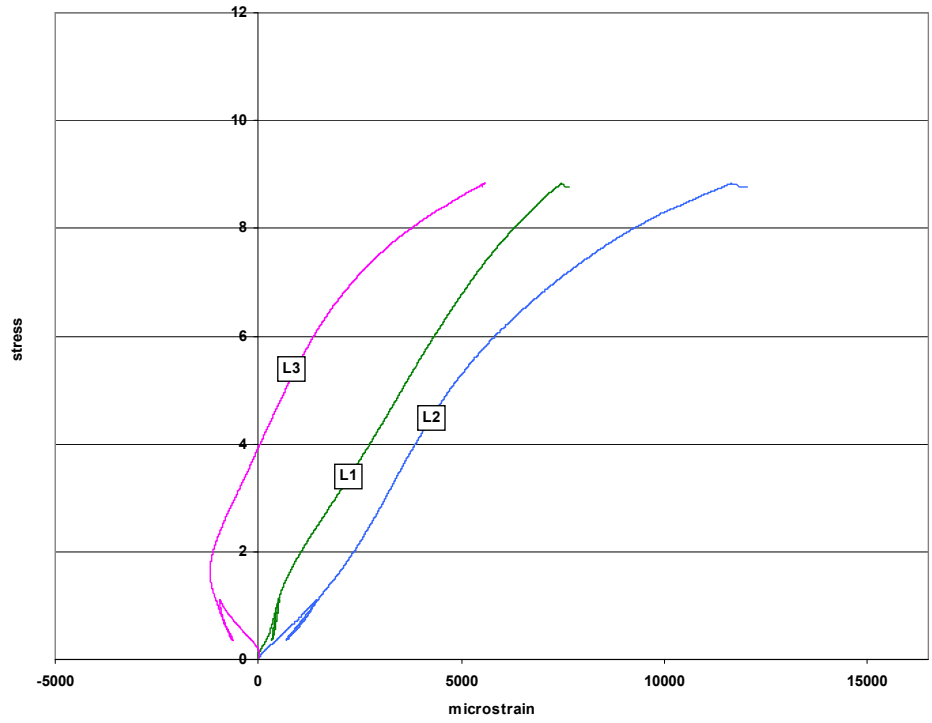

Figure 3-95 Specimen S4, Ultimate Loading, Individual Gage Data

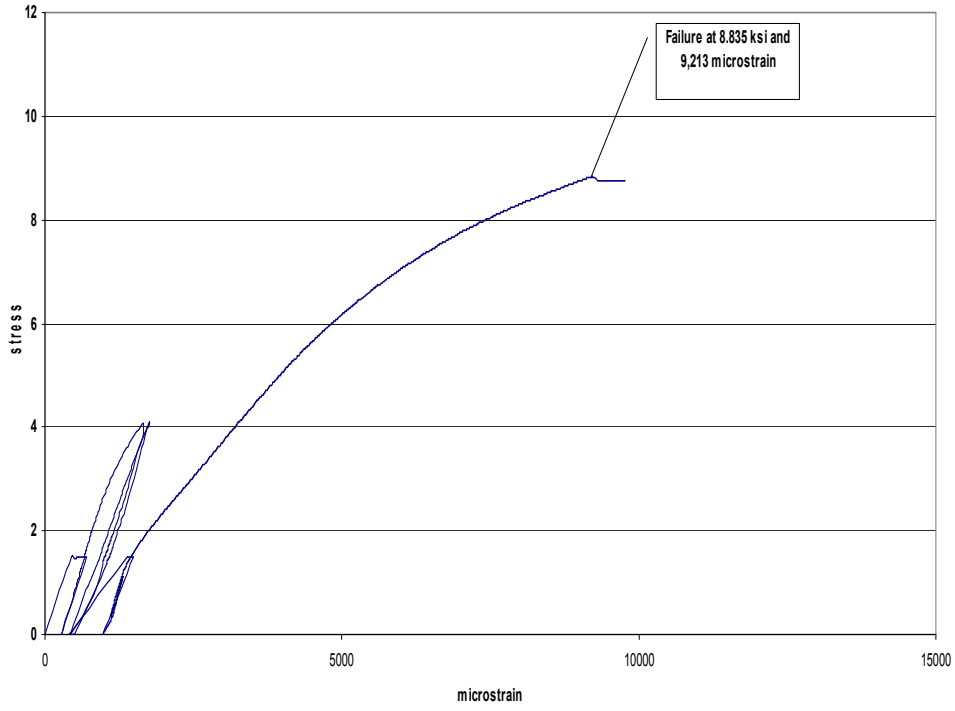

Figure 3-96 Specimen S4, Combined Stress-Strain Response

Specimen S5

Specimen S5 was placed under a sustained service load for 42 days starting on day 200. The specimen was retrofitted with FRP on day 226. Both the retrofit and FRP curing took place under the action of the sustained load. After and additional 16 days of sustained loading, specimen S5 was broken monotonically on day 242. The test took place in the load amplification device. It failed in de-lamination as shown in Figure 3-97 at 9.276 ksi and 10,548 (average total) με.

Figure 3-98 shows the strains resulting from the application of sustained load. Figure 3-99 shows the individual strain gage resulting from the ultimate loading. L4 is a correction factor necessary to correct for an excessive load eccentricity. Procedures for determining this correction are detailed in Appendix C. Figure 3-100 shows the combined stress strain response of specimen S5 to all loading events

Figure 3-97 Specimen S5, Failure Mode

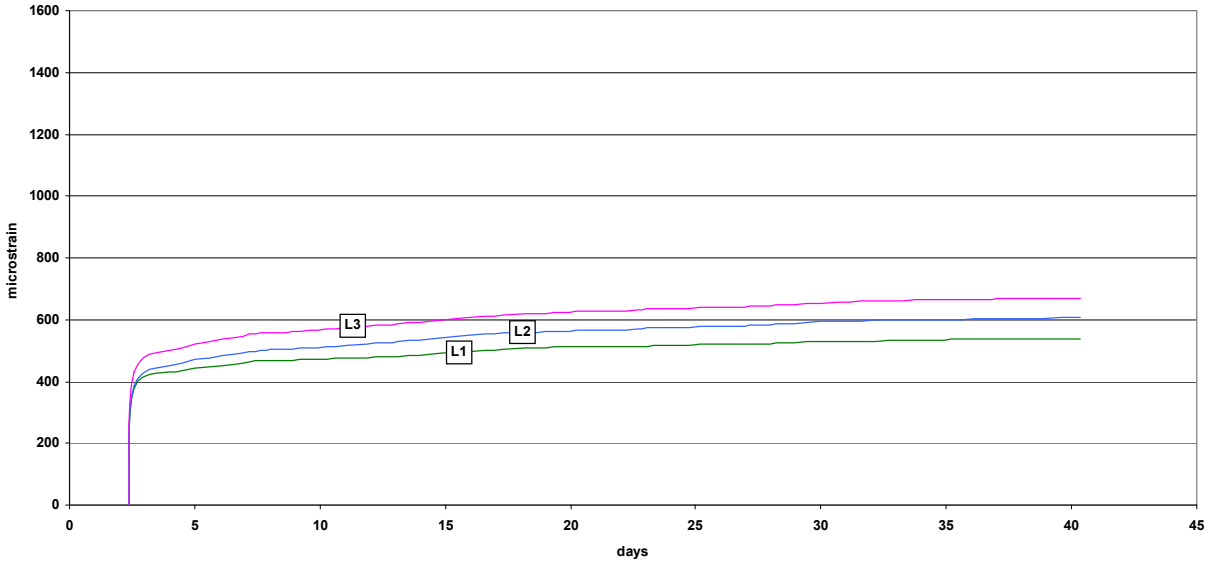

Figure 3-98 Specimen S5, Strain under Sustained Load

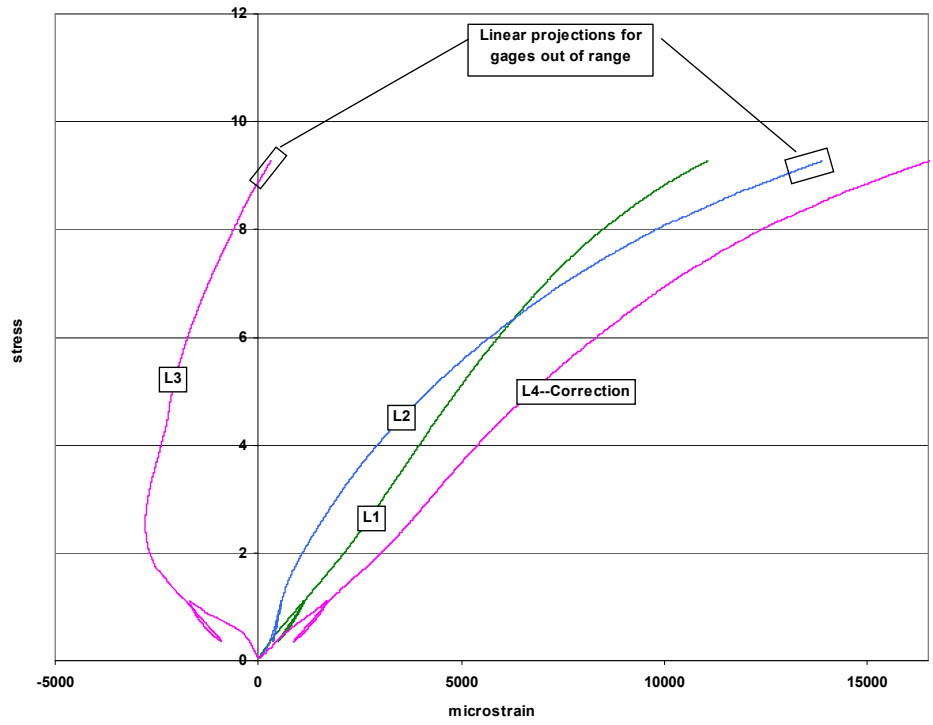

Figure 3-99 Specimen S5, Ultimate Load, Individual Gage Data

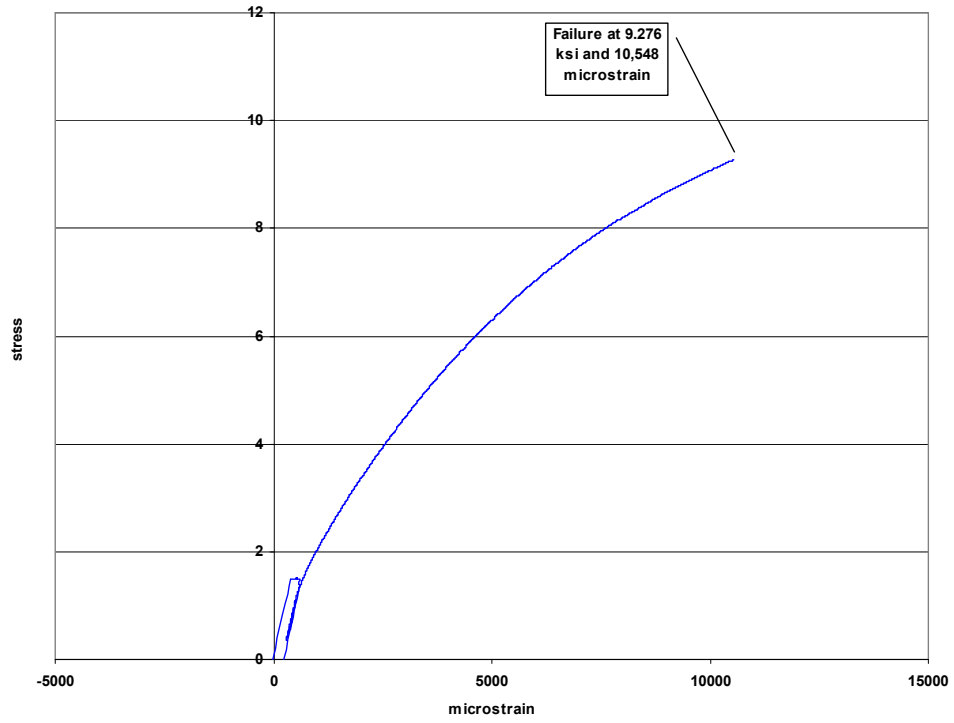

Figure 3-100 Specimen S5, Combined Stress Strain Response

Specimen S6

Specimen S6 was placed under a sustained service load for 42 days starting on day 200. The specimen was retrofitted with FRP on day 226. Both the retrofit and FRP curing took place under the action of the sustained load. After and additional 16 days of sustained loading, specimen S6 was broken monotonically on day 242. The test took place in the load amplification device. It failed in de-lamination as shown in Figure 3-101 at 9.864 ksi and 11,865 (average total) με.

Figure 3-102 shows the strains resulting from the application of sustained load. Figure 3-103 shows the individual strain gage values resulting from the ultimate loading. Figure 3-104 shows the combined stress strain response of specimen S6 to all loading events

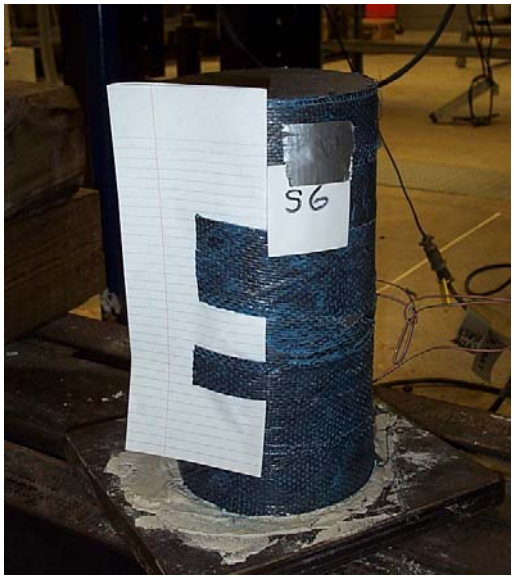

Figure 3-101 Specimen S6, Failure Mode

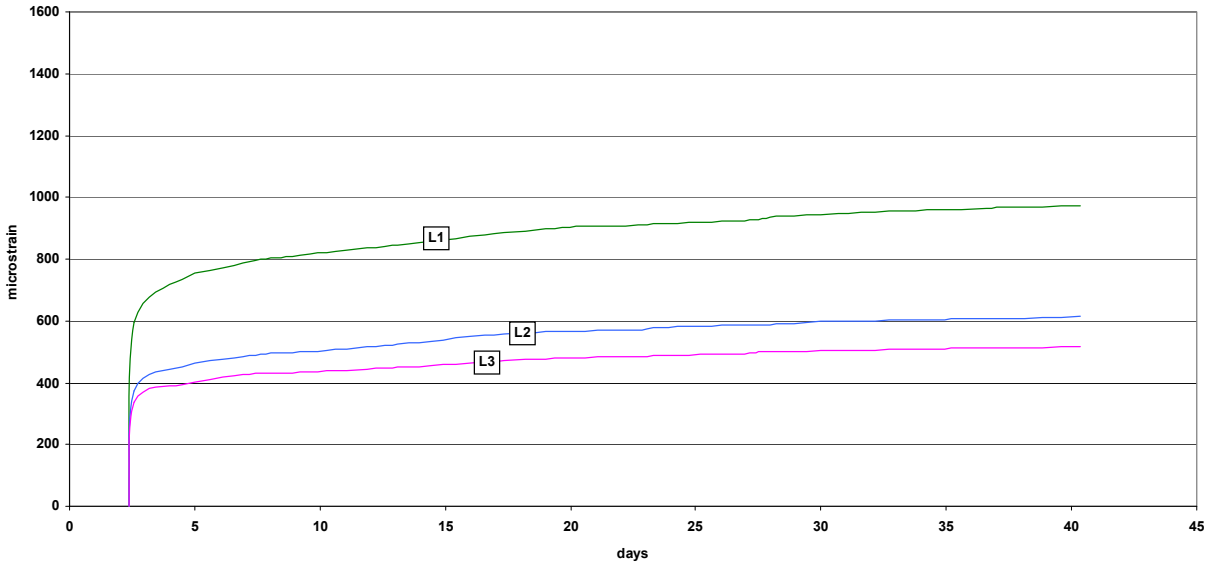

Figure 3-102 Specimen S6, Strain under Sustained Load

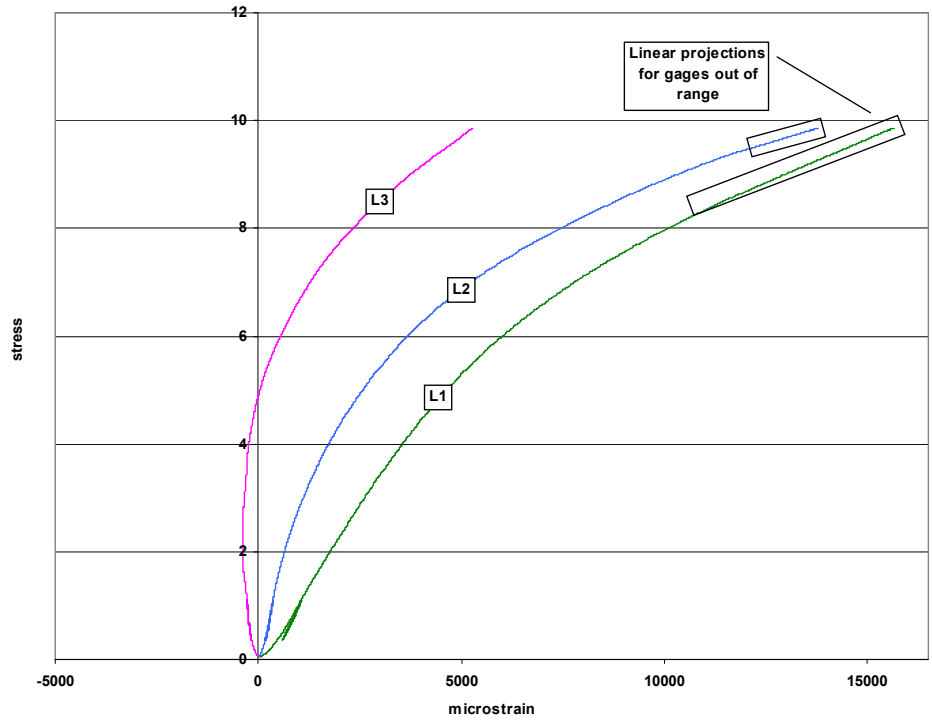

Figure 3-103 Specimen S6, Ultimate Loading, Individual Gage Data

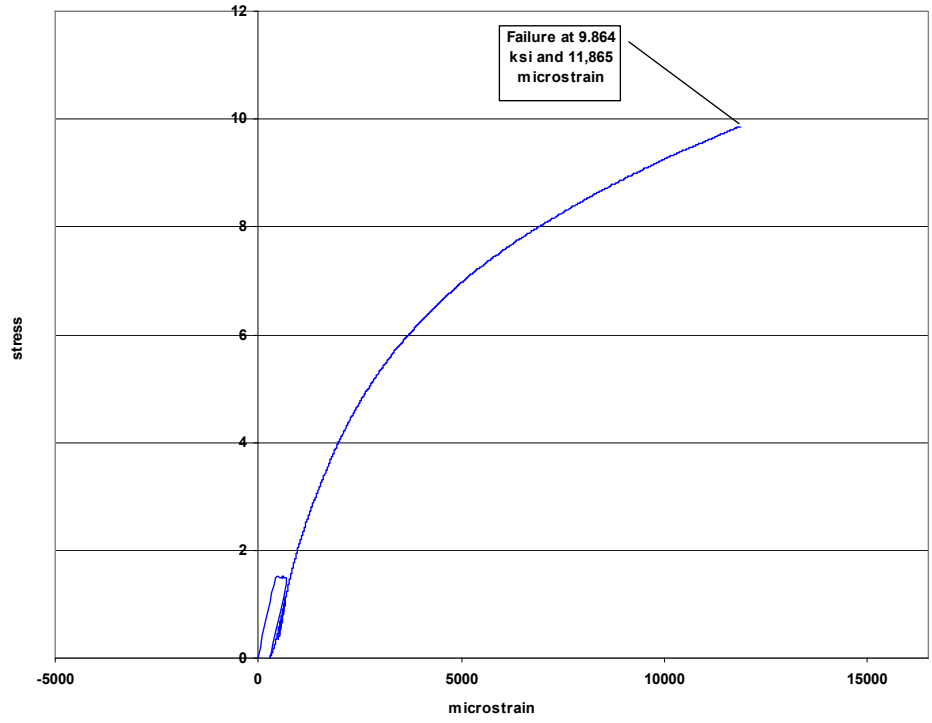

Figure 3-104 Specimen S6, Combined Stress Strain Response

Specimen S7

Specimen S7 was intended to be a calibration specimen like S8, but this specimen failed prematurely due to excessive eccentricity and did not produce useful data. It was excluded from all results.

Specimen S8

Specimen S8 was a calibration specimen used to determine the ultimate load of the steel spiral confined specimens without the presence of FRP. The specimen was broken monotonically on day 226 and failed at 5.781 ksi. A stress-strain curve was not plotted as strain readings failed as the concrete began to spall. From this specimen the stress limit for the minor critical event for this group was set at 4.0 ksi. Figure 3-105 shows the failure mode of specimen S8.

Figure 3-105 Specimen S8, Failure Mode

Steel Group Data Summary

Table 3-6 shows a summary of the ultimate data from the steel group.

Specimen	f'_{cc} (ksi)	ε_{cc} (microstrain)	Failure Mode	Sustained Load?	
				total	w/FRP
S1	5.826	unk	crushing	42 days	---
S2	5.972	n/a	crushing	42 days	---
S3	8.950	6,312	not found	42 days	16 days
S4	8.835	9,213	de-lamination	42 days	16 days
S5	9.276	10,548	de-lamination	42 days	16 days
S6	9.864	11,865	de-lamination	42 days	16 days
S7	not used				
S8	5.781	n/a	crushing	none	---

Table 3-6 Steel Group, Data Summary

4. Analytical Program

In this chapter, appropriate models representing the state of the art of FRP confined concrete modeling are selected and calibrated using the material parameters of this experimental set. The results of each experimental test are examined, refined, and where necessary, modified. Twelve investigations are described to examine the impact of each life cycle event. Findings from these investigations support the development of proposed life cycle modeling procedures. Impacts of the results are addressed along with suggestions for future research.

4.1 Selection of Current Representative Models

The following models are selected as representing the current state of the art.

4.1.1 Stress Strain Model

The stress strain model of Lam and Teng, explained in Section 2.5.3, is selected as the baseline model for three principal reasons. First, as a recent development, it takes advantage of fifteen years of experience in FRP confined concrete research. Second, it is based on 76 specimens from a variety of researchers and compares favorably with the experimental results of five different authors. Third, it is a design oriented model that provides two closed form equations which generate the complete stress strain curve based only on the input of basic material parameters.

When the parameters of these experiments are applied to the equations of Section 2.5.3, the following values result for the confining stress, ultimate strain, and ultimate stress:

Equation (2.71):

$$f_{l,a} = \frac{2(33{,}000)(0.013)(0.009786)}{6.00} = 1.399 \ ksi \quad with \quad \varepsilon_{h,rup} = 0.586(0.0167) = 0.009786 \ strain$$

Equation (2.72):

$$\varepsilon_{cu} = \left(1.75 + 5.53\left(\frac{1.399}{5.455}\right)\left(\frac{0.0167}{0.002000}\right)^{0.45}\right)0.00200 = 0.01087 \ strain$$

Equation (2.73):

$$f'_{cc} = \left(1 + 3.3\frac{1.399}{5.455}\right)5.455 = 10.07\ ksi$$

These, in turn, allow for the calculation of the transition point parameters:

Equation (2.76):

$$f_o = f'_{co} = 5.455ksi$$

Equation (2.77):

$$E_2 = \frac{10.07 - 5.455}{0.010873} = 424\ ksi$$

Equation (2.78):

$$\varepsilon_t = \frac{2(5.455)}{(4{,}210 - 424)} = 0.002882\ strain$$

Finally, the two closed form equations for the stress-strain response are $f_c = 4{,}210\varepsilon_c - \frac{(4{,}210 - 424)^2}{5{,}455}\varepsilon_c^2$ for the first branch and $f_c = 5.455 + 424\varepsilon_c$ for the second branch. When displayed in graphical form, Lam and Teng's model results in Figure 4-1.

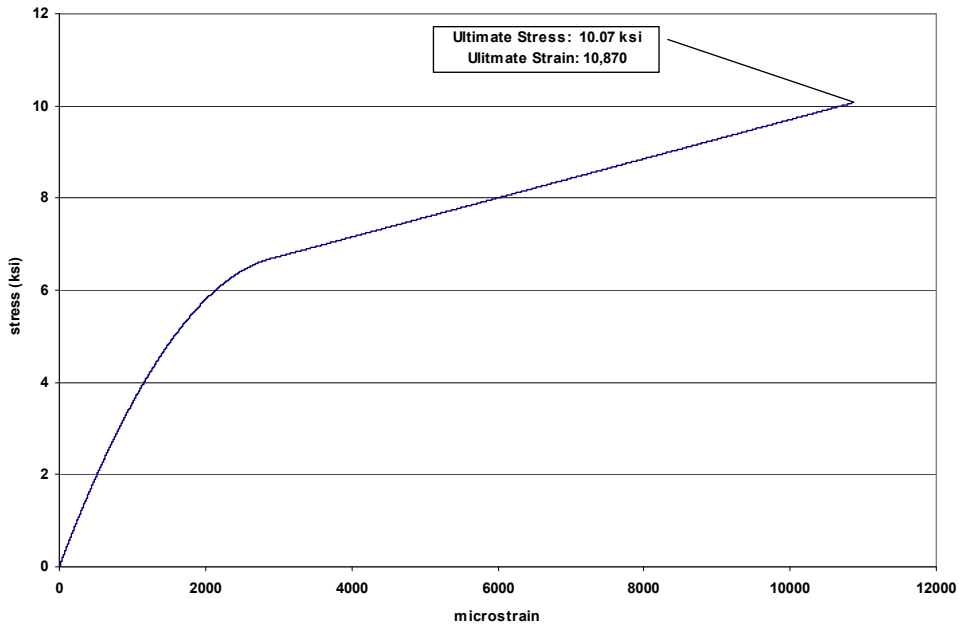

Figure 4-1 Lam and Teng (2003) Model for Experimental Material Properties

4.1.2 ACI Creep Model

Section 2.6.1 explains the provisions of ACI 209 as it pertains to the prediction of creep in a specimen. For the conditions of these experiments, the primary parameter is the age of the concrete at loading. Figure 4-2 shows the creep response predicted by ACI 209. The age of the first loading for LAB specimens was 117 days, RETROFIT 159 days, and STEEL specimens 199 days. The nominal initial elastic strain was 353 microstrain calculated by dividing the applied stress of 1.49 ksi by the nominal elastic modulus of 4,210 ksi. On average, a 42 day sustained load at 1.49 ksi produces and additional 270 microstrain due to creep.

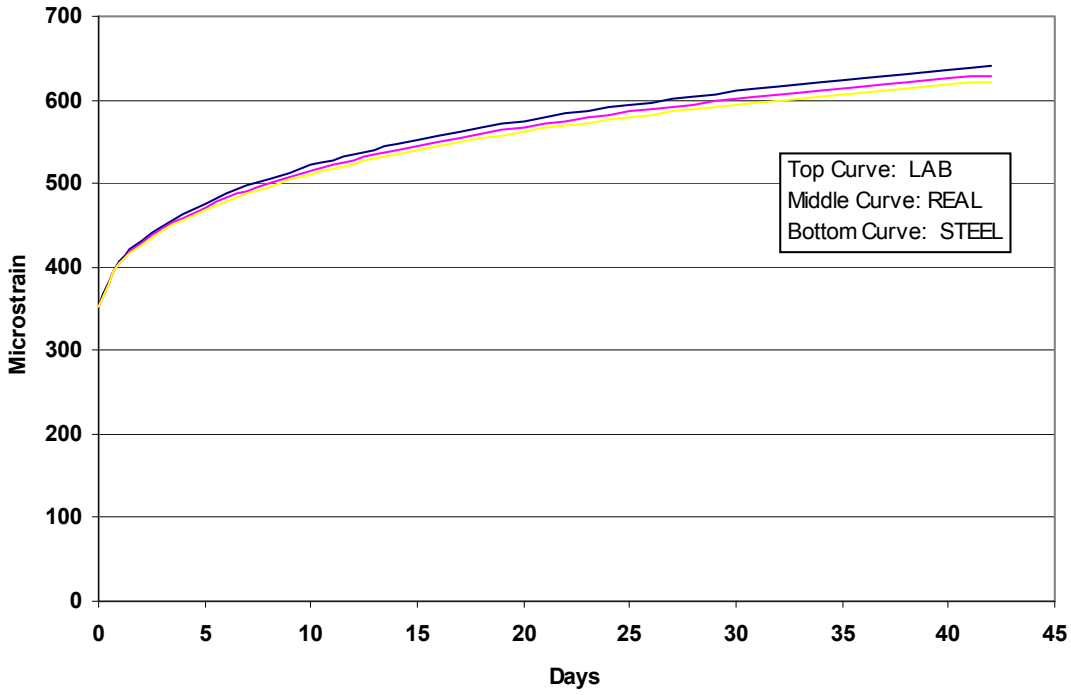

Figure 4-2 Nominal Creep Strains by ACI 209

4.2 Analysis of FRP Confined Plain Concrete Specimens under Life Cycle Loadings

4.2.1 Investigation 1: Verification of Control Group Behavior

The purpose of this investigation is to establish that the behavior of the Control Group specimens tested in the load amplification device matches the behavior predicted by the baseline model.

Exclusion of Specimens C1 and C2

The results of specimens C1 and C2 are excluded from the analysis because of inconsistent performance. Specimen C1 failed prematurely at 8.07 ksi when the FRP at the base of the specimen ruptured. As seen in Figure 4-3, both specimens C1 and C2 exhibit a strange behavior between 1.5 and 3.0 ksi which indicates either excessive deformation for the recorded load or an under-recording of the applied load. This behavior is believed to have been caused by an overly flexible support plate. After these two experiments, the thickness of the support plate was doubled and this phenomenon did not appear again.

While it may be possible to correct the data for these two specimens, the author does not believe it is prudent in this case. To remove the discrepancy between 1.5 and 3.0 ksi would require shifting the curves left, up, or some combination of both. There are no experimental data points available to indicate the direction or magnitude of the correction. Accordingly, it would be necessary to use some portion of Lam and Teng's model to calibrate the adjustment. Once this was done, a useful comparison between the experiment and the baseline model could not be made as the model would have influenced the response.

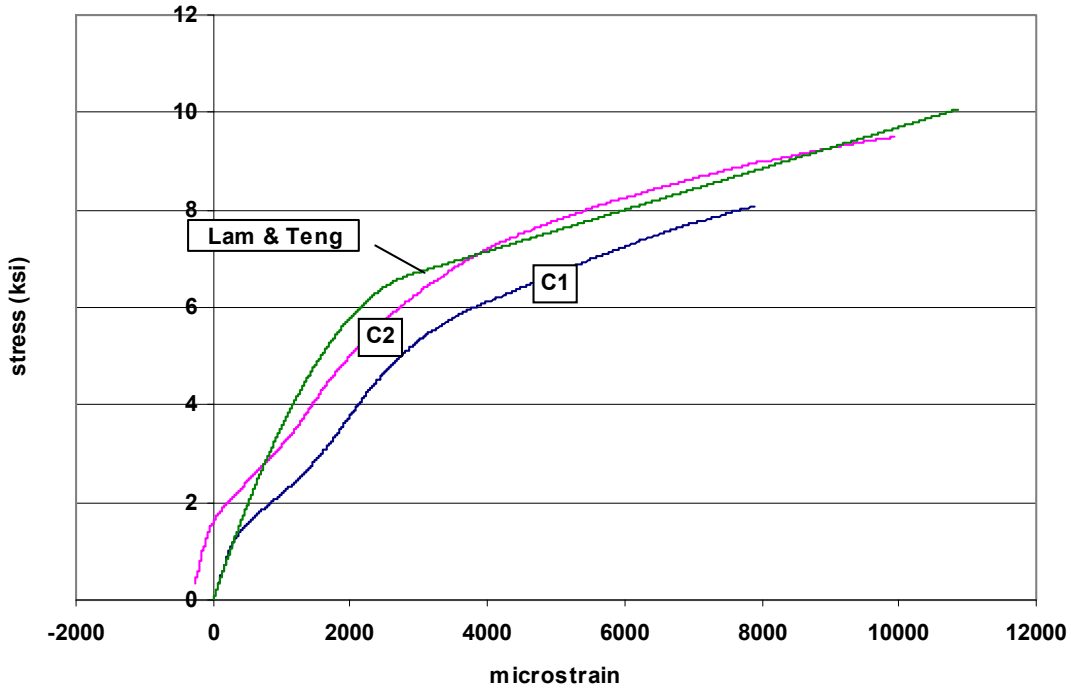

Figure 4-3 Comparison between the Baseline Model and Specimen C1 & C2

Even though the results of these two specimens will be excluded from the final analysis, some useful information can be gleaned. Up to 1.5 ksi, the behavior of specimen C1 corresponds very closely to the baseline model. The behavior of specimen C2 is comparable, but is shifted to the left due to eccentricity induced by the flexible support plate. With the exception of the discrepancy between 1.5 and 3.0 ksi, the general shape and values, the experimental response tends to follow that predicted by the model. Even with the discrepancy, specimen C2 failed at 94.2% of the predicted f'_{cc}. While the responses of these two specimens are not correct, they are close enough to the baseline model that they may also be called 'not incorrect.'

Baseline Model Verification by Specimens C3, C4, and C5

Figure 4-4 shows the comparison between the baseline model and specimens C3, C4, and C5. The response of specimens C3 and C4 are reported to failure while the response of specimen C5 is only shown through the start of the minor critical event. The average response is calculated using C3, C4, and C5 prior to the minor critical event. As seen in this figure, the average behavior of the control specimens tracks very closely with that of specimen C3 and the base line model.

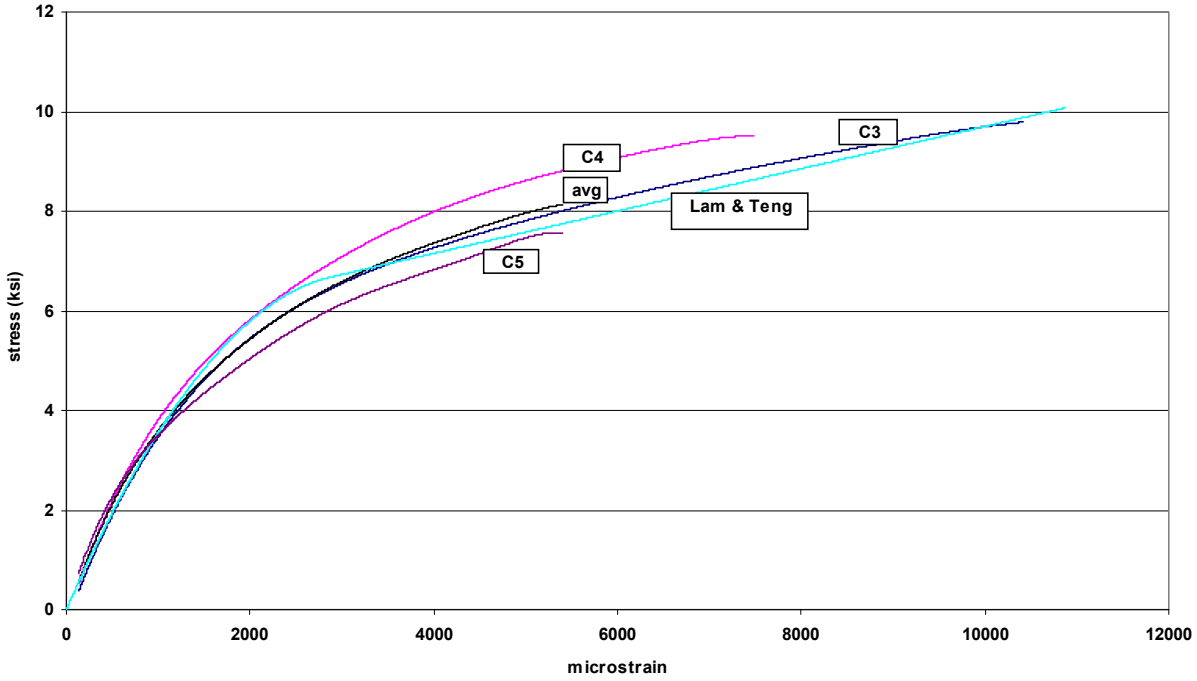

Figure 4-4 Comparison between the Baseline Model and Specimens C3, C4 and C5

Table 4-1 shows the comparison between the measured ultimate response of the specimens and that predicted by the baseline model. Specimen C3 compares favorably to the model. Specimen C4 shows reasonable agreement for strength, but failed at a substantially lower strain than predicted by the model. After both a minor critical event and a sustained load, specimen C5 failed at a lower stress than predicted, but at the predicted strain.

Specimen	f'_{cu}/f'_{cc} (as %)	$\varepsilon_{cu}/\varepsilon_{cc}$ (as %)	Failure Mode	Sustained Load?
C3	98.2%	100.6%	Yielding	No
C4	94.5%	68.9%	De-lamination,	No
C5	93.5%	101.1%	Yielding	Yes

Table 4-1 Comparison of Baseline Model Ultimate Response to Specimens C3, C4 and C5

Discussion of Specimen C6

The behavior of specimen C6 on the initial loading demonstrates one of the deficiencies of the load amplification device. Under normal conditions, the three longitudinal strain gages provide an accurate recording of the average strain. However, it is possible that the specimen can be positioned in such a way that one of the strain gages records a substantial tensile strain while the other strain gages do not record the necessary counterbalancing compressive strains.

The resulting average shows an overall tensile strain under a compressive stress as seen in Figure 4-5. As this is a physical impossibility, the error must be in the recording of the strains.

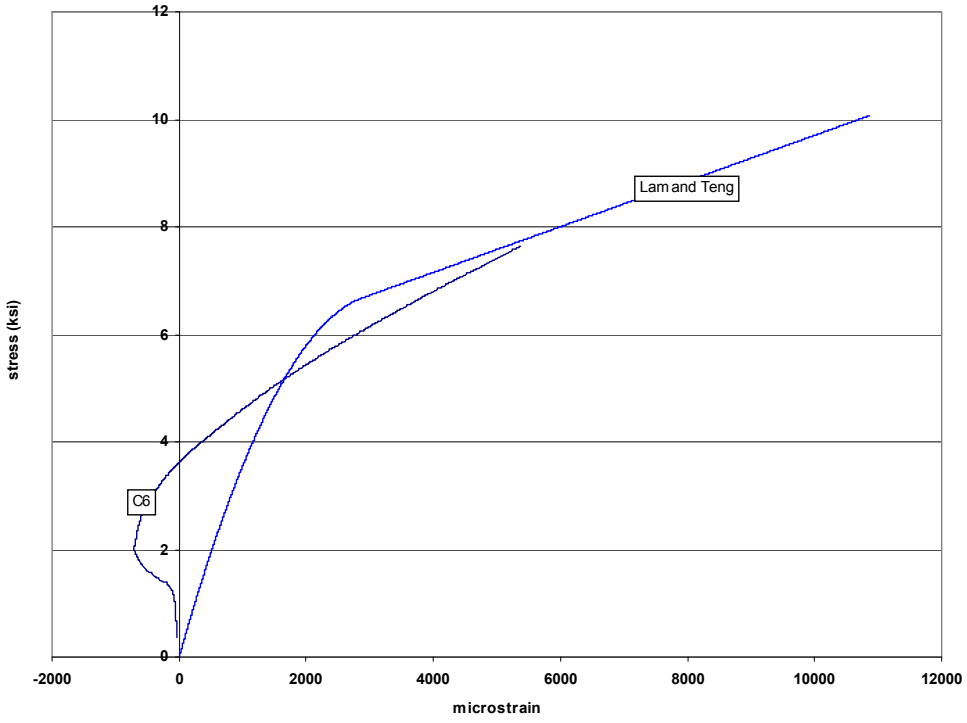

Figure 4-5 Average Response of Specimen C6

Based on the experience from this specimen, the procedures for subsequent experiments were modified. The individual strains were observed and averaged while the test was being conducted. If the average response indicated a tensile strain or if the average response deviated substantially from the baseline model, the test was terminated and the specimen rotated to gain a better recording of the average response. This technique proved successful in subsequent tests. Unfortunately, the average results in this initial loading are not useful for comparison.

Finding 1: Control Specimens Conform to Baseline Model

As exhibited in Figure 4-4, the response of specimens C3, C4, and C5 as loaded in the load amplification device shows good agreement with the baseline model. From this, it can be concluded that the specimens as prepared and tested are consistent with other experiments and published results. Furthermore, these results indicate that the Lab and Retrofit specimen groups can be compared to the baseline model to determine the impact of various life cycle factors.

4.2.2 Investigation 2: Impact of Sustained Service Load on Ultimate Stress-Strain Performance

The purpose of this investigation is to determine if and how the presence of a sustained service load impacts the ultimate stress-strain performance of an FRP confined specimen. This investigation is accomplished by comparing the results from the Lab Group tests to the baseline model which, according to Finding 1, serves as a reasonably accurate representation of the Control Group behavior.

Lab Specimen to Model Comparison

Figure 4-6 shows the comparison between the total response of specimens L1, L2, L3, and L4 to the baseline model of Lam and Teng. Specimens L1 and L2 were loaded monotonically while L3 and L4 included three cycles and were then loaded to failure. The grouping of these four specimens together is justified because after the three cycles, the response of specimens L3 and L4 returned to the envelope defined by the monotonic response. If Lam and Teng's model is plotted from zero initial strain, it initially over-predicts the response of all four specimens. Past the transition strain to the second branch, the model under-predicts the performance of specimen L2 while over-predicting the performance of L1, L3, and L4.

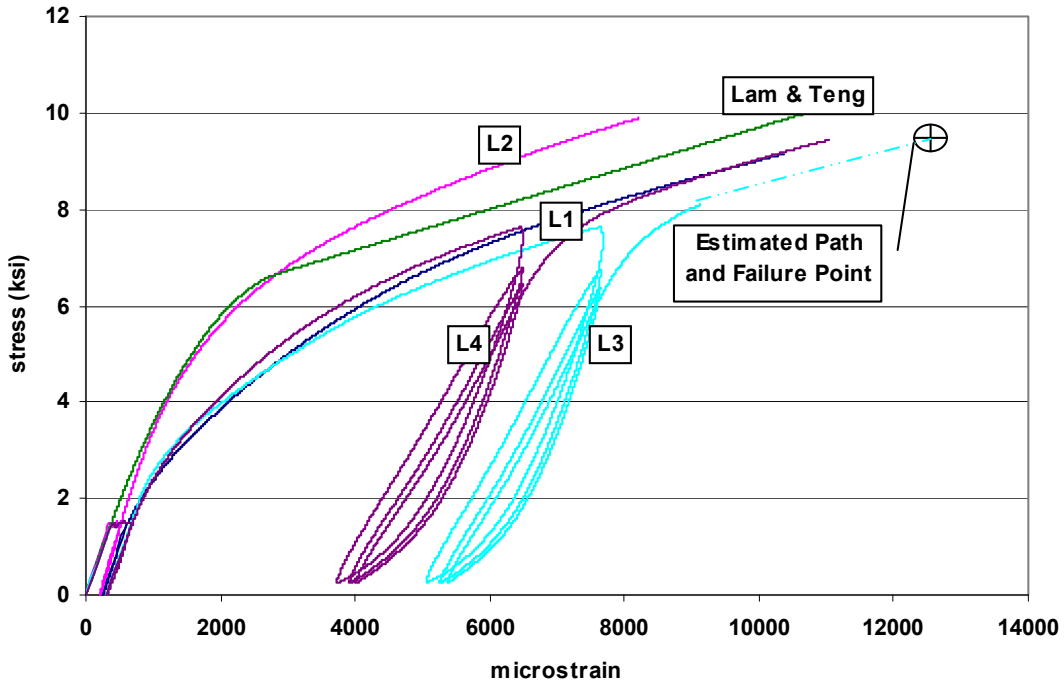

Figure 4-6 Lab Group to Baseline Model Comparison

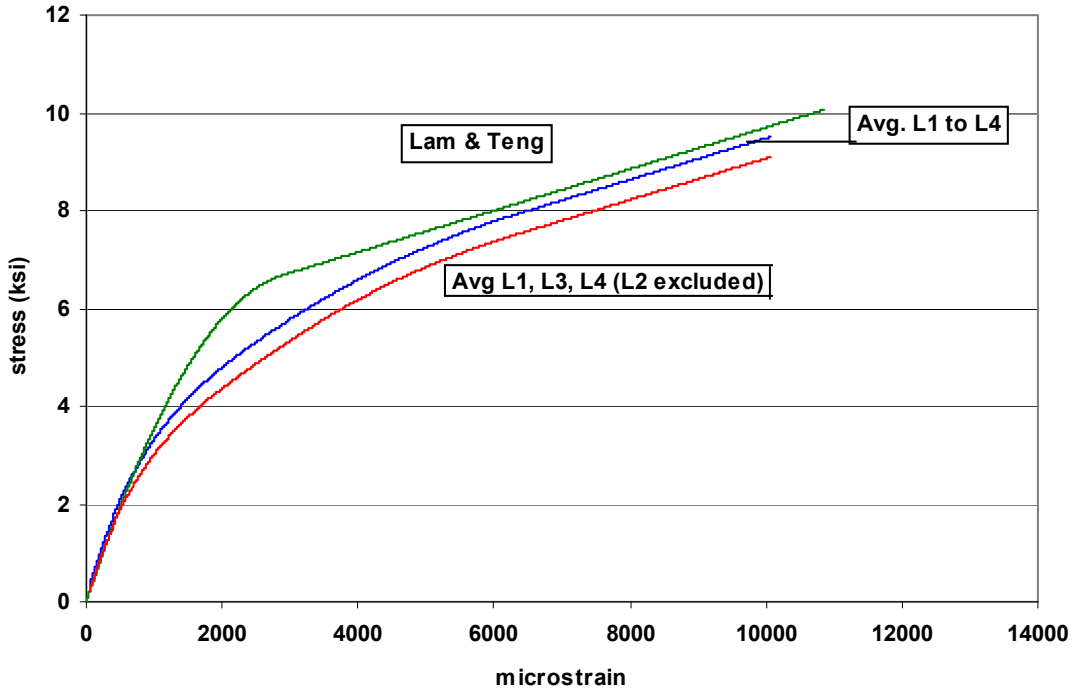

Figure 4-7 Average Behavior of Lab Group Specimens

Figure 4-7 shows the average behavior of Lab Group specimens 1 to 4 without the permanent strains due to the sustained load. The behaviors are averaged through the point where the cycles start for specimen L4. Beyond this point, the average behavior is projected forward as the tangent to the last average data point. The average terminates at the failure point of specimen L1. Two average behavior curves are shown. One includes all four specimens and one excludes specimen L2. The exclusion of L2 from the average is justified based on the observation that it seems to exhibit a different failure mode as discussed in Section 4.2.5. Corrections are clearly required to the baseline model to allow better prediction of the stress strain behavior following a period of sustained loading.

Table 4-2 shows the comparison of the ultimate response predicted by the baseline model to that achieved in the Lab Group tests. All specimens failed to achieve the predicted strength. Both specimens loaded monotonically failed to achieve the predicted strain while both specimens loaded cyclically exceeded the predicted strain. This increase in strain capacity for cyclically loaded specimens is consistent with the findings of Lam, et al. (2006) in Section 2.8.3.

Specimen	f'_{cu}/f'_{cc} (as %)	$\varepsilon_{cu}/\varepsilon_{cc}$ (as %)	Failure Mode	Sustained Load?
L1	90.8%	95.3%	de-lamination	41 days
L2	98.2%	75.6%	de-lamination	41 days
L3	95.9%	116% (estimate)	de-lamination	41 days
L4	93.7%	102%	de-lamination	42 days

Table 4-2 Comparison of Baseline Model Ultimate Response to Specimens L1 to L4

Potential Modifications of Baseline Model

To predict the effects of sustained loading on ultimate stress-strain behavior, two adjustments are required. First, the effects of the sustained loading are removed so that the specimen response starts at zero strain. Second, the second branch of the baseline model must be lowered to meet the actual stresses from the experiments. Within the linear region of the second branch, the experimental data averaged 91% of the original model values. The shift of the curve was accomplished simply by reducing the reference stress of the plain concrete from f'_c to $0.91f'_c$. Figure 4-8 shows the comparison between the average experimental data and the modifications to Lam and Teng's equations. The modified model shows good agreement with the experimental results, except in the central portion where the model over predicts the specimen's strength. This issue will be addressed in Section 4.4.2. Additionally, the discussion of ultimate stress and strain values is reserved to Section 4.2.8.

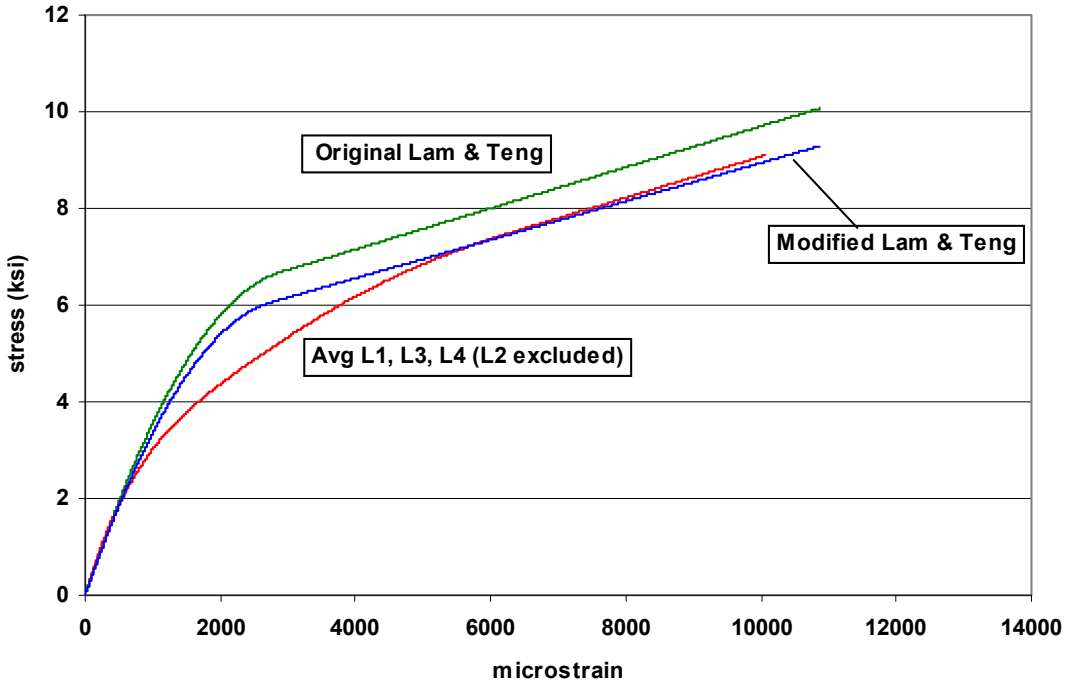

Figure 4-8 Modifications to Lam and Teng Based on Sustained Loading

Finding 2: Sustained Loads Change the Stress Strain Behavior of FRP Confined Concrete

A sustained load of $0.27f'_c$ for 41 days (±1 day) on an FRP confined concrete specimen results in a stress-strain behavior approximately 9% below that predicted by Lam and Teng's model in the second branch. Ultimate performance is also below that predicted by the model. Modifications are possible to Lam and Teng's model to allow for better prediction of post sustained load response.

4.2.3 Investigation 3: Impact of Time of FRP Application on Stress-Strain Behavior

This investigation determines if there is a difference in behavior between the Lab Group specimens which were wrapped with FRP prior to the application of sustained load and the Retrofit Group specimens which were subjected to a sustained loading prior to undergoing an FRP retrofit.

Average Response of the Retrofit Group Specimens

Figure 4-9 shows the total response of specimens R1, R2, R3, R4, and R5. The baseline model is shown as a reference only. Specimens R1, R3, and R4 underwent sustained loading for

31 days and then were retrofitted with FRP. After 10 or 11 days of additional sustained loading, the specimens were tested to failure. Specimens R2 and R5 underwent 39 days of sustained loading prior to retrofit. After an additional 2 or 3 days of sustained loading, these specimens were tested to failure.

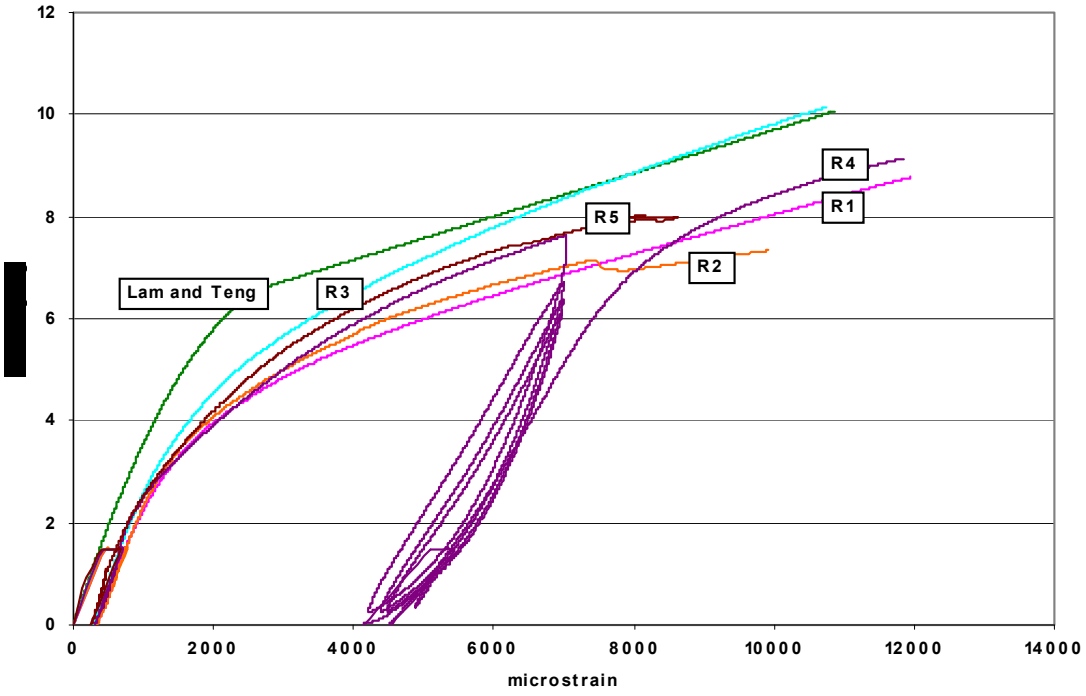

Figure 4-9 Total Response of Retrofit Group Specimens

Figure 4-10 displays the average behavior of the Retrofit Group specimens including the permanent strains from the sustained loading. The baseline model is again shown for reference only. The behavior of specimens R1 to R5 is averaged through the point when specimen R4 began to cycle. Beyond this point, the average behavior is taken as the slope of the average curve at the last points calculated.

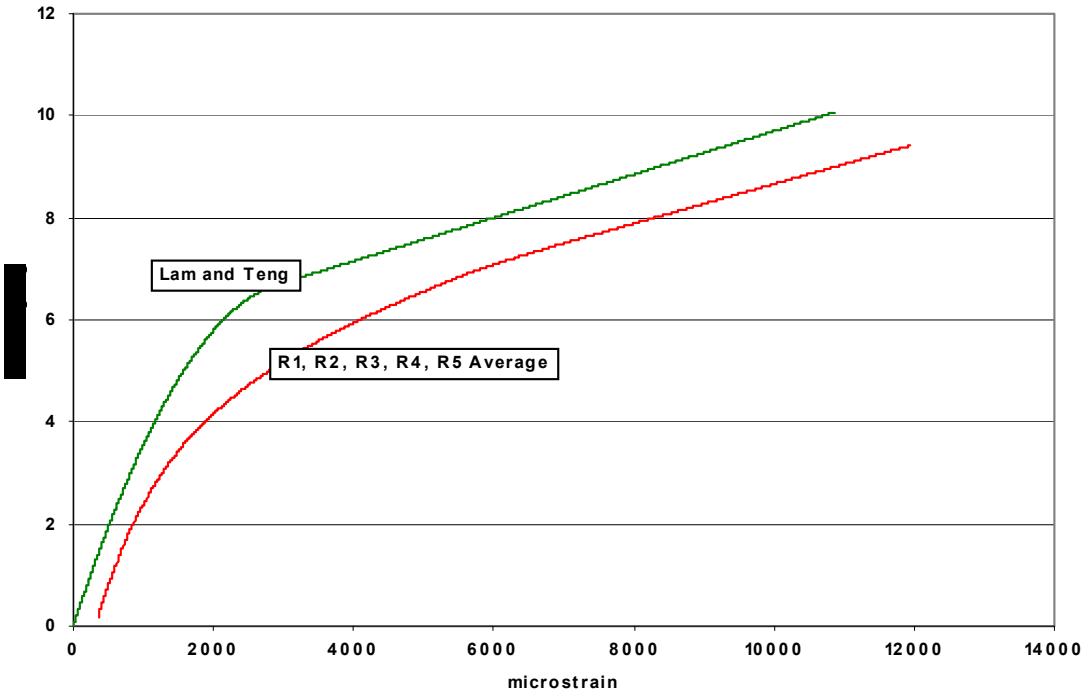

Figure 4-10 Average Behavior of Retrofit Group Specimens

Comparison of Retrofit and Lab Group Average Behavior

A comparison of Figure 4-4, Figure 4-7, and Figure 4-10 shows that the application of a sustained load prior to ultimate loading changes the stress-strain behavior of the specimen. Figure 4-11 helps to evaluate the importance of FRP in this behavior change. Below the transition point of about 6 ksi, the behavior of the Lab and Retrofit groups are essentially the same. Above this point the behavior of the Retrofit Group is slightly below that of the Lab Group. The difference, however, is very small. From Figure 4-11 it can be concluded that the application of a sustained load is a more important factor in behavior change than the point of application of FRP.

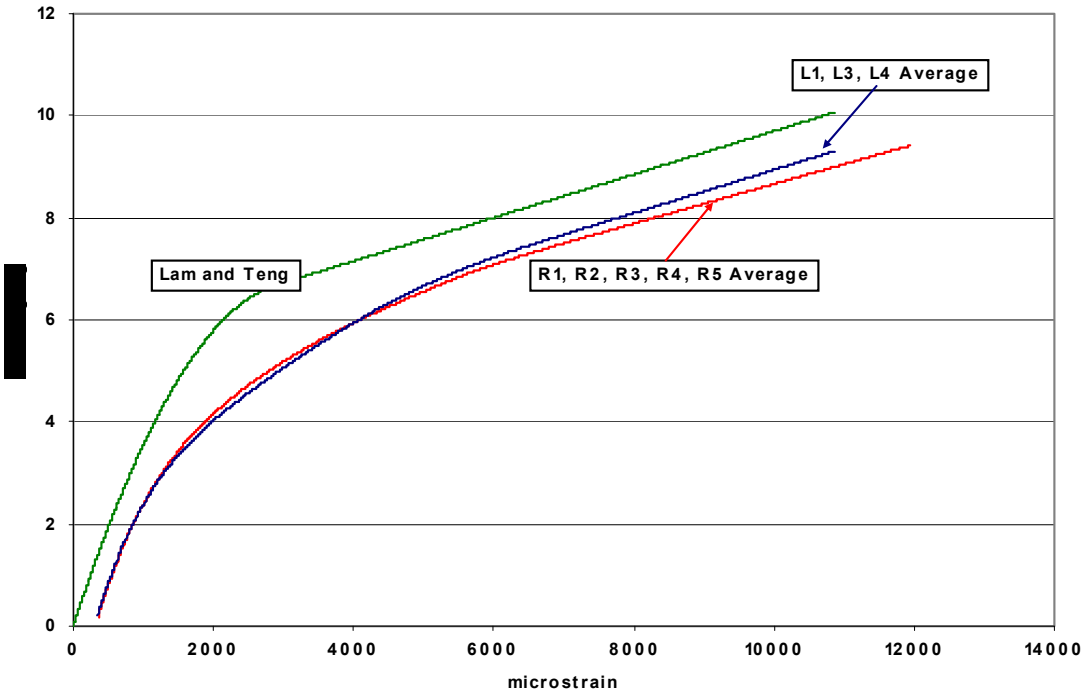

Figure 4-11 Comparison of Retrofit and Lab Groups

Retrofit Group to Baseline Model Comparison

Figure 4-12 shows the comparison between the Retrofit Group average results without the permanent strains from the sustained load and the baseline model. Lam and Teng's model clearly unconservative under these conditions. Table 4-3 shows the comparison between the ultimate response of the Retrofit Group and the ultimate stress and strain predicted by the baseline model. In general, the Retrofit Group specimens failed to achieve the predicted ultimate compressive stress. Specimen R4 which was subjected to cyclic loading exhibited the same increase in ductility as observed in the cyclically loaded Lab Group specimens and is consistent with the findings of Lam, et al. (2006) in Section 2.8.3

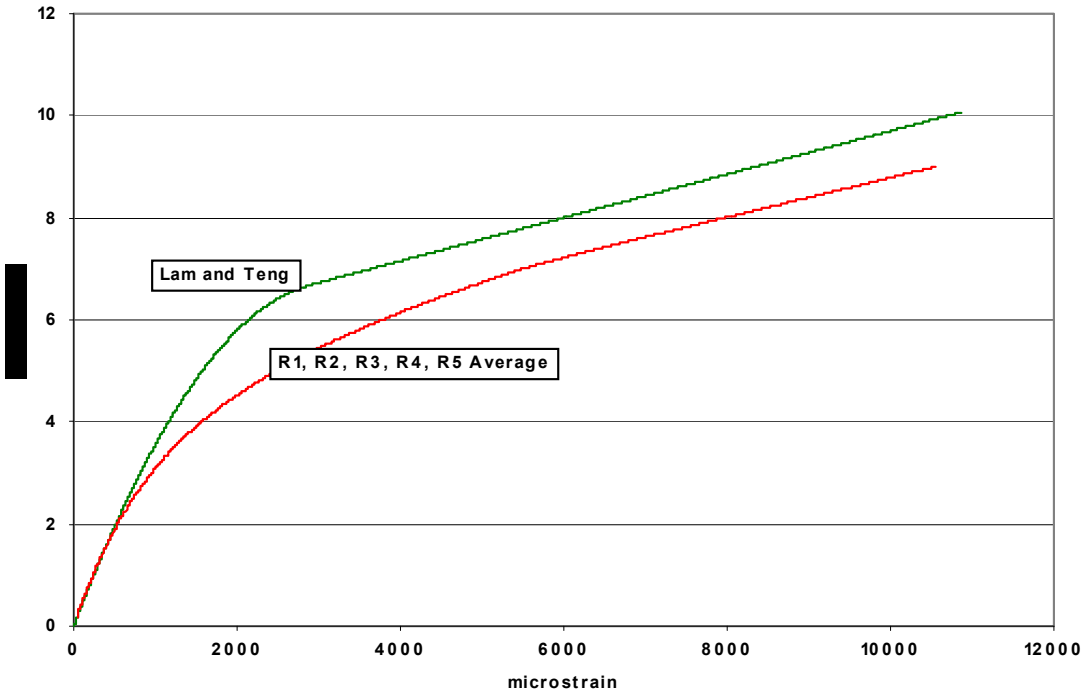

Figure 4-12 Retrofit Group and Baseline Model Comparison

Specimen	f'_{cu}/f'_{cc} (as %)	$\varepsilon_{cu}/\varepsilon_{cc}$ (as %)	Failure Mode	Sustained Load?	
				total	w/FRP
R1	87.1%	110%	rupture	42 days	11 days
R2	78.8%	88.3%	de-lamination	42 days	3 days
R3	100.7%	99.0%	de-lamination	42 days	11 days
R4	94.3%	146%	de-lamination	41 + 40 days	10 + 40 days
R5	80.3%	75.1%	de-lamination	41 days	2 days

Table 4-3 Comparison of Baseline Model to Retrofit Group Ultimate Response

Potential Modifications to Baseline Model

Similar to the results of Investigation 2, Lam and Teng's model can be applied to predict the response of the Retrofit Group. First, the Retrofit Group average response is shifted to the left to remove the residual strain from the sustained loading. Second, the reference plain concrete ultimate stress is reduced to $0.89f'_c$. 89% was selected because within the linear region of the second branch, the experimental data averaged 89% of the original model values. Figure

4-13 shows the comparison between the average experimental Retrofit Group data and the modifications to Lam and Teng's equations. The modified model shows good agreement with the experimental results, except in the central portion where the model over predicts the specimen's strength.

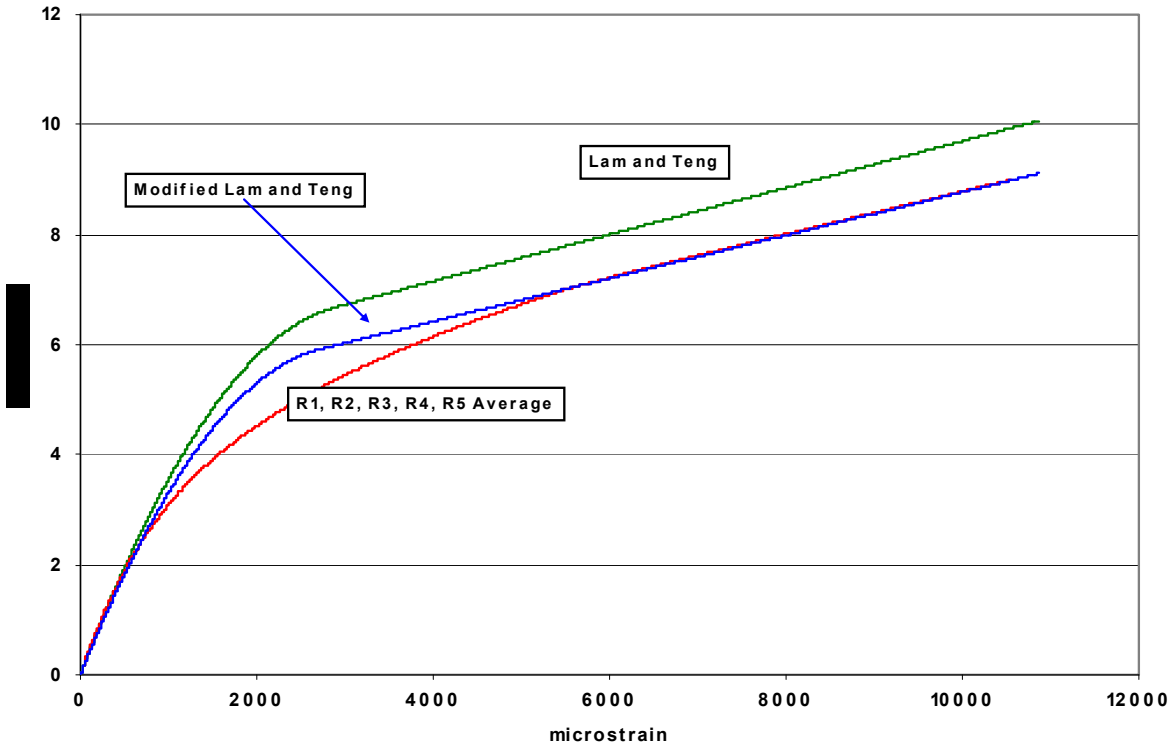

Figure 4-13 Modification to Lam and Teng Based on Retrofit Group Response

Finding 3: Age of Application of FRP has a Minimal Impact on Behavior Changes

As evident in Figure 4-11, the difference in behavior between specimens that were wrapped prior to the application of the sustained load and specimens that were wrapped after 30 or more days of sustained loading is very small. Thus, it is found that sustained loading has a larger impact on the change in stress-strain performance than the time of application of FRP.

Additional Comments on Investigation 3

Based on the explanation given in section 3.3.3 and shown in Figure 3-82 and Figure 3-83, the results of specimen R6 are excluded from the analysis. Excessive eccentricity and instability resulted in a stress-strain response that cannot reliably be compared to other results.

Specimens R1, R3, R4, and R6 were retrofitted with FRP 10 or 11 days before testing while specimens R2 and R5 were retrofitted 3 and 2 days before testing, respectively. This was done to further explore the impact of age of FRP application on stress-strain behavior. It is interesting to note that specimens R2 and R5 exhibited a similar stress-strain response to the other specimens, but failed at a substantially lower stress and strain. This premature failure may have been due to the shorter cure time or by a discrepancy in the epoxy preparation or FRP application. The author does not feel sufficient data exists to accurately determine the cause of this response.

4.2.4 Investigation 4: Impact of FRP on Creep Behavior

This investigation is accomplished by comparing the results of the sustained load response of the Lab Group (specimens wrapped with FRP) to the Retrofit Group (un-wrapped specimens)for the first 31 days of sustained loading. The comparison terminates at 31 days because the Retrofit Group specimens were wrapped with FRP on day 31 after the strain readings were taken.

Data and Model Comparison

Figure 4-14 shows the average longitudinal creep strains of all specimens in the Retrofit and Lab groups for the first 31 days of loading. During this time, the average daily stress for both groups was 1.49 ksi. Also shown are the ACI 209 creep predictions for both groups. As explained in section 4.1.2, the difference in the two curves is due to the age of the concrete at the application of the sustained load. Even with the different ages at first load, there is only a 1.5% variance in the predicted creep strains at 42 days.

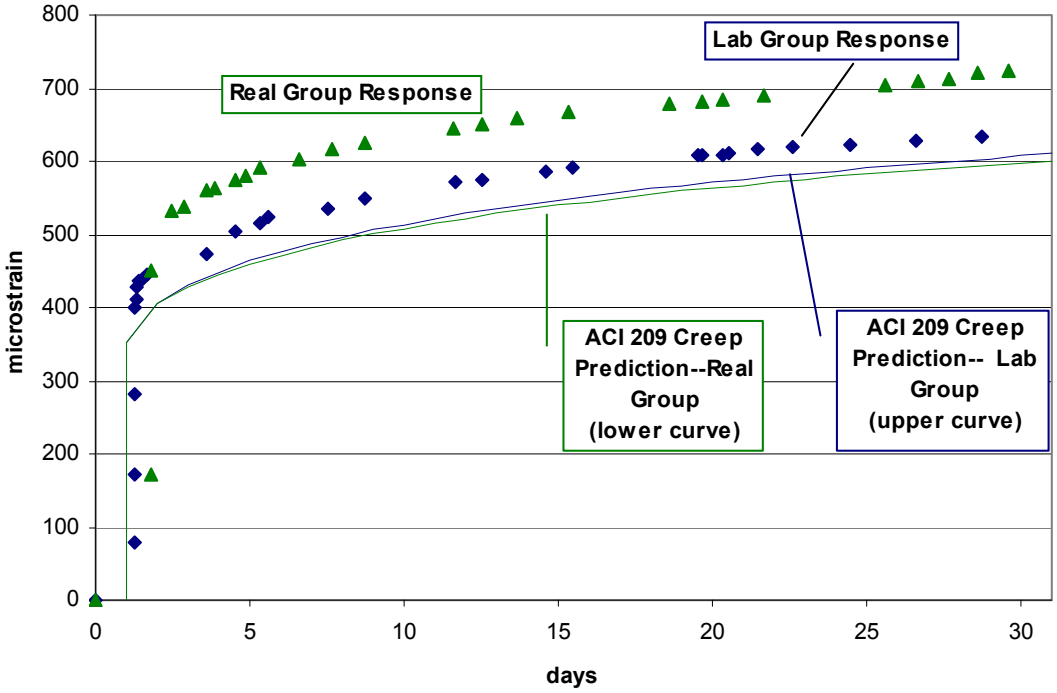

Figure 4-14 Retrofit and Lab Group Creep Behavior Compared to ACI 209 Creep Model

Creep Strain Analysis

Using the estimated elastic modulus of 4,210 ksi and an applied stress of 1.49 ksi, the initial elastic strain is 353 με. The 318 Commentary (ACI, 2005) states that the actual value of the modulus of elasticity may vary as much as 20% from the value estimated by $57{,}000\sqrt{f_c'}$. This variance places the range of initial elastic strains between 293 and 442 με. The recorded initial elastic strains were 399 με for the Lab (wrapped) Group and 451 με for the Retrofit (un-wrapped) Group. The initial elastic strain of the Lab (wrapped) Group is 88.5% of the Retrofit (un-wrapped) Group.

It is evident in Figure 4-14 that the Retrofit (un-wrapped) Group displayed greater total creep strains than the Lab (wrapped) Group. Naguib and Mirmiran (2003) give two principal reasons that FRP wrapped specimens creep less than un-wrapped ones. First, the fiber-epoxy combination acts as a sealer to prevent migration of moisture which substantially reduces drying creep and shrinkage. Second, the FRP wrap results in a triaxial state of stress which also reduces creep. The first statement is derived from the work of Russell and Corley (1977) while the second is based on Gopalakrishnan et al. (1970) and Jordaan and Illston (1971). Based on

selected points, the response of the Lab Group is 88.5% of the Retrofit Group Response when considering the impact of both initial elastic and long term creep strains. This relationship is based entirely on the initial behavior as the relationship starts at 88.5% and continues at that rate for all 32 days. This correlation is shown in Figure 4-15.

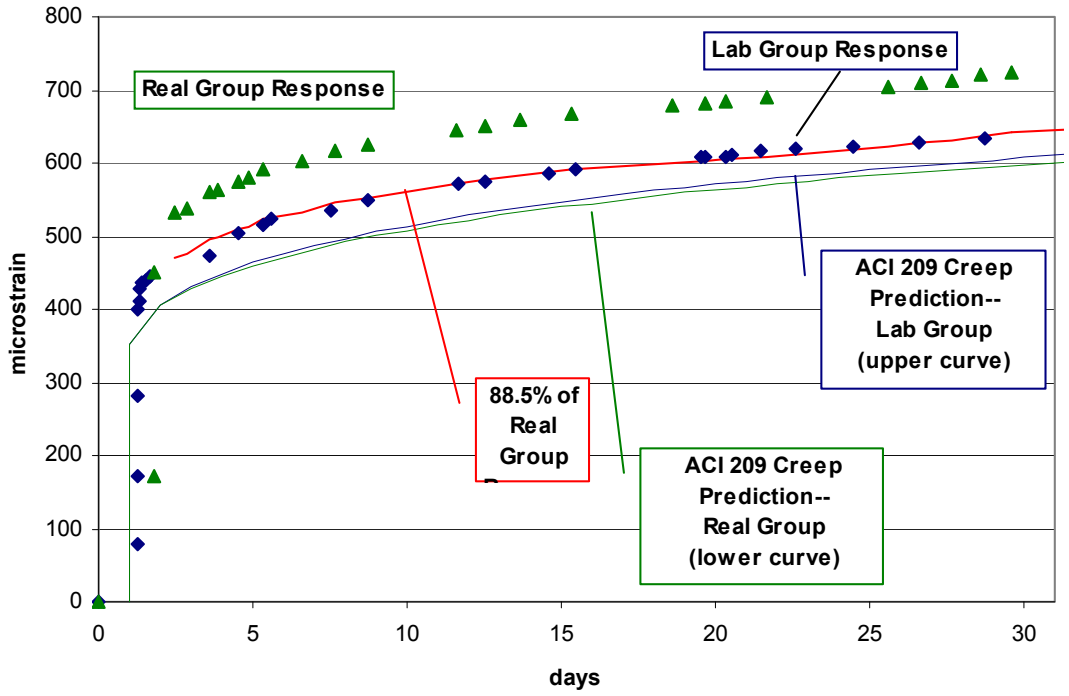

Figure 4-15 Impact of FRP on Creep Response

To remove the impact of the different levels of initial elastic strain, Table 4-4 considers only the difference between the total strain on sustained loading day 32 and the initial elastic strain recorded at the first application of the 1.49 ksi applied stress. The ACI 209 creep strain values are calculated using the recorded initial elastic strain rather than that based on the estimated elastic modulus. The result is the strain due to creep only without regard for the initial elastic strain and allows the evaluation of the ability of ACI 209 to predicted creep strains. In this table, it can be seen that the presence of the FRP on the Lab specimens resulted in a 13% decrease in the magnitude of creep strains when compared to the Retrofit Group. It can also be seen that, under these conditions, the procedures of ACI 209 for determining the magnitude of creep strains under-predicted the response of the Retrofit and Lab Groups.

	Lab Group		Retrofit Group	
Measured $\varepsilon_{32\ days} - \varepsilon_{initial}$	244	Actual creep strain is 82.2% of predicted	280	Actual creep strain is 86.4% of predicted
ACI 209 $\varepsilon_{32\ days} - \varepsilon_{initial}$	297		324	

Table 4-4 32 Day Creep Strains of Lab and Retrofit Groups

Using ACI 209 (1992) the creep coefficient at any time can be calculated by dividing the creep strains by the initial elastic strain. Under these conditions at 32 days, the creep coefficient predicted by ACI 209 (1992) was 0.71 to 0.75 while the creep coefficients found from the experimental data were 0.61 for the Lab Group and 0.62 for the Retrofit Group.

Finding 4: An FRP Jacket Reduces Creep Behavior under Sustained Loads

Under the test conditions, the Lab (wrapped) Group specimens exhibited only 88.5% of the initial elastic strain of the Retrofit (un-wrapped) Group. This relationship continued at this rate over all 32 days of the investigation. Over the same time, the creep coefficients of both groups were essentially the same—0.61 and 0.62. Thus, it can be concluded that while the creep coefficient is unaffected by FRP, the FRP does reduce the initial elastic strain and the total creep strains of the specimen. For the same time period ACI 209 predicts a creep coefficient of 0.75. Given that the ACI ultimate creep coefficient can vary form 1.3 to 4.15, these differences are within an expected range.

4.2.5 Investigation 5: Relating Sustained Load, Failure Mode, and Stress-Strain Behavior.

It has long been known that the typical stress-strain behavior of FRP confined concrete can be described with a bi-linear curve where the first branch is controlled by plain concrete behavior and the second branch is controlled by the properties of the FRP jacket. The most common failure mode is rupture of the FRP jacket. As discussed in Section 2.5.3, Lam and Teng (2003) using a database of 76 tests report that the rupture strain of FRP on a circular specimen should be taken as 58.6% of the coupon rupture strain. A significant limitation of Lam and Teng's work is that it considered FRP rupture as the only failure mode. However, other failure modes exist as discussed in Section 3.3. The epoxy can fail resulting in a de-lamination of the FRP jacket. The specimen can undergo apparent yielding where no additional load can be sustained but de-lamination or FRP rupture are not observed. Additionally, a small, but significant, portion of test specimens do not display the typical bi-linear stress-strain response.

Sustained Load and Failure Mode

Under the normal experimental conditions of cast-wrap-test, the expected failure mode is FRP rupture. Specimens C1 to C4 were prepared in this manner and tested without the application of sustained load and the failure modes can be seen in Table 4-5. Specimens C5 and 6 underwent minor critical events and then a sustained load prior to ultimate loading. All specimens in the Lab and Retrofit Groups were subjected to sustained loading prior to ultimate loading. From this table and the work of other researchers, it can be seen that FRP rupture is the expected failure mode for cast-wrap-test specimens while de-lamination predominates under the Lab (cast-wrap-sustained load-test) and the Retrofit (cast-sustained load-wrap-test) conditions.

Specimen	Control Group	Lab Group	Retrofit Group
1	Rupture	De-lamination	Rupture
2	Rupture	De-lamination	De-lamination
3	Yield	De-lamination	De-lamination
4	De-lamination	De-lamination	De-lamination
5	Yield	Rupture + Yield	De-lamination
6	Yield	De-lam. + Yield	De-lamination

Table 4-5 Failure Mode Summary for Control, Lab, and Retrofit Groups

Atypical Stress-Strain Relationship

Some tests of FRP confined concrete have resulted in failure points where the failure stress is comparable to the predicted failure stress while the failure strain is substantially lower than predicted. This manner of failure tends to result in a stress-strain relationship that is different from the typical bi-linear relationship.

As detailed in Section 2.5.2, Karabinis and Rousakis (2002) had two of twenty two specimens exhibit this behavior. These specimens failed at a comparable strength and 60% of the strain when compared to their expected failure mode counterparts. From Section 2.7.2, Naguib and Mirmiran (2003) had one specimen, FWCC 40, which also demonstrated this atypical behavior. In the current research, specimens C4 and L2 exhibited this behavior. See Figure 4-16. Table 4-6 shows the comparison of the failure points of the specimens that exhibited atypical failure points. The atypical failure stresses are very close to the expected values while the atypical failure strains are approximately 60 to 75%of the expected values. From Table 4-6, both specimens with and without sustained load have demonstrated this atypical behavior.

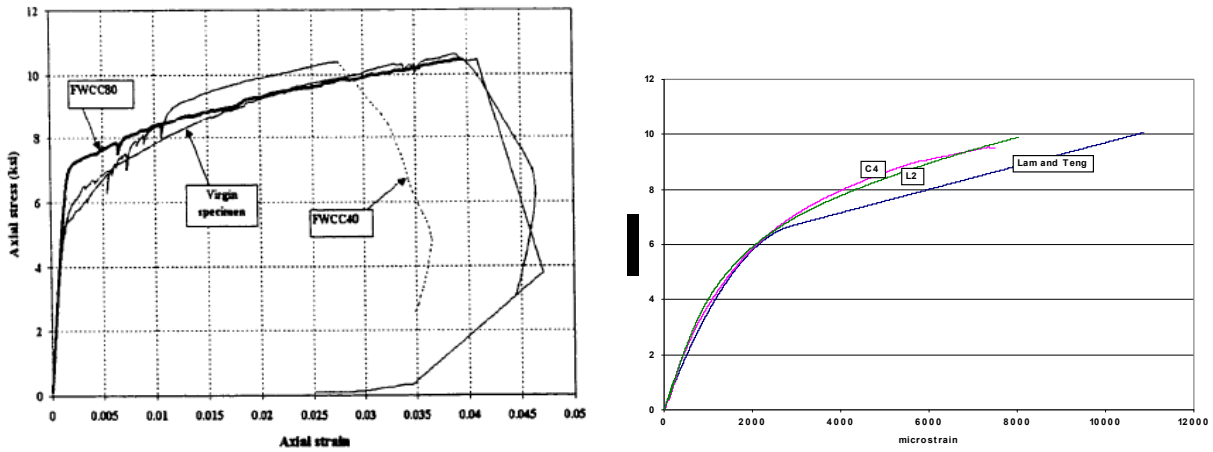

Figure 4-16 Atypical Stress-Strain Relationship from Naguib and Mirmiran (2003) and This Research

Specimen	Failure Strength actual/predicted	Failure Strain actual/predicted	Sustained Load Prior to Failure
Karabinis and Rousakis (2002)	100%	60%	No
Karabinis and Rousakis (2002)	100%	66.7%	No
Naguib and Mirmiran (2003)—FWCC40	98%(±)	70%(±)	Yes
This Research—C4	94.5%	68.9%	No
This Research —L2	98.2	75.6	Yes

Table 4-6 Comparison of Failure Points For Typical and Atypical Stress-Strain Relationships

Finding 5A: Sustained Load Changes the Expected Failure Mode

For specimens that undergo a cast-wrap-test lifecycle, the prevailing failure mode is FRP rupture. De-lamination becomes the most common failure mode for specimens with a sustained load period in the life cycle. This is possibly attributable to the fact that as the concrete creeps, the FRP creeps as well.

Finding 5B: The Atypical Stress-Strain Relationship Must Be Considered

At least three different researchers conducting independent test with varying parameters have had specimens which have demonstrated the atypical failure described above. As this failure mode occurs with limited frequency, it could reasonably be excluded from an analysis with a small number of specimens. However, when a large scale analysis is done combining the results of many researchers, this should be included in the analysis. A possible variation, even if unlikely, of 35% in the failure strain is significant. This is especially important when reliability studies are performed to determine appropriate resistance factors for FRP confined concrete.

4.2.6 Investigation 6: Impact of Prior Damage on Creep Behavior

This investigation examines the creep performance of specimens that have been damaged by minor critical events. It is related to Investigation 7 and seeks to address the issues raised by Shan, Xiao, and Gou (2006) concerning reserve capacity after loadings which exceed service levels but do not fully reach design levels. Specimens C3 and C4 underwent minor critical events then were placed in the sustained load device prior to being broken. Specimens L5, L6, and R4 were subjected to sustained loading and a minor critical event and then returned to the sustained load device for additional creep investigations prior to being broken.

Creep Performance under Service Load

Figure 4-17 shows the creep strain due to applied service loads for specimens L5, L6, and R4. The curve labeled 'ACI 209 Prediction' is calculated using an average initial age of loading of 131 days and an initial average elastic strain of 432 microstrain. Provided an accurate initial elastic strain is used, the procedures of ACI 209 provide a conservative estimate of creep behavior.

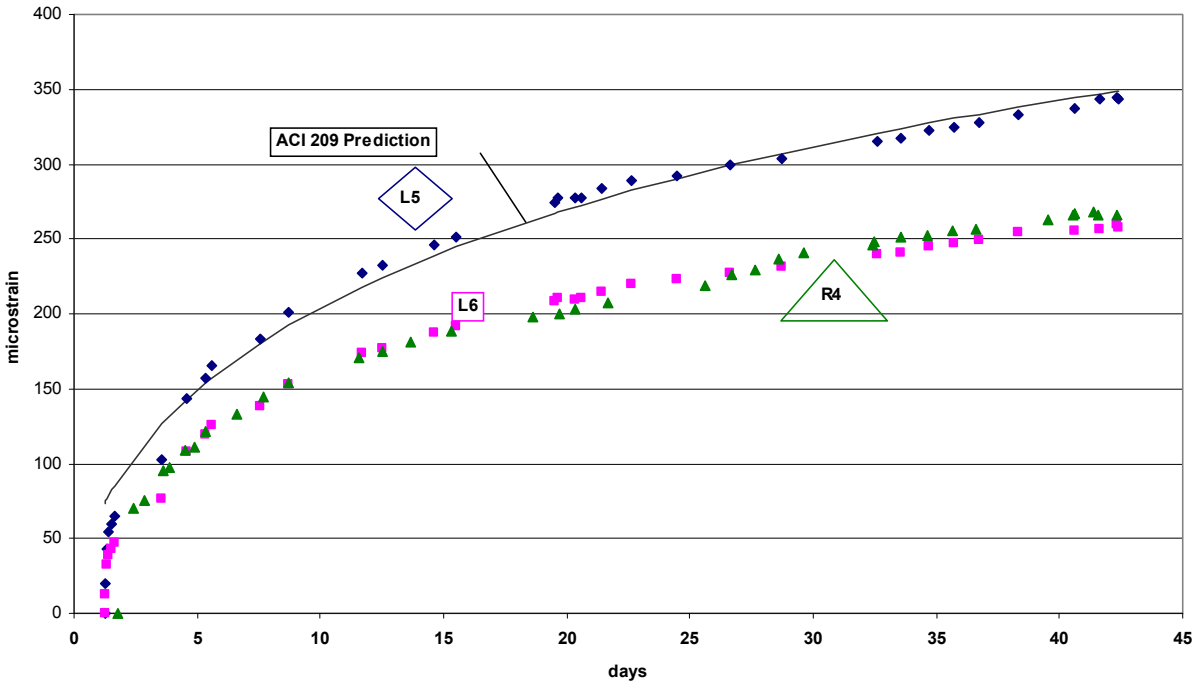

Figure 4-17 Creep Performance Under Sustained Service Loads

Creep Performance after a Minor Critical Event

ACI 209 determines creep in a specimen or a structure by multiplying the initial elastic strain by a creep coefficient. This procedure becomes problematic after a minor critical event because the specimen has been pushed beyond its elastic range and has been fractured in the process. Accordingly, when the specimen is again subjected to a service load, the elastic strain cannot be accurately calculated by dividing stress by the elastic modulus. As presented in Section 2.8.2, Shan, Xiao, and Gou (2006) suggest increasing the initial elastic strain of a damaged specimen by a factor of 1.98 and then applying the creep procedures of ACI 209.

Figure 4-18 shows the creep performance of specimens C6, C5, L5, L6, and R4 after being subjected to a minor critical event. The curve labeled 'ACI 209 using 432 microstrain' predicts the creep strains using the initial undamaged average elastic strain of 432 microstrain. This curve under predicts the creep of the damaged specimens. The curve labeled 'ACI 209 using 901 microstrain' performs the same calculations using the measured initial elastic strain of the damaged specimens. This curve provides a better estimate of creep strains and is conservative for all specimens except C6. However, it appears that if the timeframe were extended, this discrepancy would be corrected. The ratio of the undamaged to the damaged initial strains is 2.08.

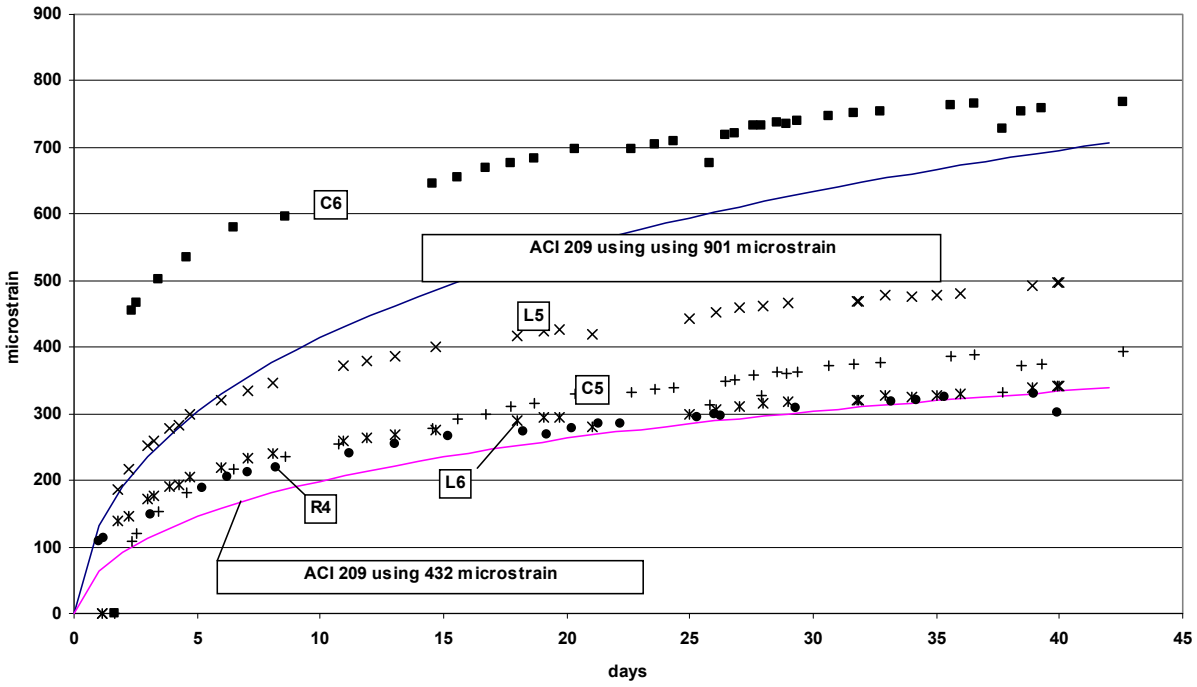

Figure 4-18 Creep Performance Following Minor Critical Event

Finding 6: Prior Damage Increases the Magnitude of Creep Strains

A specimen damaged by a minor critical event exhibits a higher initial strain under a service load and higher creep strains than an undamaged specimen. Consistent with the findings of Shan, Xiao, and Gou (2006), the procedures of ACI 209 can reasonably predict creep behavior provided the initial strain is modified according to Equation 2.87. Shan, Xiao, and Gou found the value of the coefficient α to be 1.98 for their test conditions. Under the conditions of this test, α has a value of 2.08. It can be concluded that if the initial elastic strains are doubled and the procedures of ACI 209 are applied, the creep strains of a damaged specimen can be reasonably predicted.

4.2.7 Investigation 7: Reserve Capacity Following Service Loading and a Minor Critical Event

As reported by Shan, Xiao, and Gou (2006), current seismic retrofit philosophies expect that the structure will survive one extreme seismic event. This raises issues of performance in a series of less severe seismic events as well as the economic justifications for a retrofit that may not provide long term protection. Accordingly, this investigation examines the ultimate performance of a specimen that has previously been subjected to a combination of retrofit, sustained load, minor critical event, and additional sustained load. This simulates the performance of an older structure that has been through a retrofit and at least one more frequent, less severe seismic event.

Specimen Responses

Figure 4-19 shows the stress-strain responses of all specimens that were subjected to a minor critical event (MCE)-sustained load-extreme critical event life cycle. Specimens Control 5 and 6, Lab 5 and 6, and Retrofit 4 met this criterion. Strains are shown from zero strain and do not include any of the residual strains from prior events. Table 4-7 reports the failure stresses and stains of these specimens along with the residual strain prior to the MCE and the strains recorded during the MCE. The failure strain is the combination of the two.

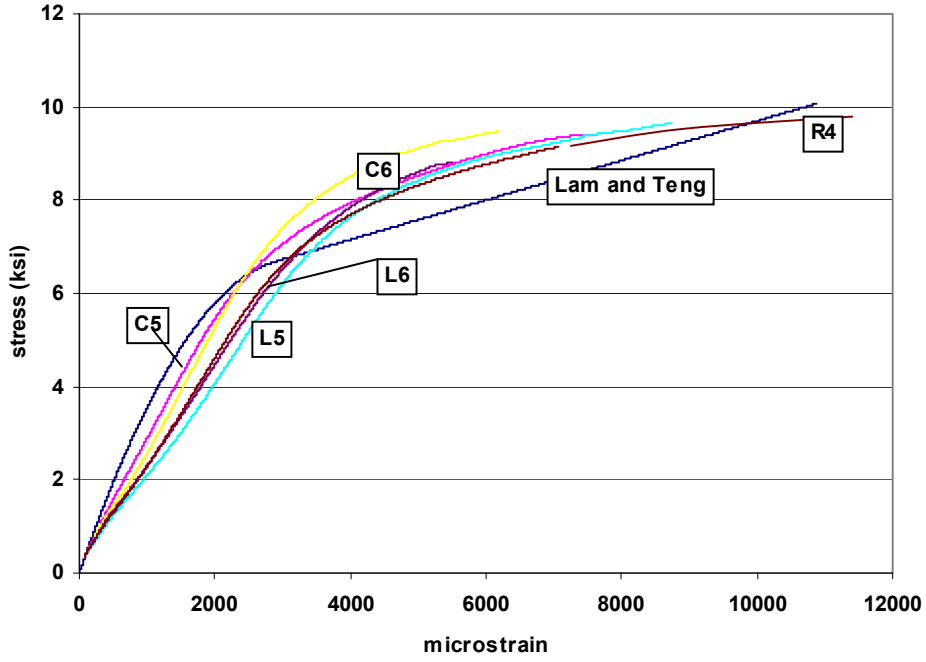

Figure 4-19 Stress-Strain Response of Post MCE Specimens without Residual Strain

	Max Stress (ksi)	Pre-MCE strains	Strains from MCE	Total Failure Strain
C5	9.41	3234	7758	10992
C6	9.48	2877	6489	9366
L5	9.66	5815	9166	14981
L6	8.81	4469	5678	10147
R4	9.79	4544	11388	15932
Average	9.43	4056	8096	12284
Lam & Teng	10.07	---	---	10870

Table 4-7 Failure Points of Post MCE Specimens

Residual Capacity Analysis

Table 4-8 shows the comparison between the failure stresses and strains recorded in the extreme critical event and the baseline model in percentage form.

	Max Stress (ksi)	Strains from MCE	Total Failure Strain
C5	93.4%	71.4%	101%
C6	94.1%	59.7%	86.2%
L5	95.9%	84.3%	138%
L6	87.5%	52.2%	93.3%
R4	97.2%	104.8%	146%
Average	93.6%	74.5%	113%
Lam & Teng	100%	---	100%

Table 4-8 Failure Point to Model Comparison for Post MCE Specimens

The specimens averaged 93.6% of the calculated ultimate strength compared to 95.4% with the control group findings reported in Section 4.2.1. When only the strains generated from the final ultimate loading are considered, the average specimen failure strain was 74.5% of the expected failure strain. However, when the total strain histories of the specimens are considered, the specimens demonstrated failure strains ranging from 86.2% to 146% of the estimated value.

Finding 7: Damaged Specimens Retain Significant, but Diminished Stress-Strain Capacity

At the levels of sustained load and minor critical events used in this study, damaged specimens retained over 90% of the stress capacity of undamaged specimens. However, only about 75% of the expected strain capacity remained. The strain capacity of a specimen is a finite quantity. Beyond the elastic range, once strain capacity is 'used', it cannot be recovered and 're-used.' If one third of the strain capacity is consumed from sustained loading and minor critical events, only two-thirds of the capacity remains to provide ductility during an extreme critical event.

4.2.8 Investigation 8: Impact of Varying Life Cycles on Ultimate Behavior

Prediction of the ultimate stress and strain of FRP confined concrete specimens has always proven problematic. Nanni and Bradford (1995) found that the model of Fardis and Khalili (1982) underestimated ultimate strains. Lam and Teng (2003) report that previous models tend to overestimate failure strains because the FRP wraps typically fail at 58.6% of the FRP coupon rupture strain. Lam and Teng, however, did not consider de-lamination as a failure mode. When all these facts are taken together, it is clear that many variables impact the ultimate stress and strain of FRP confined specimens.

Ultimate Stress and Strain Points

Figure 4-20 shows the ultimate stress-strain of all specimens in the Control, Retrofit, and Lab Groups plotted with the stress-strain response of the baseline model. Figure 4-21 shows the average failure point for each of these groups and Table 4-9 reports this information numerically. All specimens, regardless of failure mode, are included on these figures even if excluded from other investigations to show the difficulty in predicting the ultimate stress and strain. This is a different approach from some other researchers who considered only specimens with specific failure conditions.

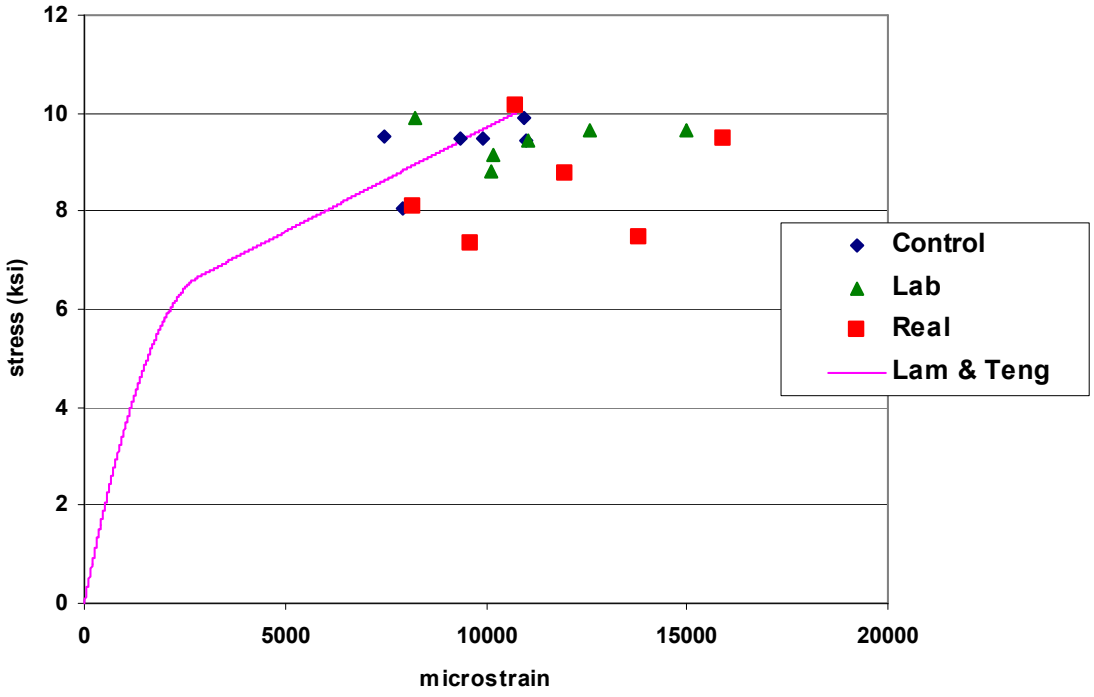

Figure 4-20 Ultimate Stress and Strain of Control, Lab, and Retrofit Groups

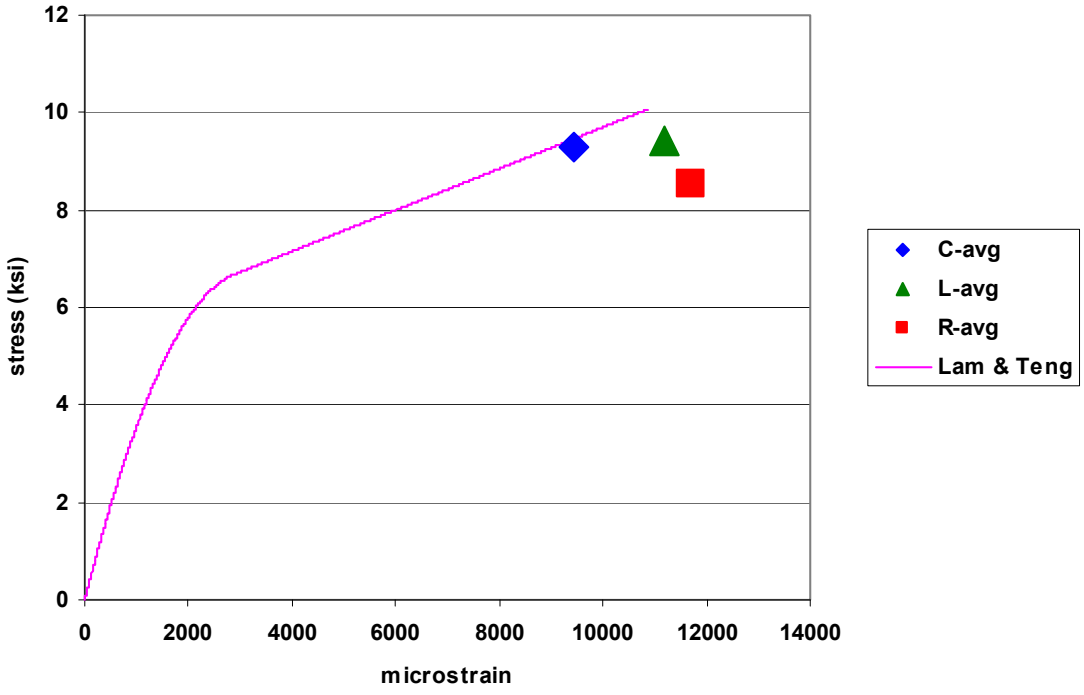

Figure 4-21 Ultimate Average Stress and Strain of Control, Lab, and Retrofit Groups

Group	Stress	Strain
Lam & Teng	100%	100%
Control	92.5%	86.8%
Lab	93.7%	103%
Retrofit	84.9%	108%
Combined	90.3%	99.1%

Table 4-9 Comparison of Average Failure Points to Baseline Model

Failure Point Analysis

When all failure modes and all life cycle histories are considered, the average failure stress was 90.3% and average failure strain was 99.1% of that predicted by the baseline model. This indicates that the ultimate stress and strain predicted by Lam and Teng's model is reasonably accurate under a variety of conditions. The problem is in the variation. Figure 4-22 shows the average failure stress and strain with two boxes that represent +/- 1 and 2 standard deviations of failure stress and strain. This large variation clearly raises issue for researchers conducting reliability studies to determine appropriate resistance factors for FRP confined concrete.

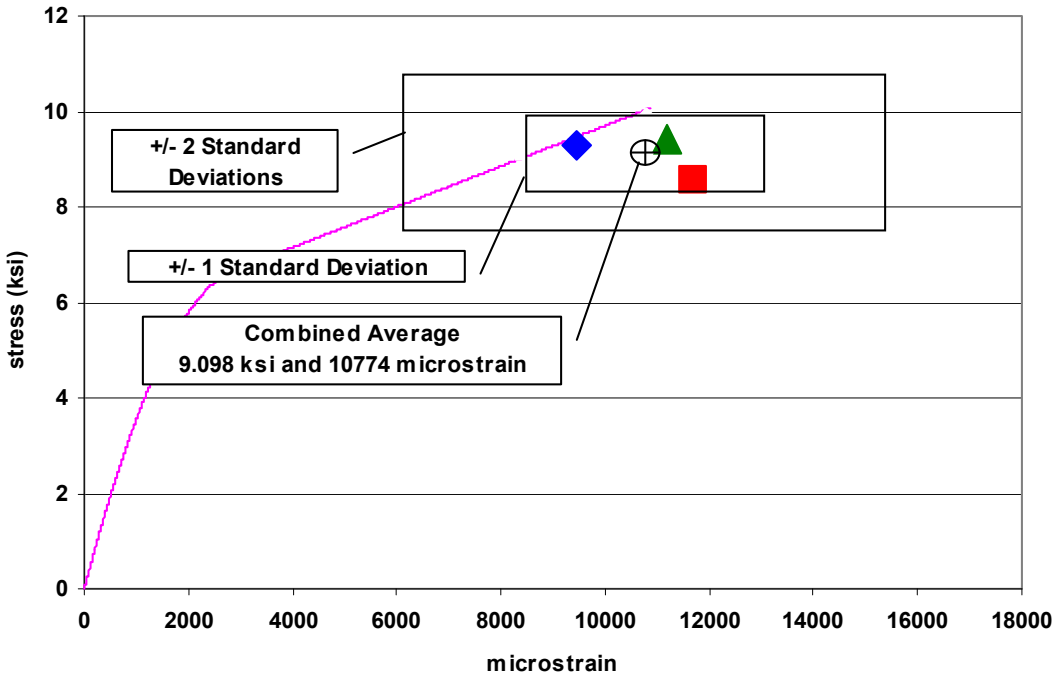

Figure 4-22 Standard Deviations of Ultimate Stress and Strain

From Figure 4-20 it is apparent that a more complex life cycle increases the variability of the failure points. The Control Group, which had the simplest life cycle, had the lowest standard deviation of results. The Lab and Retrofit Groups, which had increasing variability in life cycle events, demonstrated higher deviations in behavior. These results can be seen in Table 4-10. In this table, specimen C1 is excluded because its premature failure was due to a construction, not life cycle factor and led to changes in the construction of subsequent specimens. See Section 3.3.1.

Group	Failure Stress	1 Standard Dev.	Failure Strain	1 Standard Dev.
Control w/o C1	9.560	0.188	9741	1436
Lab	9.433	0.393	11186	2334
Retrofit	8.550	1.128	11700	2836

Table 4-10 Standard Deviations of Ultimate Stress and Strain Points

Finding 8: Average Failure Stress and Strains Do Not Present a Complete Understanding of Specimen Failure

When considering the aggregate results, the baseline model provides a good prediction of the failure strain and over predicts the failure stress by 10%. However, when the large range of failure points is considered, it is clear that the average failure point alone is not sufficient to predict failure. Failure analysis must include the substantial standard deviation of failure points and this must be included in the determination of appropriate resistance factors. Furthermore, as the number of variables like sustained loads, minor critical events, and renovations or rehabilitations under load are introduced into the life cycle, the range of failure points increases.

4.3 Analysis of Steel Spiral Confined Concrete Reinforced by FRP under Life Cycle Loadings

The preceding section examined the behavior of plain concrete specimens reinforced with FRP wraps. While this is an acceptable method for developing predictive models, it neglects a significant variable in the retrofit of actual structures. Test specimens are often constructed of un-reinforced and un-confined concrete. Retrofit structures are not. This section will extend the analysis of section 4.2 to test specimens that include a steel confining spiral. The experimental results for the Steel Group are detailed in Section 3.3.4. This group contains only 8 total

specimens so the data and results available are not as extensive as the Control-Lab-Retrofit Group combination.

4.3.1 Investigation 9: Verification of Control Behavior

The model proposed by Mander, et al.(1988) predicts a steel confined concrete strength of 7.17 ksi, but the average experimental strength of Specimens S1 and S2 was only 5.89 ksi. The steel spiral provided an 8% increase in the compressive strength over the strength of plain concrete, but it was only 82% of the strength predicted by Mander's model. This difference is most likely due to the nature of the reinforcing spirals used. Mander's model was developed for deformed reinforcing steel bars. In order to limit the strength of the confined specimens to the capacity of the laboratory equipment, smooth, mild steel, ¼" diameter rods with a yield stress of 36 ksi were used to form the spirals in lieu of standard reinforcing steel. Additionally, the pitch of the spiral was 3 inches, the maximum allowed by ACI 318. This combination of factors probably contributed to the failure of the specimens to achieve the predicted confined concrete strength. Figure 4-23 shows the relationship of the Mander, et al. and the Lam and Teng models as well as the maximum average stress achieved by Specimens S1 and S2.

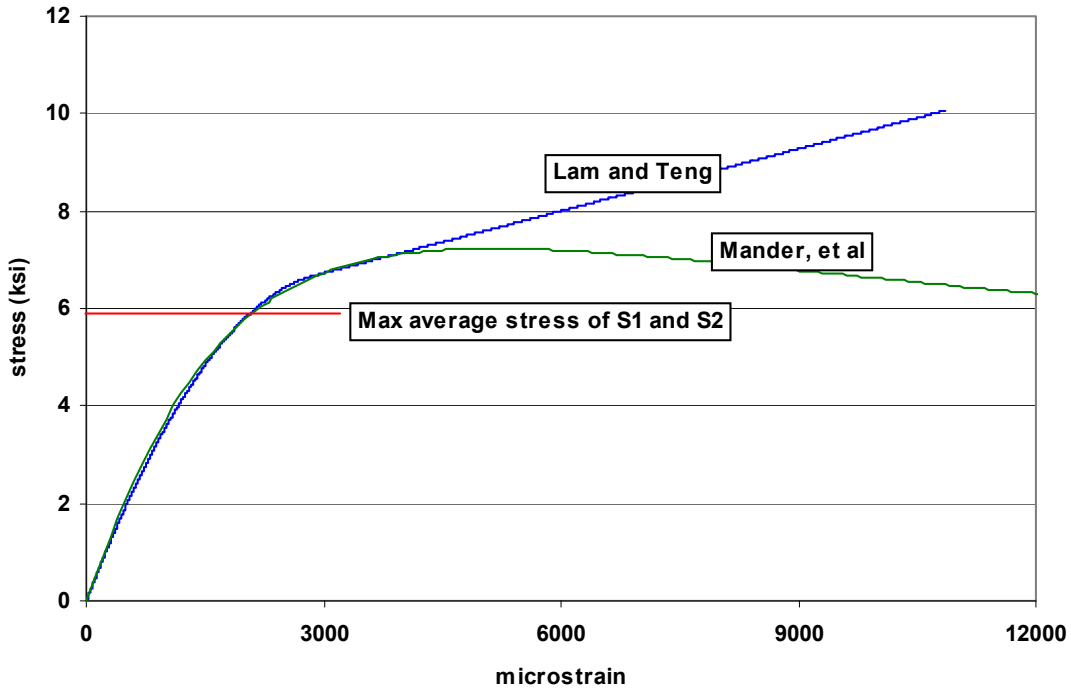

Figure 4-23 Model Comparison for Steel Group

Finding 9: Confining Steel Spirals Provide Some but Not All of the Expected Strength Increase

The steel spirals employed in the Steel Group provide increased strength and ductility over plain concrete, but not to the level predicted by the Mander Model. This issue should be attributed to the material and design parameters used, especially the distribution of the lateral steel, rather than the model.

4.3.2 Investigation 10: Impact of Sustained Service Load on an Undamaged, Retrofitted Specimen

This investigation was accomplished by comparing the results of Specimens S5 and S6 to the baseline model and to the average behavior of the Retrofit Group. All of these specimens underwent a period of sustained load without damage from a minor critical event and were then retrofitted with FRP. The results are seen in Figure 4-24. The behavior of Specimens S5 and S6 was generally comparable to average behavior of the Retrofit Group. Within the second region and at the failure stress and strain, the performance of S5 and S6 exceeded the Retrofit Group Average. Table 4-11 compares the failure stress-strain points of Specimens S5 and S6 with the average behavior of the Retrofit Group and the baseline model. Again, it is seen that the performance exceeds that of the Retrofit Group, but does not achieve that of the baseline model. This improved behavior over the average Retrofit Group behavior is attributable to the steel spiral which provides additional confinement, albeit slight. The fact that S5 and S6 do not meet the predictions of the baseline model should again be attributed to the impact of the sustained service loads.

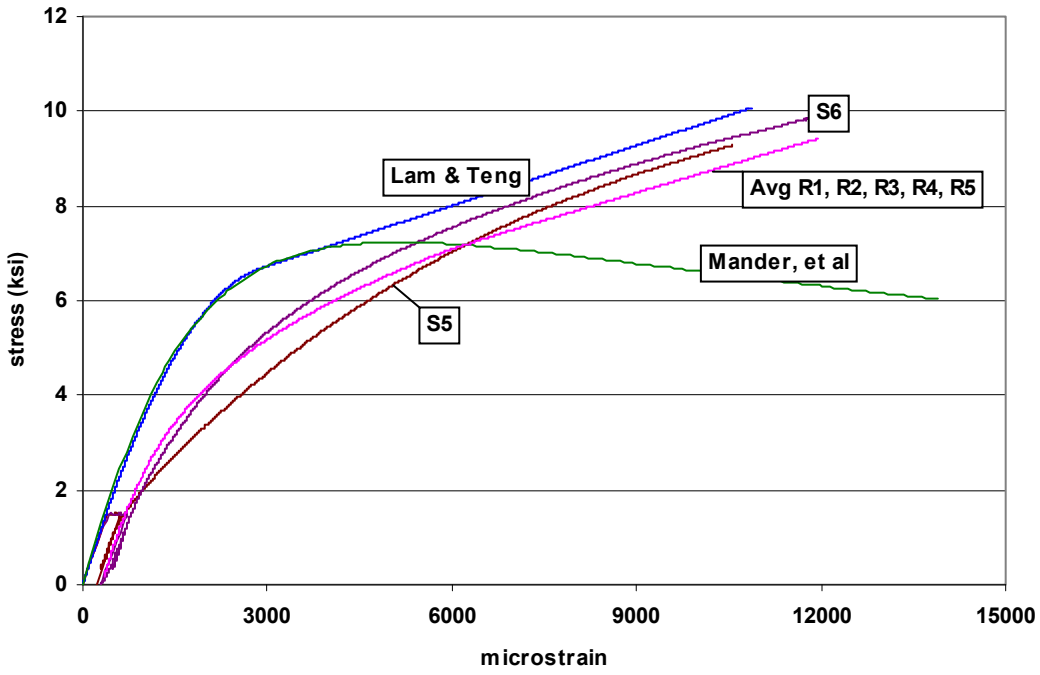

Figure 4-24 Post Sustained Load Performance of FRP Retrofitted Steel Spiral Confined Columns

Specimen	Failure Stress	Failure Strain
S5	9.276	11,548
S6	9.864	11,865
Avg S5&S6	9.57	11,706
Retrofit Average	8.76	11,281
Lam and Teng	10.07	11,870

Table 4-11 Ultimate Stress-Strain Comparison for Specimens S5 and S6

Finding 10: FRP Retrofitted Steel Confined Specimens Display Behavior Similar to FRP Retrofitted Plain Specimens

A comparison of the stress-strain history of S5 and S6 to the Retrofit Group average behavior demonstrates that both steel spiral confined and plain concrete specimens behave in a similar manner. The presence of the steel spiral improves the performance of the specimen in the second region of the stress-strain curve.

4.3.3 Investigation 11: Impact of a Sustained Load-Minor Critical Event-Retrofit Life Cycle on the Stress-Strain Behavior of a Steel Spiral Confined Specimen

This investigation evaluated the ability of an FRP retrofit to provide increased strength and ductility to a previously damaged specimen. This investigation was accomplished by comparing specimens S3 and S4 which had a sustained load-minor critical event-retrofit-extreme critical event life cycle to S5 and S6 which had a sustained load-retrofit-extreme critical event life cycle.

Figure 4-25 shows the total strain history of specimens S3, S4, S5, and S6. The sustained load creep can be seen for all four specimens while only specimens S3 and S4 show the minor critical event. The creep of the specimens is discussed in Section 4.3.4, but here it can be seen that specimen S4 exhibited substantially more creep than specimen S3 after the minor critical event. In this figure it can be seen that when subjected to an extreme critical event, all specimens behave in a similar manner. For specimen S4, the larger creep strains and softer behavior in the first region can probably be attributed to slightly more damage sustained during the minor critical event. Specimen S3 demonstrated a stiffer behavior under extreme loading when compared to S5 and S6. While this result may appear surprising at first, one must recall the discussions and findings in Section 4.2.5 about atypical stress-strain paths and failure modes. While this may not be the generally expected result, it is not an unreasonable one.

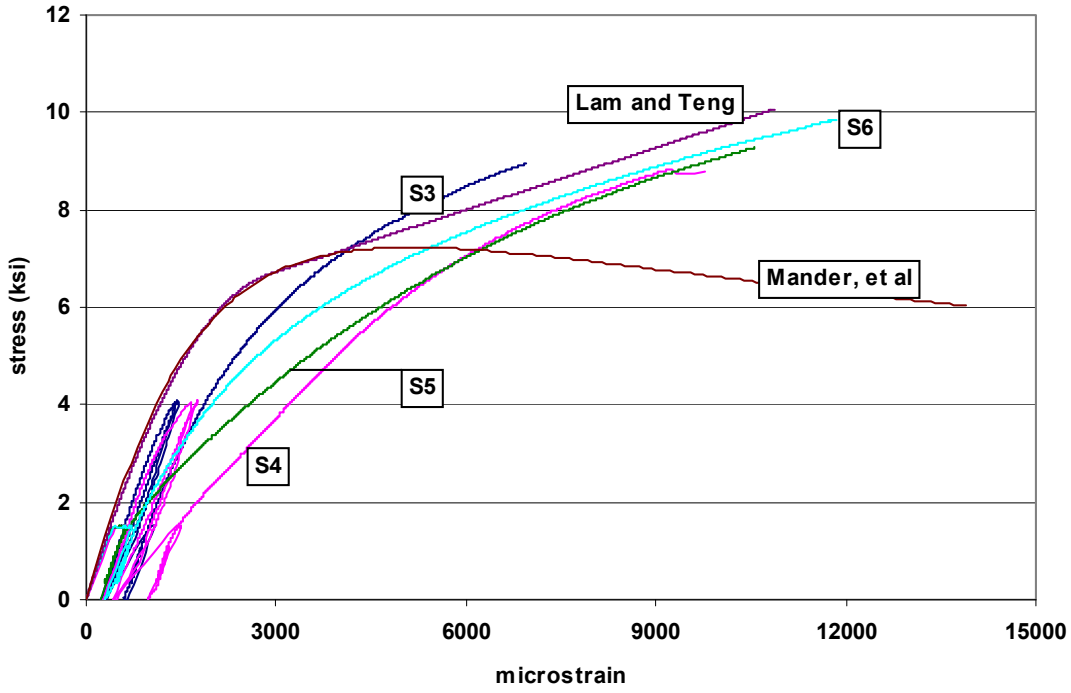

Figure 4-25 Comparison of Steel Group Behavior With and Without Minor Critical Events

While Figure 4-25 shows similar stress-strain paths for specimens S3, S4, S5 and S6, there is a clear difference in failure points. Table 4-12 lists the failure stresses and strains for these specimens. Clearly, the undamaged specimens, S5 and S6, demonstrated higher failure stresses and strains than S3 and S4 which were damaged prior to retrofit.

Specimen	Failure Stress	Failure Strain
S3	8.950	6,312
S4	8.835	9,213
S5	9.276	10,548
S6	9.864	11,865

Table 4-12 Failure Stress and Strain for S3, S4, S5 and S6

Finding 11: Damaged Specimens Retrofitted with FRP Behave in a Similar Manner, but with a Reduced Ultimate Capacity, to Un-damaged Retrofitted Specimens

Damaged and un-damaged retrofitted specimens demonstrated similar stress-strain relationships when subjected to ultimate loadings. The damaged specimens, S3 and S4, however, demonstrated only 92.8% of the capacity of the undamaged ones.

4.3.4 Investigation 12: Impact of a Minor Critical Event Creep Behavior

Strain Under Sustained Load

Steel Group Specimens S1 to S6 were subjected to sustained service loads prior to experiencing minor critical events and retrofit. The sustained loading of specimens S5 and S6 began 1 days after the sustained loading of S1 to S4, but the subsequent events occurred on the same days. Creep graphs in this section are plotted to end at the same point and show a shift of one day at the starting point. Figure 4-26 shows the total strain in each specimen from the application of a sustained service load. On Day 27 of this figure (day 199 from casting) specimens S1 to S4 were removed from the sustained load device and subjected to a minor critical event. Specimens S3 and S4 were then retrofitted with FRP and all four specimens were returned to the sustained load device. Also on Day 27 (day 199), specimens S5 and S6 were retrofitted under sustained load with FRP.

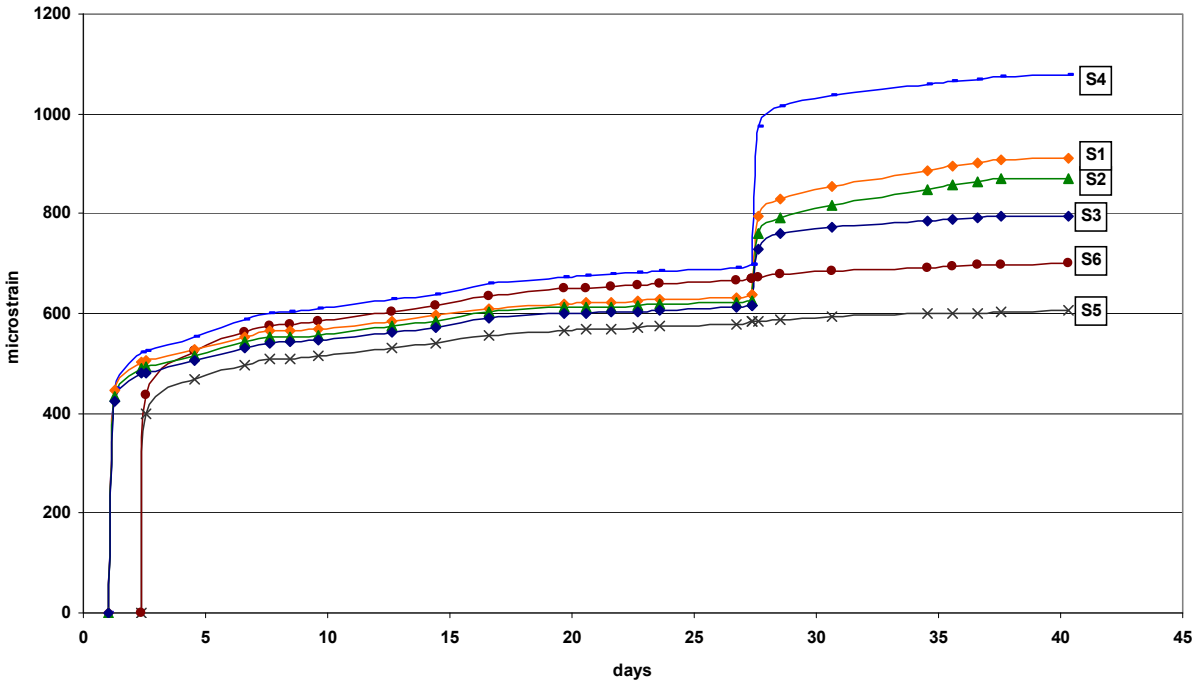

Figure 4-26 Strain s Under Sustained Load For Steel Group Specimens

Creep Strain Analysis

The effect of the initial elastic strain for each specimen has been removed from Figure 4-26 which leaves only the creep strains prior to the minor critical event in Figure 4-27. The

curve labeled 'ACI 209' represents the ACI 209 predicted creep strain using the average measured initial elastic strain. If this curve is calculated using 4,210 ksi as the estimated elastic modulus, it falls between the data for specimens S5 and S6. If the measured initial elastic strain is used, the procedures of ACI 209 provide an accurate, conservative estimate of the creep strains in the steel confined specimens.

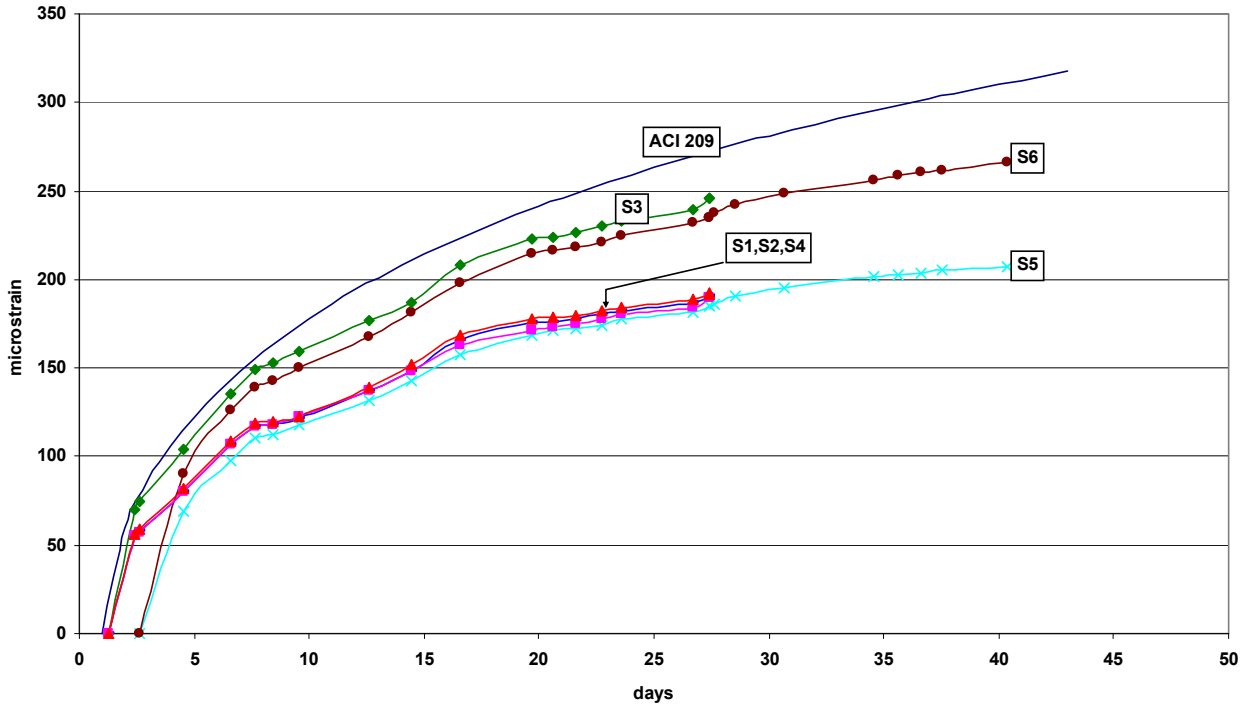

Figure 4-27 Steel Group Creep Strains Before MCE

Figure 4-28 shows the creep strains in specimens S1 to S4 following the minor critical event. These strains are calculated by taking the total strain as in Figure 4-26 and subtracting the first recorded strain when the specimens were returned to the sustained load device following the minor critical event. Also shown is the ACI 209 predicted creep strain calculated based on the first recorded following the minor critical event. Clearly, this procedure significantly over predicts the creep strains recorded in the specimens and alternate procedures are needed. The FRP retrofit seems to have little impact on the creep behavior of these specimens as the retrofitted specimens, S3 and S4, display essentially the same creep as the non-retrofitted ones, S1 and S2.

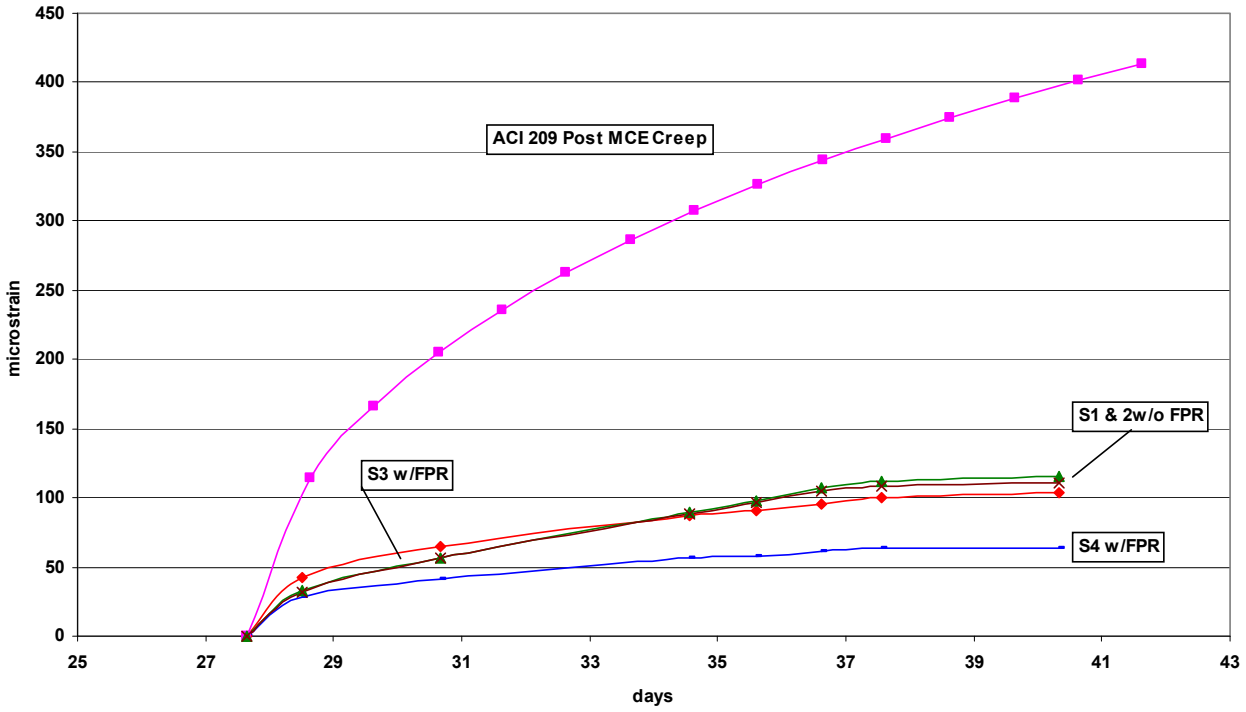

Figure 4-28 Steel Group Creep Strains After MCE

Creep Strain Modeling

The procedures of ACI 209 provide an good model for creep behavior of steel spiral confined specimens prior to a minor critical event but not following the minor critical event of the magnitude used in these experiments. From Figure 4-26 it can be seen that the rate of creep in specimens S1 to S4 is similar before and after the minor critical event. It is only the level of total strain that is different. A modification to the ACI 209 creep procedures is suggested in Figure 4-29. Following the minor critical event, the predicted creep strains are increased by the difference between the last recorded average total strain before the minor critical event and the first recorded average total strain after the minor critical event. This produces the 'Modified ACI 209' curve in Figure 4-29. It is recognized that this can be accomplished only because of the recorded data and does not provide a viable method for estimating creep strains in actual structures of this time following minor critical events. It merely indicates that, under these conditions, after a minor critical event, creep continues at the same rate, but at an increased level of total strain. Additional data points are necessary to confirm this finding and develop an appropriate correlation between damage and additional creep.

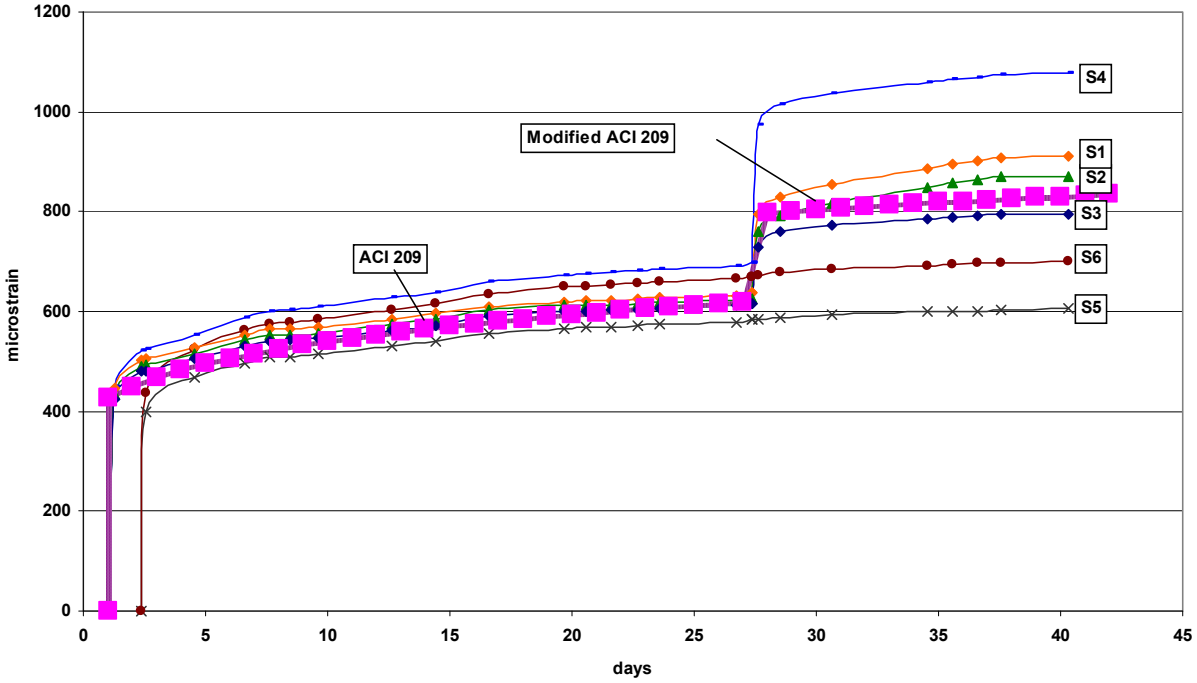

Figure 4-29 Modified ACI 209 Creep Predictions

Finding 12: ACI 209 Accurately Predicts Creep in Steel Confined Specimens Prior to the Minor Critical Event, but Not After It

As with the FRP confined specimens, the creep predictions of ACI 209 are accurate under sustained service loading prior to the specimens experiencing minor critical events. Following the minor critical event, alternate procedures are necessary to account for the consistent rate of creep with an increased level of total strain. This research does not provide sufficient data to determine the necessary procedures.

4.4 Life Cycle Modeling of a Structure

The twelve findings of the previous two sections describe how life cycle factors affect the behavior of confined concrete columns. These findings are summarized in the following key points:

- Sustained service loads change the stress-strain behavior of FRP confined concrete columns. The age of the concrete at FRP application is a less significant factor than the presence of the sustained service load.

- The ACI 209 creep model is effective for FRP confined specimens and can be effectively adapted to predict creep in damaged specimens.
- Failure modes, paths, and points are highly variable with large standard deviations.
- Specimens damaged by minor critical events retain significant residual strength capacity, but have substantially reduced strain capacity.
- The behavior of steel spiral confined specimens is comparable to plain specimens in all regards except post-damage creep.

The models and modeling procedures proposed in this section account for these changes in behavior in the test specimens. The proposed models are calibrated to and validated against experimental results. A hypothesis is offered to extend the model to loading with durations greater than the 42 days of these experiments. The issues of modeling minor critical events and reserve capacity are then addressed.

4.4.1 Modeling Creep in Un-damaged and Damaged Specimens

Un-damaged Specimens

This research confirms that the procedures of ACI 209 provide accurate predictions of the creep behavior of a specimen subjected to sustained service loads. This accuracy is improved by using the recorded initial elastic strain when load is first applied or using a measured modulus of elasticity rather than estimating the elastic strains using the modulus estimated by $\mathbf{57{,}000}\sqrt{f_c'}$. If the estimated value of E_c is used, it is recommended that additional creep calculations be performed using $0.8E_c$ and $1.2E_c$ to account for the acknowledged variability in this value and determine the possible range of creep values. In this manner, a designer may determine a reasonable level of strain already present in a concrete structure at the start of a subsequent event.

Damaged Specimens

This research confirms the post minor critical event creep modeling parameters of Shan, Xiao, and Gou (2006) explained in 2.8.2, but found a slightly different modeling parameter. In Equation 2.87, Shan, Xiao, and Gou recommend a value for α of 1.98 where this research found a value of 2.08. In the absence of better information, a value of α =2.0 would seem reasonable

for general use. Therefore, using α =2.0, Equation 2.87, and the procedures of ACI 209, an engineer can accurately model concrete creep in a damaged, FRP, confined concrete specimen.

It would be beneficial for future research to vary the level and manner of damage from a minor critical event as well as the sustained service load level to further refine the value for α.

4.4.2 Modeling Monotonic Stress-Strain Behavior with Sustained Load Effects

One of the principal objectives of this research is to model the stress-strain behavior of an FRP confined concrete specimen after the application of sustained loads. This may be accomplished by modifying an existing model or developing a new one. The model of Lam and Teng (2003) was selected as the baseline model as detailed in section 4.1.1. In sections 4.2.2 and 4.2.3, Figure 4-8 and Figure 4-13 show that this model can be modified to provide a reasonable prediction of the stress-strain behavior, but that transition zone between the first and second branches is not well modeled. Additionally, the modified model is unconservative in this area which is not acceptable for a design model. Lam and Teng's model does not lend itself to further modification because it does not contain a parameter to adjust the curvature in this region. Therefore, another model that contains appropriate curve fitting parameters is needed.

Proposed Monotonic Stress-Strain Model

The stress-strain model of Sammaan, Mirmiran, and Shahawy (1998) is selected for modification because it contains a curve fitting parameter that allows for the modification of the shape of the stress-strain response in the transition region. This model modified Richard and Abbot's (1975) equation based on tests of specimens confined by FRP tubes, and, therefore, requires re-calibration for use in this research. Furthermore, as this research demonstrates, the behavior of FRP confined concrete changes over time so these equations must be re-cast in variable form which can account for the effects of time. Equations 2.11 to 2.15 are renumbered below and variables inserted to allow for calibration to the current results.

Equation (4.1) [also (2.28)] is the closed form equation that models the entire stress-strain curve based on the variation of the longitudinal strain, ε_c. The curve fitting parameter, n, is left as a variable and will be determined based on fitting the curve to the data.

$$f_c = \frac{(E_1 - E_2)\varepsilon_c}{\left[1 + \left(\frac{(E_1 - E_2)\varepsilon_c}{f_o}\right)^n\right]^{\frac{1}{n}}} + E_2\varepsilon_c \tag{4.1}$$

Equation (4.2) is unchanged as it is the confining pressure provided by the FRP. For this research, the confining pressure is a constant 2.383 ksi when using the reduced FRP rupture strain suggested by Lam and Teng in Section 2.5.3, Equation (2.71).

$$f_l = \frac{2 f_{frp} t}{d} \tag{4.2}$$

Equation (4.3) is a modification of Equation (2.30). The coefficient of f'_{co} is changed from 0.872 to 0.838 and the constant 0.908 has been replaced with the reference stress coefficient **A**. All stresses are in ksi.

$$f_o = 0.838 f'_{co} + 0.632 f_l + A \left[ksi\right] \tag{4.3}$$

Equation (4.4) is a modification of Equation (2.31) which is the calculation of modulus of elasticity proposed by Ahmad and Shah (1982). For this research, the coefficient is 54.158 which is higher than that found by Ahmad and Shah, lower than the 57.00 used by ACI 318, and within the 20% possible variation reported in the ACI 318 commentary. For this research, E_1 has a constant value of 4,000 ksi.

$$E_1 = 54.158\sqrt{1{,}000 f'_{co}} \quad \left[ksi\right] \tag{4.4}$$

Equation (4.5) is a modification of Equation (2.32) where the coefficient of the second term becomes 3.1667. For this research, E_2 has a constant value of 300 ksi.

$$E_2 = 52.411 f'^{0.2}_{co} + 3.1667 \frac{E_{frp} t}{d} \quad \left[ksi\right] \tag{4.5}$$

It is important to note that E_1 and E_2 are related to the slope in the first and second regions of the stress-strain curve, but are not truly slopes as this model does not possess any linear regions. These values ensure good agreement between the proposed model and the data.

This proposed model builds on past research, but is calibrated to the results of the current research. It retains the closed form equation of a design oriented model, uses only readily available material properties as inputs, and contains coefficients to account for the effects of time.

Calibration of the Proposed Model to Control Group Behavior

Figure 4-30 shows the performance of the proposed model with n=1.7 in Equation (4.1) and A=1.59 in Equation (4.3) and the Lam and Teng model for reference. Good agreement can be seen between the proposed model and the Control Group average behavior found in Section 4.2.1. Additionally, the proposed model and the Lam and Teng model predict a consistent stress at the ultimate strain of 10,870 microstrain.

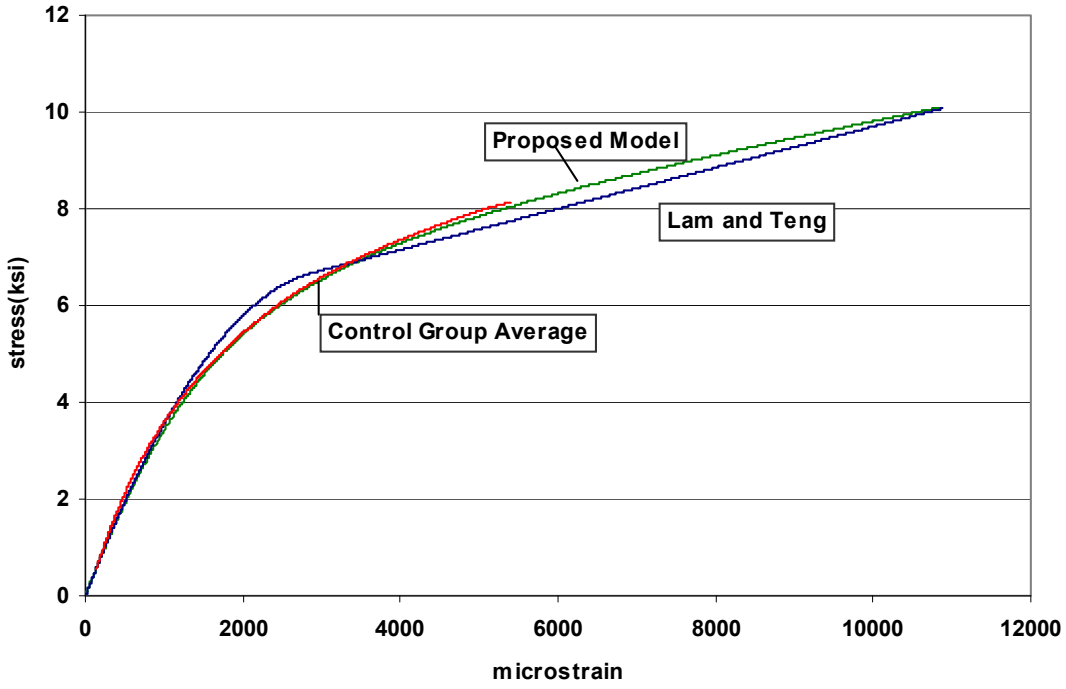

Figure 4-30 Calibration of Proposed Model to Control Group

Calibration of Proposed Model to Lab and Retrofit Groups

Figure 4-31 shows the performance of the proposed model with n=1.2 and A=1.09. Good agreement can be seen between the proposed model and the average behavior of both the Lab and Retrofit Groups. The variation between the Proposed Model and the recorded data is under 3%. For this calibration, the average responses of both the Lab and Retrofit Groups were shifted left by the average value of the residual strains in the specimen groups so that the response starts at zero.

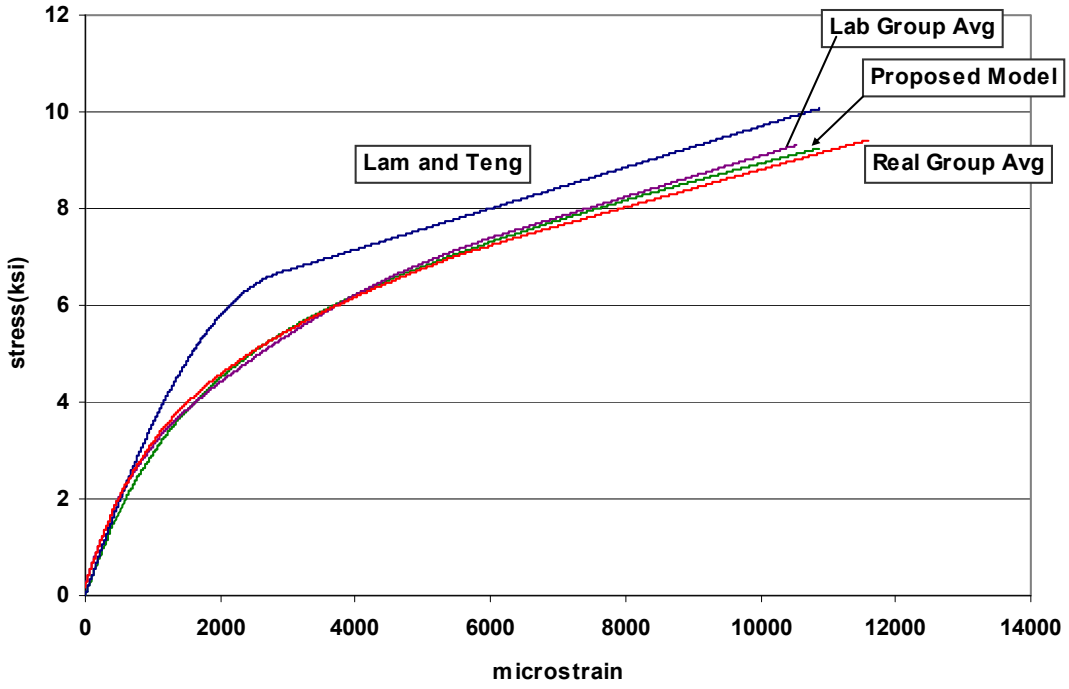

Figure 4-31 Calibration of Proposed Model to Lab and Retrofit Groups

Relating the Sustained Load Parameters 'n' and 'A' to Duration of Load

The limiting constraint of this research is that it essentially produced only two data points: The control behavior and the behavior after 42 days of a sustained 1.49 ksi stress. One would not expect that two data points could be extracted to predict long term performance. However, by employing an understanding of creep behavior, a hypothesis can be formulated that relates 'n' and 'A' to duration of loading.

The first requirement is to estimate the rate of change of these parameters over time. As sustained load causes both the creep and behavior changes seen in this research, it is logical to conclude that the rate of change in the stress-strain parameters should be similar to the rate of change in the creep parameters. Equation (4.6) is the time parameter extracted from the ACI 209 creep coefficient equation and is here designated as φ.

$$\phi = \frac{t^{0.6}}{10 + t^{0.6}} \tag{4.6}$$

The value of φ increases with time t, but this needs to be reversed to get a parameter that decreases at a corresponding rate. The parameter θ can then be calculated by Equation (4.7) where t is time in days and φ_{365} is the value of φ at 365 days. A time of 365 days was selected because almost all time dependent behavior changes have reached a near maximum value after one year. See the work of Song, et al.(1995) outlined in Section 2.7.1.

$$\theta_t = \phi_{365} - \phi_t \tag{4.7}$$

Figure 4-32 shows the values of φ and θ over time. Now, the time relationship, θ, must be adapted to relate the curve parameter n and reference stress coefficient A to time.

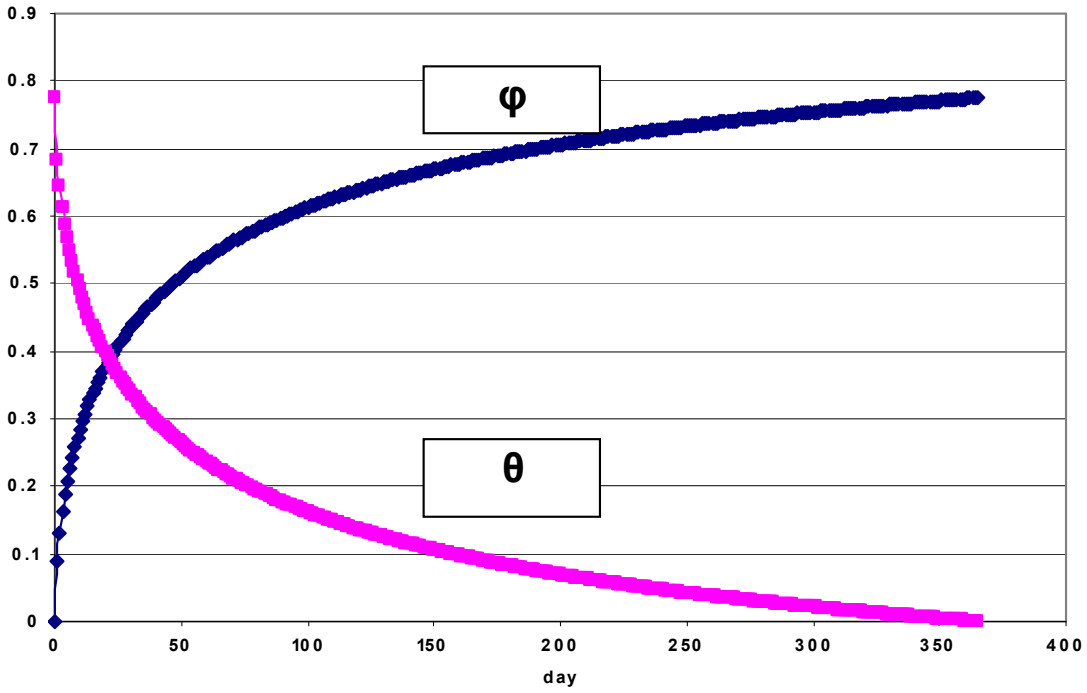

Figure 4-32 Time Parameters φ and θ

In Figure 4-33, the curve θ ranges from 0.775 at t = 0 days to 0 at t = 365 days. This curve is shifted up to a value of 1.7, the initial value of n, simply by adding 0.925 to the value of θ at each time. This curve gives a value of n at 42 days of 1.22. As related above, experimental value of n at 42 days is 1.2. Since the behavior of the proposed model is not very sensitive to small variations in n, this curve provides good agreement with the experimental data. At 365 days, the value of n reaches its minimum value of 0.925.

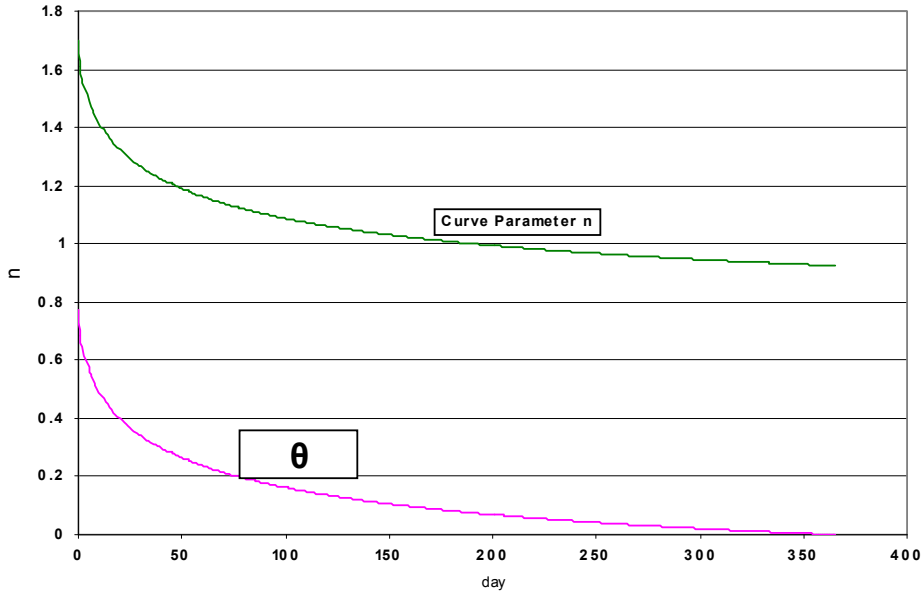

Figure 4-33 Values of the Curve Parameter n Over Time

Scaling the curve for θ to predict the reference stress coefficient A is equally easy. At a time of zero, the value of A is 1.59. In Figure 4-34, the values of A are found by adding 0.815 to the value of θ at each day. When the curve for θ is shifted in this manner, the A value predicted at 42 days is 1.105 which compares favorably with the 1.09 found from the experimental data. At a time of 365 days, A reaches it minimum value of 0.815.

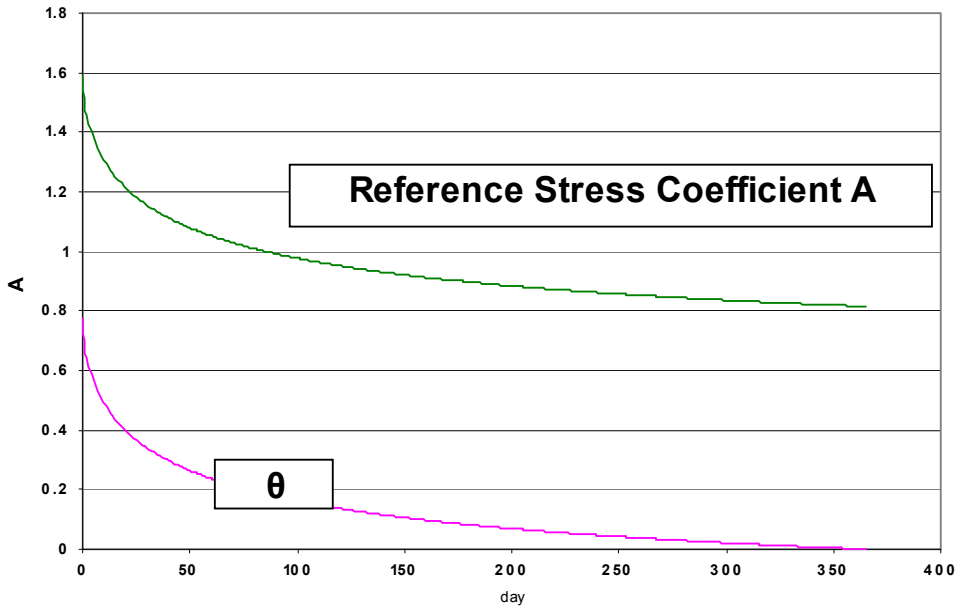

Figure 4-34 Values of the Reference Stress Coefficient A Over Time

In lieu of using Figure 4-33 and Figure 4-34 for the finding n and A, Equation (4.8a) can be used to find n_t and Equation (4.8b) to find A_t where φ_t is found from Equation (4.6)

$$n_t = 0.925 + \theta_t \tag{4.8a}$$

$$A_t = 0.815 + \theta_t \tag{4.8b}$$

It must be noted that at this time, these relationships are only a hypothesis. The only data points that this research has produced are at times of 0 and 42 days of sustained loading. Further research is necessary to confirm the relationships in Figure 4-33 and Figure 4-34.

Behavior of the Proposed Model Over Time

Figure 4-35 shows the application of the proposed model over time using the suggested equations. The response for times of 0 and 42 days are confirmed by experimental results. The response at 365 days is hypothesized as explained above and should be confirmed by future research. Table 4-13 shows the values of the model variables and predicted ultimate strength over time.

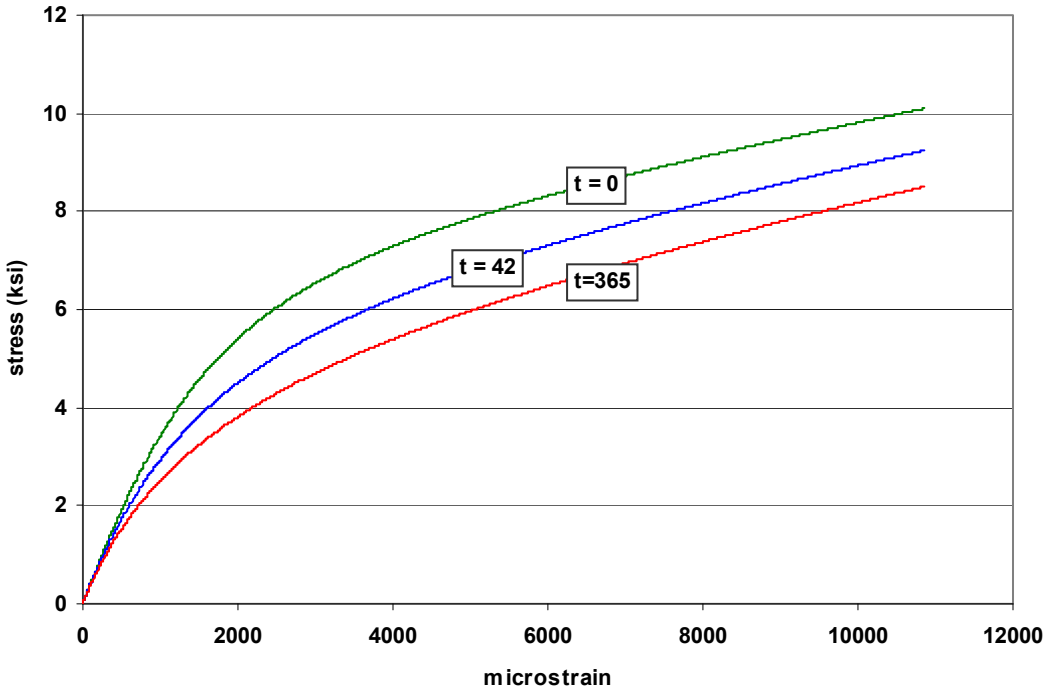

Figure 4-35 Behavior of Proposed Model Over Time

time (days)	n	A	f'_{cc} (ksi)
0	1.7	1.59	10.1
42	1.2	1.09	9.24
365	0.925	0.815	8.51

Table 4-13 Impact of Time of Proposed Model Variables

Integrating Strains from Sustained and Ultimate Loadings

The effects of creep strain modeling and stress strain modeling can be combined by superposition. First, the creep strains are calculated then the stress-strain model is shifted to the right by the magnitude of the creep strains. The initial elastic strain can also be included if a stress-strain plot showing behavior over time is desired.

Validation of the Proposed Stress-Strain Modeling Procedures Using the Steel Group

The procedures explained above will be compared to the results of specimens S5 and S6 from the Steel Group. These specimens were not used in the calibration of the model, but experienced a similar strain history to the Lab and Retrofit specimens used for the calibration.

If the proposed model procedures are applied to parameters of the Steel Group, the following values result:

$E_1=E_c$=4,000 ksi

$\varepsilon_{initial\ elastic}$ = 373 microstrain

$\varepsilon_{creep\ only}$ = 462 microstrain

n=1.2

A=1.09

When these are applied to the proposed model, the stress-strain curve shown in Figure 4-36 results. (Lam and Teng's model is shown for reference only.) The plateau at 1.49 ksi represents the creep strains from the 42 day sustained load. The proposed model, when shifted for creep strains, shows good agreement with the results of these two specimens. Within the first region the proposed model is very close to the average behavior of S5 and S6. Within the second region, the proposed model performs about 4% below the average behavior. This is probably due to the additional confinement provided by the steel spiral which is not included in this model.

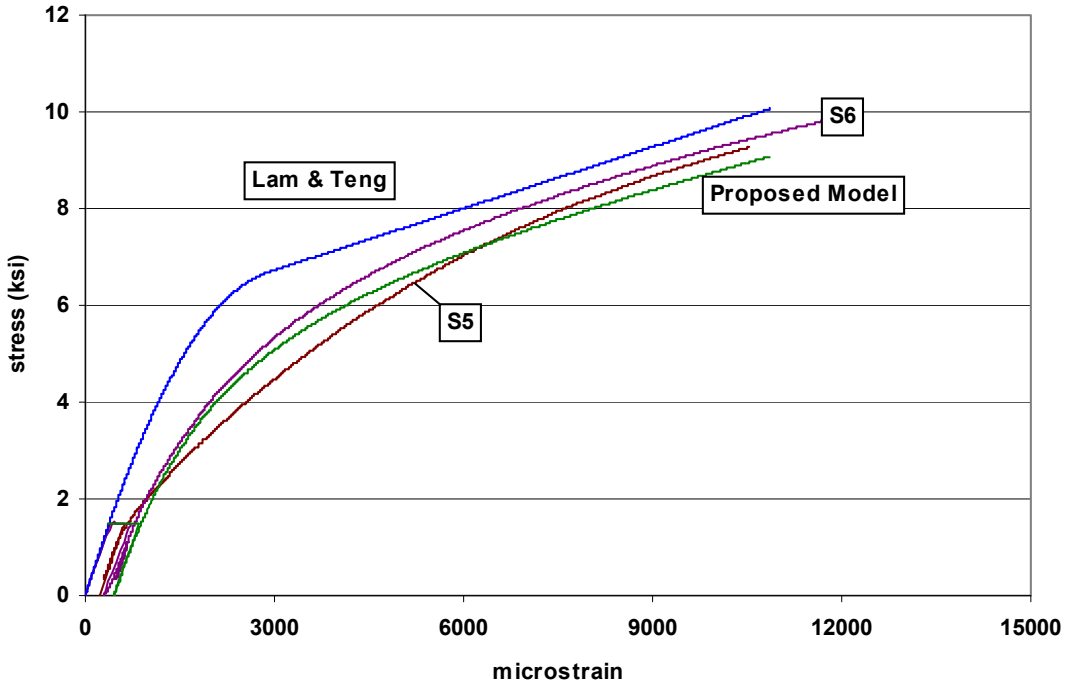

Figure 4-36 Proposed Model vs. Specimens S5 and S6

Prediction of Ultimate Stress and Strain

The prediction of ultimate stress and strain values is one of the most challenging aspects of FRP modeling. The failure point is affected by failure mode, failure path, material properties, and hoop rupture strain of the FRP material. Additionally, it seems that specimen failure occurs when either a failure stress or a failure strain is reached. The atypical failure modes and stress-strain relationships discussed in Section 4.2.5 show specimens that reach the predicted failure stress, but achieve only 60% to 70% of the predicted failure strain. On the other hand, the average failure strain of all specimens in the Control, Lab, and Retrofit Groups, regardless of sustained loadings, minor critical events, failure modes, and failure paths, is 10,774 microstrain which is practically the same at the 10,870 microstrain predicted by Lam and Teng. This behavior seems to indicate that there is a finite, set stress and strain capacity and when one of these limits is reached, the specimen fails.

Base on the results of Investigation 8 in Section 4.2.8, Equations (2.71) and (2.72) from Lam and Teng (2003) were selected for the calculation of the ultimate strain and returned a value of 10,870 microstrain for these specimens. When this value is used in Equation (4.1) of the

proposed model, the value of f'_{cc} decreases over time as seen in Table 4-14. Good agreement is shown with the ultimate stress averages from the experimental data.

Time	f'_{cc} (ksi)	Recorded Avg Failure (ksi)
0 days	10.1	9.32
42 days	9.24	8.99
365 days	8.51	---

Table 4-14 Ultimate Strength From the Proposed Model

4.4.3 Modeling Cyclic Stress-Strain Behavior

A model capable of predicting behavior under cyclical and post-cyclical loadings is essential to any examination of the residual capacity and behavior. While various models are available for cyclic behavior of steel spiral confined concrete, few have been adapted to FRP confined concrete. The principal difference between the two confinement models—ascending vs. descending second branch—leads to substantial modifications of a steel based model to enable it to predict FRP confined concrete behavior under cyclic loads. Based on the model of Mander et al.(1988), a modified model is proposed which accounts for the unloading, reloading, and transition stress-strain relationships of FRP confined concrete when the cycles start in the second branch. The proposed model, summarized in Figure 4-37, uses three equations to describe the cyclic response. It was validated against the experimental data where cycles took place between a designated unloading strain and a reloading point near zero stress. Once the unloading point is designated, the model predicts the response based only on material parameters. The model was validated using complete cycles, but should function for partial unloading cycles as the level of unloading is not a parameter. There is no experimental data available in this research to validate this point.

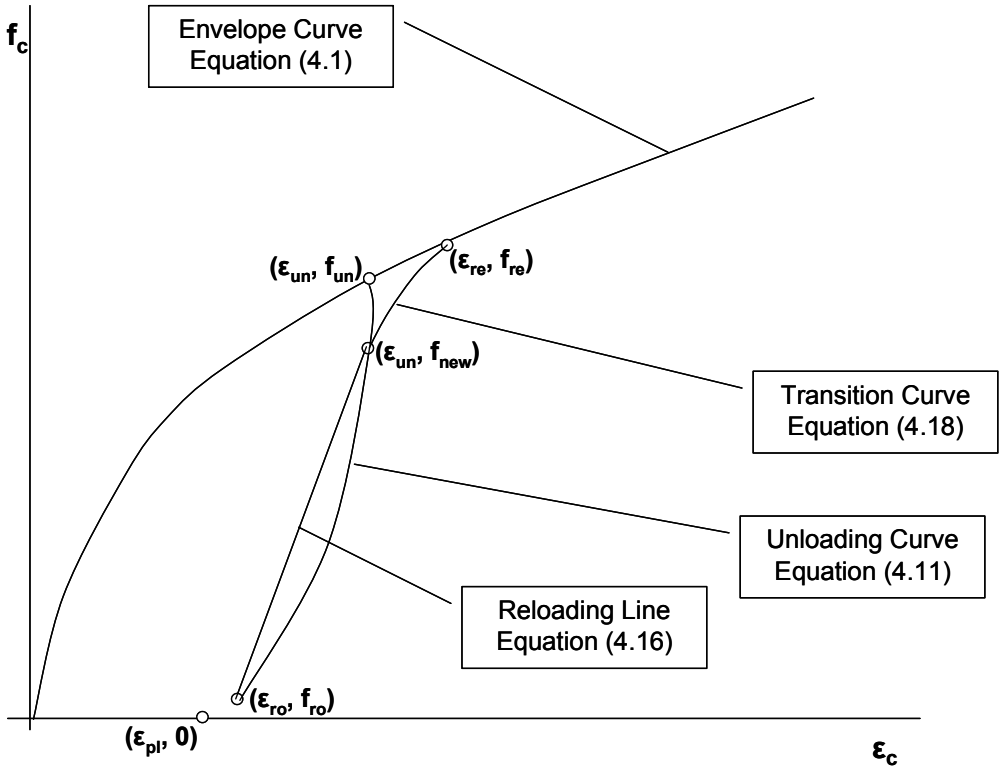

Figure 4-37 Proposed Cyclic Model

Proposed Cyclic Stress-Strain Model

The proposed cyclic behavior model begins in the second branch of FRP confined concrete response at the unloading strain-stress point of (ε_{un}, f_{un}). First the plastic strain, ε_{pl}, is calculated using Equation (4.9) and the unloading modulus, E_u, is found using Equation (4.10) where E1 is from Equation (4.4). These equations are modified versions of those proposed by Mander et al. For ε_{pl}, Equation (2.6) will not function properly for FRP confined concrete as it employs the value for ε_{cc} which is located at a different point on the stress-strain response and has a different physical meaning for FRP and steel confined concrete. For E_u, Equation (2.13) does not correlate with the results of these experiments.

$$\varepsilon_{pl} = \varepsilon_{un} - \frac{f_{un}}{E_1} \tag{4.9}$$

$$E_u = \frac{4}{3} E_c \tag{4.10}$$

Using these values, the unloading curve is modeled using Equation (4.11) supported by Equations (4.12), (4.13), and (4.14). These are the same equations as proposed by Mander, et al. but yield different results because of the different inputs from Equations (4.9)and (4.10).

$$f_c = f_{un} - \frac{f_{un}\, x\, r}{r - 1 + x^r} \tag{4.11}$$

$$r = \frac{E_u}{E_u - E_{\sec}} \tag{4.12}$$

$$E_{\sec} = \frac{f_{un}}{\varepsilon_{un} - \varepsilon_{pl}} \tag{4.13}$$

$$x = \frac{\varepsilon_c - \varepsilon_{un}}{\varepsilon_{pl} - \varepsilon_{un}} \tag{4.14}$$

The unloading branch ends and the reloading branch begins at the reload strain-stress point (ε_{ro}, f_{ro}). A linear relationship is used between the reload point and a new reference point, (ε_{un}, f_{new}) which represents the loss of capacity due to the cyclic loading. The new reference stress is found using Equation (4.15). In this Equation, the coefficient of f_{un} is increased from 0.92 used in Equation (2.16) to 0.95 to account for the difference in behavior between steel and FRP confined concrete. Equation (4.17) gives the modulus of the reloading curve and Equation (4.16) calculates the stress along the reloading curve. Equations (4.16)and (4.17) are identical to those proposed by Mander, et al.

$$f_{new} = 0.95 f_{un} + 0.08 f_{ro} \tag{4.15}$$

$$f_c = f_{ro} + E_r\left(\varepsilon_c - \varepsilon_{ro}\right) \tag{4.16}$$

$$E_r = \frac{f_{ro} - f_{new}}{\varepsilon_{ro} - \varepsilon_{un}} \tag{4.17}$$

The cycle ends when the stress-strain response returns to the unloading strain ε_{un} at the stress given by Equation (4.16). This point now becomes the starting strain-stress (ε_{un}, f_{un}) for the next cycle. These procedures are repeated for the desired number of cycles. Unlike the

model of Shao (2003, 2006), this modeling procedure accounts for the continued stress-strain deterioration under cyclic loading described by Lam, et al. (2006).

When the response moves beyond ε_{un} back to the monotonic curve proposed in Section 4.4.2 it follows the path given by Equation (4.18).

$$f_c = \frac{(E_1 - E_2)(\varepsilon_c - \varepsilon_{tr})}{\left[1 + \left(\frac{(E_1 - E_2)(\varepsilon_c - \varepsilon_{tr})}{f_{tr}}\right)^{0.5}\right]^2} + E_2(\varepsilon_c - \varepsilon_{tr}) + f_{tr} \tag{4.18}$$

where:

ε_{tr} is the value of ε_{un} for the final cycle

f_{tr} is the stress given by Equation (4.16) at the end of the final cycle

E_1 is given by Equation (4.4)

E_2 is given by Equation (4.5)

Clearly this is an adaptation of the monotonic model proposed in Section 4.4.2. Use of the (ε_c-ε_{tr}) term along with a value for n of 0.5 enables the curvature of the model to match the experimental results while the use of f_{tr} shifts the model to the correct stress. Under the cyclic loading conditions, the value of n does not seem to vary substantially with time. This curve terminates when it reaches the monotonic stress strain curve. This point is located by setting Equation (4.1) equal to Equation (4.18) and solving for the value of ε_c which is designated ε_{re}, the return strain.

Comparison of Proposed Models and Experimental Data

In all figures in this section, the blue curve is the experimental data, the red is the proposed cyclic model, and the green is the proposed monotonic model where applicable. Additionally, the initial stress-strain due to the sustained load is removed from all figures for Lab Group specimen shown in this section. This effect could be re-introduced into these figures by simply shifting them to the right by the creep strains, but it would not change the results.

Figure 4-38, Figure 4-39, and Figure 4-40 show the comparison of the proposed cyclic response model to the data collected for Specimens C5, L3, and L5 respectively. The proposed model functions well for all specimens regardless of life cycle history. Specimen C5 underwent only a monotonic loading prior to the three cycles shown. Specimen L3's life cycle was sustained service load then a monotonic load followed by three cycles and ending with a

monotonic load to failure. Specimen L5 underwent a sustained load—minor critical event (monotonic + three cycles)—sustained load—monotonic load to failure life cycle. The response of unloading, reloading, and transition curves the proposed model is shown in these figures. In these figures, the model stops when the transition curve returns to the second branch of the monotonic response. The proposed model shows good agreement with the experimental values as seen by the R^2 values shown in Table 4-15. These values are calculated based on the unload, reload, and transition curves of the proposed cyclic model.

Specimen	R^2 Value
C5	0.996
L3	0.994
L5	0.973

Table 4-15 R^2 Values for Proposed Cyclic Model

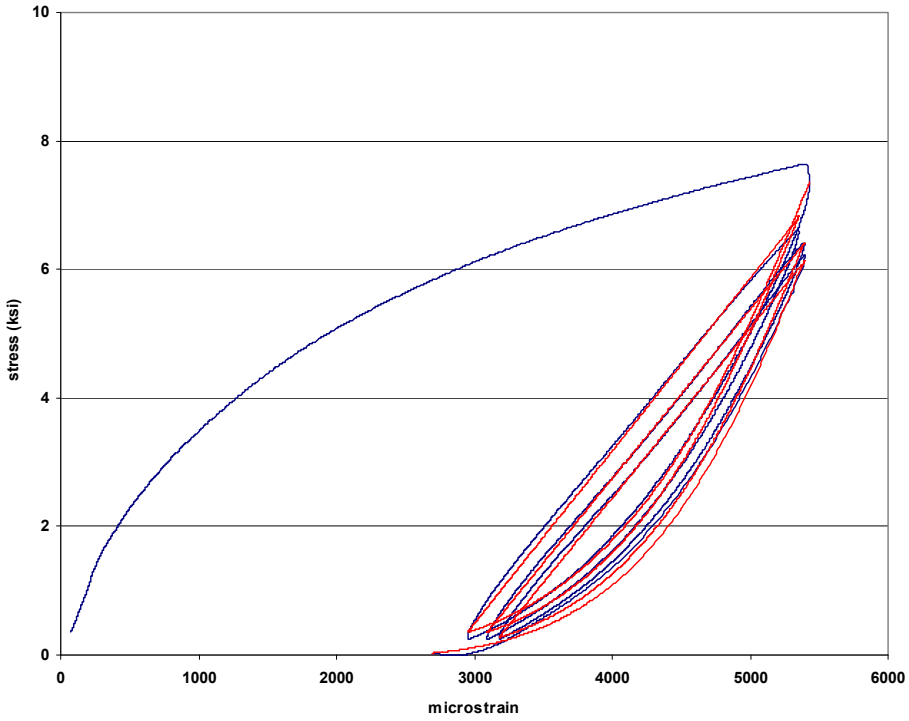

Figure 4-38 Proposed Cyclic Model and Specimen C5

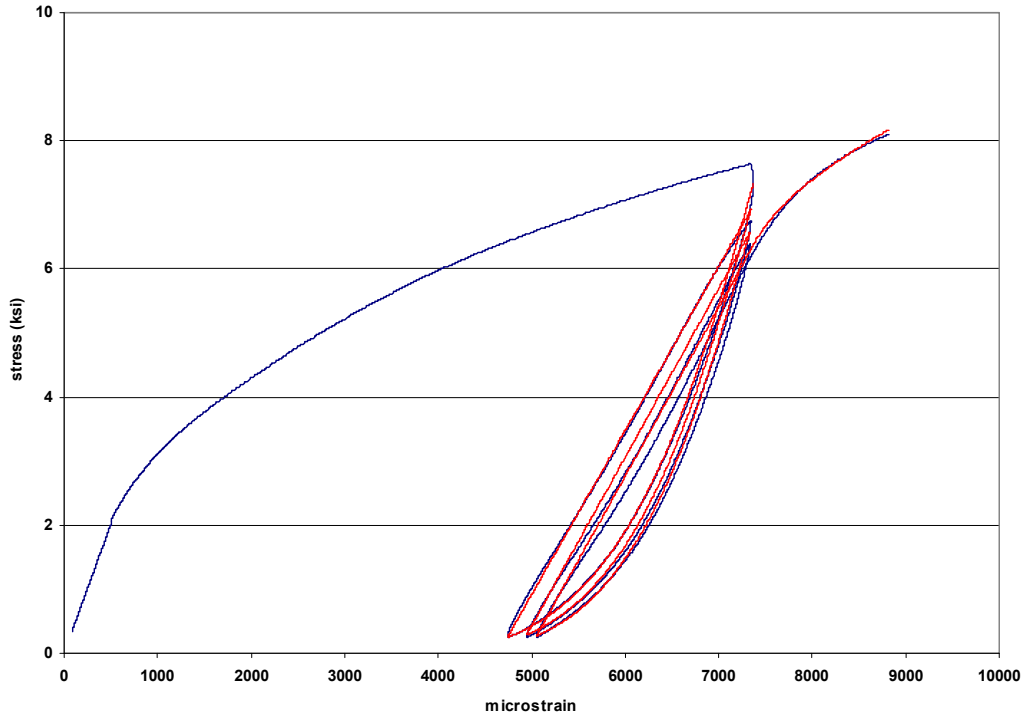

Figure 4-39 Proposed Cyclic Model and Specimen L3

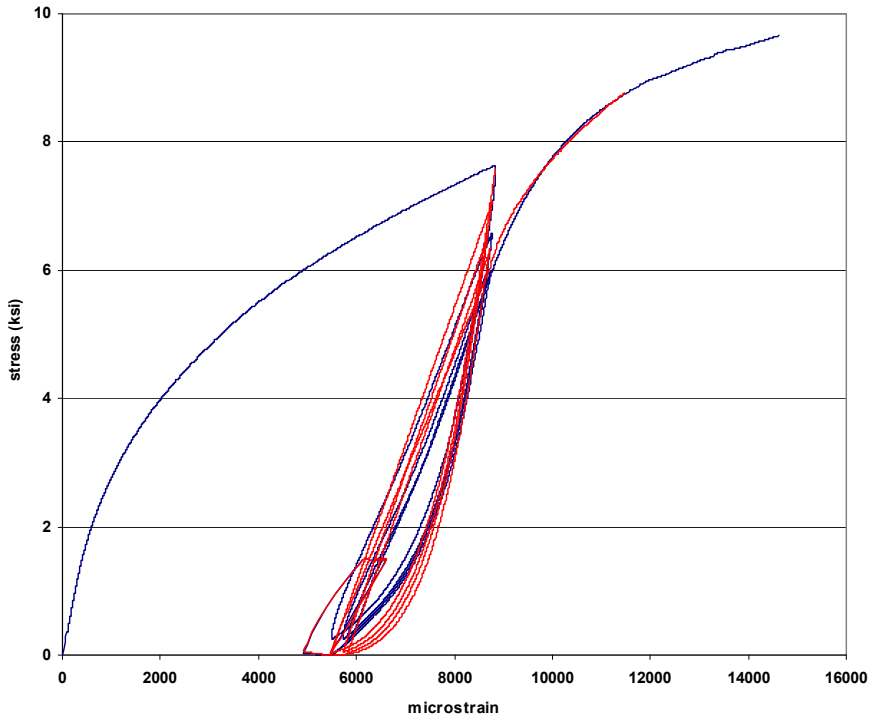

Figure 4-40 Proposed Cyclic Model and Specimen L5

Figure 4-41 and Figure 4-42 show the experimental data, proposed monotonic curve, and proposed cyclic response for Specimens L4 and L6. L4 and L3 had the same life cycles as did L6 and L5. The monotonic model is included in these graphs as the response of L4 and L6 tracked closely with the average data and therefore the proposed monotonic model. These figures demonstrate the return of the transition curve to the monotonic model. Again good agreement is seen between all three parts of the proposed cyclic model and the experimental data as seen in Table 4-16.

Specimen	R^2 Value
L4	0.997
L6	0.994

Table 4-16 R^2 Values for L4 and L6

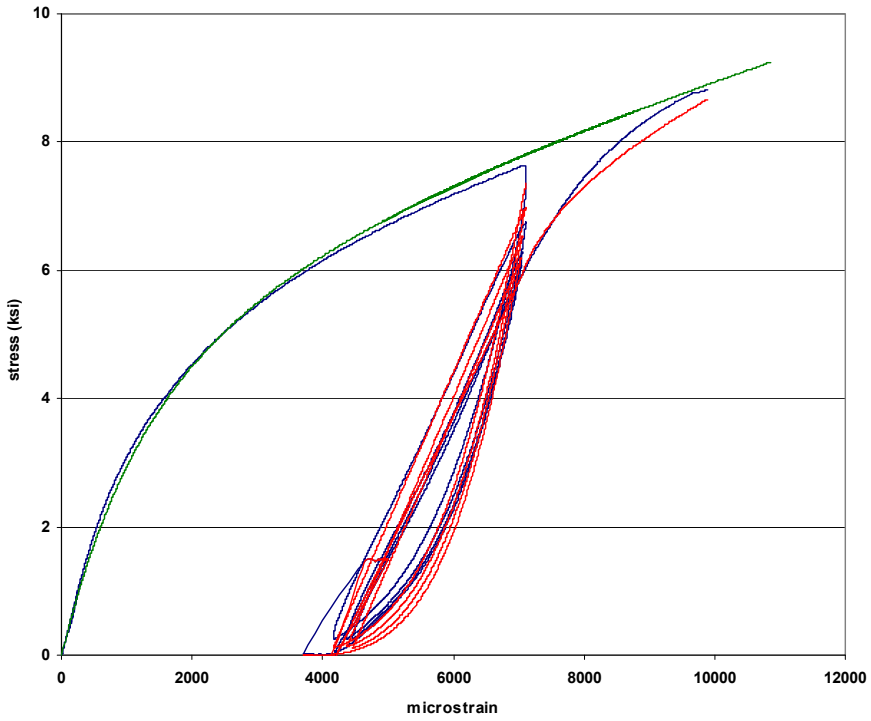

Figure 4-41 Proposed Monotonic and Cyclic Models and Specimen L6

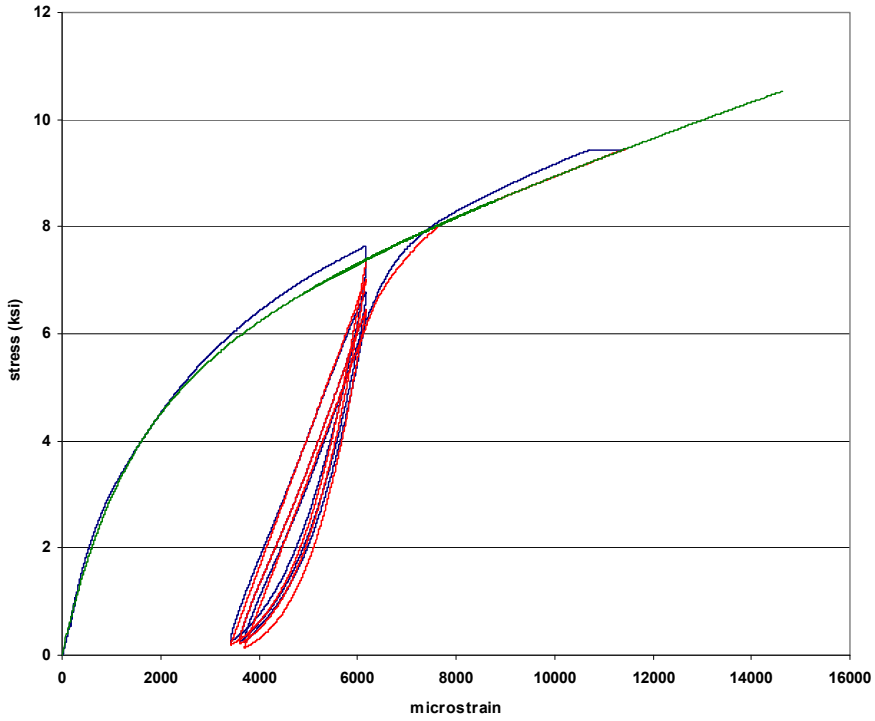

Figure 4-42 Proposed Cyclic and Monotonic Models and Specimen L4

Modeling the Cyclic Load-Sustained Load-Monotonic Load Condition

This condition occurs for specimens L5 and L6 and is evidenced by the sustained load plateau seen observe in Figure 4-40 and Figure 4-41. This behavior is accounted for in the model simply by using the stress and strain at the end of the sustained load period as the as the values for the reload point (ε_{ro}, f_{ro}). The unload point values (ε_{un}, f_{un}) are taken from the start of the prior unloading cycle. When the monotonic load starts, it follows the proposed reloading and transition paths then the proposed monotonic model beginning at the return strain, ε_{re}.

4.5 Impact of Results

The two items presented in this section could be termed, "A blinding flash of the obvious." While these impacts may be known intuitively, the scope of this research broadens our understanding of these behaviors, begins to quantify what we know intuitively, and provides potential avenues for future research.

4.5.1 Impact of Findings on Current Model Earthquake Codes

As described in detail in the introduction and Hart and Esmaeily (2007), the FEMA 450 model earthquake code proportions structures based on the most severe design requirements, a procedure which is expected to provide acceptable performance (i.e. less damage) in lesser events. The FEMA 356 model code seeks to model structural performance in a variety of events using a Performance Based Earthquake Engineering approach. Both of these codes rely on an understanding of the inelastic behavior based on a combination of analysis and observed building performance. Both codes ensure that a structure will not collapse from the forces induced by the design earthquake or lesser events. Even with all this experience, the question, as raised by Shan, Xiao, and Gou (2006), of how previous strain histories affect future performance remains. As detailed in Section 4.2.7, substantial reserve strength but lower levels of reserve strain capacity remain after a minor critical event. Even though a structure retains significant residual strength, the decrease in ductility can significantly alter both seismic analysis and behavior.

Impact on a FEMA 356 Analysis

FEMA 356 calls for all elements to be classified as either 'force-controlled' or 'deformation-controlled' based on the force-deformation curves in Figure 1-1. This behavior is considered ductile if the inequality $\varepsilon > 2\gamma$ is satisfied. Models and prior research show that FRP confined concrete columns under axial load should exhibit the behavior of a Type 2 Curve. Figure 4-43 and Figure 4-44 show that the Control Group specimens without sustained load and the Lab Group specimens with sustained load are sufficiently ductile to be classified as 'deformation-controlled' members under the provisions of FEMA 356. It is clear that the presence of the sustained load has a minimal impact on specimen ductility and member classification.

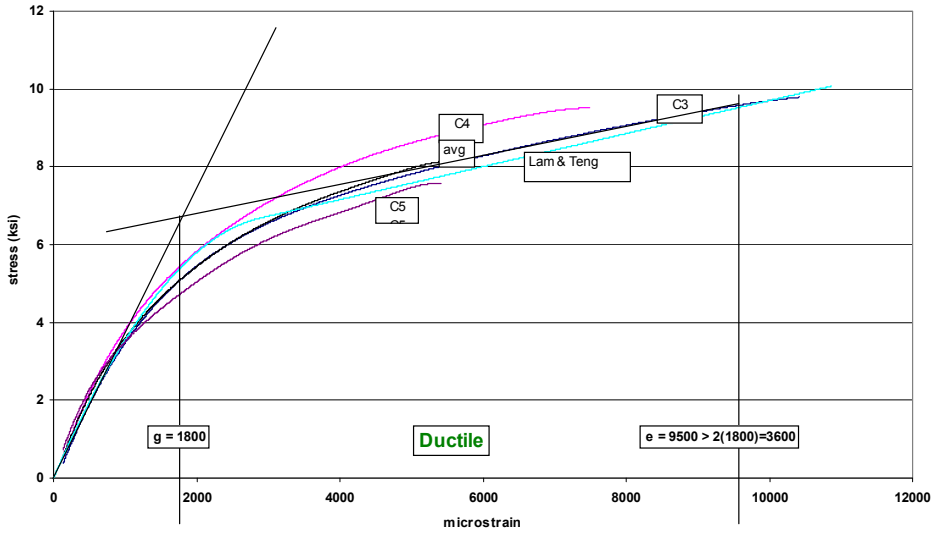

Figure 4-43 Control Group Ductility Calculation

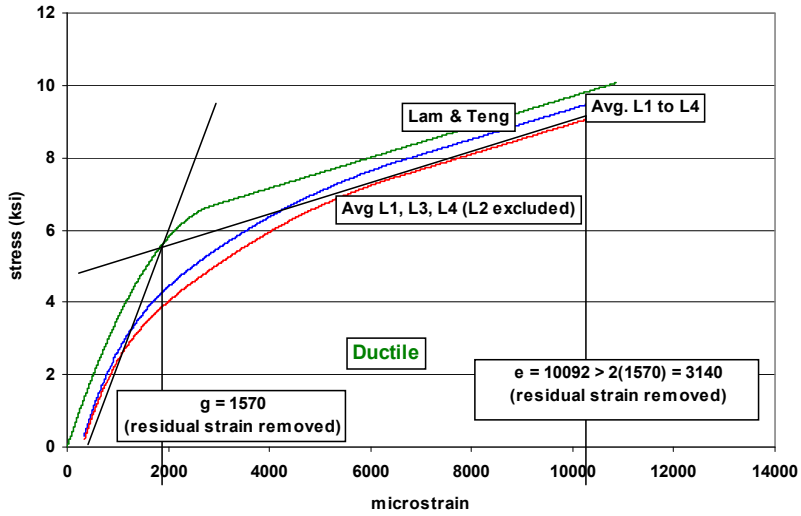

Figure 4-44 Lab Group Ductility Calculation

Figure 4-45 to Figure 4-49 show the ductility checks for specimens C5, C6, L5, L6, and R4 based on the extreme critical event which took place after a life cycle that included sustained loads, retrofit, and minor critical events. Strains are plotted from zero so the behavior shown represents the residual capacity of the specimens. Specimens C5, L5, and R4 retain sufficient ductility to be classified a 'deformation-controlled' while specimens C6 and L6 are no longer ductile and now these formerly 'displacement controlled' members are now 'force-controlled' members. It must be noted that L5 is ductile by the slimmest of margins.

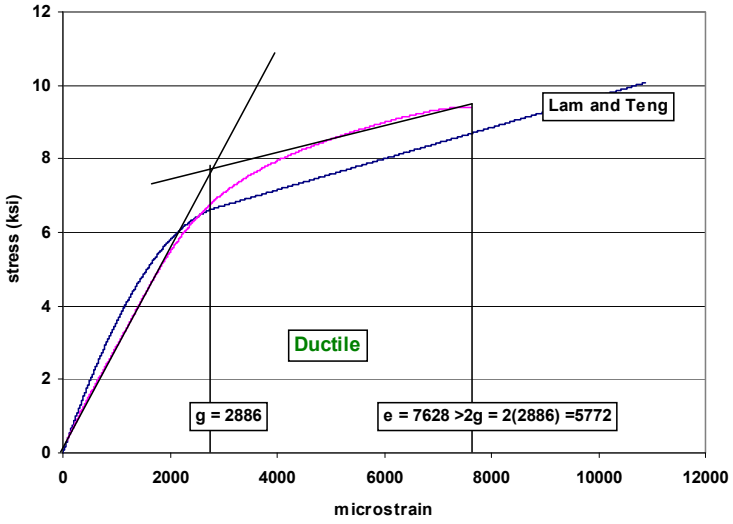

Figure 4-45 Specimen C5 Post MCE Ductility Calculation

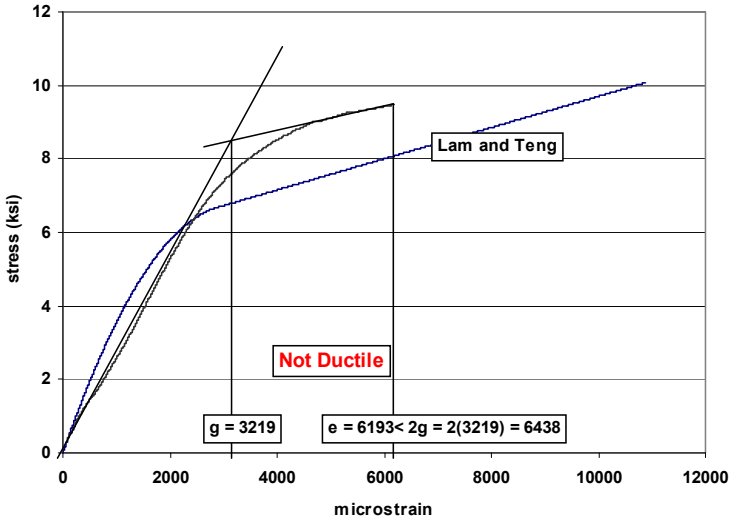

Figure 4-46 Specimen C6 Post MCE Ductility Calculation

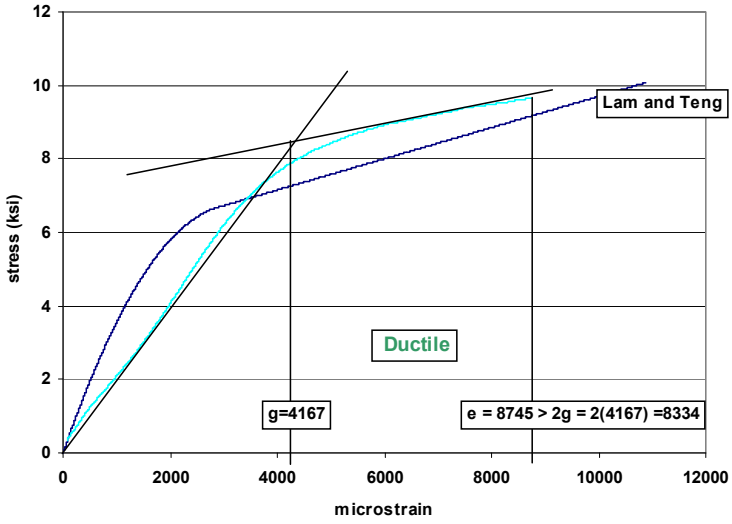

Figure 4-47 Specimen L5 Post MCE Ductility Calculation

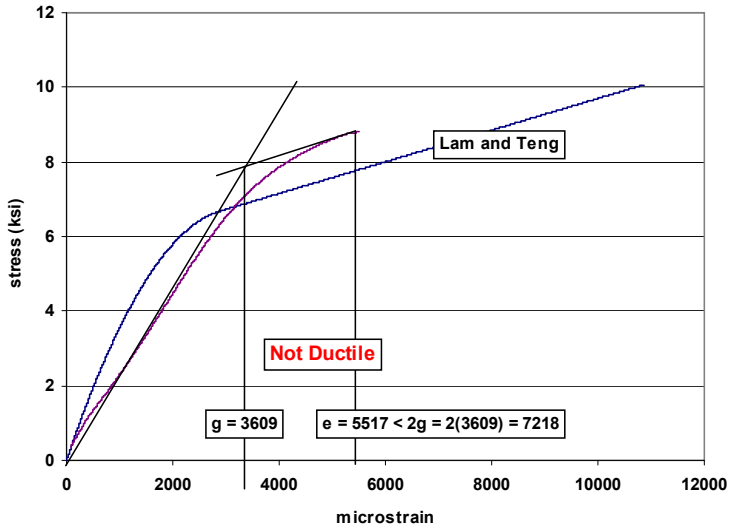

Figure 4-48 Specimen L6 Post MCE Ductility Calculation

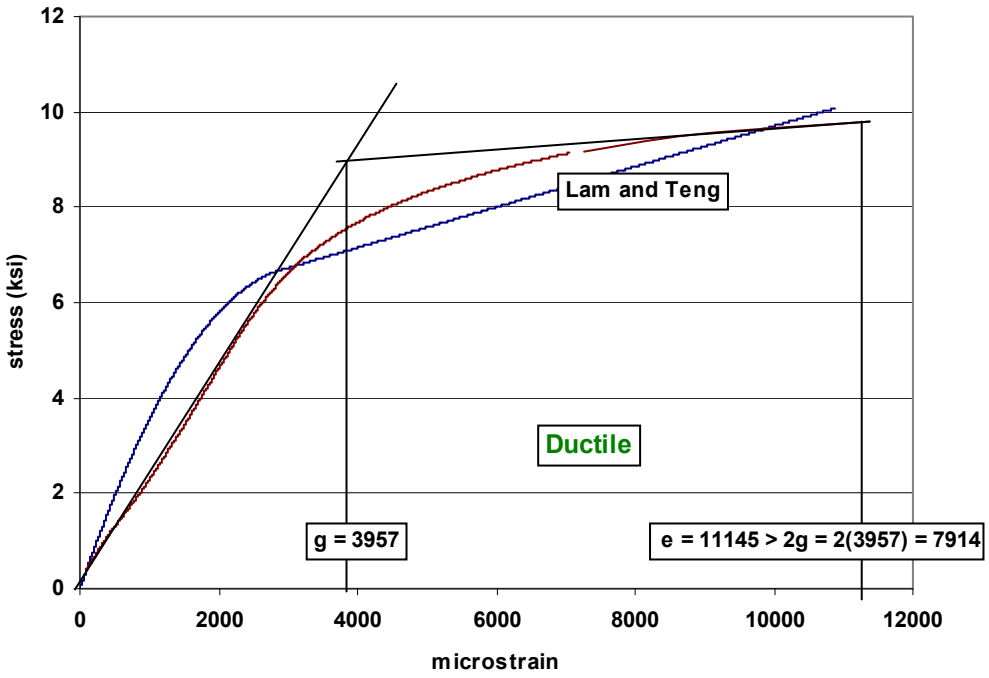

Figure 4-49 Specimen R4 Post MCE Ductility Calculation

Even though the damaged specimens have retained over 90% of the strength and 60% of the ductility of the undamaged specimens, their performance in subsequent seismic events will be substantially impacted under the procedures of FEMA 356. Members that are considered 'deformation controlled' have their allowable strength increased by a demand modification factor, m, which typically has a value of 2 to 4 but can be as high as 10 depending on various parameters. The demand modification factor does not apply to 'force controlled' members. Thus, when a member switches from deformation to force controlled, its usable strength under the FEMA 356 design procedures is substantially reduced. It follows that a structure damaged in a moderate earthquake may then lack sufficient residual ductility to achieve the desired performance level in subsequent, more severe seismic events. See Appendix D for a more detailed explanation of the FEMA 356 design procedures.

Table 4-17 demonstrates the impact of switching a member from 'deformation controlled' to 'force controlled'. From the reference cited in Appendix D, the design strength of a selected 'deformation controlled member' is given and found to be adequate. If a loss of ductility in a seismic event were to switch the member's classification to 'force controlled,' the design strength would drop by 75% and the member would not longer be adequate for the

desired performance level. Even though this member retained of 90% of its original strength, the loss in ductility as demonstrated in specimens C6, L5, and L6, caused such a change in behavior that the member is no longer adequate for the design seismic event.

Member Type	Required Strength	m-factor	Design Strength	Adequate?
Deformation Controlled	1233 k-ft	4	1472 k-ft	Yes
Force Controlled	1233 k-ft	1	368 k-ft	No

Table 4-17 Design Strength of Force and Displacement Controlled Members

Impact on a FEMA 450 Analysis

The impacts of a loss of ductility on the procedures of FEMA 450 are easier to explain qualitatively. FEMA 450 recognizes that when a structure behaves inelastically, it dissipates earthquake energy. Elements and structures with large inelastic capacities are more flexible. More flexible structures have lower fundamental periods. Lower fundamental periods mean lower design accelerations. This behavior is modeled by giving more ductile structures higher response modification factors (R factors) to reduce the seismic design forces. Table 4-18 shows R factors for three types of reinforced concrete moment frames and their relative ductility. .

Seismic Force Resisting System	R Factor	Relative Ductility
Special Reinforced Concrete Moment Frame	8	high
Intermediate Reinforced Concrete Moment Frame	5	medium
Ordinary Reinforced Concrete Moment Frame	3	low

Table 4-18 R Values for Concrete Moment Frames from FEMA 450

Under the procedures of FEMA 450, as R decreases, the seismic base shear increases. For the example structure described in Appendix D the variation of base shear with R can be seen in Table 4-19. If, through damage or modification, a structure were to lose ductility, the required seismic loads would increase. A structural system proportioned based on an R-factor of 8 could easily prove inadequate if the system no longer possesses that level of ductility.

R Factor	Seismic Base Shear (kips)
8	882
5	1411
3	2352

Table 4-19 Relationship of Seismic Base Shear to R-Factor

Table 4-20 shows the impact of changing the R-Factor in the analysis of the example structure in Appendix D. The R-factor decreases with loss in ductility which results in a corresponding increase in the required strength of a selected member. Under these procedures, the required strength changes while the design strength remains constant. Clearly, a member

adequately proportioned under an R-Factor of 8 or 5 would fail if the R-Factor were dropped to 3. If the damage resulting from a seismic event reduces ductility to the point where the original R-Factor is no longer justified, the structure may not be adequate for future events.

R-Factor	Required Strength	Design Strength	Adequate?
8	162 k-ft	368 k-ft	Yes
5	259 k-ft	368 k-ft	Yes
3	432 k-ft	368 k ft	No

Table 4-20 Impact of Ductility Loss on R-Factor and Required Strength

Residual Behavior Means More than Residual Capacity

In raising the issue of structural performance in a series of seismic events, Shan, Xiao, and Gou (2006) state:

> It has been suggested that the rupture of several glass FRP (GFRP) jackets installed on the columns of the I-5 and Freeway 2 interchange in Los Angeles were due to the insufficient residual capacity after the columns were subjected to the shaking of ht e1994 Northridge earthquake.

The term 'residual capacity' could be incorrectly interpreted as asking, "What percentage of the original strength and ductility remains?" where the correct issues is, "How does a structure that survived this earthquake perform in the next one?" When the issue is properly framed, it is clear that an engineer must consider the interaction between the strength and ductility remaining in each member and how a structure and its elements would behave based on the code classifications using this remaining ductility. As the severity of minor seismic events approaches that of the design seismic event, the probability that the structure will retain sufficient residual behavior to survive subsequent events decreases. In other words, a seismic event below design level, could preclude a structure surviving a subsequent design level seismic event.

The observations from this research do not indicate that damage from a moderate seismic event always leads to failure in a future seismic event of equal or greater magnitude. Rather, the observations indicated an alternative way of viewing the problem. After a moderately sever earthquake which causes structural damage a structure that remain standing must be considered as a 'new', or at least 'different' structure where each member and the structure as a whole possess new strength and ductility parameters. Subsequent analysis in accordance with an

appropriate design code or model must be based on the new properties if the issue of residual behavior is to be correctly addressed.

4.5.2 Impact of Findings on Reliability Studies

The strength of plain concrete is a function of many variables including aggregate strength, cement strength, cement gradation, curing temperature and humidity, vibration and compaction, and moisture content. When the concrete is reinforced with steel, the steel introduces additional variables like steel strength, confined core dimensions, and spiral pitch. When the concrete is retrofitted with FRP, even more variables arise: FRP material properties, quality of installation, and fiber orientation. This research has shown that the presence of sustained loading, failure mode, and typical vs. atypical stress-strain relationships are also among the significant variables.

In assessing this daunting number of variables, researchers have made hundreds, if not thousands, of test results available. Within these publications, models tend to be based on a relatively small sample size and compared to the equally small samples of other researchers. Within small samples, there is a tendency to attribute atypical results to errors in the experimental process and exclude them from new proposed models or diminish their importance. Even Lam and Teng's (2003) extensive database contained only 76 specimens. Any specimen that did not fail in FRP rupture was excluded. Their model shows good agreement with experimental results within the confines of original data set, but does not work as well for atypical failures. With the large number of published results now available, these atypical failure modes and paths should now be seen as unlikely, but legitimate, variations in behavior.

If externally applied FRP laminates are to become widely used and accepted, standardized ultimate strength or LRFD procedures compatible with those currently in use under ACI 318 must be developed. As this work proceeds it is necessary for researchers to proceed beyond results that "show good agreement with the proposed model" and analyze the impact of all the results that don't. Many FRP confined concrete columns display a clear bi-linear behavior, but some do not. Many FRP confined concrete columns fail in FRP rupture at about 60% of the ultimate coupon strain, but some delaminate. FRP confined columns display substantially increased strength over plain concrete, but the presence of a sustained load is detrimental to the level of performance. Safe, reliable, and usable design standards for FRP

confined columns require more than models that 'show good agreement with the results of this experiment.' The design standards must also provide reliability by addressing the wide variance generated by atypical results and the variety of possible life cycles.

4.6 Suggestions for Future Research

4.6.1 Creep Modification Factor α

Both this research and that of Shan, Xiao, and Gou (2006) found the value of the creep modification factor, α, to be about 2.0. When this value is used in Equation (2.108) and the resulting modified initial elastic strain used in the procedures of ACI 209, a reasonable creep prediction results. In both sets of experiments, the level of damage was such that the specimens exceeded their elastic limit and were pushed into the second region of the FRP confined concrete stress-strain curve. This research also found that this procedure did not produce suitable results for the Steel Group specimens which did not experience substantial in-elastic behavior during the minor critical event. Creep strains for these less damaged specimens exceeded that of ACI 209, but the procedure suggest by Shan, Xiao, and Gou did not accurately predict these strains. It is recommended that research be conducted to establish procedures for predicting creep in specimens with low levels of damage resulting from lower load levels as well as verifying values for the creep modification factor, α, at other levels of in-elastic loading and damage.

4.6.2 Sustained Load Parameters n and A

The proposed model quantified the effect of a sustained load on the stress-strain behavior of FRP confined concrete. The duration of the sustained load is related to the curve fitting parameter n and the reference stress parameter A using a relationship derived from the creep coefficient of ACI 209. A limitation of this research is that only two time data points at one stress are available: no applied stress at time equal zero and 1.49 ksi for 42 days. Future research conducted at this stress for longer durations and other stresses for similar durations would further validate and improve the proposed model.

4.6.3 Application of Life Cycle Analysis to Standard and Performance Based Earthquake Engineering

The results of this research show that minor critical events can significantly reduce the ductility of damaged components. This loss of ductility can result in a change in classification under either of the two model earthquake codes discussed. As the member or structure classification changes, so do the results of the structural analysis. Current code procedures ensure that the structure survives the first earthquake, but do not take into account performance in subsequent events. Research should be conducted on structural performance under a random series of seismic events. After each event, the damage to the structure should be established and this 'new' structure used as the basis for the next seismic event. While this type of analysis would not replace field inspections following an actual earthquake, it would enable engineers to predict a sequence of events expected to result in a required rehabilitation to maintain a desired performance level.

For example, consider a structure designed using the Performance Based Earthquake Engineering approach of FEMA 356. Assume the structure is designed to achieve the Life Safety performance level under a 10% probability of exceedence (P.E.) in 50 year earthquake. If this is the first earthquake to occur following the construction, the structure should perform as planned. Life cycle analysis would address the issue of sequential performance if the structure experienced a 20% P.E./50 year earthquake and then a 50% P.E./50 year earthquake prior to the maximum expected earthquake. Life cycle analysis where strength and ductility are modified after each event would enable engineers to predict the need for future inspections and rehabilitations. This approach could prove beneficial to increasing safety, better structural performance, and reduced economic losses.

4.6.4 Toward LRFD for FRP

> New construction technologies will not be widely accepted without supporting structural design standards to facilitate their introduction into professional practice. A probability-based LRFD standard for engineered composite structures would remove a major barrier to their implementation in civil construction.
>
> (Ellingwood, 2003)

For over 25 years, papers presenting experimental data and proposing stress-strain models for FRP confined concrete have been published. While data and models abound,

standards do not. The ACI publication concerning FRP is over 12 years old and is more of an information paper than a design specification. Perhaps the greatest difficulty is establishing standards for FRP composite applications in civil engineering is the variability in materials, application methods, models, and results. However, there are procedures for dealing with these issues.

Load and Resistance Factor Design, under different names, has a more that 50 year history and the procedures for its implementation are well established. Concrete, steel, and timber structures are now designed under LRFD based formats. The processes used in an LRFD methodology contain the tools necessary to assess the variability seen in the results of FRP confined concrete research. It is time for the results of the 25 year history of FRP confined research to be consolidated and used to establish appropriate resistance factors which will then lead to the publication of a complete design specification.

4.6.5 Development Length

When using standard 6" by 12" specimens, most researchers use a one quarter wrap overlap to ensure the full development of the FRP strength. When considering the effects of sustained load, this overlap may prove insufficient. Experiments should be conducted on specimens subjected to sustained loading with different overlap lengths to determine if longer overlaps can prevent delamination and return the expected failure mode to FRP rupture.

5. Conclusions

5.1 Research Summary

One inspiration for this research was a favorite statement of Dr. Rich Barker of Virginia Tech: "The trouble with engineers is that they don't know how to build buildings." Dr. Barker was speaking of the problems that arise from constructing a computer model of a 100 story building and, when the model is complete, "flipping a switch to turn on gravity." In reality, gravity acts on the structure as member is added to member and substantial deformation due to gravity has already occurred by the time the owner takes possession of the building. In this research, Dr. Barker's observation has been applied to the behavior of FRP confined concrete.

A principal selling point of externally applied FRP wraps is their ability to provide additional strength and ductility to existing structural members that do not meet current code standards. The literature review of Chapter 2 leads to the conclusion that this claim is accurate, but is based on models that have not investigated the effects of time of FRP wrapped members. This observation led to the basic question of this research program: Does an experimental based model which experiences construction, loading, and destruction in a matter of weeks accurately reflect the behavior of a retrofit structure which experiences long term sustained service loading prior to critical events?

To answer this question, this research employed the concept of 'life cycle modeling' to simulate the critical events in a building's history so that the impact of these events on the ultimate performance of the structure could be assessed. The experimental program of life cycle modeling was explained in Chapter 3. Critical life cycle events were defined and experimental devices constructed to allow the modeling of these events. Load magnitudes and durations were selected to approximate real world behavior within the time constrains of a Ph.D. research program. While not long enough to see the full effects of time, they are sufficiently long to see many of the effects of time. Life cycle stress and strain data were recorded and reported in Chapter 3 for each specimen and group of specimens.

The analytical program explained in Chapter 4 began by selecting the stress-strain model of Lam and Teng (2004) as representative of the current understanding of the behavior of FRP confined concrete and the creep model of ACI 209 for creep predictions. Using the experimental

data, 12 investigations were conducted examining individual aspects of life cycle behavior. The resulting 12 findings establish that the control behavior is consistent with the model of Lam and Teng; sustained loading results in a degradation of the stress-strain behavior; creep of a damaged specimen can be predicted based on a modified form of the ACI 209 creep model; the variation in behavior increases with increasing complexity of the life cycles; and FRP retrofit of a damaged steel spiral confined specimen produces a stress-strain response 8% below that of an undamaged specimen. Analysis of these findings led to the proposed model which accounts for all elements in the life cycle behavior of a specimen.

5.2 Proposed Model

The proposed model has three elements to deal with creep, monotonic loading, and cyclic loading. It is a design oriented model where the only required inputs are unconfined compressive strength of the concrete and the strength, elastic modulus, and ultimate strain of the FRP. The input parameters and the forms of the equations are consistent for the monotonic and cyclic models. The proposed model is explained fully in Section 4.4 and the highlights are repeated in the next three sub-sections.

5.2.1 Proposed Creep Modeling

Creep modeling of an undamaged, FRP confined specimen can be accomplished by using the procedures of ACI 209. A more accurate prediction is achieved if the actual initial elastic strain is used rather than a strain estimated by the estimated value of E_c. For a specimen damaged by a minor critical event, the procedures of ACI 209 can be used provided the initial elastic strain is modified using Equation (2.108). Experimental values of α are 1.98 and 2.09. A value of 2.0 may be used in the absence of other information.

$$\varepsilon_{ia} = \alpha \varepsilon'_{ia}$$

5.2.2 Proposed Monotonic Model

The proposed monotonic model is given by Equation (4.1) supported by Equations (4.2) to (4.5). The values for the curve fitting parameter n and the reference stress coefficient A can be found from Figure 3-32 and Figure 3-33 or Equations (4.8a) and (4.8b) respectively.

$$f_c = \frac{(E_1 - E_2)\varepsilon_c}{\left[1 + \left(\frac{(E_1 - E_2)\varepsilon_c}{f_o}\right)^n\right]^{\frac{1}{n}}} + E_2\varepsilon_c \tag{4.1}$$

$$f_l = \frac{2 f_{frp} t}{d} \tag{4.2}$$

$$f_o = 0.838 f'_{co} + 0.632 f_l + A[ksi] \tag{4.3}$$

$$E_1 = 54.158\sqrt{1{,}000 f'_{co}} \quad [ksi] \tag{4.4}$$

$$E_2 = 52.411 f'^{0.2}_{co} + 3.1667 \frac{E_{frp} t}{d} \quad [ksi] \tag{4.5}$$

The stress strain curve terminates at an ultimate strain as predicted by Equation (2.72) from the model of Lam and Teng (2004) and the stress predicted by Equation (4.1) using this strain.

5.2.3 Proposed Cyclic Model

The proposed cyclic model uses three equations to model the three parts of the response: unloading, reloading, and transition back to the stress-strain envelope. The unloading branch begins at a strain-stress point (ε_{un}, f_{un}) and is a curve given by Equation (4.11) supported by values from Equations (4.9), (4.10), (4.12), (4.13), and (4.14).

$$\varepsilon_{pl} = \varepsilon_{un} - \frac{f_{un}}{E_1} \tag{4.9}$$

$$E_u = \frac{4}{3} E_c \tag{4.10}$$

$$f_c = f_{un} - \frac{f_{un}\, x\, r}{r - 1 + x^r} \tag{4.11}$$

$$r = \frac{E_u}{E_u - E_{\sec}} \tag{4.12}$$

$$E_{\sec} = \frac{f_{un}}{\varepsilon_{un} - \varepsilon_{pl}} \tag{4.13}$$

$$x = \frac{\varepsilon_c - \varepsilon_{un}}{\varepsilon_{pl} - \varepsilon_{un}} \tag{4.14}$$

The unloading branch ends and the reloading branch begins at the reload strain-stress point (ε_{ro}, f_{ro}). Equation (4.16) predicts the reloading branch between the reload point and a new reference point, (ε_{un}, f_{new}) which represents the loss of capacity due to the cyclic loading. Equations (4.15)and (4.17) support the calculation of the reloading branch.

$$f_{new} = 0.95 f_{un} + 0.08 f_{ro} \tag{4.15}$$

$$f_c = f_{ro} + E_r (\varepsilon_c - \varepsilon_{ro}) \tag{4.16}$$

$$E_r = \frac{f_{ro} - f_{new}}{\varepsilon_{ro} - \varepsilon_{un}} \tag{4.17}$$

The reload cycle ends when the stress-strain response returns to the unloading strain ε_{un} at the stress given by Equation (4.16). This point now becomes the starting strain-stress (ε_{un}, f_{un}) for the next cycle. These procedures are repeated for the desired number of cycles. When the response moves beyond ε_{un} back to the monotonic curve proposed in Section 4.4.2 it follows the path given by Equation (4.18).

$$f_c = \frac{(E_1 - E_2)(\varepsilon_c - \varepsilon_{tr})}{\left[1 + \left(\frac{(E_1 - E_2)(\varepsilon_c - \varepsilon_{tr})}{f_{tr}}\right)^{0.5}\right]^2} + E_2(\varepsilon_c - \varepsilon_{tr}) + f_{tr} \tag{4.18}$$

5.2.4 Sequential Application of Models

The models for creep, monotonic behavior, and stress-strain behavior can be combined to get the stress-strain history of a specimen. Events can be sequenced in any order with the starting strain in any event being the ending strain in a prior event. Input parameters and equation forms are consistent across the different model elements for ease of application and consistency of results.

5.3 Conclusion

The answer to the fundamental question of this research program is that the behavior of a real structure which experiences a varied life cycle is not completely predicted by an experimental based model which experiences construction, loading, and destruction in a matter of weeks. Critical differences between traditionally developed models and life cycle modeling are:

- Ultimate stress-strain performance is degraded following the sustained application of a service load. This degradation may be accounted for using the proposed model. The model is based on one level of sustain load and one time duration. Future studies should include more variation in these parameters.
- Increasing the variation of life cycle events increases the variability of failure modes, paths, and values. This variation must be addressed in future reliability studies.
- Saying a specimen retains 'significant reserve capacity' is not a sufficient condition to ensure the desired behavior in subsequent seismic events. After a specimen or structure is damaged, it must be re-evaluated with the members and structural system reclassified using the remaining strength and ductility rather than the original values.
- The behavior of a retrofitted damaged steel confined specimen is 8% below that of a retrofitted undamaged steel confined specimen. Therefore an increased level FRP rehabilitation of damaged specimens may be necessary to achieve the performance calculated using a model derived from undamaged specimens.

Using a life cycle approach to model development improves the verisimilitude of material models by developing them under conditions that simulate actual structural life cycles. An improved material model combined with a life cycle focus enhances performance based engineering because the effects of time can be explicitly included and analyzed. This, in turn, allows engineers and facility managers to better predict different life cycle events that would trigger a need for inspection and, possibly rehabilitation, to ensure the desired performance levels are maintained in future events. When the life cycle of a building is viewed and modeled holistically, better decisions can be made from structural, maintenance, and economic perspectives. From these improved decisions flow safety, economic, and operational benefits for clients, the engineering profession, and society.

References

Ahmad, S.M., and Shah, S.P. (1982). "Stress-strain Curves of Concrete Confined by Spiral Reinforcement." *Journal of the American Concrete Institute*, v79, n6, 484-490.

American Concrete Institute, Committee 440.2R-02 (2002). Design and Construction of .Externally Bonded Systems for Strengthening Concrete Structures.

American Concrete Institute, Committee 209. (1997). Prediction of Creep, Shrinkage, and Temperature Effects in Concrete Structures.

ASTM International. (2002). Standard Test Method for Static Modulus of Elasticity and Poisson's Ratio of Concrete in Compression.

American Society of Civil Engineers. 2000. Prestandard and Commentary for the Seismic Rehabilitation of Buildings.

Atadero, R.A. and Karbhari, V.M. (2005). "Determination of Design Values for FRP Used for Strengthening." *Proceedings, International SAMPE Symposium and Exhibition, 141-156.*

Berthet, J. F., Ferrier, E., and Hamelin, P. (2006). "Compressive behavior of concrete externally confined by composite jackets: Part B: Modeling." *Constr.Build.Mater.,* 20 338-347.

Berthet, J. F., Ferrier, E., and Hamelin, P. (2005). "Compressive behavior of concrete externally confined by composite jackets. Part A: experimental study." *Construction & Building Materials,* 19 223-32.

Berthet, J. -., Ferrier, E., Hamelin, P., Al Chami, G., Theriault, M., and Neale, K. W. (2006). "Modeling of the creep behavior of FRP-confined short concrete columns under compressive loading." *Materials and Structures/Materiaux Et Constructions,* 39(28), 53-62.

Building Seismic Safety Council. 2003. NEHRP Recommended Provisions for Seismic Regulations for New Buildings and Other Structures.

Cusson, D. and Paultre, P. (1985). "Stress-Strain Model for Confined High-Strength Concrete" *ASCE Journal of Structural Engineering*, Vol. 121, No. 3, p. 468-477.

Ellingwood, B.R. (2003). "Toward Load and Resistance Factor Design for Fiber-Reinforced Polymer Composite Structures." *ASCE Journal of Structural Engineering*, Vol. 129, No. 4, p. 449-458.

Fafitis A., and Shah, S. P. (1985). "Lateral Reinforcement for High-Strength Concrete Columns" ACI Special Publication, SP 87-12, p. 213-232.

Fardis, M. N., and Khalili, H. H. (1982). "FRP-Encased Concrete As A Structural Material." *Magazine of Concrete Research,* 34(12), 191-202.

Gopalakrishnan, K.S., Neville, A.M., and Ghali, A. (1970). "A Hypothesis on Mechanism Creep of Concrete with Reference to Multiaxial Compression." *ACI Journal.* v67, n3, 29-35.

Han, L., Tao, Z., and Liu, W. (2004). "Effects of sustained load on concrete-filled hollow structural steel columns." *J.Struct.Eng.,* 130 1392-1404.

Harmon, T., Slattery, K., and Ramakrishnan, S. (1995). "The Effect of Confinement Stiffness on Confined Concrete." *Proceedings of the Second International RILEM Symposium,* 548-592.

Hart, S.D. and Esmaeily, A (2007). "A Comparison of Two Earthquake Design Methodologies." *Proceedings, 3rd International Conference on Structural Engineering, Mechanics, and Computation, 329-334.*

Jordaan, I.J. and Illston, J.M. (1971). "Time-dependent Strains in Sealed Concrete Under Multi-Axial Compressive Stress." *Magazine of Concrete Research,* v23, n75-76, 79-88.

Karabinis, A. I., and Rousakis, T. C. (2002). "Concrete confined by FRP material: A plasticity approach." *Eng.Struct.,* 24 923-932.

Kawashima, K., Hosotani, M., and Hoshikuma, J. (1997). "Composite Jacketed Concrete under Uniaxial Compression: Verification of Simple Design Equations." *J. Mat. in Civ. Engrg.,* ASCE v9. n4, 195-193.

Lam, L., and Teng, J. G. (2003). "Design-oriented stress-strain model for FRP-confined concrete." *Constr.Build.Mater.,* 17(6), 471-489.

Lam, L., Teng, J.G., Cheung, C.H., and Xiao, Y. (2006). "FRP-Confined Concrete under Axial Cyclic Compression." *Cement and Concrete Composites.*, v28, n10, 949-958.

Maalej, M., Tanwongsval, S., and Paramasivam, P. (2003). "Modeling of rectangular RC columns strengthened with FRP." *Cement and Concrete Composites,* 25 263-276.

Mander, J. B., Priestley, M. J. N., and Park, R. (1988). "Theoretical Stress-Strain Model for Confined Concrete" Journal of Structural Engineering, ASCE, V. 114, No. 8, p. 1804-1825.

Mansur, M.A., Wee, T.H., and Chin, M.S. (1995). "Derivation of the Complete Stress-Strain Curves for Concrete in Compression." *Magazine of Concrete Research,* v47, n173, 285-290.

Matthys, S., Toutanji, H., and Taerwe, L. (2006). "Stress-Strain Behavior of Large-Scale Circular Columns Confined with FRP Composites." *Journal of Structural Engineering,* ASCE, v.132, n. 1. 123-133.

Mirmiran, A., and Shahawy, M. (1997). “Behavior of Concrete Columns Confined by Fiber Composites.” *J. Struct. Engrg.,* ASCE, 123(5), 583-590.

Miyauchi, K., Nishibayashi, S., and Inoue, S. (1997). “Estimation of Strengthening Effects with Carbon Fiber Sheet for Concrete Column.” *Proceedings of the Third International RILEM Symposium,* 217-224.

Moran, D. A., and Pantelides, C. P. (2002). "Stress-strain model for fiber-reinforced polymer-confined concrete." *J.Composite Constr.,* 6 233-240.

Murray, T. (1997). Steel II Course Notes, Virginia Tech.

Naguib, W. (2001). “Long Term Behavior of Hybrid FRP-Concrete Beam-Columns.” Ph.D. dissertation, University of Cincinnati.

Naguib, W., and Mirmiran, A. (2003). "Creep analysis of axially loaded fiber reinforced polymer-confined concrete columns." *J.Eng.Mech.,* 129(1), 1308-1319.

Nanni, A., and Bradford, N. M. (1995). "FRP jacketed concrete under uniaxial compression." *Constr.Build.Mater.,* 9 115-124.

Oline, R. A. and Karbhari, (2003). “An Approach to the Establishment of LRFD for FRP Strengthening.” *Proceedings, International SAMPE Symposium and Exhibition*, 2104-2114.

Pantazopoulou, S.J. and Mills, R.H. (1995). “Microstructural Aspects of the Mechanical Response of Plain Concrete.” *ACI Materials Journal.* v92, 605-616.

Popovics, S. (1973). "Numerical Approach To The Complete Stress-Strain Curve Of Concrete." *Cem.Concr.Res.,* 3 583-599.

Picher, F., Rocherre, P. and Labossiere, P. (1996). “Confinement of Concrete Cylinders with CFRP.” *Proceedings, First International Conference on Composites in Infrastructure,* 829-841.

Richard, R.M. and Abbott, B.J. (1975). “Versatile Elastic-Plastic Stress-Strain Formula.” *J.Eng.Mech.,* 101(EM4), 551-515.

Richart, F.E., Brandtzaeg, A., and Brown, R.L., (1928), “Study of the Failure of Concrete under Combined Compressive Stresses,” *Bulletin 185,* University of Illinois Engineering Experiment Station, Champaign, Illinois.

Russell, H.G. and Corley, W.G. (1977). “Time-dependent behavior of Columns in Water Tower Place.” *Research and Development Bulletin RD025B,* Portland Cement Association, Skokie, Ill.

Saadatmanesh, H., Ehsani, M. R., and Li, M. W. (1994). "Strength and ductility of concrete columns externally reinforced with fiber composite straps." *ACI Structural Journal (American Concrete Institute),* 91 434-447.

Saafi, M., Toutanji, H. A., and Li, Z. (1999). "Behavior of concrete columns confined with fiber reinforced polymer tubes." *ACI Mater.J.,* 96 500-509.

Saadatmanesh, H., Ehsani, M.R., and Li, M. W. (1994). "Strength and Ductility of Concrete Columns Externally Reinforced with Fiber Composite Straps." *ACI Structural Journal,* v91, n4, 434-447.

Saatcioglu, M. and Razfi, S.R. (1992). "Strength and Ductility of Confined Concrete." *ASCE Structural Journal,* v118, n6, 1590-1607.

Samaan, M., Mirmiran, A., and Shahawy, M. (1998). "Model of concrete confined by fiber composites." *J.Struct.Eng.,* 124 1025-1031.

Sargin, M. (1971). "Stress-Strain Relationships for Concrete and the Analysis of Structural Concrete Sections," *Study No. 4*, Solid Mechanics Division, University of Waterloo, Ontario, Canada.

Shan, B., Xiao, Y., and Guo, Y. (2006). "Residual performance of FRP-retrofitted RC columns after being subjected to cyclic loading damage." *J.Composite Constr.,* 10 304-312.

Shao, Y (2003). "Behavior of FRP-Confined Concrete Beam Columns under Cyclic Loading." PhD Thesis, North Carolina State University.

Shao, Y., Zhu, Z., and Mirmiran, A. (2006). "Cyclic Modeling of FRP-Confined Concrete with Improved Ductility." *Cement and Concrete Composites.*, v28, n10, 959-968.

Sheikh, S. A., and Uzumeri, S. M. (1982). "Analytical Model for Concrete Confinement in Tied Columns" Journal of Structural Engineering, ASCE, V. 108, No. ST12, p. 2703-2722.

Spoelstra, M. R., and Monti, G. (1999). "FRP-confined concrete model." *J.Composite Constr.,* 3 143-150.

Teng, J.G. and Lam L (2004). "Behavior and Modeling of Fiber-Reinforce Polymer Concrete." *Journal of Structural Engineering.,* v124, n9, 1713-1723.

Takiguchi, K., et al. (1976). "Analysis of Reinforced Concrete Sections Subjected to Biaxial Bending Moments." *Transaction, Architectural Institute of Japan,* 250, 1-8.

Toutanji, H. A. (1999). "Stress-strain characteristics of concrete columns externally confined with advanced fiber composite sheets." *ACI Mater.J.,* 96 397-404.

Young-Chul Song, Dae-Soo Lee, Myung-Suk Cho, and Jang-Hwa Lee. (1995). "A study on the long-term properties of concrete." *Sixteenth Annual Conference 1995,* Canadian Nucl. Soc, Saskatoon, Sask., Canada, 401-12.

Appendix A Notation

A_{st} cross sectional area of FRP strap, particularly in Saadatmanesh, et al.(1994)

A reference stress parameter in the proposed monotonic model

d diameter of

E_1 elastic modulus for the 1st branch of an FRP confined concrete stress-strain curve. depending on the model, this may or may not equal E_{co}

E_2 elastic modulus for the 2nd branch of an FRP confined concrete stress-strain curve

E_{co} elastic modulus of plain concrete

E_{frp} elastic modulus of fiber reinforced polymer material

E_P modulus calculated at the peak compressive stress. Used by Richard and Abbott (1975)

E_r reloading modulus under cyclic loading

E_{re} transition modulus from cyclic to monotonic model

E_u initial unloading modulus

f_c concrete stress in a specimen at a given point

f'_{co} or f'_c maximum compressive stress of plain concrete

f'_{cc} maximum compressive stress of confined concrete

f_{frp} or f_{ju} ultimate stress of FRP material in a coupon test

f_l or f'_l or f_{lu} maximum confining stress provided by steel spiral or FRP jacket

$f_{l,a}$ actual maximum confining stress provided by steel spiral or FRP jacket

f_{new} reloading reference stress

f_o a reference stress, usually related to the y-intercept of the 2nd branch of an FRP confined concrete stress strain curve

f_{re} transition stress from cyclic to monotonic model

n curve fitting parameter in the proposed monotonic model

s width of FRP strap, particularly in Saadatmanesh, et al.(1994)

t total thickness of FRP jacket

ε_c concrete strain in a specimen at a given point in the axial (or longitudinal) direction

ε_{cc} confined concrete strain at f'_{cc}

ε_{co} ultimate rupture strain of plain concrete

ε_{cu} ultimate rupture strain of confined concrete

ε_{frp} rupture strain of FRP as determined by coupon test

$\varepsilon_{h,rup}$ rupture strain of FRP in a hoop configuration (i.e. wrapped around a cylinder)

ε_{re} transition strain from cyclic to monotonic model

ε_{un} cyclic unloading strain

ε_{pl} plastic strain on unloading

ε_{r} radial strain

ε_{t} concrete strain at the point of transition between the 1st and 2nd branches of an FRP confined concrete stress-strain curve

μ dilation ratio

σ_{o} reference stress found by projecting E_p back to the σ-axis. Used by Richard and Abbott.

ν_{c} ratio of longitudinal to axial strain in a concrete specimen

ν_{co} Poisson's ratio of plain concrete

subscript a denotes axial direction

subscript r denotes radial direction

Appendix B Sustained Load Device

The sustained load device was an essential part of this research. It was required to simulate the long term service load on a structure. One technique to apply these loads is creep frames consisting of steel tension rods, plates, and springs. The principal drawback of this method is that as the concrete creeps, the load on the specimens decreases unless constant adjustments are made. A second technique uses an air over hydraulic pump to maintain a relatively constant load on a specimen in a load frame. Drawbacks to this method include susceptibility to power failure and irregularities in the force applied. For this research, an additional disadvantage of these methods was that the lab did not have this equipment available. The available assets to apply a sustained load included space, three 200 kip hydraulic cylinders, two 300-kip load cells, and shop equipment. These were used to design and build the sustained load device for this research.

The sustained load device used the basic engineering principles to enable 1.5 kips of load to apply 42 kips of force to the specimens. The system was self equilibrating so that it cannot apply more load and it will not apply less.

The system used a lever with a 3:1 mechanical advantage where the weight of a water tank was counterbalanced by a small hydraulic cylinder as seen in Figure B-1. The small hydraulic cylinder then actuated the three large bore loading cylinders with a mechanical advantage of over 10:1. In this way, 1.4 kips of load, multiplied by 3 then by 10 became 42 kips of load on the test specimens. The load on the specimens was equilibrated using end plates and eight tension rods. The load was verified by means of 300 kips load cells seen in Figure B-1. The system was designed to carry a maximum load of 80 kips on the specimens.

They system proved able to maintain a very steady load over time as proven in Figure 3-3. This is principally because the system is self-equilibrating. As the concrete specimens creeped and shortened, the large hydraulic cylinders expanded because the water tank on the lever arm maintains a constant hydraulic pressure in the small cylinder. This worked fine in theory, but neglects the friction in the system. In reality, the friction force could be as large as 3 kips. To overcome this problem, each morning the lever arm was manually bumped up or down and the load reset using the load cells. To remove the small elastic strain changes that resulted

from this adjustment, strains were recorded in the afternoon. This method was simple and effective.

Figure B-1 Sustained Load Device Loading Lever

Figure B-2 Sustained Load Device Loading Cylinders and Frames

Two extremely useful features of the system were the come-along and hydraulic refill pump. The come-along seen in Figure B-3 enabled the entire system to be unloaded without draining the water tank. Tightening the come-along raised the water tank and removed all load from they hydraulic cylinders and allowed adjustments and changes to the system to be made quickly and easily. As is true with all hydraulic jacks, a small movement in the large cylinders

produced a large movement in the small one. In this case, a 1/8 inch movement in the large cylinders meant over 4 inches of movement in the small one. To maintain a near horizontal position of the lever, it was necessary to add more fluid to the system. This was accomplished by means of a hydraulic jack seen in Figure B-4. The jack was able to add fluid but the system pressure did not change because the equilibrium condition of the lever. If the pressure increased, it simply moved the water tank up until equilibrium was re-established.

Figure B-3 Sustained Load Device Come-Along

Figure B-4 Sustained Load Device Hydraulic Fluid Refill Pump

Appendix C

Load Amplification Device

The load amplification device is proof that Civil Engineering is a contact sport! This device was necessary to test the FRP confined specimens because the capacity of the MTS servo controlled hydraulic actuator was 150 kips while the strength of the specimens was almost 300 kips. The device was nicknamed the 'nutcracker' because it was inspired by the common household nutcracker which places a nut near a pivot point while a hand squeezes long handles.

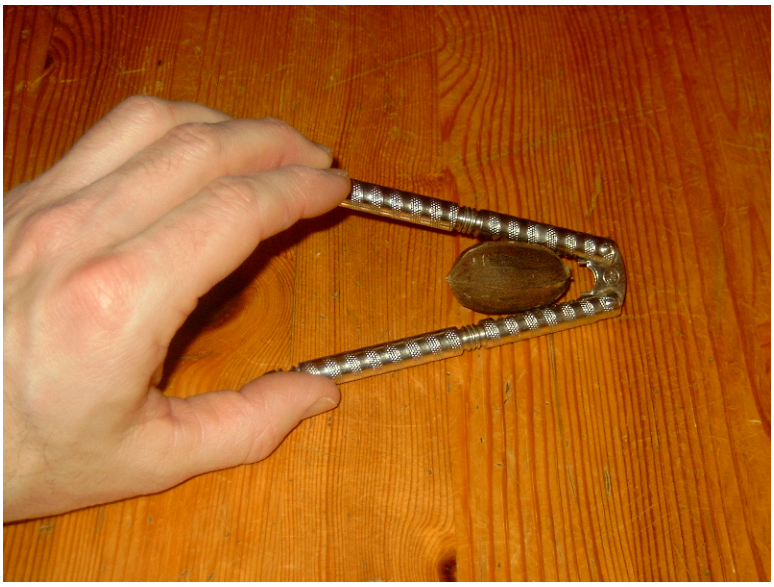

Figure C1 Household Nutcracker

The load amplification device consisted of an immobile base beam, two tie bars and a movable top beam. See Figure C2. The moment arm from the pivot point to the specimen was 1 foot and to the hydraulic actuator was 3 feet. This resulted in a mechanical advantage of 3:1 and allowed the 150 kip actuator to break specimens with a strength of over 300 kips.

Figure C2, Load Amplification Device

The device was designed in accordance with the 2005 Manual of Steel Construction for all applicable limit states and fabricated by the author and the staff of the KSU Civil Engineering Lab. Both the bottom and beams were built up using C10x25, Grade 50 sections. The bottom beam, shown in Figure C3, had two shorter center sections (5 feet) and two longer outer sections (10 feet) to facilitate securing the device to the strong floor. The half sections consisting of one longer and one shorter piece were bolted together with spacer plates as seen in Figure C4. The bolts, 1 inch diameter, A325N type, were sufficient to transfer any applied force from one beam to the other to ensure the built up member acted as a unit. The spacer plates provided the space necessary to insert the two tie rods. The two half sections were then welded together to form the bottom beam. The top beam was fabricated in the same manner as the bottom beam, except that it was only five feet long. See Figure C5.

Figure C3, Bottom Beam, Load Amplification Device

Figure C4, Bottom Beam, Load Amplification Device

Figure C5, Top Beam, Load Amplification Device

One of the reasons for using C10x25 channels was that they have a very thick web, 0.526 inches, and demonstrate better behavior in the limit states of web crippling, web buckling, and web yielding. As an added reinforcement, full depth web stiffeners of 3/8 inch by 2¼ inch, A36 plate were added to the interior channels of both the bottom and top beams. The stiffeners can be seen in Figures C6 and C7.

Figure C6, Web Stiffeners on One Member

Figure C7, Web Stiffeners on Built Up Section

The tie bars were two 6 inch by 1 inch, A36 plates. For consistency in hole spacing, the two bars and both the top and bottom beams were assembled and gang drilled. This operation can be seen in Figures C8 and C9. The beams and tie bars were connected using pins fabricated from 1½ inch diameter Viscount 44® tool steel.

Figure C8 Gang Drilling Bottom Beam

Figure C9 Gang Drilling Top Beam

The load amplification device was designed to provide a mechanical advantage of 3:1. This was verified by placing a 300 kip load cell at the specimen location and recording the value of the specimen load at each increment of actuator load. In Figure C10, the x-axis is the load recorded using the load cell on the MTS actuator while the y-axis is the load recorded at the specimen location by the 300 kip load cell. The specimen load in kips was then be calculated using the equation shown in Figure C10.

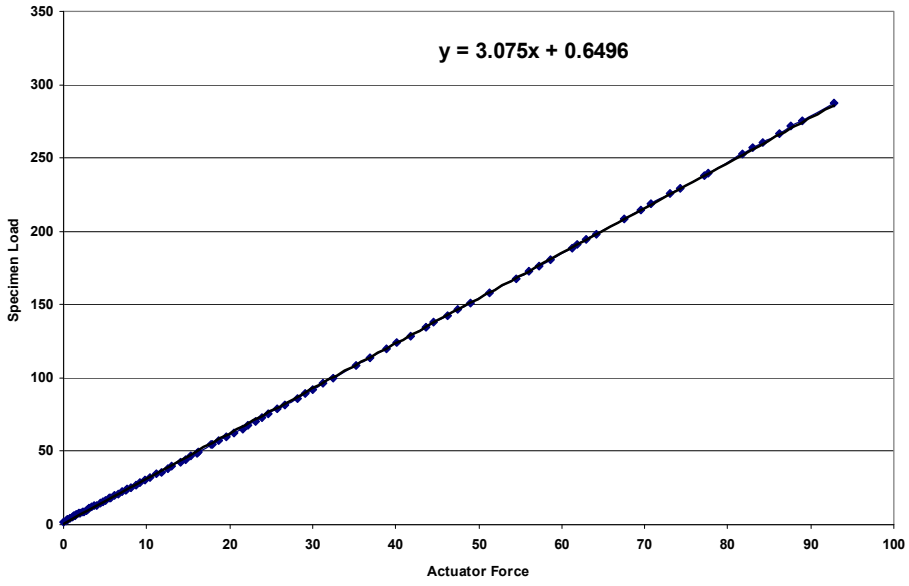

Figure C10, Load Amplification Device Calibration

The most difficult aspect of operating the load amplification device was maintaining a concentric load. Space requirements did not allow for the use of a ball and socket system, and sometimes the load was eccentric. Usually, the eccentricity was small and could be corrected by simply averaging the three strain gage values. Sometimes, an unacceptably large eccentricity was identified during the preliminary loading of a specimen. This was normally corrected by stopping the test, rotating the specimen, and re-initializing the test. In the case of Specimen S5, this still did not yield good results. For this specimen, strain gage L3 reported tensile strains for the entire test, and although strain gages L1 and L2 reported compressive strains, the three gages did not average well. It was apparent that the influence of L3 was excessively weighted in tension while L1 and L2 did not fully counterbalance this with compression. As the values of the three gages were consistent, they were used to estimate a value of a virtual strain gage labeled L4 as seen in Figure C11. With the inclusion of L4, the specimen response was consistent with the expected behavior.

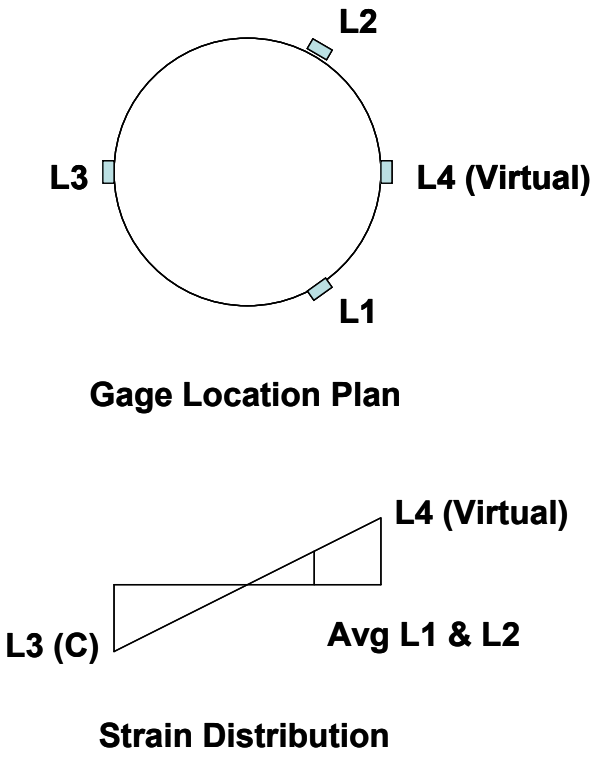

Figure C11, Specimen S5 Correction Algorithm

Appendix D

FEMA 356-FEMA 450 Comparison

This appendix refers the reader to "A Comparison of Two Earthquake Design Methodologies" published in the *Proceedings, 3rd International Conference on Structural Engineering, Mechanics, and Computation,* in September, 2007 by the author and his major professor. This paper explains the different design and analysis approaches in FEMA 356 and FEMA 450. The paper provides the results of sample calculations performed on a multi-story reinforced concrete frame using data from the Pacific Earthquake Engineering Research Center (PEER) website, http://peer.berkeley.edu/peertestbeds/van%20nuys.htm. It is the analysis of this structure, as reported in this paper, which provides the values for the design strengths and required strengths used for illustration purposes in Section 4.5.1.